Division of Drug Delivery
School of Pharmacy

A novel approach toward colon cancer treatment involving mucoadhesion and tumour-targeting of curcumin-containing nanoparticles

Rayan Sabra
BSc, MRes

Thesis submitted to the University of Nottingham for the degree of Doctor of Philosophy

May 2019

Dedicated to my beloved parents and brothers, for their love, endless support, encouragement & sacrifices.

This thesis is the result of the author's original work except for quotations and citations, which have been duly acknowledged. It has not been previously or concurrently submitted for any degree at the University of Nottingham Malaysia or any other institution.

Abstract

Curcumin is a natural, lipid-soluble compound extracted from turmeric with no perceptible toxicity. Recent studies have shown that curcumin has distinctive anticancer properties against colorectal cancer (CRC). However, oral administration of curcumin results in low absorption, rapid metabolism and elimination, and limited systemic bioavailability. To surmount these limitations, nano-encapsulation technology may be applied. Various polymers have been utilised to fabricate the encapsulant in nanoparticles, yet those of natural origin are more favoured since they are biocompatible, biodegradable and cause no toxicity. Thus, encapsulating curcumin in natural polymeric nanoparticles that offer opportunities for targeted delivery, are a promising means for improving treatment of CRC through increased local drug concentration and minimising side effects on surrounding healthy cells in the colon. Moreover, incorporating targeting ligands on the nanoparticles introduces cell specificity through receptor-specific binding and tissue uptake, enabling curcumin to reach intracellular targets. This thesis describes the development of curcumin-containing cetuximab-modified citrus pectin-chitosan nanoparticles for the aim of delivering curcumin to colon cancer tissue when administered orally.

Initially, modified pectin-chitosan curcumin-containing nanoparticles (MCPCNPs) were fabricated by ionic gelation. The formulated MCPCNPs registered a mean size of 178 nm (± 0.896) and a surface charge of +35.7 mV (± 1.41). The nanoparticles presented a high mucoadhesion propensity in the colonic region/media and a minimal mucoadhesion in pH 1.2 medium (stomach). In the presence of mucin, there was a reduction in zeta potential (ZP)

of the MCPCNPs at pH 1.2 and a more significant reduction at 7.0, both of which were mucin concentration-dependent. A reduction in ZP correlates with mucoadhesive propensity. Nanoparticle tracking analyses (NTA) revealed an increase in the hydrodynamic radii of the MCPCNPs from 218.1 (± 4.9) nm to 291.7 (± 7.8) nm upon exposure to mucin at pH 7.0. Moreover, there was approximately 18% curcumin release at pH 1.2 over 2 h and up to 68% release in 33% (w/v) caecal medium over 24 h.

In order to augment the targeting capability of the MCPCNPs to relevant tumour sites within the colon, the carboxylic functionality in the modified pectin was conjugated with the amine-terminated aspect of cetuximab (Cet) antibody through a two-step carbodiimide (EDC) approach. Our data revealed that 61.37 ± 0.70% of the Cet added was incorporated on the surface of the nanoparticles, which resulted in a slight increase in the mean size (249.33 ± 5.15 nm) and surface charge (+39.1 ± 0.87 mV) of the MCPCNPs. An encapsulation efficiency of about 68.43 ± 2.4% was achieved with more than 63.79 ±0.66 % of curcumin released in a 24 h. Crucially, the mucoadhesive properties of the MCPCNPs were not altered after Cet-conjugation. The *in vitro* cytotoxicity studies revealed that Cet-MCPCNPs induced cell apoptosis in CRC models. Results from the cellular uptake studies confirmed that the incorporation of Cet to MCPCNPs enabled curcumin to be retained longer within Caco-2 cells compared to MCPCNPs or free curcumin. Cet-MCPCNPs also induced cell cycle arrest at G2/M phase in CRC cell lines.

These studies validate the potential of Cet-MCPCNPs as a platform for targeted delivery in CRC, forming a compelling validation for further pre-clinical evaluation of this system for safety and efficacy *in vivo*.

Publications during candidature

Peer-reviewed papers

1. Sabra, R.; Roberts, C.J.; Billa, N., 2019. Courier properties of modified citrus pectinate-chitosan nanoparticles in colon delivery of curcumin. (under peer-review by J. Colloid Interface Sci. when this thesis is submitted).

2. Sabra, R., Billa, N., Roberts, C.J., 2018. An augmented delivery of the anticancer agent, curcumin, to the colon. React. Funct. Polym. 123, 54–60. https://doi.org/10.1016/j.reactfunctpolym.2017.12.012

Conference abstracts

3. Sabra R, Billa N. and Roberts C, 2018. Curcumin-encapsulated polymeric nanoparticles for colon cancer treatment. 23rd International Conference on Nanomaterials and Nanotechnology, London, United Kingdom (poster presentation).

4. Sabra R, Billa N. and Roberts C, 2018. A novel approach toward mucoadhesive and tumour targeting curcumin nanoparticles for colon cancer treatment. 2nd International Conference and Exhibition on Nanomedicine and Drug Delivery, Tokyo, Japan (oral presentation).

Presentations

5. Sabra R, Billa N. and Roberts C, 2017. Mucoadhesive and tumor-targeting curcumin nanoparticles for colon cancer treatment. FOS PGR Student Conference Support Poster Competition, University of Nottingham, Malaysia (poster presentation).

6. Sabra R, Billa N. and Roberts C, 2017. Curcumin nanoparticles for colorectal cancer treatment. Faculty of Science Research Talk, University of Nottingham, Malaysia (oral presentation).

7. Sabra R, Billa N. and Roberts C, 2017. Spicing the road for a new anti-cancer hope. Postgraduate Research Showcase, University of Nottingham, Malaysia (oral presentation).

8. Sabra R, Billa N. and Roberts C, 2017. Curcumin Nanoparticles for treating colon cancer. 3MT® Competition, University of Nottingham, Malaysia (oral presentation).

Acknowledgments

I would like to thank Almighty Allah for bestowing me resoluteness and strength to accomplish my research. His ceaseless blessings and mercy were with me throughout my life and ever more during the tenure of my research.

My profound and sincere gratitude goes to my supervisor Prof. Nashiru Billa, for his assistance, insightful guidance and inspiring comments that shaped the success of this research. Your constant understanding, encouragement and great support made my study in UNM to be an amazing experience to remember. I would also like to sincerely thank my co-supervisor, Prof. Clive J. Roberts for his support throughout my stay on the UK campus. Thank you for your valuable comments and constructive criticisms that helped in channelling my project on the right course. The time and effort, you placed into my project are deeply appreciated.

I am indebted to the technical staff in both Campuses UK and Malaysia for their helpful discussions on my experimental problems. I am also appreciative to the Graduate school of the UNM for the training courses, which I found to be very resourceful throughout my research. I am especially thankful for the friends I made here who did not stop at making a mark on me professionally. You were a sounding board for anything I needed, and you made my days in Malaysia remarkable. A special thanks also go to my lab mates for their support and cooperation.

I am forever grateful to all members of my family. Mom and Dad, your unconditional support give me confidence to pursue my biggest dreams. You have sacrificed so much to provide for all of us, and I cannot imagine where we would be without you. My dear brothers, Abbas and Zein, I am so lucky to have

you always by my side. Your invaluable support and humour over the years helped me find the strength to continue my work here.

To those who indirectly contributed in this research, thank you very much.

Rayan Sabra, 2019

Table of Contents

Abstract iv

Publications during candidature vi

Acknowledgments vii

List of Figures xiv

List of Tables xix

List of Equations xx

Abbreviations xxi

Chapter 1 Introduction and Literature Review 1

1.1 General overview 2

1.2 Colon and Colorectal Cancer 4

1.2.1 Colon 4

1.2.2 Statistics, diagnosis and staging of CRC 6

1.2.3 Treatment of Colorectal Cancer 9

1.2.3.1 Epidermal growth factor (EGF) 10

1.3 Monoclonal antibodies 13

1.4 Curcumin 16

1.4.1 Anti-cancer activity 18

1.5 Nanoparticle technology 21

1.5.1 Organic nanoparticles 23

1.5.1.1 Liposomal nanoparticles 24

1.5.1.2 Solid lipid nanoparticles 25

1.5.1.3 Polymeric nanoparticles 26

1.5.2 Inorganic nanoparticles 27

1.6 A review of some polymeric formulation techniques used to fabricate curcumin nanoparticles 29

1.6.1 The two-step procedure 30

1.6.1.1 Solvent removal 30

1.6.1.2 Polymerisation 35

1.6.2 The one-step procedure 35

1.6.2.1 Nanoprecipitation 35

1.6.2.2 Spray-drying 37

1.6.2.3 Ionic gelation 39
1.7 Colon-specific nano-carrier systems 41
1.7.1 Prodrug-based approach 41
1.7.2 Time-dependent systems 42
1.7.3 pH-dependent devices 42
1.7.4 Microflora-activated systems 43
1.7.5 Choice of appropriate polymer 44
1.7.5.1 Chitosan 44
1.7.5.2 Pectin 45
1.8 Mucoadhesion 49
1.9 Physical techniques for NP characterisation 50
1.9.1 Zeta Sizer Nano Series® 51
1.9.2 Scanning Electron Microscopy 53
1.9.3 Atomic Force Microscopy 55
1.9.4 Nanoparticle Tracking Analysis 56
1.9.5 Fourier Transform Infrared Spectroscopy 57
1.9.6 Differential Scanning Calorimetry 59
1.9.8 Micro-bicinchoninic acid assay 61
1.10 Thesis objectives 62

Chapter 2 Formulation and *in vitro* evaluation of modified citrus pectin-chitosan nanoparticles containing curcumin 64
2.1 Introduction 65
2.2 Materials: 67
2.3 Methods: 67
2.3.1 Modifying citrus pectin 67
2.3.2 Formulating MCP-chitosan nanoparticles 69
2.3.3 Physical properties of the nanoparticles 70
2.3.3.1 The hydrodynamic size and surface charge of nanoparticles 70
2.3.3.2 The morphology of the MCPCNPs 70
2.3.3.3 The FTIR spectra of the polymers and nanoparticle solids 70
2.3.3.4 The thermal response profile of MCPCNPs 70
2.3.4 Time-of-Flight Secondary Ion Mass Spectrometry (TOF-SIMS) 71
2.3.5 High Performance Liquid Chromatography (HPLC) for quantifying curcumin 71
2.3.5.1 HPLC method validation 72

2.3.6 Encapsulation efficiency and curcumin loading within MCPCNPs 72
2.3.7 Stability studies 73
2.4 Results and discussion 73
2.4.1 Modification of citrus pectin 73
2.4.2 MCP-chitosan nanoparticle formulations 75
2.4.3 Physical characterisation of MCPCNPs 78
2.4.3.1 The hydrodynamic size and surface charge of MCPNPs 78
2.4.3.2 The morphology of MCPCNPs 79
2.4.3.3 FTIR spectra 80
2.4.3.4 Thermal analyses 82
2.4.4 ToF-SIMS analysis of MCPCNPs 83
2.4.5 Validation of HPLC method 86
2.4.6 Encapsulation efficiency and drug loading 89
2.4.7 Stability studies 91
2.5 Conclusion 93

Chapter 3 Evaluating the mucoadhesion propensity and release profile of curcumin from MCPCNPs 95
3.1 Introduction 96
3.2 Materials 97
3.3 Methods 97
3.3.1 MCPCNPs matrix swelling studies 97
3.3.2 Mucin adsorption studies 98
3.3.3 Zeta Potential Measurements 98
3.3.4 Morphological analyses 99
3.3.5 AFM 99
3.3.6 NTA 99
3.3.7 Mucoadhesion based on everted caecal sac 100
3.3.8 Freeze-drying of MCPCNPs 101
3.3.9 Preparation of 33% w/v rat caecal content 102
3.3.10 Curcumin release from the MCPCNPs 102
3.4 Results and discussion 103
3.4.1 Swelling of MCPCNPs matrices 103
3.4.2 Mucin adsorption assay 104
3.4.3 Zeta- potential as a function of pH 107
3.4.4 Morphological analyses 109

3.4.5 AFM....111
3.4.6 NTA analysis....113
3.4.7 Everted caecal sac....116
3.4.8 Curcumin release studies....116
3.5 Conclusion....119

Chapter 4 Formulation and *in vitro* evaluation of cetuximab conjugated to MCPCNPs....121
4.1 Introduction....122
4.2 Materials....123
4.3 Methods....124
4.3.1 Preparation of MCPCNPs....124
4.3.2 Preparation of Cet-MCPCNPs....124
4.3.4 Physiochemical characterisation....125
4.3.5 Entrapment efficiency of curcumin and *in vitro* drug release from Cet-MCPCNPs....125
4.3.6 Mucin adsorption studies....126
4.4 Results and discussion....126
4.4.1 Preparation of Cet-MCPCNPs....126
4.4.2 Physiochemical characterisation....128
4.4.3 Entrapment efficiency and *in vitro* curcumin release....133
4.4.5 Mucin adsorption studies....136
4.5 Conclusion....137

Chapter 5 *In vitro* cell evaluation of formulations....138
5.1 Introduction....139
5.2 Materials....140
5.3 Methods....140
5.3.1 Maintenance of cell culture....140
5.3.2 Subculture of cells....141
5.3.3 Cell counting....141
5.3.4 Cell cytotoxicity....142
5.3.5 Cellular uptake....143
5.3.5.1 Qualitative cellular uptake....143
5.3.5.2 Quantitative cellular uptake....143
5.3.6 Cellular apoptosis....144
5.3.7 Cell cycle....144

5.3.8 Statistical analysis.....145
5.4 Results and discussion.....145
Section I:.....146
5.4.1 Maintenance of cell culture 146
5.4.2 Cell cytotoxicity assay.....148
5.4.3 Cellular uptake studies through fluorescent microscopy and HPLC 152
Section II: 156
5.4.4 Maintenance of cell culture 157
5.4.5 Cell cytotoxicity assay.....157
5.4.6 Cellular uptake.....161
5.4.7 Cell apoptosis 164
5.4.8 Cell cycle 168
5.5 Conclusion.....173
Chapter 6 General conclusions and Future directions 174
6.1 General conclusion.....175
6.2 Future work 178
References 182

List of Figures

All figures are drawn by author, unless otherwise stated

Figure 1.1 The anatomy **(a)** and the wall layers of human colon (**b)** 5
Figure 1.2 Summary of the EGFR signaling process pathway 12
Figure 1.3 The antibody structure 13
Figure 1.4 Schematic description of the mAb synthesis 15
Figure 1.5 The chemical structures of the curcuminoids 17
Figure 1.6 Example of organic nanoparticle platforms for drug delivery 23
Figure 1.7 Example of inorganic nanoparticle platforms for drug delivery ...28
Figure 1.8 Schematic representation of the preparation of NPs by emulsion evaporation method. 32
Figure 1.9 Schematic representation of the preparation of nanocapsules by emulsion diffusion method. 33
Figure 1.10 Schematic representation of the preparation of NPs by salting-out method. 34
Figure 1.11 Schematic representation of the preparation of NPs by nanoprecipitation method. 37
Figure 1.12 Schematic representation of the preparation of NPs by spray-drying method. 38
Figure 1.13 Chemical structure of chitosan, comprising N-acetyl-D-glucosamine 44
Figure 1.14 Chemical structure of pectin 46
Figure 1.15 The binding process of modified citrus pectin with galectin-3 ...48
Figure 1.16 Schematic illustration of the techniques associated with the Zeta sizer Nano series®. Adapted and modified from (Horiba Scientific, 2016) 52
Figure 1.17 Schematic diagram of SEM. 54
Figure 1.18 An outline of the basic principles of the AFM 55
Figure 1.19 Schematic illustration of NTA 57
Figure 1.20 Basic principle of FTIR 58
Figure 1.21 Schematic diagram of the DSC 59
Figure 1.22 An example of a DSC thermogram 60

Figure 1.23 An outline of the micro-BCA principle.....61
Figure 2.1 Schematic illustration of pectin modification.....68
Figure 2.2 The different techniques carried out to develop the most ideal method of MCP-chitosan nanoparticles 69
Figure 2.3 FT-IR spectra of CP **(a)** and MCP **(b).**.....74
Figure 2.5 Zeta-potential from the different formulation techniques 77
Figure 2.4 Size and PDI obtained from the different techniques followed.....77
Figure 2.6 Schematic representation of the MCPCNP formation.....78
Figure 2.7 SEM image of the MCPCNPs 79
Figure 2.8 FTIR spectra of chitosan, STPP, MCP, curcumin, MCP-chitosan nanoparticles and MCPCNPs. 81
Figure 2.9 DSC profiles of chitosan, STPP, MCP, curcumin and MCPCNPs82
Figure 2.10 Negative ion mass spectra obtained by ToF-SIMS analysis of MCPCNPs between 0 and 80 mass (u).....84
Figure 2.11 Negative ion mass spectra obtained by ToF-SIMS analysis of raw materials and MCPCNPs between 327 and 339 mass (u) 85
Figure 2.12 Standard calibration curve of curcumin.....86
Figure 2.13 Representative chromatograms of curcumin at concentrations 0.625 µg/ml and 10 µg/ml 87
Figure 2.14 The encapsulation efficiency and drug loading of curcumin in MCPCNPs and CPCNPs 89
Figure 2.15 Mean particle size, encapsulation efficiency and drug loading values of MCPCNPs at days 0, 7, 14 and 21 during storage at 4 ^{0}C.....91
Figure 2.16 Morphology of MCPCNPs at day 0 **(a)**, 7 **(b)**, 14 **(c)** and 21 **(d)** during storage at 4 ^{0}C 92
Figure 3.1 Illustration of the everted intestinal sac procedure.....101
Figure 3.2 Swelling profile of MCPCNPs in pH 1.2, 5.5 and 7.0. 103
Figure 3.3 The calibration curves of mucin in pH 1.2, 5.5, 6.2 and 7.0 105
Figure 3.4 Mucin adsorption of MCPCNPs at different pH 106
Figure 3.5 Z-potential of NPs incubated in different pH without mucin for specific time intervals.....107
Figure 3.6 Z-potential of NPs incubated in different pH with mucin for specific time intervals. 108

Figure 3.7 SEM images of MCPCNPs **(a)** MCPCNPs exposed to mucin in pH 7.0 **(b)** MCPCNPs exposed to mucin in pH 1.2 **(c)**.....110
Figure 3.8 AFM images with 5 μm x 5 μm scan sizes of pure MCPCNPs **(a)** and MCPCNPs incubated with mucin in pH 7.0 **(b)**.....112
Figure 3.9 NTA results with **(a)** and **(b)** presenting the video snapshots of MCPNPs before and after the addition of mucin, respectively, while **(c)** and **(d)** portray the size distribution profiles of MCPNPs prior to and 30 minutes after addition of mucin, respectively. 115
Figure 3.10 Standard calibration curves of curcumin prepared in pH 1.2 **(a)** and 33 % caecal content buffer **(b)** 117
Figure 3.11 In vitro drug release profile of curcumin from MCPCNPs in pH 1.2 for 2 h and 33 % caecal medium for 24 h.....117
Figure 4.1 Schematic representation of the EDC/NHS conjugation that was employed to crosslink Cet to MCPCNPs 128
Figure 4.2 STEM image of the Cet-MCPCNPs.....129
Figure 4.3 FT-IR spectra of Cet-MCPCNP **(a)** and MCPCNP **(b)**.....131
Figure 4.4 EDX chemical mapping of MCPCNPs (**a**) Cet-MCPCNPs (**b**) on a STEM copper grid 132
Figure 4.5 *In vitro* drug release profile of curcumin from Cet-MCPCNPs in pH 1.2 for 2 h and 33 % caecal medium for 24 h.....134
Figure 4.6 Mucin adsorption of Cet-MCPCNPs at different pH 136
Figure 5.1 Schematic representation of a haemocytometer (a) and its counting grids (b) 142
Figure 5.2 HT-29 cells **(a)**, HCT-116 **(b)** and MRC-5 cells **(c)** viewed under an inverted microscope under 10× magnification 147
Figure 5.3 Cytotoxicity of MCPCPs, CPCNPs and curcumin solution on HCT-116 (a-c) and HT-29 (e-f) after 24, 48 and 72 h incubation (mean± S.D, n=3). Significance denoted as *($p < 0.05$), ** ($p < 0.01$), *** ($p < 0.001$), **** ($p < 0.0001$). 149
Figure 5.4 Cytotoxicity of MCPCPs, CPCNPs and curcumin solution on MRC-5 (a-c) after 24, 48 and 72 h incubation (mean± S.D, n=3). Significance denoted as *($p < 0.05$), ns (not significant). 151
Figure 5.5 Cellular uptake of MCPCNPs, CPCNPs and curcumin solution at 20 μg/mL and 2.5 μg/mL after 4 h incubation [10-20x magnification].....153

Figure 5.6 Cellular uptake of MCPCNPs, CPCNPs and curcumin solution at 20 μg/mL and 2.5 μg/mL after 4 h incubation [10-20 x magnification] 154
Figure 5.7 Amount of curcumin retrieved from HCT-116 and HT-29 cells after treatment with 20 μg/mL and 2.5 μg/mL of MCPCNPs, CPCNPs and curcumin solution after 4 h incubation. Averaged mean values and standard deviations of triplicates are presented 156
Figure 5.8 Caco-2 cells viewed under an inverted microscope under 10× magnification 157
Figure 5.9 Cytotoxicity of Cet-MCPCPs, MCPCNPs and curcumin solution on HCT-116 (a-c) and Caco-2 (e-f) after 24, 48 and 72 h incubation (mean± S.D, n=3). Significance denoted as *($p < 0.05$), ** ($p < 0.01$), *** ($p < 0.001$), **** ($p < 0.0001$). 158
Figure 5.10 Cytotoxicity of Cet-MCPCPs, MCPCNPs and curcumin solution on MRC-5 after 24, 48 and 72 h incubation (mean± S.D, n=3). Significance denoted as *($p < 0.05$), ns (not significant). 159
Figure 5.11 Cellular uptake of Cet-MCPCNPs, MCPCNPs and curcumin solution at 20 μg/mL and 2.5 μg/mL after 4 h incubation [10-20x magnification].....162
Figure 5.12 Cellular uptake of Cet-MCPCNPs, MCPCNPs and curcumin solution at 20 μg/mL and 2.5 μg/mL after 4 h incubation [10-20x magnification].....163
Figure 5.13 Amount of curcumin retrieved from HCT-116 and Caco-2 cells after treatment with 20 μg/mL and 2.5 μg/mL of Cet-MCPCNPs, MCPCNPs and curcumin solution after 4 h incubation. Averaged mean values and standard deviations of triplicates are presented. 164
Figure 5.14 Fluorescence micrographs of treated and untreated HCT-116 cells after DAPI staining (20x magnification) 166
Figure 5.15 Fluorescence micrographs of treated and untreated Caco-2 cells after DAPI staining (20x magnification). 167
Figure 5.16 DNA histogram of HCT-116 cells treated with control, DMSO, 20 μg/ml free curcumin, 20 μg/ml MCPCNP and 20 μg/ml Cet-MCPCNP analysed by flow cytometry. 170

Figure 5.17 DNA histogram of Caco-2 cells treated with control, DMSO, 20 μg/ml free curcumin, 20 μg/ml MCPCNP and 20 μg/ml Cet-MCPCNP analysed by flow cytometry.....171

List of Tables

Table 1.1 The stages of CRC adapted from (American Cancer Society, 2018)8

Table 1.2: The anti- EGFR FDA-approved mAbs used in cancer treatment..15

Table 2.1 Characteristic negative fragments of raw materials used for MCPCNPs fabrication.....84

Table 2.2 Precision and accuracy of the HPLC method 88

Table 3.1 Correlation coefficients of best fits to studied models.....118

Table 5.1 IC50 values in µg/mL of MCPCNPs, CPCNPs and curcumin on HCT-116 and HT-29 cell lines. Each value represents means of triplicate determinations (mean ± S.D).....150

Table 5.2 IC50 values in µg/mL of Cet-MCPCNPs, MCPCNPs and curcumin on Caco-2 and HCT-116 cell lines. Each value represents means of triplicate determinations (mean ± S.D).....160

Table 5.3 Percentage (%) of cells in the respective phases analysed by flow cytometry. Each value represents means of triplicate determinations (mean ± S.D).....172

List of Equations

(2.1): $Encapsulation\ efficiency\ (\%) = \frac{\text{Amount of curcumin added} - \text{unbound curcumin}}{\text{Amount of curcumin added}} \times 100$

(2.2): $Loading\ capacity\ (\%) = \frac{\text{Entrapped curcumin}}{\text{Curcumin loaded NP weight}} \times 100$

(2.3): $Accuracy = \frac{\text{mean concentration found}}{\text{concentration taken}}\ x\ 100$

(2.4): $LOD = 3.3 \times \frac{\text{Standard deviation of low concentration}}{\text{Slope of curve}}$

(2.5): $\text{LOQ} = 10 \times \frac{\text{Standard deviation of low concentration}}{\text{Slope of curve}}$

(3.1): $Swelling\ capacity\ (\%) =$

$$\frac{Z-average \text{ of MCPCNPs at time (t)} - \text{ Initial z-average of MCPCNPs}}{\text{Initial z-average of MCPCNPs}} \times 100$$

(3.2): $Mucin\ adsorption\ (\%) = \frac{\text{Amount of mucin added} - \text{Amount in supernatant}}{\text{Amount of mucin added}} \times 100$

(3.3): $Attachment\ of\ MCPCNPs\ to\ caecam\ (\%) =$

$$\frac{\text{Weight of MCPNPs added} - \text{Weight of unattached MCPNPs}}{\text{Weight of MCPNPs added}} \times 100$$

(3.4): $Percentage\ released\ (\%) = \frac{\text{Amount of curcumin released}}{\text{Amount of curcumin in the NPs}} \times 100$

(4.1): $Encapsulation\ efficiency\ (\%) = \frac{\text{Amount of curcumin encapsulated}}{\text{Total amount of curcumin added}} \times 100$

Abbreviations

1-LV	Leucovorin
5-FU	5-fluorouracil
AFM	Atomic force microscopy
ATP	Adenosine triphosphate
CCD	Charge-coupled device
Cet	Cetuximab
Cet-MCPCNPs	Cetuximab-modified citrus pectin-chitosan-curcumin nanoparticles
CP	Citrus pectin
CPCNPs	Curcumin-containing nanoparticles prepared with citrus pectin
CPT-11	Irinotecan
CRC	Colorectal cancer
CUR-FLs	Curcumin-loaded flexible liposomes
CUR-LCL	Curcumin-long-circulating liposomes
CUR-SLs	Silica-coated flexible liposomes loaded with curcumin
DMSO	Dimethylsulfoxide
DLS	Dynamic Light Scattering
DSC	Differential scanning calorimetry
EDC	1-ethyl-3-(3-dimethylaminopropyl)carbodiimide hydrochloride
EDX	Energy dispersive X-ray
EggPG	Egg yolk phosphatidylglycerol

EGF	Epidermal growth factor
EPHB2	Ephrin type-B receptor 2
EPR	Enhanced permeability and retention
FDA	Food and Drug Administration
FIT	Faecal immunochemical test
FT-IR	Fourier Transform-Infrared Spectroscopy
Gal-3	Galectin-3
gFOBT	Guaiac-based faecal occult blood test
GIT	Gastrointestinal tract
GLOBOCAN	Global Cancer Incidence, Mortality and Prevalence
GRAS	Generally recognized as safe
GRB2	Growth factor receptor-bound protein 2
GTP	Guanosine-5'-triphosphate
H	Hour
HAT	Hypoxanthine-aminopterin-thymidine medium
HCl	Hydrochloric acid
HDAC4	Histone deacetylase 4
HG	Homogalacturonan
HPLC	High Performance Liquid Chromatography
Ig	Immunoglobulins
KBr	Potassium bromide
L-OHP	Oxaliplatin
mAb	Monoclonal antibodies
MCP	Modified citrus pectin
MCPCNPs	Modified citrus pectin-chitosan-curcumin nanoparticles

MES	2-(N-morpholino) ethanesulfonic acid
Micro-BCA	Micro-bicinchoninic acid
MRI	Magnetic resonance imaging
NaOH	Sodium hydroxide
NF-κB	Nuclear factor- kappa B
NHS	N-hydroxysuccinimide
NPs	Nanoparticles
NTA	Nanoparticle tracking analysis
o/w	Oil-in-water
pAbs	Polyclonal antibodies
PALS	Phase analysis light scattering
PBS	Phosphate buffered saline
PDI	Polydispersity index
PE	Phosphatidylethanolamines
PEG	Polyethylene glycol
PET	Positron emission tomography
PIP2	Phosphatidylinositol-4,5-bisphosphate
PIP3	Phosphatidylinositol-3,4,5-trisphosphate
PKC	Protein kinase C
PLA	Poly-lactic-acid
PLGA	Poly-lactic-co-glycolic-acid
RES	Reticule endothelial system
RG-I	Rhamnogalacturonan-I
RG-II	Rhamnogalacturonan-II
RTK	Receptor tyrosine kinases

SEM	Scanning electron microscopy
SEPP1	Selenoprotein P
SLN	Solid lipid nanoparticle
SOS	Son of sevenless
Sp-1	Specificity protein 1
STAT3	Signal-transducer-and-activator-of-transcription-3
STEM	Scanning transmission electron microscope
STPP	Sodium tripolyphosphate
TCS	Thermocouple sensors
TOF-SIMS	Time-of-Flight Secondary Ion Mass Spectrometry
TPGS	Vitamin E polyethylene glycol succinate
TRAIL	Tumour necrosis factor-related apoptosis-inducing ligand
VEGF	Vascular epithelial growth factors
w/o	Water-in-oil

Chapter 1 Introduction and Literature Review

1.1 General overview

Colorectal cancer, also known as bowel cancer, is the term used to describe malignant tumours found in the colon and rectum. It is the second leading cause of cancer death globally in both sexes combined (Bray et al., 2018). Fortunately, it is one of the easily treatable cancers if detected early. Surgery is considered the first treatment option, whilst chemotherapy and/or radiotherapy are often used in combination to eradicate residual cancer cells. Chemotherapy is the least invasive of the first-line choices outlined above. However, the powerful cytotoxic effects of chemotherapeutic drugs cause damage not only to tumour sites but to healthy cells and tissues as well, leading to severe side effects in patients. Thus, the constraint in delivering optimal therapeutic doses to the tumour site, whilst at the same time addressing the distribution of the drug in healthy tissues, has led to the emergence of anticancer agents of plant origin. Plants, are becoming serious contenders as chemotherapeutic alternatives due to their manifestation of reduced toxicity to adjoining cells (Jagetia and Aggarwal, 2007). One such example is curcumin, a major chemical constituent in turmeric which has received much attention in the past decade because of its 'acceptability' as it is derived from natural sources (Hua, 2014). Furthermore, it is used extensively as a spice, all of which gives the perception will manifest fewer side effects when used therapeutically. Aptly, extensive research has elaborated the therapeutic potential of curcumin against a range of cancers and distinctly against colorectal cancer (Chuah et al., 2011). However, the systemic bioavailability following oral administration of curcumin is poor due to the low solubility and rapid metabolism when administered orally (Prasad et al., 2014). To overcome this constraint, polymer-based nanoparticles have been proposed

as a possible delivery intervention. These can be formulated so that they traverse the gastrointestinal epithelia effectively and therefore circumvent the metabolic constraints that the payload is subjected to within the gastrointestinal tract. In the context of colorectal cancer management, an attractive feature for the delivery system is attendant mucoadhesion within the colon cancer epithelia. Mucoadhesive polymers usually offer the possibility of controlled release capability through diffusion of the cargo from the particles and allowing specific targeting and uptake of the particles by Peyer's patches (Boddupalli et al., 2010). Active targeting approaches with the coupling of antibodies, particularly monoclonal, to the surface of nanoparticles are regarded to be efficient "magic bullets" for cancerous tissues and other disease treatments (Shafras M, Rafeek R.A.M, 2017). Recent clinical trials suggest that targeting tumour-specific receptors with monoclonal antibody offers the most effective therapeutic approach for the treatment of colorectal cancer (Krzemieniecki et al., 2006). Hence, in the present pursuit, our aim is to formulate a novel mucoadhesive curcumin-containing tumour targeting nanoparticulate drug delivery system. Such a delivery system would significantly reduce the dosing frequency and thus undesirable side-effects manifested by the conventional delivery approach. We have also sought to utilise polymers that have minimal toxicity to tissue. Chitosan, for example is non-toxic, biodegradable, biocompatible and shown to be mucoadhesive as well (M. Ways et al., 2018). It has been used in conjunction with modified pectin in the present work because of the possible protective effect it might have on the curcumin nanoparticulate delivery system in the upper GI tract (Wong et al., 2011). Furthermore, modified pectin essentially inhibits the growth of colon cancer and migration due to its antagonism with

galectin-3, which is vastly expressed on tumour cell surface. The modified pectin binds to the colonic mucin with an altered carbohydrate structure which inhibits tumour growth, cell to cell adhesion, and metastasis (Glinsky and Raz, 2009). There is a significant expression of antigens on cancerous cells, therefore, a final feature of the present investigation is to couple the surfaces of the nanoparticles with monoclonal antibodies, to further improve the cancer targeting capability of the particles to cancer tissue (Chu et al., 2015). In this context, I will examine whether the anti-tumour activity of curcumin-loaded nanoparticles is further enhanced by coupling them with antibodies that target tumour-specific receptors such as the epidermal growth factor receptor (EGFR). In this fashion, the anticancer effects of curcumin will be augmented. The above approach would require a lesser drug payload than conventional formulations, which means manifestation of fewer side effects and cost-effectiveness – both features of which would be attractive to the pharma industry.

1.2 Colon and Colorectal Cancer

1.2.1 Colon

The colon, also known as the large intestine, is approximately 1.5 m long and located immediately after the small intestine in the human gastrointestinal tract (Irving and Catchpole B, 1992). It can be functionally divided into two parts, the right and the left colon (Figure 1.1 (a)). The right colon (caecum and ascending colon) plays a major role in adsorption of water and fermentation of undigested sugars, while the left colon (descending colon, sigmoid colon and rectum) is primarily responsible for storage and evacuation of stool (Shaffer A. Eldon et al., 2005).

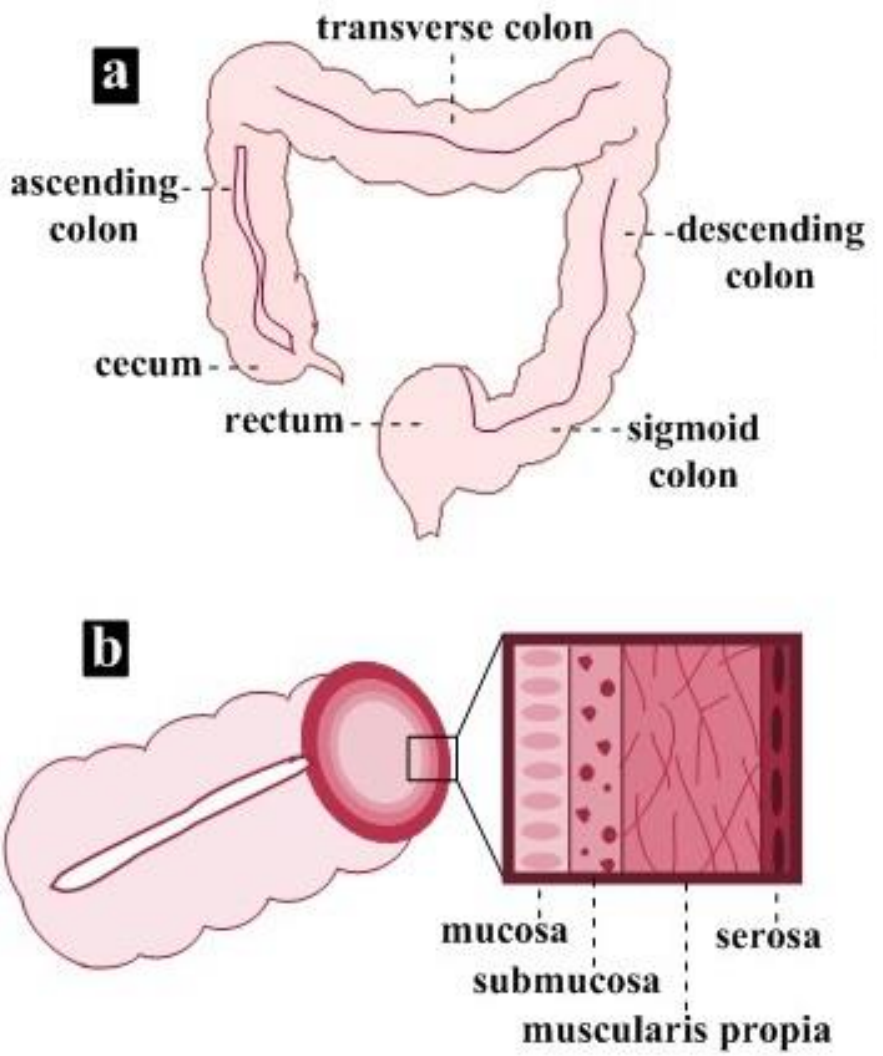


Figure 1.1 The anatomy **(a)** and the wall layers of human colon (**b)**

The walls of the colon are made of inner and outer layers: the mucosa, the submucosa, the muscularis propria and the serosa that covers most of the colon excluding the rectum (Rao and Wang, 2010) (Figure 1.1(b)). The colonic mucosa is made of numerous crypts composed of goblet cells which secret mucus that facilitates the mobility of the colonic contents. There are numerous microflora consisting of about 400 bacterial species, 18 of which accounts for vitamin synthesis and metabolism of residual nutrients in the luminal content (Nugent et al., 2001). Under normal physiological conditions, the colonic pH

varies between 5.66-6.72 and 5.20-7.02 in the ascending and descending colon, respectively (Khutoryanskiy, 2015). Cancer that is manifested in the colon and rectum is usually coined as colorectal cancer (CRC), colon and rectal cancer are usually grouped together since they present similar pathological features (Y.-C. Lee et al., 2013). Cancer originates when cells in the body start to grow out of control. It follows that cells in almost any part of the body can develop into cancer and can spread to other areas of the body.

1.2.2 Statistics, diagnosis and staging of CRC

According to Global Cancer Incidence, Mortality and Prevalence (GLOBOCAN) 2018, CRC is the third most common cancer in men (1,006,019 cases) and the second in women (794,958 cases) worldwide (Bray et al., 2018). Approximately, over 1.8 million new CRC cases were diagnosed globally in 2018, with nearly 881,000 deaths attributed to this statistic (Bray et al., 2018). Most CRCs develop slowly over several years. It starts as polyps -a non-cancerous growths- and eventually becomes malignant under uncontrolled growth that begins within the mucosa of the colon and spreads to some or to the rest of the colon layers to form a solid tumour. Usually, colorectal polyps and early-stage cancer are asymptomatic, however, cancers that have grown large enough, might cause symptoms such as change in bowel habits, rectal bleeding, persistent abdominal discomfort and unexplained weight loss (Astin et al., 2011). Therefore, it is recommended that women and men at average risk, start a regular screening for CRC at the age of 50 and people with positive family history begin at an earlier age (Rex K. Douglas et al., 2009).

There are several screening tests available for monitoring and detecting colorectal polyps or cancer inside the colon such as: stool DNA testing, guaiac-

based faecal occult blood test (gFOBT), faecal immunochemical test (FIT), colonoscopy, double-contrast barium enema, Flexible sigmoidoscopy and imaging tests such as magnetic resonance imaging (MRI) scan, chest x-ray and positron emission tomography (PET) scan (Janz et al., 2016). However, these imaging and screening tests alone cannot distinguish between cancerous cells and benign cells. Biopsy is the only way to make a definitive diagnosis, in which tissue sampled from the suspicious region is observed under a microscope (Ma and Coombes, 2014). Biopsy along with screening/imaging tests guides clinicians in diagnosing and staging CRC and to determine the suitable treatment option for patients and monitor the treatment outcome. The most commonly used staging system for colorectal cancer is the TNM staging system, where **T** stands for how far the **t**umour has grown into the colon wall and nearby areas, **N** specifies whether the cancer has spread to nearby lymph **n**odes and **M** for cancer **m**etastasis to other distant parts of the body (American Cancer Society, 2018). Table 1.1 summarizes the details of each stage.

Table 1.1 The stages of CRC adapted from (American Cancer Society, 2018)

Stage	Other names	Stage sub-division	Stage Explanation
0	Carcinoma *in situ*		Malignant cells have not grown beyond the mucosa of the colon.
I	Dukes A		The cancer has grown through the mucosa into the submucosa and might have also grown into the thick muscle layer. It has neither spread to nearby lymph nodes nor to distant sites
II	Dukes B	IIA	The cancer has only spread and not grown into the serosa of the colon. It has not reached to nearby organs, lymph nodes or distant sites.
		IIB	The cancer has grown into the serosa of the colon, but has not reached nearby organs, lymph nodes or distant sites.
		IIC	The cancer has grown through the wall of the colon and has grown into other nearby organs. But, has not yet spread to nearby lymph nodes or distant sites.
III	Dukes C	IIIA	Cancer has spread through the mucosa to the submucosa, and has spread to at least 3-4 lymph nodes, but not reached to distant sites.
		IIIB	Cancer has spread to the muscle layer of the colon or to the outmost layers of the colon. Cancer has also spread to as many as 3 nearby lymph nodes or tissues but no distant sites.
		IIIC	Cancer has spread through the outmost layers of the colon and reached nearby organs. It has also spread to at least 3 nearby lymph nodes but no distant sites.
IV	Dukes D		Cancer have spread through the colon to nearby organs and/or lymph nodes. It has also spread to at least one distant lymph node or organ, such as liver or ovary.

1.2.3 Treatment of Colorectal Cancer

The prognosis and treatment options for CRC mainly rely on the stage of the cancer, tumour recurrence, and patient's general health. The four prevalent CRC treatment procedures are: surgery, chemotherapy, radiotherapy and targeted therapy (Watanabe et al., 2012). Surgery, is the first therapeutic approach and primary procedure used to treat CRC and can be performed either as a local excision or as a colon resection (Nakayama et al., 2014). In local excision, a tube with cutting capability is inserted through the rectum into the colon to remove the cancer without cutting through the abdominal wall. In colon resection, part of the colon containing the tumour is removed, then either anastomosis (joining back the ends of the colon together) or colostomy, in which an opening is made on the outside of the body for waste to pass through, is performed (Mastalier B et al., 2012). Usually surgery is combined with chemotherapy and/or radiation therapy in order to avoid the residual tumour recurrence. In radiotherapy, energy and irradiated volume of X-rays produced by a linear accelerator are employed to destroy cellular DNA and inhibit cell proliferation (Kim H. John, 2017). Chemotherapy relies on cytotoxic drugs utilised to inhibit the growth of cancer cells and kill them (Wu et al., 2012). It is either taken before surgery to shrink the tumour or after surgery (adjuvant chemotherapy). Commonly Food and Drug Administration (FDA)-approved chemotherapeutic drugs for CRC treatment are: 5-fluorouracil (5-FU), irinotecan (CPT-11), leucovorin (l-LV), oxaliplatin (L-OHP) and capecitabine (Jeught et al., 2018). 5-FU was initially among the first synthesized anti-cancer drugs back in the 1950s, however up to 80% – 85% of parenterally administered 5-FU dose is usually broken down to inactive metabolites in the liver making

its half-life approximately 10-15 minutes (Jordan, 2016). Thus, capecitabine, an orally administrated prodrug of 5-FU, is usually used instead due to the higher tumour response rate, ≈100% bioavailability and lower incidence of side effects (Miura et al., 2017). Due to the limited efficacy of chemotherapeutic drugs taken orally or parenterally through non-specificity to tumour sites, targeted therapy has been developed.

In targeted therapy, drugs are targeted to specific receptors present in cancer cells or in cells related to cancer growth, like blood vessels. It has been developed to block cancer cell proliferation and metastasis by inhibiting specific mediators such as epidermal growth factor (Masoud and Pagès, 2017). The effectiveness of targeted therapy depends on the release of the therapeutic at the cancer target site, as well as diminishing the off-target side effects caused to normal tissues (Padma, 2015).

1.2.3.1 Epidermal growth factor (EGF)

EGF is a low-molecular-weight polypeptide that stimulates cell growth, proliferation, and differentiation by binding to its receptor EGFR. EGFR is a member of the viral oncogene, ErbB, family of four receptors closely related to receptor tyrosine kinases (RTK). It is present on the cell surface with an extracellular ligand-binding domain and a cytoplasmic region that modulates cellular responses (Singh B et al., 2016). In normal cells, the expression of EGFR ranges from 40,000 to 100,000 receptors per cell (Herbst, 2004). The activation of the EGFR begins when the ligand, EGF, binds to the receptor, EGFR, in the extracellular domain. This will form an active EGFR-homodimer or heterodimer (if further bound to another member of the ErbB family) that stimulates the adenosine triphosphate (ATP) phosphorylation of the tyrosine

residues in the intracellular domain. As a result, a complex program of intracellular signal transduction is activated. The two well-known intracellular pathways are: the Ras-RAF-MEK-ERK pathway, which controls the cell proliferation, cell-cycle progression and gene transcription, and the PI3K-Akt pathway, which activates a cascade of anti-apoptotic and pro-survival signals (Riesco et al., 2017). In the Ras-RAF-MEK-ERK pathway, the cytoplasmic protein, Growth factor receptor-bound protein 2 (GRB2), binds to the tyrosine kinase residue and recruits a set of genes known as the son of sevenless (SOS) to the membrane. SOS triggers the Guanosine-5'-triphosphate (GTP) exchange which recruits RAS, that phosphorylates RAF then MEK, which thus stimulates the ERK that induces cell growth and proliferation. In the PI3K-Akt pathway, however, the adaptor protein, GRB2, recruits PI3Ks. PI3Ks then converts Phosphatidylinositol-4,5-bisphosphate (PIP2) to Phosphatidylinositol-3,4,5-trisphosphate (PIP3). Consequently, PIP3 recruits PDK1, which phosphorylates AKT, which in turn, regulate the activity of various proteins that mediate protein synthesis or apoptosis (Oda et al., 2005). Figure 1.2 summarizes the signal transduction process of EGFR. The EGFR signals become inactivated through the endocytosis of receptor-ligand complex and are then either degraded or recycled to the cell surface, ready for another cycle of active growth-factor signalling (Normanno et al., 2006).

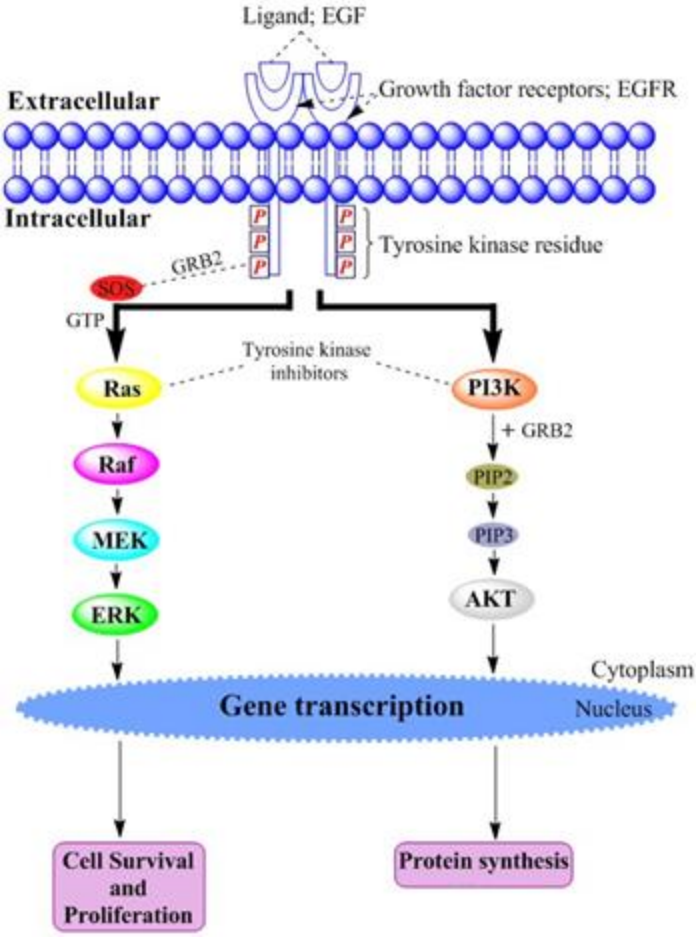


Figure 1.2 Summary of the EGFR signaling process pathway

The overexpression of EGFR plays a key role in the development and growth of tumour cells, specifically in CRC, in which EGFR is estimated to be overexpressed in 60%-80% of tumours (Pabla B. et al., 2015). Thus, the identification of EGFR as an "oncogene" has encouraged the development of therapeutic targeting agents which specifically block the growth factor pathways that are dysregulated in tumour cells. Most targeted therapies are either small-molecule drugs (drugs that attack proteins inside cancer cells) or monoclonal antibodies (mAbs) (drugs that attack proteins on cancer cell surface). Although the development of mAb requires relatively complex processes with huge monetary costs compared with small-molecule inhibitors,

mAbs have displayed higher approval success rates than small-molecule agents, especially in the field of oncology (Ecker et al., 2015).

1.3 Monoclonal antibodies

Antibodies, also known as immunoglobulins (Ig), are Y-shaped proteins produced by the immune system to identify and neutralize foreign objects (Janeway et al., 2001) (Figure 1.3).

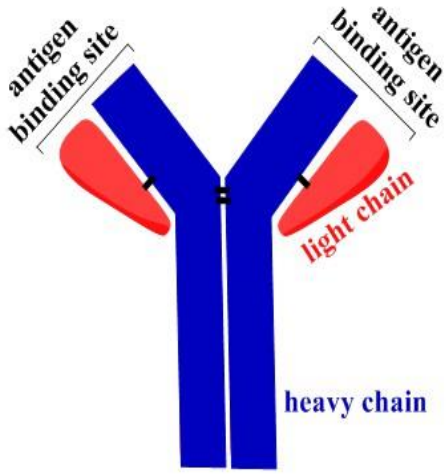


Figure 1.3 The antibody structure

They are either produced by clones derived from a single parent cell (monoclonal antibodies) or from several different immune cells (polyclonal antibodies). Monoclonal antibodies specifically target a unique epitope, or binding site, on a single antigen, while polyclonal antibodies (pAbs) recognize multiple epitopes on an antigen (Ascoli and Aggeler, 2018). mAbs are preferred over pAbs in targeted cancer treatment and therapeutic drug development, due to its batch to batch homogeneity and high specificity to a single epitope (Lipman et al., 2005). Cesar Milstein and Georges Kohler were the first scientists to produce mAbs from lymphocyte fusion back in the 1975 (Geng et al., 2015). Generation of mAbs starts by immunizing a mouse with appropriate

antigen to stimulate cells that produce antibodies known as B-lymphocyte cells. The mouse is then sacrificed, and its spleen is removed and disrupted by mechanical or enzymatic methods to release the B-cells. Spleen cells are then fused, in the presence of polyethylene glycol (PEG), with myeloma cells to create an immortalized hybrid that can undergo many passages *in vitro*. Myelomas can be induced in a few strains of mice by injecting mineral oil into the peritoneum. To inhibit the myeloma cells in the hybrid from synthesizing their own antibodies, the hybridoma is cultured in the hypoxanthine-aminopterin-thymidine medium (HAT), that inhibits DNA synthesis via aminopterin. In this case, only B-cells in the hybrid can overcome culturing in HAT medium as they possess thymidine kinase which allows them to synthesize requisite DNA polymerase precursors from the HAT medium supplied thymidine. Subsequently, the hybridoma cells are screened to identify the desired antibody. ELISA and RIA are the two common screening techniques used, in which the antibody binds to the specific antigen and the unbound antibody is washed off. Therefore, the antibody secreted by the hybridomas is named as monoclonal antibody (Greenfield, 2014) (Figure 1.4).

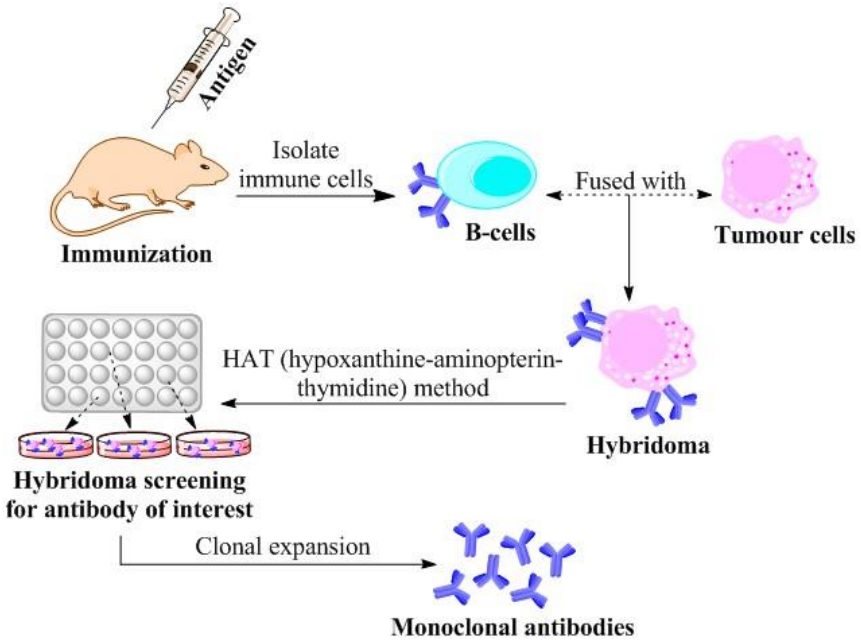


Figure 1.4 Schematic description of the mAb synthesis

Currently, therapy with mAbs is the largest growth area in pharmaceutical industry (Liu, 2014). So far there is a total of 58 mAbs approved either for therapeutic or diagnostic purposes in Europe and the United States since 1986 (Awwad and Angkawinitwong, 2018). FDA-approved mAbs that are currently being used to target EGFR for treating cancer are listed in Table 1.2.

Table 1.2: The anti- EGFR FDA-approved mAbs used in cancer treatment

Product	Type	Approval year	Therapeutic indication(s)	Status	References
Cetuximab (Erbitux)	IgG1	2004	Head and neck or colorectal cancer	Phase I/II/III	(Krzemieniecki et al., 2006)
Panitumumab (Vectibix)	IgG2	2006	Metastatic colorectal carcinoma	Phase II/III	(Rocha-Lima et al., 2007)
Necitumumab (Portrazza)	IgG1	2015	Carcinoma or non-small-cell lung cancer	Phase I/II	(Greillier et al., 2015)

mAbs are currently approved in several countries as monotherapy or in combination with chemotherapeutic agents. Even though targeted therapy has emerged as an approach to conquer the lack of specificity in conventional chemotherapy, there are potential risks and challenges associated with this novel strategy. For example, some cancer cell types develop resistance over the drug treatment course, thereby rendering the targeted therapy ineffective by driving the drug out of the cancer cells and decreasing the intracellular drug concentration (Moorthi and Kathiresan, 2013). Therefore, in most cases targeted therapy is used in combination with chemotherapy, however, this strategy does not reduce the toxicity experienced with chemotherapeutic drugs. To overcome the aforesaid constraints, scientists are considering natural herbal compounds as alternative anticancer agents due to their relatively safer profile and lack of discernible toxicity profiles to normal cells. One such extensively studied agent is curcumin, a component of the spice turmeric (Jagetia and Aggarwal, 2007).

1.4 Curcumin

Curcumin is a hydrophobic orange-yellow crystalline phytochemical derived from the rhizomes of turmeric (*Curcuma longa*), a plant which grows in the Indian subcontinent and tropical countries in South East Asia (Moorthi and Kathiresan, 2013). Apart from curcumin which is also called diferuloylmethane, two other bioactive analogues can be extracted from turmeric known as demethoxycurcumin and bisdemethoxycurcumin. The chemical structures of the three curcuminoids are presented in Figure 1.5.

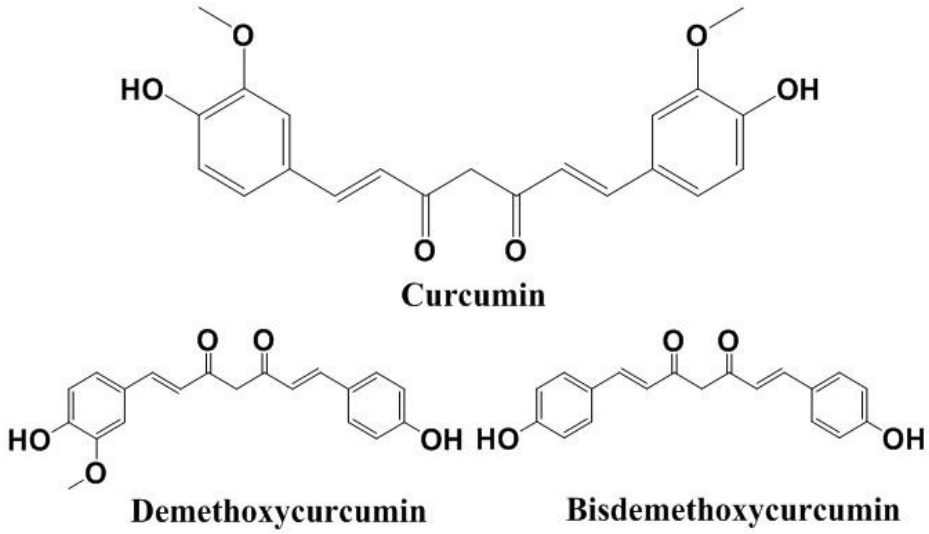


Figure 1.5 The chemical structures of the curcuminoids

However, curcumin is considered the principal curcuminoid that exhibits the majority of the therapeutic activities in turmeric (Subramani et al., 2017). Curcumin has an IUPAC name of (1,7-bis (4-hydroxy-3-methoxy-phenyl) hepta-1, 6-diene-3, 5-dione) with a molecular weight of 368.37, melting point of 183 ^{0}C and three pKa values of 7.80, 7.35 and 9.0 (Jagetia and Aggarwal, 2007). It demonstrates keto-enol tautomerism, with the predominant keto- form in acidic and neutral solutions and a stable -enol form in alkaline media (Yallapu et al., 2013). Besides, curcumin is a lipophilic polyphenol, thus it is insoluble in water but soluble in organic solvents like dimethylsulfoxide (DMSO), methanol, acetone and ethanol (Wilken et al., 2011). The most compelling and key rationale for the therapeutic use of curcumin as an anticancer alternative is its extremely superior safety profile, thus it is declared as GRAS (generally recognized as safe) by the FDA (Hewlings and Kalman, 2017). Additionally, curcumin has pleiotropic properties that modulate numerous targets including proteins (protein kinase C (PKC), 5-lipoxygenase, and tubulin), transcription factors, growth factors and their receptors, cytokines, enzymes, and gene

regulating, cell proliferation and apoptosis (Yallapu et al., 2013). Because of this multi-targeted properties, curcumin exhibits a wide spectrum of pharmacological activities and is used in the treatment of various other diseases including inflammatory bowel disease, Alzheimer's disease, atherosclerosis, lung diseases, diabetes mellitus and Parkinson's disease (Moorthi and Kathiresan, 2013). Many researchers also reported the antioxidant, antimalarial, antimicrobial, antifungal and anti-inflammatory properties of curcumin (Duvoix et al., 2005; Menon and Sudheer, 2007; Padmanaban et al., 2012). Furthermore, extensive emphasis has elaborated the therapeutic potential of curcumin against a range of cancers including breast cancer, hepatic cancer, colorectal cancer and kidney cancer. It is worth noting that the epidemiological studies attribute the low incidence of CRC in Indian subcontinent to the chemo-preventive properties of diets rich in curcumin (Wilken et al., 2011).

1.4.1 Anti-cancer activity

The main anticancer mechanisms of curcumin are cell cycle inhibition and induction of apoptosis (programmed cell death) (Mulik et al., 2010). Curcumin inhibits the signal-transducer-and-activator-of-transcription-3 (STAT3) and the nuclear factor- kappa B (NF-κB) signalling pathways, which play key roles in cancer development and progression. NF-κB is an ubiquitous transcription factor that regulates many genes implicated in growth regulation, inflammation and carcinogenesis (Betancur et al., 2010). STAT3 is an ubiquitously expressed member of the STAT family of transcription factors that is activated by tyrosine phosphorylation via upstream receptors, such as EGF, and is one of the major mediators of carcinogenesis as well (Mulik et al., 2010). Activation of NF-κB and STAT3 is increased in many cancers, and has been involved in the induction

of resistance to apoptosis in a number of cancer cells (Viennois et al., 2013). They are associated with various steps in the development of malignancy such as expression of anti-apoptotic genes, angiogenesis, tumour promotion and metastasis. Curcumin has been shown to suppress their activation (Marquardt et al., 2015). Usually, the inhibition of the specificity protein 1 **(**Sp-1) and its housekeeping gene expressions such as vascular epithelial growth factors (VEGF) and EGFR, may serve as important hypotheses to preventing cancer formation, migration, and invasion (Chen et al., 2013). Sp-1 is a transcription factor highly expressed in tumour cells compared to normal cells and has been demonstrated to interact with co-activators and co-repressors thereby, activating multiple biological functions, including cell cycle and carcinogenesis (Archer, 2011). Recent data have suggested that curcumin may act by suppressing the Sp-1 activation and its downstream genes, including calmodulin, ephrin type-B receptor 2 (EPHB2), histone deacetylase 4 (HDAC4), and selenoprotein P (SEPP1) in a concentration dependent manner in CRC cell lines; these results are consistent with other studies, which have reported that curcumin could suppress the Sp-1 activity in bladder cancer and could decrease DNA binding activity of Sp-1 in non-small cell lung carcinoma cells (Vallianou et al., 2015).

A number of studies have confirmed the potential of curcumin in suppressing various chemokines. Chemokines are small, chemotactic cytokines, which direct leukocyte migration, activate inflammatory responses, and help regulate tumour growth (Aggarwal et al., 2003). Curcumin has been shown to enhance the cell death-promoting activity of tumour necrosis factor-related apoptosis-inducing ligand (TRAIL) by inducing DNA fragmentation thus making TRAIL-resistant cells amenable to TRAIL therapy (Deeb et al., 2003). Further analyses

have highlighted the potency of curcumin to induce apoptosis and cause down-regulation of EGFR by inhibiting its tyrosine phosphorylation (Lev-Ari et al., 2006). There is a long list of literature that reviews the mechanism of curcumin against cancer assuring its use as a safe, non-toxic anti-cancer drug (Churchill et al., 2000; Huang et al., 2008; Kim et al., 2007; Tuorkey, 2014).

However, all the preclinical and clinical data from oral administration of curcumin have revealed that it has poor systemic bioavailability and high susceptibility to metabolic degradation, whereby only about 2.30 $\mu g.ml^{-1}$ of curcumin was registered in serum levels after oral administration of 10 g curcumin (Anand et al., 2007). This shows that curcumin undergoes extensive metabolic degradation prior to absorption or in the intestine and liver, which thus, hinders the systemic usefulness of curcumin in the treatment of cancer. To overcome this constraint, a number of dual-drug combination therapy were initially used, such as piperine-curcumin nanoparticles in which the inhibitory effects of piperine on hepatic and intestinal glucuronidation of curcumin promotes 2000 % bioavailability in humans (Moorthi et al., 2012). Even though this attempt does improve the bioavailability of curcumin, it does not assure the fate of curcumin to tumours, which is crucial in the present pursuit. This necessitates the use of alternate strategies. One area of research that is gaining traction more recently is the incorporation of curcumin in fabricated nanoparticles. In the subsequent section, some of the past and current trends in the utilisation of nanoformulation for the delivery of curcumin to achieve meaningful plasma concentration profiles will be discussed.

1.5 Nanoparticle technology

Nanoparticle technology is a multidisciplinary field that utilises principles from chemistry, biology, physics, and engineering to design and fabricate submicronic (< 1 μm) colloidal systems (Brigger et al., 2002). Nanotechnology has several pharmaceutical and medical applications, with oncology being a significant benefactor of these novel advances. Nanoparticles (NPs) employed in delivery of therapeutic agents are particles with sizes comparable to large biological molecules such as enzymes, receptors and antibodies and about 2-4 orders less in magnitude of human cells (Xing et al., 2014). Because of this unique physical property, NPs demonstrate promising interactions with biomolecules both on the cancer tissue surface and inside the cancer cells. According to the National Cancer Institute, nanotechnology has the potential of improving the current status of cancer detection, treatment and prevention (Alexis et al., 2010). Nanodrug delivery utilises nanotechnology in promoting innovation in the treatment of cancer. The effectiveness of the nanoscale drug delivery vehicles lies on their ability to attain the following properties (Thakor and Gambhir, 2013):

- The nanoparticle must be able to bind or contain the appropriate drug.
- The nanocarrier must stay stable in the serum to allow systemic delivery of the therapeutics and only release the drug once at the site of the tumour.
- The nanoparticle-drug complex has to reach the tumour cells either via receptor-mediated interactions or by the enhanced permeability and retention (EPR) effect.
- The residual nanoparticle carrier should ideally be made of a biological or biologically inert material with a limited lifespan to allow safe degradation.

NPs can be tuned to deliver drugs specifically to cancer cells with minimal interaction with healthy cells. Such targeting of NP to cancer tissue is classified as either passive- or active-targeting (Bertrand et al., 2014). The passive-targeting mechanism, also known as EPR effect occurs when NPs are in the range of 10~100 nm and when in circulation, can selectively enter tumours through the leaky surrounding of the blood vessels and interstitial space (Danhier et al., 2010). Typically, NPs that employ the EPR effect to deliver drugs are intravenously administered since absorption of orally administered NPs from the gastrointestinal tract has several hostile barriers to traverse before entering the systemic circulation. However, the active targeting of NPs to cancer cells entails specific ligand-receptor recognition and interaction on the cell surface. Usually, cancer cells express higher levels of cell-surface receptors (section 1.2.3.1), compared to normal cells. This allows NPs conjugated with a targeting ligand to explicitly interact with them via receptor-mediated molecular recognition. There are several examples of curcumin-nanoparticle delivery systems, which may be subdivided into organic and inorganic NPs (Romero and Moya, 2012). Their particle size, surface charge (ζ potential), hydrophilicity/hydrophobicity, composition, etc. can be tailored for a diverse array of applications (Lacour, 2013). However, the primary consideration when designing any drug delivery system is to control the drug concentration in the therapeutic window and improve patient compliance in order to maintain effective treatment cycles with minimal recovery period.

1.5.1 Organic nanoparticles

Organic nanoparticles (Figure 1.6) are described as solid particles composed of organic compounds (mainly lipids or polymeric) ranging in the diameter from 10 nm to 1 µm (Allouche, 2013).

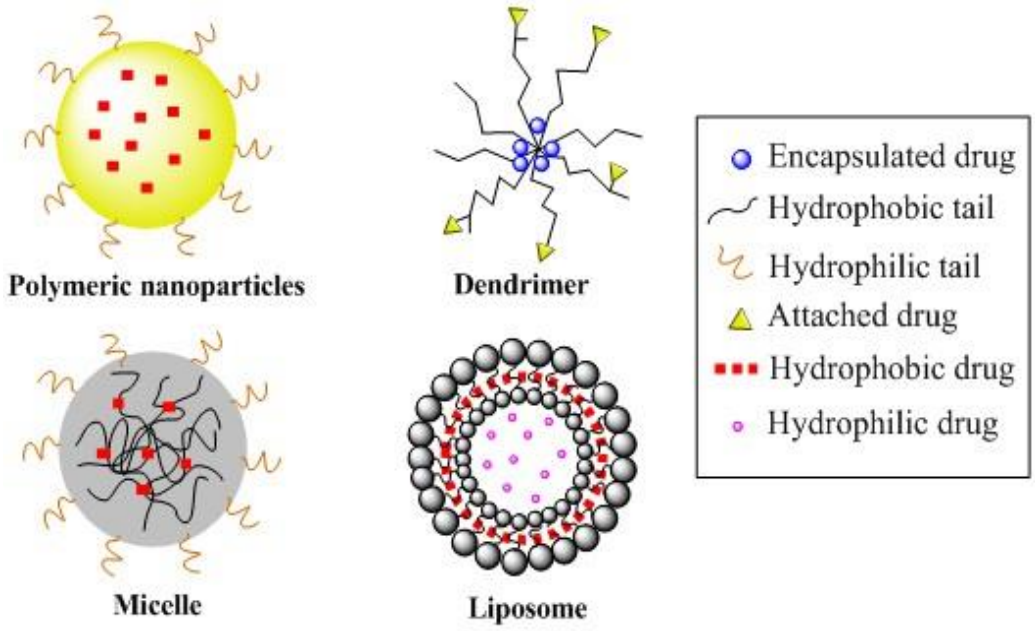


Figure 1.6 Example of organic nanoparticle platforms for drug delivery

They offer relatively simple formulation techniques for the encapsulation of curcumin or any other therapeutic agents. The compounds used for the fabrication of organic NPs are biodegradable which makes them appealing for drug delivery and biomedical applications (Romero and Moya, 2012).

Liposomal, polymeric and solid lipid nanoparticles are examples of commonly used organic NPs for nano-sized drug delivery systems. Each system possesses unique physiochemical properties inducing distinct *in vitro* and *in vivo* behaviour. In addition to the aforementioned organic nanoparticle systems, others (e.g. micelles, dendrimers etc.) have been also explored in literature as

effective curcumin-nanocarriers in cancer prevention and treatment (Din et al., 2017; Gurunathan et al., 2018). A detailed review of some of these NPs is presented below.

1.5.1.1 Liposomal nanoparticles

Liposomal formulations have demonstrated multiple benefits as drug delivery vehicles. They are biologically based nanoparticle system made from a self-assembled concentric lipid bilayer composed of amphipathic phospholipids with an enclosed interior aqueous space (Çağdaş et al., 2014). Lipids used to prepare vesicular formulations are either naturally found and approved by the FDA, such as egg yolk phosphatidylglycerol (EggPG) or synthetically established like phosphatidylethanolamines (PE) (van Hoogevest and Wendel, 2014). Liposomes can be designed to adhere to cell membranes and release drugs encapsulated in the central aqueous interior after endocytosis. Their physicochemical properties can be specifically altered to control surface charge, functionality and size by simply mixing commercially available lipid molecules. This makes them attractive over other carriers that require more elaborate and controlled synthesis steps and additional chemical modifications (Bozzuto and Molinari, 2015). However, liposomes pose many challenges such as instability in the bloodstream and burst release of cargo, which may be checked by either adding additives such as morpholine in the lipid formulation (Sercombe et al., 2015) or coating the surface of liposomes with hydrophilic polymers such as PEG to form long-circulating liposomes (Feng et al., 2017). In a study conducted by You et al., curcumin-long-circulating liposomes (CUR-LCL) demonstrated sustained-release effect and after tail intravenous administration,

half-life of CUR-LCL in rats was 13 times that of curcumin suspension and 1.8 times that of curcumin-liposomes (You et al., 2014).

1.5.1.2 Solid lipid nanoparticles

Solid lipid nanoparticle (SLN) are drug carrier systems in the submicron size range made from biocompatible lipids which are solid at room and body temperature (Pragati et al., 2009). Westesen, Müller and Gasco were the first group to invent lipid-based solid particles in the submicron range during the 1990s (Mehanna et al., 2012). SLNs are composed of 0.1% to 30% solid (w/w) lipid dispersed in an aqueous medium and, if necessary, stabilized with 0.5% to 5% (w/w) surfactant (Thakor and Gambhir, 2013). SLNs are more stable than liposomes in biological systems due to their rigid core of hydrophobic lipids surrounded by a monolayer of phospholipids and they are less toxic than polymeric nanoparticles as they are biodegradable (Pragati et al., 2009). Moreover, SLNs provide a natural platform to incorporate lipophilic anticancer drugs. For example, Guorgui et al. reported that curcumin formulated in SLN resulted in higher curcumin plasma levels in mice compared to native curcumin, additionally, curcumin-SLNs reduced Hodgkin's lymphoma xenograft growth by 50.5% while curcumin reduced it by 35.8% (Guorgui et al., 2018). Mulik et al. also proved that the use of transferrin-mediated solid lipid nanoparticles increased the photostability of curcumin and enhanced its anticancer activity against breast cancer cell line (Mulik et al., 2010). However, the quick elimination of SLNs from the blood flow by reticule endothelial system (RES) and the difficulty in controlling the rate and extent of drug release from SLNs restrain them from becoming effective nanocarriers in anticancer drug delivery (Din et al., 2017).

1.5.1.3 Polymeric nanoparticles

According to Alexis F. et al., polymeric nanoparticles may represent the most effective nanocarrier system for prolonged drug delivery (Alexis et al., 2010). The successful development of polymeric nanoparticle, poly-alkyl-cyanoacrylate-loaded with doxorubicin, back in the 1980s paved the road for using polymeric nanoparticles for cancer therapy and other diseases (Yordanov Georgi, 2012). A polymeric nanoparticle is a mutual phrase apt to any type of polymer nanoparticle, particularly to nanospheres and nanocapsules. Nanospheres are usually spherical and solid particles with molecules attached or adsorbed to their surface, while nanocapsules are vesicular systems with substances confined within a cavity consisting of a liquid core (either water or oil) surrounded by a solid shell (Guterres et al., 2007). Polymeric nanoparticles provide significant flexibility in design due to the fact that polymers can be biodegradable or non-biodegradable, and can be made synthetically or derived from natural sources (Rao and Geckeler, 2011). Some common synthetic polymers utilised in drug delivery include poly-lactic-co-glycolic-acid (PLGA), poly-lactic-acid (PLA) whilst natural polymers include gelatine, dextran, and chitosan (Sionkowska, 2011). Another interesting characteristic of polymers is that their physiochemical properties such as molecular weight, hydrophobicity, and crystallinity can be easily manipulated to allow controlled drug release kinetics and entrapment of therapeutic agents (Chan et al., 2010). Various polymeric-based curcumin nanoparticles for different therapeutic targets have been presented by many groups (Rachmawati, 2013). For example, Yallapu et al. investigated the comparative cellular uptake and cytotoxicity evaluation of polymeric, magnetic and dendrimer-based curcumin nanoformulations in

prostate cancer cells. They proved that polymeric nanoparticles, in particular curcumin loaded cellulose nanoparticles, exhibited the highest cellular uptake and caused maximum ultrastructural changes related to apoptosis in prostate cancer cells. Moreover, the cellulose-curcumin formulation showed enhanced anti-cancer efficacy compared to free curcumin (Yallapu et al., 2012). In another study by Kumar et al., curcumin loaded poly (2-hydroxyethyl methacrylate) nanoparticles revealed better tumour cells regression activity and significant reduction in G0/G1 cells than free curcumin in ovarian cancer cells (SKOV-3) (Kumar et al., 2014). Anitha et al. showed that curcumin loaded thiolated chitosan nanoparticles showed a sustained release profile over a period of 4 days, enhanced *in vitro* anticancer effects in colon cancer (HT-29) cells to 3-fold and improved plasma concentrations compared to bare curcumin (Anitha et al., 2014).

1.5.2 Inorganic nanoparticles

Inorganic nanoparticles represent a wide spectrum of nanoparticles synthesized from metals, metal oxides, and metal sulphides (Bhattacharyya et al., 2011). Gold, silica and superparamagnetic oxide nanoparticles are among the long list of inorganic nanoparticles (Figure 1.7). They have been widely studied for imaging using magnetic resonance and high-resolution superconducting quantum interference devices, and their intrinsic properties have been utilised for therapy (Huang et al., 2011). Inorganic nanoparticles can be easily conjugated with ligands for tumour targeting and/or with chemotherapeutics for tumour therapy. Additionally, their surface composition can also be feasibly manipulated to create nanoparticles that can escape the RES (Xu et al., 2006). Usually inorganic nanoparticles are more stable than liposomes and SLNs over

a large range of pH and temperatures. For instance, Li et al. showed that silica-coated flexible liposomes loaded with curcumin (CUR-SLs) demonstrated significantly higher stability against artificial gastric fluid and more sustained drug release in artificial intestinal fluid compared to curcumin-loaded flexible liposomes (CUR-FLs). Moreover, the silica coating exhibited a 3.31-fold increase in bioavailability compared with CUR-FLs (Li et al., 2012). However, there are many concerns regarding the degradation and elimination of inorganic nanoparticles from the body due to their slow dissolution rates and inadequate biodegradability properties (Soenen et al., 2011).

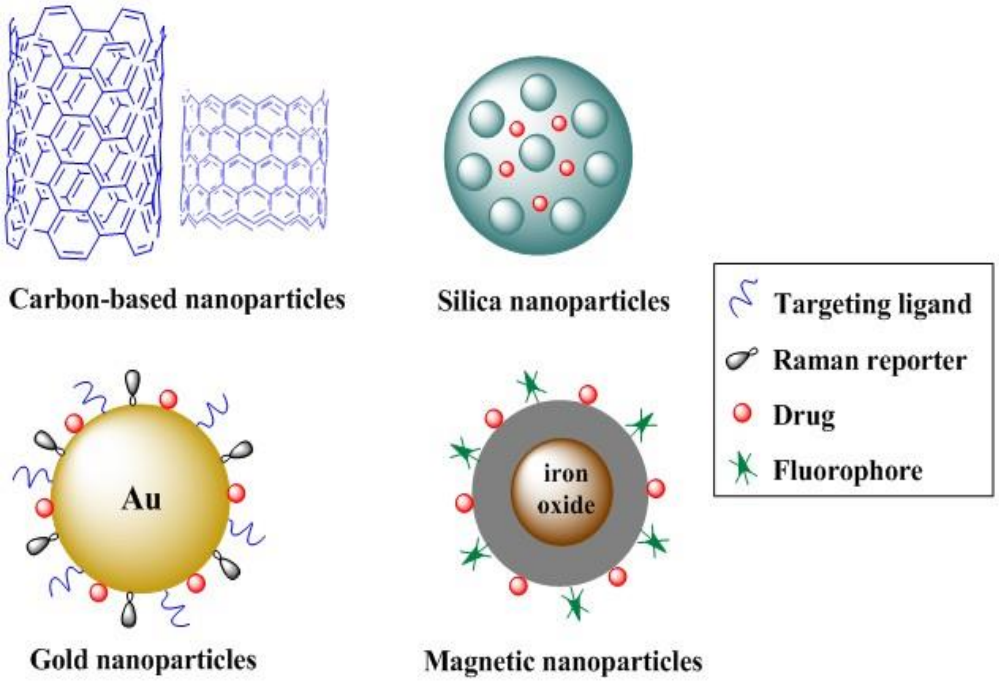


Figure 1.7 Example of inorganic nanoparticle platforms for drug delivery

Inorganic NPs differ conceptually from organic NPs in terms of fabrication principles. Inorganic NPs are normally formed by the precipitation of inorganic salts, which are linked in a matrix. While, most organic NPs are formed by several organic molecules which are driven together by self-organization or

chemical binding (Romero and Moya, 2012). Both organic and inorganic nanoparticles are highly promising contenders for the evolution of drug delivery systems in cancer treatment and their success is already established in several clinical applications. Nevertheless, among all listed types of both organic and inorganic nanoparticles, polymeric nanoparticles are emerging as one of the best options because of their higher stability, enhanced drug payload, improved physicochemical properties, higher drug circulation times and more controlled drug release compared with their colloidal counterparts (Din et al., 2017; Rao et al., 2014). All of the aforementioned features are vastly desirable in the context of cancer treatment. Thus, in the present proposal, curcumin will be loaded into polymeric nanoparticles and emphasis on the most common methods of preparation will be detailed in the next section.

1.6 A review of some polymeric formulation techniques used to fabricate curcumin nanoparticles

In order to achieve the desired properties of interest such as particle size, particle size distribution and area of application, the mode of preparation of polymeric nanoparticles plays an essential role. In general, the preparation of curcumin-polymeric nanoparticles is essentially divided into two initial approaches. The first approach is based on a two-step procedure, where in the first step an emulsification system is carried out to generate nanodroplets of definite sizes in which organic compounds (polymer, monomer, and lipid) are previously solubilized, then in the second step the nanoparticles are formed by various mechanisms such as precipitation or polymerization (Romero and Moya, 2012). The second approach consists of a one-step procedure in which emulsification is not required and the nanoparticles can be directly generated via different

mechanisms such as nanoprecipitation, ionic gelation or using more technological ways like spray-drying methods (Kumar and Lal, 2014).

1.6.1 The two-step procedure

This procedure starts with emulsification which is defined as the mixing of two or more totally or partially immiscible liquids (usually an organic "oil" and water) obtained in the presence or absence of a surfactant (Allouche, 2013). Formulated emulsions can either be single emulsion, termed as oil-in-water (o/w) or water-in-oil (w/o), or multiple emulsions of different kinds (w/o/w, o/w/o, w/o/o) (Particle Sciences, 2009). The formation of emulsion is a very crucial step since the size of the emulsion droplet is directly related to the size of the NP. To obtain emulsions with nano-scaled droplets and consequently polymeric NPs, either the low- or the high-energy emulsification technique is required. The low-energy method, also called the condensation method, is based on the phase transitions taking place during the emulsification process, while the high-energy method, relies on applying high mechanical energy during emulsification, mostly via high shear stirring, high pressure homogenizers and/or ultrasound generators (Sadtler et al., 2012). Conversion of nano-emulsions into nanoparticles can be done subsequently in the second step through several ways including solvent removal or polymerization.

1.6.1.1 Solvent removal

Nano-emulsions dissolved in the dispersed phase of the emulsion undergo precipitation upon removal of the organic solvent via either solvent evaporation, solvent diffusion or salting out procedure (Allouche, 2013).

1.6.1.2.1 Solvent evaporation

In this method, polymeric nano-emulsions are formulated whereby curcumin is dissolved in a volatile solvent and mixed via sonication or high-speed stirring (Nagavarma et al., 2012). In the past, dichloromethane and chloroform were utilised, but due to toxicity concerns, ethyl acetate has become more favourable (Wang et al., 2016). Basically, the emulsion droplets are converted into nanoparticle suspension as the volatile solvent evaporates by either continuous magnetic stirring at room temperature or under reduced pressure. The nanoparticle suspensions are then centrifuged, washed with distilled water to remove additives such as surfactants and finally lyophilized (Bennet and Kim, 2014). Figure 1.8 represent a schematic illustration of the solvent evaporation method. This technique possesses several advantages such that low temperature is required for evaporation of solvent and thermal deposition can be avoided (Dhivya and Rajalakshmi, 2018). In a study by Rachmawati et al., curcumin was encapsulated in poly (lactic acid) nanoparticles via the emulsification-solvent evaporation method using dichloromethane as the solvent and vitamin E polyethylene glycol succinate (TPGS) as the surfactant. The fabricated NPs produced a size of 300nm with an encapsulation efficiency of 89.42 % (Rachmawati et al., 2016). The concerns regarding the use of this method are mainly related to the potential hazards that the residue of the volatile solvent inside the NPs might possess in *in vivo* therapy.

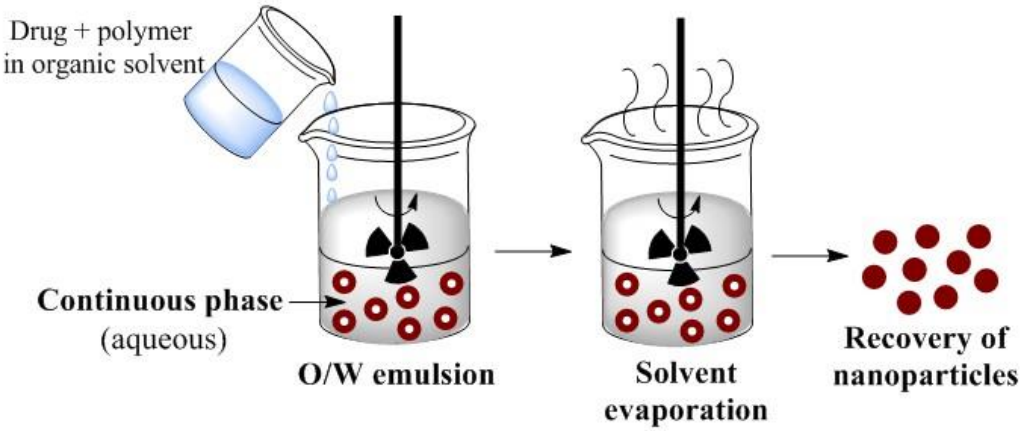


Figure 1.8 Schematic representation of the preparation of NPs by emulsion evaporation method.

1.6.1.2.2 Solvent diffusion

In the solvent diffusion method, a partially water-miscible solvent (e.g. dichloromethane; propan-2-one), saturated with water may be used to dissolve the polymer and curcumin. For curcumin-containing polymer precipitation which results in the formation of NPs, the organic solvent is diffused to the aqueous phase by diluting it in excess of water. The supersaturated solution of o/w droplets is then emulsified in an aqueous solution containing stabilizer (such as poly(vinylpirrolidone)), causing the diffusion of the solvent into the external phase composed of curcumin, polymer and an organic solvent. This eventually leads to the formation of nanospheres or nanocapsules (Pal et al., 2011). The solvent is then eliminated by evaporation or filtration and the solidified nanoparticles are collected by freeze-drying. Figure 1.9 represent a schematic illustration of the solvent diffusion method. This technique presents several advantages, such as high batch-to-batch reproducibility, ease of scale-up, simplicity and narrow size distribution. Chen et al. encapsulated curcumin into poly (lactic-co-glycolic acid) nanoparticles via solvent diffusion. They

proved that adjusting the volume ratio of binary organic solvents (acetone and ethylene for dissolving the polymer and curcumin, respectively) and the concentration of surfactant (polyvinyl alcohol) improved the formulation characteristics including smaller size, narrow size distribution and high drug loading. Moreover, they showed that the fabricated curcumin NPs exhibited a controlled curcumin release profile and enhanced the inhibition of human leukemic (HL60) and hepatoma (HepG2) cells, in comparison with free curcumin (Chen et al., 2014). However, the requirement to eliminate high volumes of water from the suspension and the leakage of water-soluble drug into the saturated-aqueous external phase during emulsification, reduces the encapsulation efficiency (Nagavarma et al., 2012). This justifies the low encapsulation efficiency obtained by Chen et al. (33.5 %) (Chen et al., 2014).

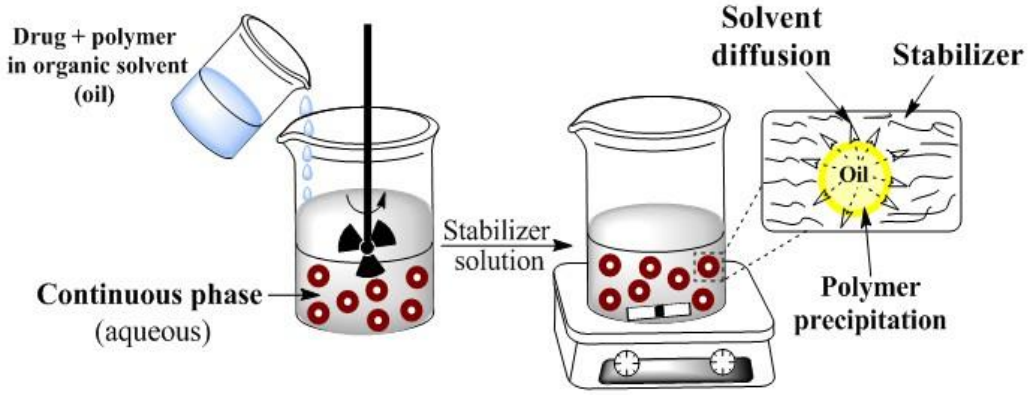


Figure 1.9 Schematic representation of the preparation of nanocapsules by emulsion diffusion method.

1.6.1.2.3 Salting out

In this method, a totally water-miscible solvent, such as acetone, is usually used to dissolve the polymer and curcumin in the presence of a high concentration of a salting-out agent (electrolytes, such as magnesium chloride, calcium chloride, and magnesium acetate, or non- electrolytes such as sucrose) and a colloidal stabilizer such as polyvinylpyrrolidone or hydroxyethylcellulose (Nagavarma et al., 2012). Subsequently, the solvent is diffused with sufficient volume of water in the continuous phase to drop the salt concentration and thus induce particle precipitation. Then, both the solvent and the salting-out agent are eliminated by cross-flow filtration. Figure 1.10 represent a schematic illustration of the salting-out method. However, there are no reports found in literature of curcumin polymeric nanoparticles being prepared via this method maybe due to the fact that salting-out procedure requires an extensive nanoparticle washing step which significantly affects the encapsulation efficiency of curcumin (Ahmed and Aljaeid, 2016).

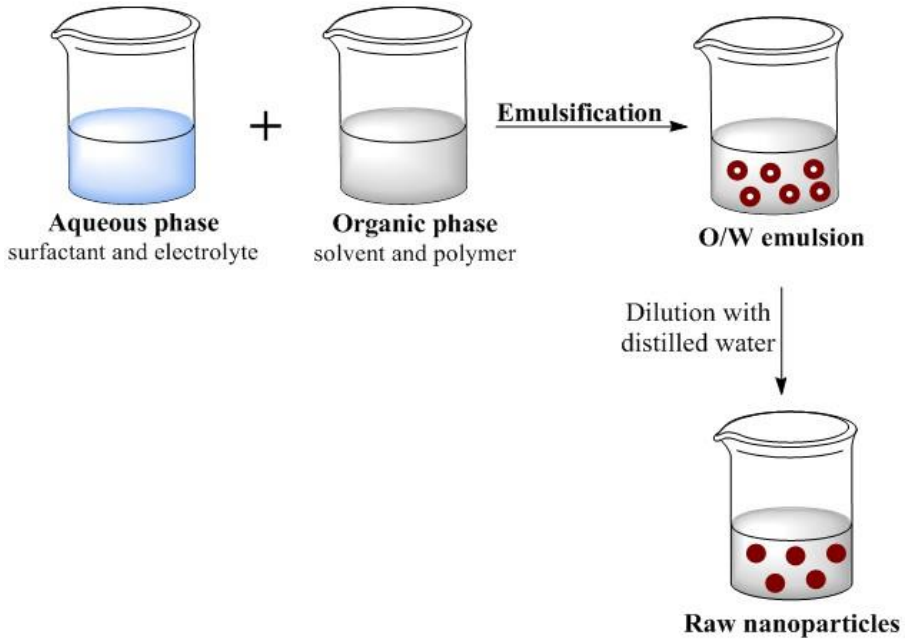


Figure 1.10 Schematic representation of the preparation of NPs by salting-out method.

1.6.1.2 Polymerisation

Polymerization techniques can be classified as emulsion polymerization, interfacial polymerization and controlled radical polymerization process. Controlled radical polymerization offers a better control of the polymer characteristics in comparison to other conventional polymerization techniques (Allouche, 2013). All of the aforementioned methods involve polymerisation of monomers by introducing the monomer to an aqueous phase or dissolving the monomer in a non-solvent of the polymer. To trigger polymerisation, an initiator molecule (ion or free radical) or high-energy radiation (gamma radiator or UV light) is required. Subsequently, curcumin either covalently bonds to the polymer or adsorbs onto the surface of the particle. Finally, purification is carried out to remove any undesirable residual monomers and initiators in the final nanoparticle formulation (Villiers M. Melgardt et al., 2008). Mulik et al. showed that the encapsulation of curcumin in poly(butyl) cyanoacrylate nanoparticles using the polymerisation method, improved the chemical and physical stability of curcumin in which the fabricated NPs can be exploit as a stealth system in blood for targeting the malignant tissues passively (Mulik et al., 2009). The main drawback of this technique is that it requires the use of high temperatures and irradiations.

1.6.2 The one-step procedure

1.6.2.1 Nanoprecipitation

Nanoprecipitation is one of the first methods developed to encapsulate drugs within polymer nanospheres by Fessi and co-workers in the 1989 (Morales-Cruz et al., 2012). It enables production of particles in the 100–300 nm range. It is one of the easiest formulation procedure for polymeric nanospheres that does

not require extended shearing/stirring rates, ultra-sonification, or high temperatures (Morales-Cruz et al., 2012). Additionally, this procedure is reproducible, fast and requires use of performed polymers as starting materials rather than monomers. Three ingredients are required to achieve the process: the polymer, the polymer solvent and the non-solvent of the polymer. Surfactants can be added as well. Ideally, the nanoparticles are generated by a rapid diffusion of the polymer solvent in the non-solvent phase by mixing the polymer solution with the latter. Consequently, the interfacial tension between the two phases drops, generates an increased surface area and rapid precipitation of the polymeric nanoparticles (Allouche, 2013). Curcumin can either be dissolved or dispersed with the polymeric solution. The lipophilic polymer solution is commonly added dropwise to the non-polymer solvent to establish a proper polymer deposition on the surface of the dispersed aqueous droplets (Yadav and Sawant, 2010). Figure 1.11 represent a schematic illustration of the nanoprecipitation method. Since nanoprecipitation method is typically appropriate for hydrophobic compounds that are soluble in ethanol or acetone and insoluble in water, an incredibly number of drugs, other than curcumin, were encapsulated into polymeric NPs using this method. For example, Barichello et al. obtained encapsulation efficiencies close to 100% with the lipophilic drugs cindomethacin and cyclosporine, but less than 15% for the hydrophilic drugs vancomycin and phenobarbital (Morales-Cruz et al., 2012). In another report by Chin et al., curcumin loaded onto starch nanoparticles yielded an encapsulation efficiency of 78% with a sustained curcumin release of 93% under physiological pH over a period of 10 days. However, the conventional nanoprecipitation method is stilled limited to lab use and small-

scale yields due to its dropwise operation and the complications of extraction and reservation of NPs (Miladi et al., 2016).

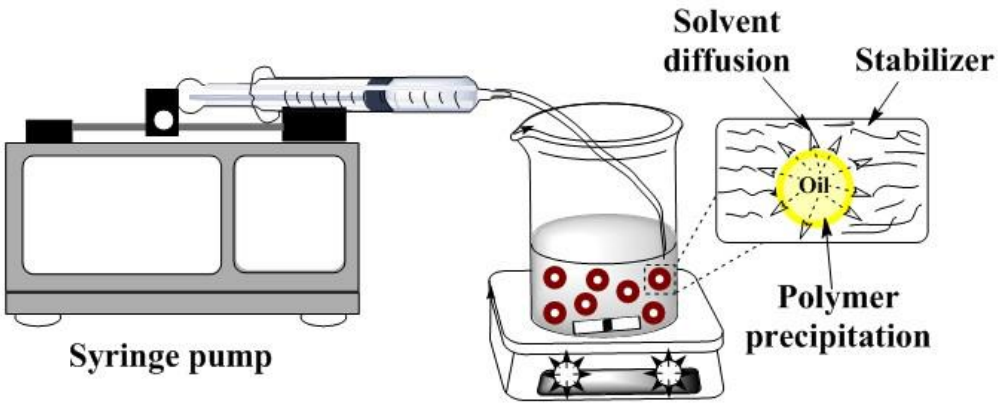


Figure 1.11 Schematic representation of the preparation of NPs by nanoprecipitation method.

1.6.2.2 Spray-drying

Spray-drying technology has gone through constant evolution in the past years. The most distinctive emergence is the synthesis of polymeric nano-sized particles obtained in a one-step procedure by the spray-drying of the polymer solution. In this method, the dispersion, emulsion or suspension of curcumin and polymer in a solution is atomised into a spray of fine droplets in a drying chamber. The small droplets are then brought in contact with a hot drying gas to evaporate the moisture which subsequently leads to the formation of the solid product, that is finally recovered via a cyclone unit (Ahmed and Aljaeid, 2016). The spray flow rate, atomisation pressure or the inlet air pressure can be adjusted to obtain a desired particle size. Figure 1.12 represent a schematic illustration of the spray-drying method. Usually spray-drying yields high particle production ranging between 70–95 % (Allouche, 2013). For example, the micro-encapsulation of curcumin by spray-drying, using gum arabic as an encapsulating agent in three different concentrations by Bucurescu and his

colleagues yielded an encapsulation between 75 and 85%, being higher for the particles prepared with higher concentrations of encapsulating agents (Bucurescu et al., 2018). However, this technique requires large volume of hot air to dry polymer droplets, thus spray-drying is not a convenient procedure for the encapsulation of heat sensitive materials such as vaccines and proteins.

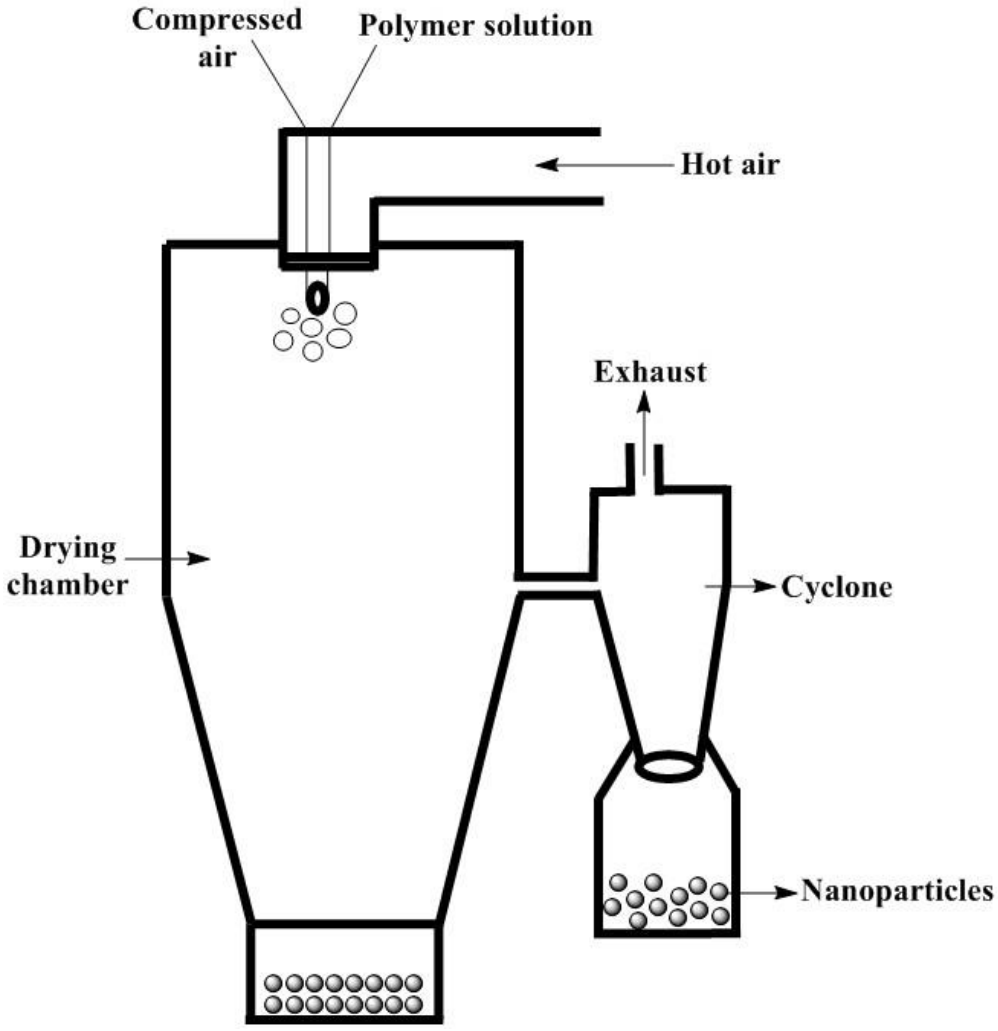


Figure 1.12 Schematic representation of the preparation of NPs by spray-drying method.

1.6.2.3 Ionic gelation

Also known as ionotropic gelation or polyelectrolyte complexation, is one of the most renowned encapsulation techniques used with chitosan-based delivery systems (Hamman, 2010). This technique involves the dropwise addition of a cross-linking agent (tripolyphosphate, glutardehyde etc.) into an aqueous solution of biodegradable hydrophilic polymers (chitosan, alginate, etc.) under continuous stirring to form hydrogels (Rajalakshmi et al., 2014). The polyanions from the cross-linker form a meshwork of structures by interacting with the polyvalent cations of the polymer hence inducing gelation (Sarmento et al., 2006). Curcumin can be loaded into these hydrogels during the production where it becomes encapsulated. There are diverse forms of cross-linkers and the choice may be made based on safety profiles and degree of cross-linking. For example, glutardehyde which chemically crosslink with polymers is known for its toxicity and poor mechanical stability. The poor mechanical strength of glutaraldehyde cross-linked product is due to its double bonding pattern (–C=N–) with the amine group containing polymer (Mitra et al., 2014). Genipine-cross-linked with chitosan, for instance, display slower degradation rate and higher biocompatibility in comparison to glutaraldehyde-cross-linked. However, genipine is incompatible with curcumin loaded into NPs (Ahmadi et al., 2015). On the other hand, sodium tripolyphosphate displays better crosslinker characteristics because it is nontoxic, relatively inexpensive, multivalent, has quick gelling property and has been widely utilised as an effective crosslinker in chitosan-based nanoparticles (Lange et al., 2014; Zhao et al., 2011). The main advantages of ionic gelation include its general capability of protecting the encapsulated molecules and retaining their activity during the

encapsulation (Usmiati et al., 2014). Additionally, reversible physical crosslinking by electrostatic interaction instead of chemical crosslinking avoids the possible toxicity of reagents and other undesirable effects (Ahirrao et al., 2013).

Generally, both the two-step and one-step procedures may allow the encapsulation and loading of curcumin into nanocarriers to improve its effects in cancer therapy. However, ionic gelation technique is the chosen encapsulation technique in this project because it is one of the simplest methods and utilises very mild conditions, avoiding harmful organic solvents or high shear forces (Usmiati et al., 2014). The majority of curcumin-loaded nanoparticles have been intended for intravenous (i.v.) administration, seeking to accumulate in tumour regions, as they circulate in blood vessel and eventually kill cancer cells. However, recent reports showed that i.v. administration caused high drug distribution in major organs which are highly perfused (e.g. kidney, lung, etc.) compared to tumour sites. This high perfusion of blood may cause impairment to the organs upon long-term i.v. administration (Attili-Qadri et al., 2013; Patel, 2014). Thus, research is focused on alternative modes of delivery, in particular, oral delivery. This is true for CRC treatment as in other cancers (Date et al., 2016; Sharma and Saltz, 2000). Oral delivery of anticancer agents not only reduces the stress and discomfort associated with i.v. treatments but also afford flexibility to patients in that, they may forgo hospital visits (Eek et al., 2016). Moreover, oral administration of therapeutics for action at the colon improves the efficacy of the former and enables localized treatment, which reduces systemic toxicity. However, one key consideration in the localised delivery of therapeutics to the colon via the oral route is that the formulation

should protect the drug-loaded NPs from premature release in the upper gastrointestinal tract. Premature release of the payload may render them to multi-drug efflux pumps and metabolic enzymes (e.g. cytochrome P450 enzymes) present on the epithelium of the gastrointestinal tract (Katragadda et al., 2005) and degradation by gastric pH. Usually, the colon has comparatively less harsh environment due to reduced digestive enzymatic activity. Furthermore, the colon transit time is relatively long (from 6 to 48 h). Both of the preceding features are desirable and favour enhanced bioavailability and action of the drug at that site (Mathew, 2011). Formulations of oral drug delivery systems capable of overcoming the harsh pH conditions in the stomach and the duodenum along with intestinal enzymatic metabolism such that, drug release proper occurs upon arrival at the colon are termed by "colon-specific delivery systems". In the next section, some of the pharmaceutical strategies designed for the development of colon targeted therapy are discussed.

1.7 Colon-specific nano-carrier systems

Most of the colon-specific drug delivery systems outlined in literature are based on four main approaches: prodrug-based approach, time-dependent systems, pH-dependent devices and microflora-activated systems (Nicholas E. Madhu et al., 2011).

1.7.1 Prodrug-based approach

A prodrug is a pharmacological substance administered in an inactive form of the parent drug that will be transformed *in vivo* to the active form of the parent drug (Singh and Khanna, 2012). For colon-targeting, prodrugs are usually designed to be hydrophilic by coupling drug molecules to hydrophilic small

molecules (e.g. amino acids and sugars) or polymers (e.g. poly (L-aspartic acid) and dextran) (Jain and Jain, 2008). This hydrophilicity helps in restricting the absorption of the prodrug in the upper gastrointestinal tract (GIT) and allows the transit to the colon where, colonic enzymes such as azo-reductase and glycosidase produced by the colon microflora degrade the prodrug to release active drug. However, the clinical application of prodrugs is limited since their manufacture depends on the availability of functional groups within the drug molecule suitable for chemical linkages. In addition, the prodrug function and safety profile is still ambiguous (Ettmayer et al., 2004).

1.7.2 Time-dependent systems

Time-dependent systems are designed to release their loaded drug in the colon at a pre-set lag time following administration, mainly being controlled by the coating layer used in the system (Gazzaniga et al., 2006). One typical example is the Time Clock® system coated with hydrophobic polyoxyethylene sorbitan monooleate and water soluble hypromellose in which the coating disintegrates in an aqueous environment at a rate proportional to the coating thickness and gradually exposes the drug core for dissolution (Pozzi et al., 1994). Nevertheless, time-dependent systems are unreliable due to the variation in their transit time through the gastrointestinal tract, influenced by the variability of the gastric emptying time, food intake, size and density of the formulation.

1.7.3 pH-dependent devices

pH-dependent devices employ the pH changes along the GI tract to control drug release. Wide range of coatings made of pH-responsive polymers, such as Eudragit® L100-55, Eudragit® S100 and hydroxypropyl methyl cellulose

phthalate, are usually used for site-specific drug delivery to the lower GI tract (Jain and Jain, 2008). These polymers have high pH threshold (at least 5.0) for dissolution and are able to resist disintegration from the gastric acid and small intestinal fluids for several hours. However, the site specificity of pH responsive dosage systems might be inadequate in some individuals due to factors such as closeness of the luminal and colonic pH, which might cause premature drug release (Ibekwe et al., 2008).

1.7.4 Microflora-activated systems

Microflora-activated systems typically refer to colon-specific carriers based on polysaccharides which can be digested by bacteria available in the colon. The colonic bacteria usually produce a number of enzymes such as: glucoronidase, xylosidase, arabinosidase, galactosidase, etc. to act on specific substrates that have been left undigested in the small intestine (Sinha and Kumria, 2003). Substrates for these enzymes include polysaccharides such as chitosan, alginate and pectin which have been used as coatings in delivery systems (Jain and Jain, 2008). These polysaccharides shield the drug from the environments of stomach and small intestine and are able to deliver the drug to the colon. On reaching the colon, they undergo degradation by enzyme or break down of their polymer back bone leading to reduction in their molecular weight and thereby loss of structural integrity. Subsequently they are unable to hold the drug entity any longer, which activates drug release.

Because the biodegradable enzymes are only present in the colon, the use of biodegradable polymers for colon-specific drug delivery seems to be a more site-specific approach when compared to transit time or pH change systems.

1.7.5 Choice of appropriate polymer

In trying to achieve site-specific delivery employing any of the aforementioned approaches, the choice of the polymer is crucial. In the present pursuit, I intend to deliver curcumin to the colon region following oral administration of the nanoparticulate delivery system. In the next section I will review key polymers used to achieve the above objective whilst rationalising the specific use of two of them (chitosan and pectin) in the project.

1.7.5.1 Chitosan

Chitosan is a hydrophilic, cationic polysaccharide subjected to degradation by the bacterial enzymes, e.g. lysozymes, generated by the colonic microflora. It is the N-acetylated derivative of chitin, a natural polysaccharide found in the shells of marine crustaceans. It comprises of β- [1–4] -linked D-glucosamine and N-acetylated units (Figure 1.13) (Jonassen et al., 2012).

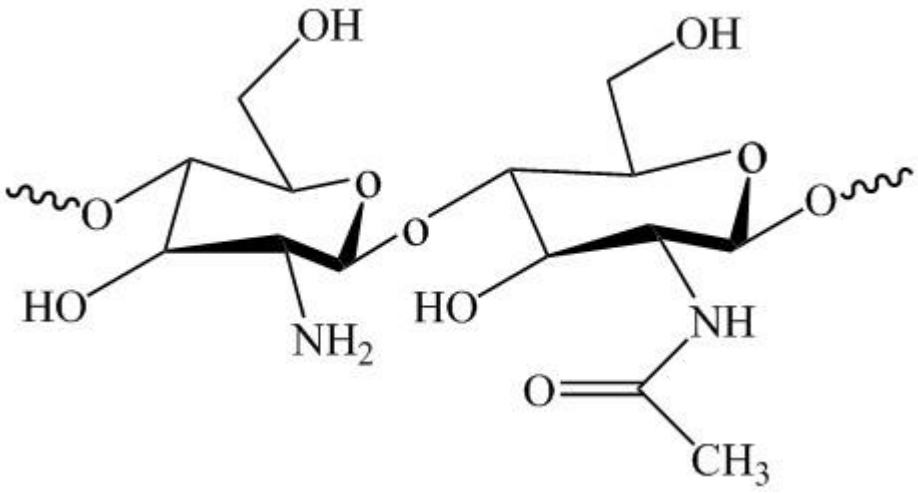
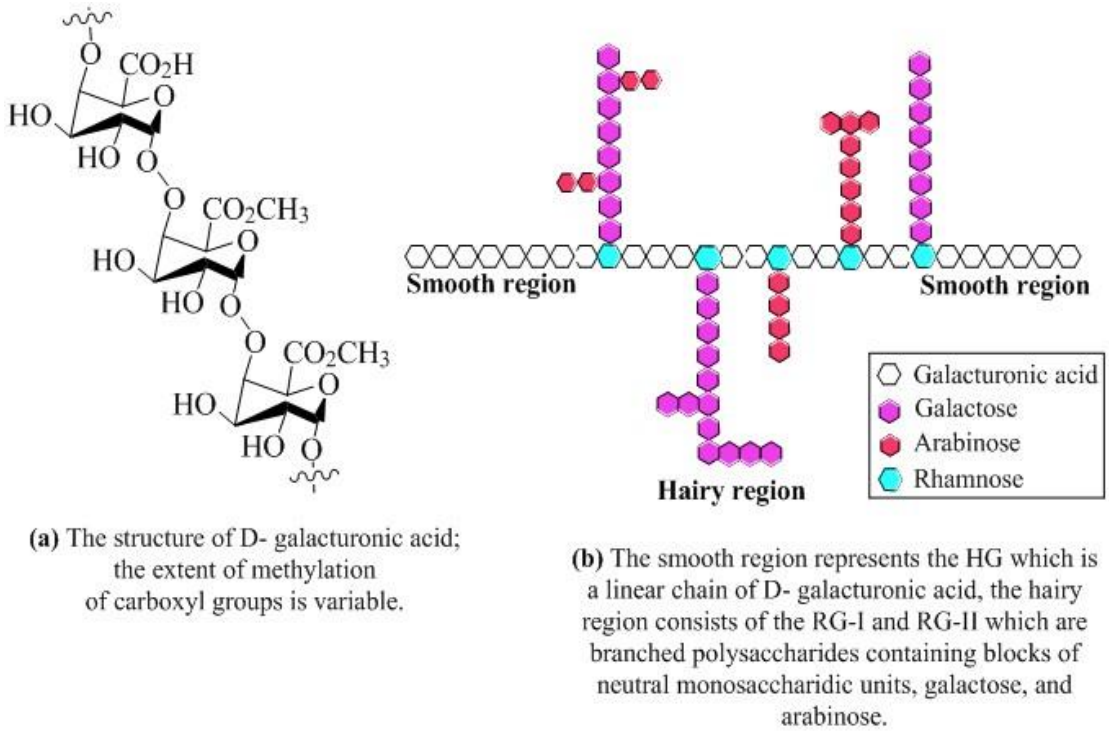


Figure 1.13 Chemical structure of chitosan, comprising N-acetyl-D-glucosamine **(right)** and D-glucosamine **(left)** units

It is soluble in acidic media due to the presence of the protonated amine groups (NH_3^+), hence possessing the ability to effectively form electrostatic interactions with negatively charged species (Kavitha et al., 2011). The positively charged moieties of chitosan also interact with the tight junction of the intestinal epithelial cells and thus modulate drug permeation and absorption through the para-cellular route (Muheem et al., 2014). One of the features I wish to impart in the development of a colon-targeted delivery system is the mucoadhesive functionality. Chitosan is considered a well-suited polymer for targeted drug delivery to the colon due to its biodegradability, low toxicity, and bio-adhesive properties (Rampino et al., 2013). Therefore, in the present project, chitosan is utilised as one of the matrix-forming polymers.

1.7.5.2 Pectin

Pectin is a negative hetero-polysaccharide extracted from the cell wall of plants. It possesses a poly α- [1–4] - linked D-galacturonic acid units with varying degrees of methylation of carboxylic acid functional groups (Figure 1.14 a) (Mishra et al., 2012).



(a) The structure of D- galacturonic acid; the extent of methylation of carboxyl groups is variable.

(b) The smooth region represents the HG which is a linear chain of D- galacturonic acid, the hairy region consists of the RG-I and RG-II which are branched polysaccharides containing blocks of neutral monosaccharidic units, galactose, and arabinose.

Figure 1.14 Chemical structure of pectin

Pectin with greater than 50 % carboxyl methylation is identified as high-methoxyl pectin, whilst those with less than 50 % are known as low-methoxyl pectin. Pectin consists mainly of three polysaccharides: the homogalacturonan (HG), the rhamnogalacturonan-I (RG-I) and the rhamnogalacturonan-II (RG-II) (Sharma et al., 2006) (Figure 1.14 b). To date, the way in which the three domains are connected to one another to form the pectin macromolecule is still vague (Kaya et al., 2014). Pectin shares very similar properties with chitosan such as non-toxic, biodegradable, highly available and resistant to the digestive enzymes in the GI tract and only degraded by the microflora in the colon (Mishra et al., 2009). In addition, pectin has moieties that have anticancer properties. This makes the use of a pectin-chitosan composite a favourable approach in the present project.

The anticancer properties of pectin may be ameliorated after modification via pH/thermal treatment (Glinsky and Raz, 2009). The pH modification begins with increasing the alkaline pH of the polymer to disrupt the rhamnogalacturan side chain and thus de-polymerises the backbone side chain and de-esterifies the HG regions. This is followed by an acid treatment that ultimately cleaves the rhamnogalacturans to arabinose and galactose. This modification process of pectin results in the production of neutral sugar sequences with a low degree of branching but rich in galactose. Galactose is capable of inhibiting the growth of colon cancer and migration since it is a remarkable antagonist to galectin-3 (Gal-3) (Leclere et al., 2013; Venzon et al., 2015).

Gal-3 is a member of the galectin super-family with a carbohydrate-binding domain that exhibits high affinity to β-galactoses (Barrow et al., 2011). It is vastly expressed on tumour cell surfaces and more specifically, it is expressed at higher levels in colon cancer than normal colon tissue. Gal-3 binds to the colonic mucin with an altered carbohydrate structure causing tumour growth, cell to cell adhesion and metastasis (Wong et al., 2011). Modified pectin, rich in galactose, binds to the carbohydrate recognition domain of the Gal-3, consequently restricting the capacity of Gal-3 to stimulate cell adhesion and migration and thus, preventing tumour growth (Venzon et al., 2015) (Figure 1.15).

In addition to all the desirable properties that chitosan and pectin exhibit and make collectively suitable for use in developing colon-targeted systems, they are also considered as effective mucoadhesive polymers. Thus, chitosan and pectin (after modification) composite would be used in the fabrication of the curcumin nanoparticle delivery system. As mentioned earlier, mucoadhesion at

colonic mucosa is a key aspect of the present investigation and in the subsequent section I shall discuss the key aspects as they relate to colon-targeted drug delivery.

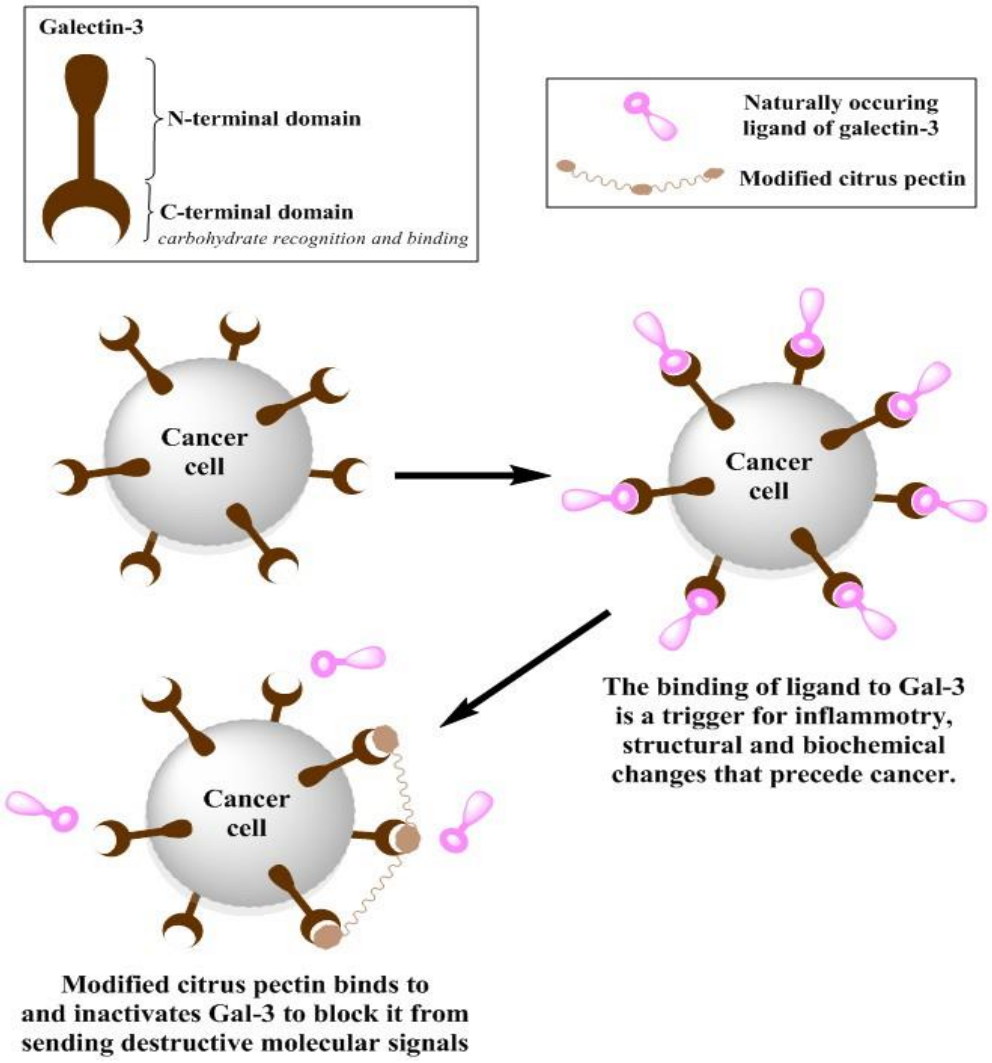


Figure 1.15 The binding process of modified citrus pectin with galectin-3

1.8 Mucoadhesion

Mucoadhesion is the adhesion between two materials, at least one of which is a mucosal surface. It is a promising strategy that can be exploited to improve the bioavailability of drugs through prolonged residence of dosage forms in the gastrointestinal tract. Mucoadhesive polymers can be used as a mean of improving drug delivery via various routes such as: the buccal /oral route, nasal route, ocular route and the gastrointestinal route. Nanoparticles designed using the aforementioned natural polymers possess promising mucoadhesive properties to the colon due to their hydrogen bond forming moieties, cationic/anionic moieties and flexibility to penetrate the mucus network (Shaikh et al., 2011). It is worth noting that various synthetic polymers such as polylactic acid, polyadipic acid and cellulose derivatives are also widely used in formulating mucoadhesive systems. However, the use of natural polymers is preferred over the synthetic ones because the former usually exhibit less toxicity, widely available and have lower production costs (Kavitha et al., 2011).

Prolonged gastrointestinal residence improves the contact time of dosage forms with epithelia and hence improves drug adsorption (Mazzarino et al., 2012). The mucosal layer is a viscoelastic fluid made up of gel-like mucus which is secreted by the goblet cells (Shaikh et al., 2011). It consists of water, mucin (an anionic polyelectrolyte), proteins, lipids and muco-polysaccharides. Mucoadhesion basically occurs in two steps: the contact stage and the consolidation step. The contact stage is manifested between the mucoadhesive polymer and the mucus membrane, with spreading and swelling of the formulation (Boddupalli et al., 2010). The consolidation step involves the activation and bonding of

mucoadhesive material in the presence of moisture that plasticizes the system, allowing the mucoadhesive molecules to break free and to link up by Van der Waals and hydrogen bonds (Boddupalli et al., 2010). Due to the complexity of the mucoadhesion process, numerous theories have been proposed to explain the aforesaid mechanisms. For simplification purposes the theories are classified into two categories: i) the chemical method which involves the electronic and the adsorption theories; ii) the physical method which include the wetting, the diffusion and the cohesive theory (Tao et al., 2014).

In general, the colon is regarded as a more suitable site for mucoadhesion compared to the stomach and small intestine due to the presence of a thicker mucus layer and reduced colonic motility in the former. Therefore, mucoadhesive drug delivery systems targeting the colon allows for effective targeting and localisation of drug to the colon with prolonged residence time as well as intimate contact between the delivery system and the absorptive mucosa. This prolonged residence results in higher drug flux across the colon membrane compensated for by the longer residence time. Nanoparticle delivery systems are well suited for use in the present context because of their large surface area to volume ratio. Mucoadhesion is also affected due to the dispersibility of the nanoparticles.

1.9 Physical techniques for NP characterisation

To characterize formulated curcumin-loaded NPs, there are number of analyses that can be performed, such as: size distribution, surface charge, morphology, physical status of the drug within the carrier systems, drug release and encapsulation efficacy. The commonly used techniques for particle size analyses are dynamic light scattering, nanoparticle tracking analysis, scanning

electron microscopy (SEM) and atomic force microscopy (AFM). SEM and AFM can also provide information on surface morphology. Differential scanning calorimetry is often used to examine the physical state of the drug in NP, in which the thermogram of drug-loaded particles is compared to that of raw drug and particles without drug incorporation. To confirm the successful curcumin incorporation to the NPs, available methods, include high performance liquid chromatograph and/or Fourier transform infrared spectroscopy. These characterisation methods validate the composition of particulate carriers (especially the drug encapsulation) thus are typically conducted to establish the optimal formulation for *in vitro*/*vivo* efficacy evaluation. *In vitro* drug release studies can be used to evaluate the potency of carrier systems for colon-specific delivery. It utilises different buffers and incubation times to simulate the gastrointestinal conditions that a test formulation may endure after oral administration. To evaluate the vulnerability of microflora-activated systems to the *in vivo* colonic microflora environment, colonic enzymes are usually included in the simulated colonic fluids. Although the *in vitro* release model cannot represent the full factors of *in vivo* milieu, it is still considered a useful tool for the development of the formulation as it compares the response of different formulations to mimic biological factors (e.g. transit time, pH or colonic enzymes).

In the following sections therefore, some of the adopted techniques for characterizing the formulated nanoparticles will be briefly reviewed.

1.9.1 Zeta Sizer Nano Series®

The Zeta sizer Nano Series (Figure 1.16) is a high-performance system that incorporates combination of particle size and zeta potential analysis, for

enhanced detection of aggregates and measurement of small or dilute samples (MALVERN, 2017).

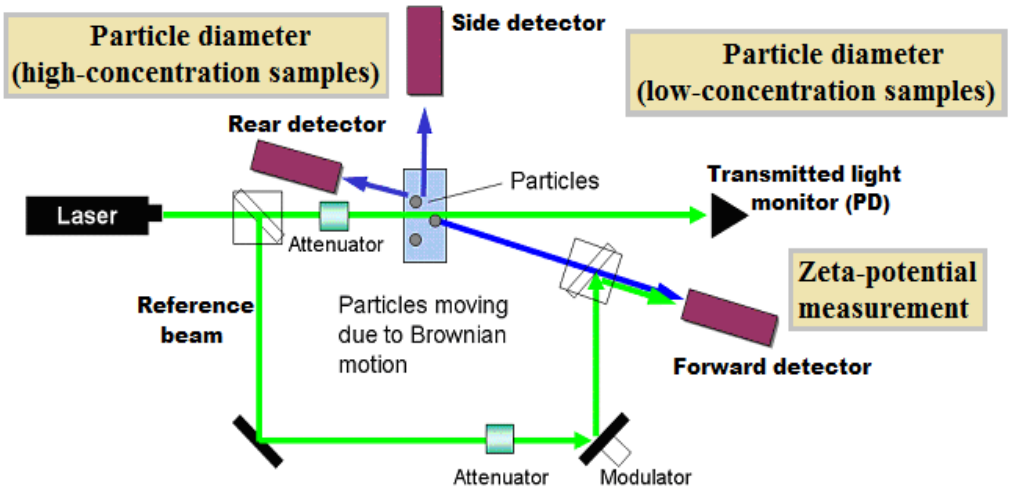


Figure 1.16 Schematic illustration of the techniques associated with the Zeta sizer Nano series®. Adapted and modified from (Horiba Scientific, 2016)

It associates two techniques in a single compact unit to simplify the measurement of different sample types. The first technique is known as the "Laser Doppler Micro-electrophoresis" which is used to measure zeta potential (surface charge of the nanoparticles or colloidal particles). Zeta potential values of typically ±30 mV are representative of stabilised particle (Vogel et al., 2017). Usually, an electrical field is applied to a solution of molecules or a dispersion of particles, which then move with a velocity due to the interaction between the charged particle and applied field. The direction and velocity of the motion is a function of particle charge, the suspending medium, and the electric field strength. This velocity is measured using a patented laser interferometric technique called M3-PALS (phase analysis light scattering) by observing the Doppler shift in the scattered light. This enables the calculation of electrophoretic mobility, hence the zeta potential is proportional to the electrical

potential of the particle at the shear plane (Malvern Instruments Ltd., 2016). The other technique is the Dynamic Light Scattering (DLS), one of the most popular light scattering techniques that measures the particle size down to 1 nm diameter. It measures the diffusion of particles moving under Brownian motion and converts this to size and a size distribution using the Stokes-Einstein relationship. Size distribution is usually referred to as the "Polydispersity index" (PDI), where a high PDI shows a poly-dispersed sample with large size distribution and a low PDI value displays a monodisperse sample with narrow size distribution. Any numerical value of PDI that is below ≤0.1 is considered highly monodisperse, if ranges between 0.1–0.4 then it is moderately polydisperse and any value above 0.5 is highly polydisperse (Bhattacharjee, 2016).

DLS is a non-invasive technique, which provides good statistics regarding the *in-situ* measurements of the size and PDI, however, it does not display the morphology of the nanoparticles (e.g. spherical, cylindrical) and it assumes any aggregation of several vesicles as one single particle (Danaei et al., 2018). Microscopic techniques, on the contrary, provide a detailed view of the morphology of nanostructures as well as the presence/absence of any aggregation. Such examples include scanning electron microscope, atomic force microscopy, etc.

1.9.2 Scanning Electron Microscopy

SEM is an instrument that utilizes vacuum conditions and electrons instead of light to form a largely magnified image with better resolution (Bogner et al., 2007). Initially, a beam of electrons is produced at the top of the microscope by an electron gun as voltage is applied. The electron beam follows a vertical path

through the microscope and travels through electromagnetic fields and lenses, which focus the beam down toward the sample. Once the beam hits the sample, electrons and X-rays are ejected from the sample. Detectors collect these X-rays, backscattered electrons, and secondary electrons and convert them into a signal that is sent to a screen similar to a television screen, producing the final image (Figure 1.17) (Leonard et al., 2012).

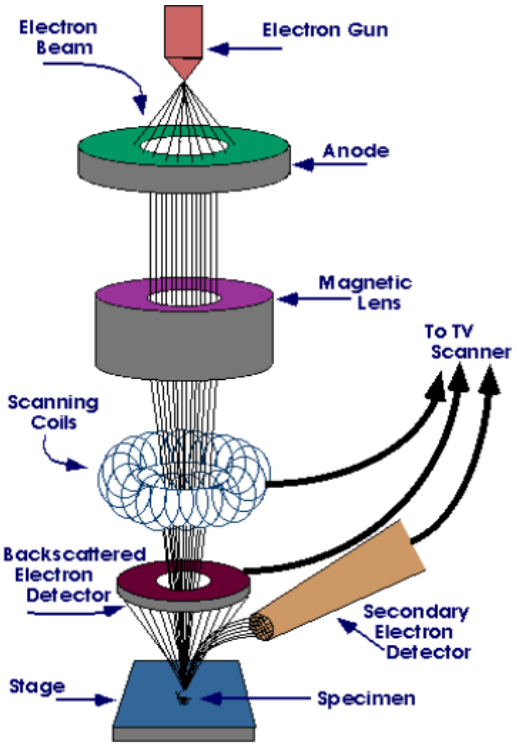


Figure 1.17 Schematic diagram of SEM.
Adapted from [Bogner et al., 2007]

The SEM is one of the most useful instruments in nanotechnology research today due to its flexibility in controlling the degree of magnification as it utilises electromagnets rather than lenses (Voutou and Stefanaki, 2008).

1.9.3 Atomic Force Microscopy

AFM is a prevailing surface analytical technique used in air, liquid or vacuum to generate three-dimensional, high-resolution topographic images of samples at sub-micron level. It also provides some information about the nanoscale mechanical (modulus, stiffness, viscoelastic, frictional) properties. In AFM, a sharp tip of atomic scale, attached to a cantilever, is scanned across a sample. The deflection of the cantilever caused by forces between the tip and the sample surface, is monitored by a laser and photodiode. This generates a topographical map of the sample. The AFM can image in a number of ways using either contact or tapping mode. In contact mode, the topographical map is generated by tapping the probe on to the surface across the sample while in the tapping mode, the probe hovers over the conducting surface without contacting the surface (Figure 1.18) (Pal et al., 2011).

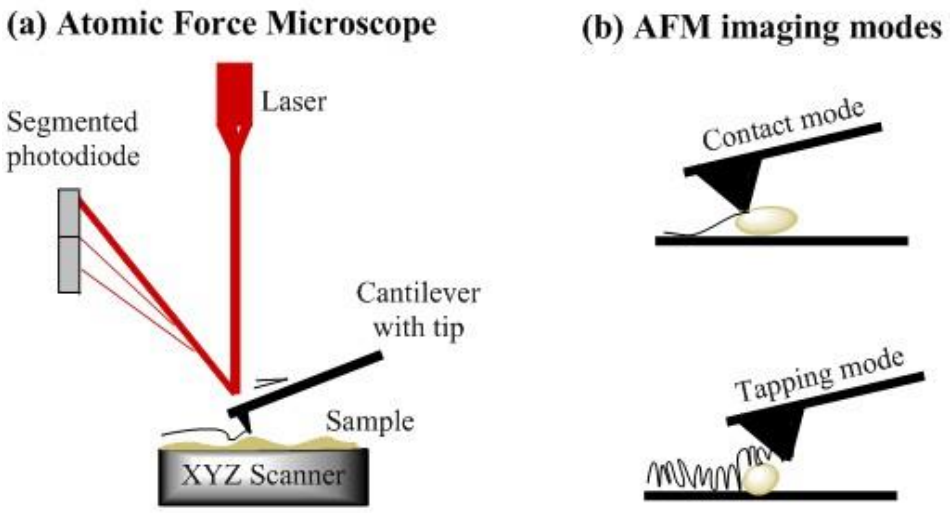


Figure 1.18 An outline of the basic principles of the AFM

Even though, AFM and SEM converge in their abilities to offer nanometer scale lateral information, they differ in the fact that SEM provides elemental analysis

using X-ray detection, while the AFM presents compositional information based on physical properties. The AFM can produce a 3-dimensional topography using just a single scan, whereas the SEM can only produce 2-dimensional images (Eaton et al., 2017). Although, AFM has higher resolution than SEM and requires no mathematical treatment, on relatively rough surfaces, SEM's large depth of field and large lateral field gives it a significant advantage over AFM (Batchelor and Russell, 2013). Therefore, both SEM and AFM can complement each other very well and provide a wealth of information about a sample.

1.9.4 Nanoparticle Tracking Analysis

NTA is another high-resolution technique that is capable of tracking and measuring the size, size distribution and concentration of a single nanocarrier moving under Brownian motion (Saveyn et al., 2010). For NTA analysis, the sample is first injected into the special cell and then illuminated by a laser light with 635 nm wavelength. Refraction occurs, and NPs contained in the sample are visualised under the microscope as small points of light moving under Brownian motion (Tian et al., 2016). Usually bigger NPs and heavy aggregates move with a slow speed, while smaller NPs, which have less weight, move faster. The motion of the nanocarriers is then recorded as a video of typically 30 seconds, using a conventional charge-coupled device (CCD) camera supported on the C-mount of the microscope (Danaei et al., 2018) (Figure 1.19). The NTA software concurrently locates and tracks the centre of each particle throughout the length of the video and relates it to the size of the particles. The hydrodynamic size and size distribution of the NPs is then calculated by the

Stokes–Einstein equation, taking into account the particle diffusion coefficient (Danaei et al., 2018).

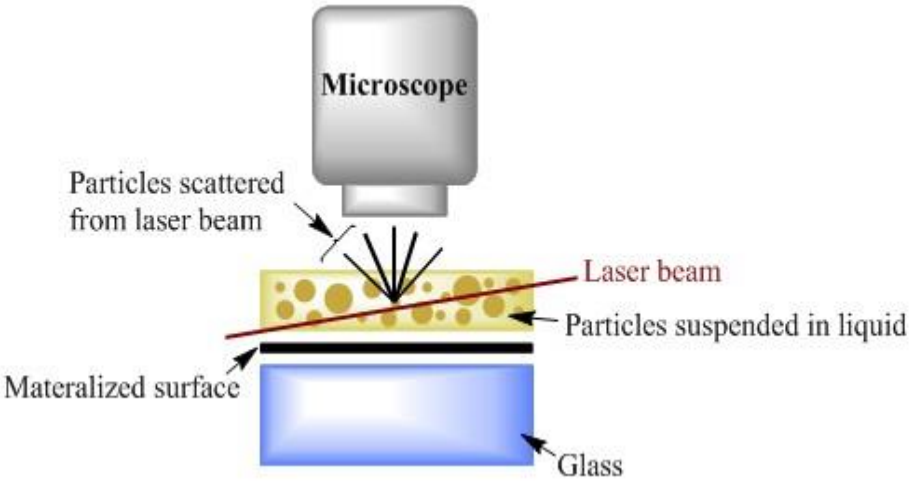


Figure 1.19 Schematic illustration of NTA

A significant advantage that NTA offers in comparison with other size measurement techniques is that it is not biased toward larger NPs or aggregates. Additionally, its confirmed accuracy and reproducibility verified the suitability of NTA to determine the size populations of both monodisperse and polydisperse samples (Mourdikoudis et al., 2018).

1.9.5 Fourier Transform Infrared Spectroscopy

FT-IR is an analytical technique used to identify organic (and in some cases inorganic) materials. This technique measures the absorption of infrared radiation to identify the molecular components and structures (Bunaciu et al., 2010). In an infrared spectroscopy, IR radiation with a specific wavelength, modulated by an interferometer, is passed through the sample. The sample will absorb some of the infrared radiation and the rest will be transmitted and measured by a detector. The signal obtained from the detector is an

interferogram, which must be analysed with a computer using Fourier transforms to obtain a single-beam infrared spectrum (Figure 1.20) (Doyle, 1992).

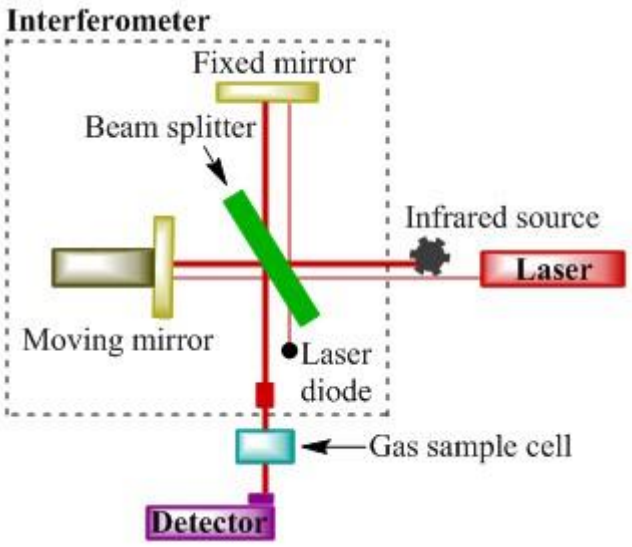


Figure 1.20 Basic principle of FTIR

The resulting spectrum is presented as a plot of intensity (% of transmittance or absorbance) versus wavenumber (in cm^{-1}), creating a molecular fingerprint of the sample. Like a fingerprint, no two unique molecular structures produce the same infrared spectrum. This makes infrared spectroscopy useful for several types of analysis (Nicolet and All, 2001). The obtained IR absorption spectrum is usually compared with standard spectra in computer databases to identify the functional groups present in the sample. Absorption bands in the range of 1500 - 400 cm^{-1} wavenumbers are referred to as the fingerprint region, which are generally due to intramolecular phenomena and are highly specific to each material (Simonova and Karamancheva, 2013).

1.9.6 Differential Scanning Calorimetry

DSC is a technique that studies the thermal transitions of polymers by measuring the energy absorbed (endotherm) or produced (exotherm) as a function of time or temperature (Gill et al., 2010). It is used to characterize melting, crystallization, heat capacity and other processes involving an energy change. In the DSC chamber, the sample pan and an empty reference pan are placed on small platforms with thermocouple sensors (TCS) lying underneath (Figure 1.21).

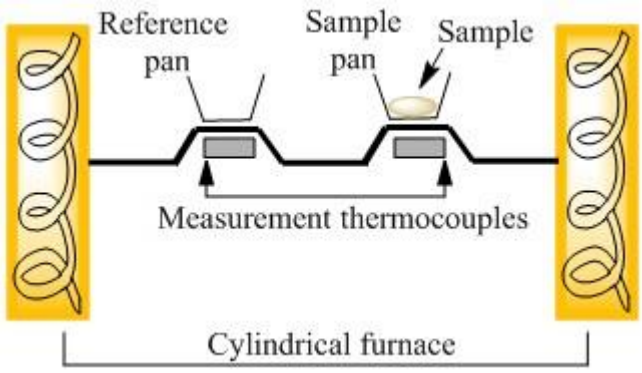


Figure 1.21 Schematic diagram of the DSC

Then the analysis can be made in two ways: either by measuring the electrical energy to be provided to the TCS to maintain the same temperature (power compensation) at both pans, or by measuring the heat flow (differential temperature) as a function of sample temperature (heat flux) (Danley, 2002). The DSC ultimately outputs the differential heat flow (heat/time) between the material and the empty reference pan. Heat capacity may be determined by taking the ratio of heat flow to heating rate. The increase or decrease of heat flow determines whether the change is endothermic or exothermic, respectively

(Mutlur, 2004). The three most common states a substance undergoes are presented in Figure 1.22.

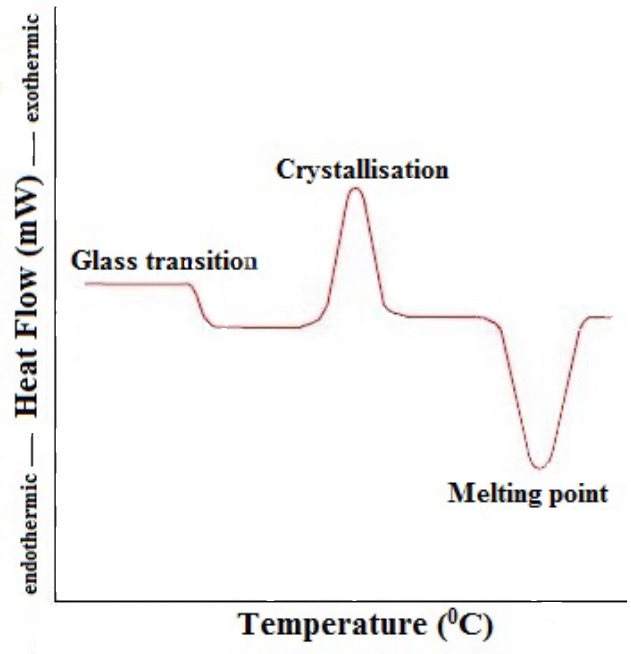


Figure 1.22 An example of a DSC thermogram

In glass transition state, which is an endothermic event, a heated amorphous substance undergoes a transition from a glassy state to a rubbery state. As the viscosity of a material increases, it experiences a transition from the hard and brittle 'glassy' state to the elastic and flexible 'rubbery' state. This known as the crystallisation state and it is an exothermic event, in which the molecules within a material partially aligns into a crystalline form. As heating is continued the material undergoes a melting point state, in which the solid state of the material changes to liquid, forming an endothermic event (Chiu and Prenner, 2011).

1.9.8 Micro-bicinchoninic acid assay

The micro-bicinchoninic acid (micro-BCA) protein assay is employed to quantitate the amount of protein in a sample. The theory behind this assay is that proteins can reduce Cu^{2+} to Cu^{1+} in an alkaline solution, then two molecules of the BCA chelate with each Cu^{+} forming a purple-coloured complex that strongly absorbs wavelength at 562nm (Figure 1.23).

Unlike Bradford assay, the BCA assay is more objective as the universal peptide backbone also conduces to colour formation. One drawback of the BCA assay compared to the Bradford assay is that it is vulnerable to intrusion by some chemicals present in protein samples, including reducing agents, copper chelators and buffers with high concentration, however this can be avoided by generating diluted samples (Olson and Markwell, 2007).

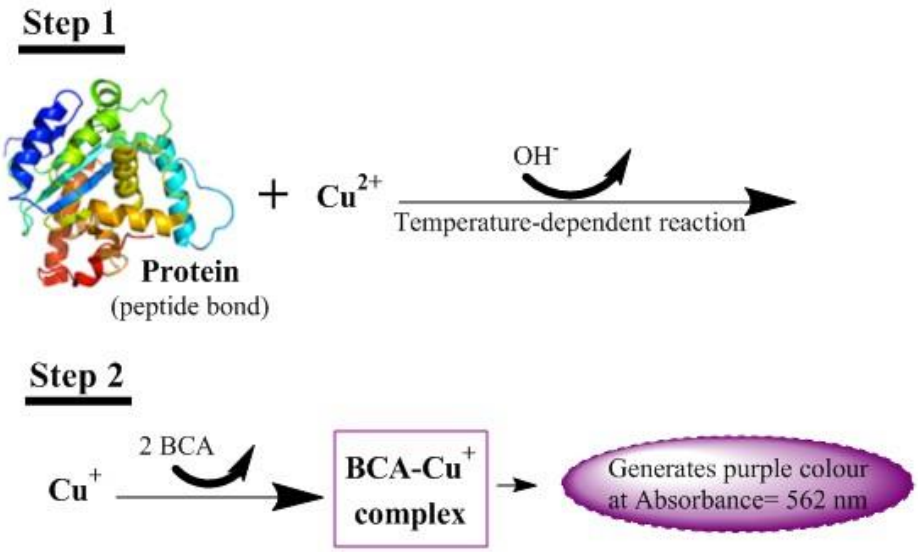


Figure 1.23 An outline of the micro-BCA principle

1.10 Thesis objectives

In view of the above very detailed discussion and the continued quest for alternative and more patient-acceptable solutions in anticancer therapy, I have sought to propose the development of a novel colon cancer delivery system that harnesses maximum therapeutic potential, whilst keeping side effects at the minimum. Consequently, I aim to formulate an oral colon cancer delivery system made from nanoparticles using curcumin as the therapeutic agent. In order to improve specificity of the anticancer agent to cancer tissue, the surface of the nanoparticles would be modified with antibodies that target the tumour-specific receptors within the colorectal cancer tissue. The choice for chitosan as a delivery vehicle is based on its documented mucoadhesive properties coupled with its biocompatibility, whilst pectin is used in a modified form to augment the anti-cancer properties of curcumin through the yield of galactose moiety described earlier. Specifically, the objectives of this project are:

- To develop a mucoadhesive curcumin-containing nanoparticle delivery system using chitosan and modified pectin
- To extensively characterise the above delivery system in terms of physical properties and mucoadhesion potency.
- To develop an efficient synthetic means for introducing tumour-targeting antibody to the surface of the curcumin nanoparticles.
- To examine the cytotoxicity and potential of the mucoadhesive, tumour-targeted nanoparticle formulations on well-defined colorectal cancer cell surface biomarkers and normal cell.

This thesis comprises of six chapters that elucidates the research conducted towards accomplishing the above objectives. Chapter 2 describes the development and the *in vitro* evaluation of modified citrus pectin-chitosan nanoparticles containing curcumin. Chapter 3 evaluates the mucoadhesion propensity of the curcumin-containing NP system. Chapter 4 describes the conjugation of the antibody on the surface of the nanoparticle with evaluation of its physical and *in vitro* release profile. Chapter 5 studies the *in vitro* cytotoxicity and cellular uptake of the composite nanoparticle antibody curcumin delivery system. Chapter 6 recaps the fundamental findings of this project and deliberates the future approach of the research.

Chapter 2 Formulation and *in vitro* evaluation of modified citrus pectin-chitosan nanoparticles containing curcumin

2.1 Introduction

Chitosan is a cationic polysaccharide that is obtained by alkaline deacetylation of chitin (Quiñones et al., 2018). Its biocompatibility, biodegradability and nontoxicity properties present a platform that make chitosan a good candidate for pharmaceutical applications. Although chitosan remains indispensable in drug formulations, it has a limited capacity for controlling drug release from formulated oral dosage forms due to rapid dissolution in the stomach (Jana et al., 2014). However, this limitation can be addressed through chemical modifications with other polymers or cross linkers. Sodium tripolyphosphate has been widely utilised as an effective crosslinker in chitosan-based nanoparticles because it is non-toxic, relatively inexpensive and has quick gelling property (Lange et al., 2014; Zhao et al., 2011).

The interaction between sodium tripolyphosphate and chitosan leads to the spontaneous formation of biocompatible nanoparticles which can efficiently modulate drug release (Bhumkar and Pokharkar, 2006). To improve the stability of nanoparticles and control curcumin release, alongside the use of crosslinker, other polymers may be used in conjunction with chitosan. Chitosan-based polyelectrolyte complexes have been developed for oral, nasal or systemic administration of drugs and biodrugs (Andriani et al., 2015). Polyelectrolyte complexes are usually formed by electrostatic interaction between polyanions and polycations (Maciel et al., 2017). These complexes display distinctive physical and chemical properties, as the electrostatic interactions within the polyelectrolyte complex gel are significantly stronger than most secondary binding interactions (Jana et al., 2014). Several studies have addressed the employment of polyelectrolyte complexes of chitosan and polyanions for

pharmaceutical applications. Pectin, a natural non-toxic polysaccharide, is among the long list of different polyanions that can be used for chitosan-based polyelectrolyte complexes. Pectin has the desirable stability under acidic conditions even at higher temperature which makes it an ideal candidate in drug delivery systems (Mishra et al., 2012). Polyelectrolyte complexes based on chitosan and pectin ameliorates the mechanical properties of resulting matrices (Maciel et al., 2017). The electrostatic attractions between the ionised amino groups (NH_3^+) of chitosan and the ionised carboxyl acid groups (COO^-) of pectin are key interactions in the formation of the pectin/chitosan nanoparticles (Sh Rashidova et al., 2004). The stability of these complexes depends on pH, temperature, charge density and ionic strength among other environmental conditions (Recillas et al., 2011).

Many studies have addressed the potential of chitosan/pectin polyelectrolyte complexes in drug delivery applications, specifically for colon targeted drug delivery (Bigucci et al., 2008; Das et al., 2011; Ghaffari et al., 2007; Oliveira et al., 2010; Pandey et al., 2013). Crucially, pH-thermal treatment of pectin yields chemical moieties that demonstrate chemo-preventive activities against cancers (Glinsky and Raz, 2009). In this regard, the modified pectin would serve the dual function of retaining the integrity of the nanoparticles within the acidic pH of the upper gut and also yielding the galactose moiety, which is known to manifest anticancer properties against galectin-3 in the colon (Johnson et al., 2007).

In this chapter, the modification method of pectin alongside the optimal conditions used to obtain desirable physical properties of nanoparticles based on ionic gelation were investigated. Moreover, the physical properties of the

synthesized chitosan-modified pectin cross linked by sodium tripolyphosphate nanoparticles as nanocarrier of curcumin (MCPCNPs) were also evaluated.

2.2 Materials:

Chitosan (low molecular weight, DE acetylated chitin, Poly (D- glucosamine) was purchased from Sigma Aldrich, Iceland and low methoxyl citrus pectin (DE lower than 50) from Genu, CPKelco® (Limeira- SP, Brazil) were utilized as coating polymers. Curcumin was bought from Fluka, China. Sodium tripolyphosphate (STPP) (Sigma Aldrich, USA) was used as the cross-linker with chitosan. Potassium bromide (KBr) (Nacalai Tesque, Japan) was used for the FT-IR analysis. Acetic acid (R&M chemicals, UK), hydrochloric acid (HCl) (R&M chemicals, UK), sodium hydroxide (NaOH) (Merck, Germany), ethanol (R&M chemicals, UK), acetone (R&M chemicals, UK), acetonitrile (RCI Labscan, Thailand) and methanol (R&M chemicals, UK) were expended as solvents or pH modifiers.

2.3 Methods:

2.3.1 Modifying citrus pectin

The low-methoxyl citrus pectin (CP) was chemically modified as ascribed by Venzon et al. (Venzon et al., 2015) with some modification. 1.5 g of the powdered CP was dissolved in 100 ml ultra-pure water and the pH adjusted to 10.0 using 3 M NaOH followed by gentle stirring at 60 °C for an hour. The mixture was allowed to cool at room temperature; its pH was adjusted to 3.0 with 3 M HCl and then stored at 4 °C overnight. Subsequently, the modified citrus pectin (MCP) was precipitated in the sample with 95 % ethanol and then washed with 100% acetone, followed by drying at 60 °C for an hour. Finally,

the semi-dried MCP was frozen at −20 °C and then lyophilized. Figure 2.1 summarizes the steps:

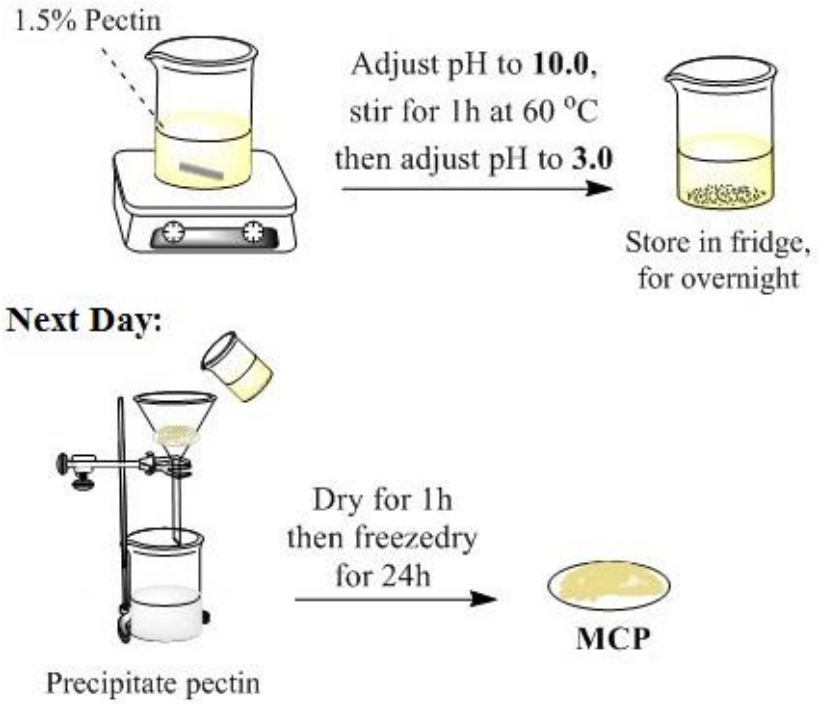


Figure 2.1 Schematic illustration of pectin modification

2.3.2 Formulating MCP-chitosan nanoparticles

Chitosan solutions (1, 1.5 and 2.5 mg/ml) were prepared in 2 % (v/v) acetic acid, and pH adjusted to 5 using 2 M NaOH. 0.5 mg/ml of MCP was dissolved in ultra-pure water for 30 minutes at 57 ± 2 ^{0}C. 10 ml of MCP solution was added dropwise to 10 ml of chitosan solution, followed by dropwise addition of 10 ml of STPP (0.5 mg/ml) and then stirred at 500 rpm for 20 minutes. The different techniques used are illustrated in Figure 2.2:

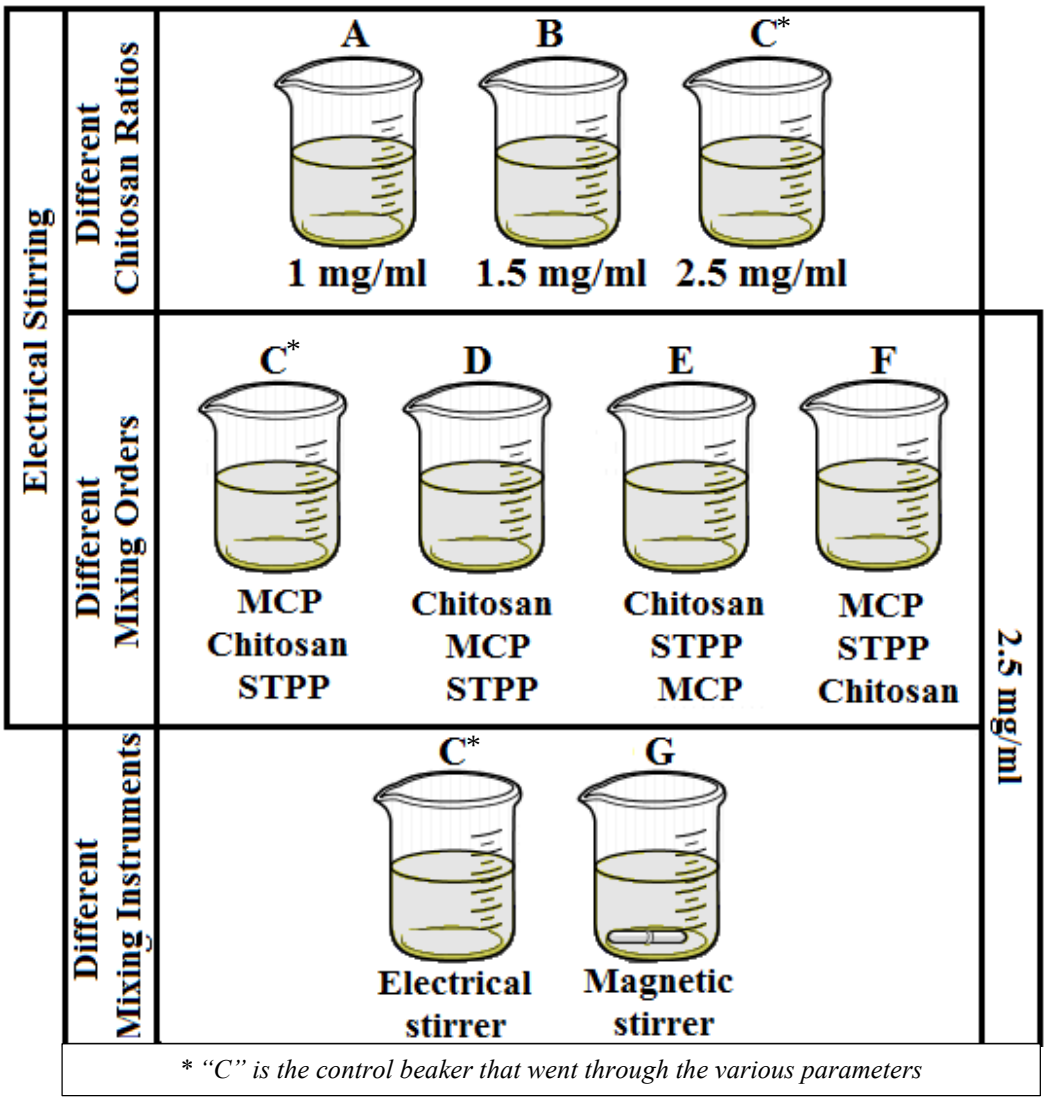


Figure 2.2 The different techniques carried out to develop the most ideal method of MCP-chitosan nanoparticles

2.3.3 Physical properties of the nanoparticles

2.3.3.1 The hydrodynamic size and surface charge of nanoparticles

The hydrodynamic size distribution (expressed as average diameter) and surface charge (expressed as zeta- potential) of the nanoparticles (NPs) were determined after dilution using a Zeta Sizer Nano Series® (Malvern Instruments Ltd., UK) equipped with a 4 mW He-Ne laser at a wavelength of 633 nm. The average diameter and zeta-potential were measured by means of Dynamic Laser Scattering and Laser Doppler Anemometry (LDA), respectively. Samples were run in triplicates and presented as mean (± SD).

2.3.3.2 The morphology of the MCPCNPs

The morphology of the MCPCNPs was observed using a SEM (Model Quanta 400F, FEI Company USA) equipped with a backscattered electron detector at 3 kV. 100 µl of the sample was placed on the SEM imaging stub with carbon layer and left under a drying chamber for 24 h at room temperature before viewing.

2.3.3.3 The FTIR spectra of the polymers and nanoparticle solids

The FTIR spectra of compacts from the MCPCNPs and excipients were reviewed after compressing them with KBr into compact discs at a pressure of 5t for 5 min. Spectra were obtained for chitosan, MCP, STPP, curcumin, MCP-chitosan nanoparticles and MCPCNPs using a Perkin-Elmer FTIR spectrometer (Spectrum RX I) with scans run between 400 and 4000 cm^{-1} at a resolution of 4 cm^{-1} and interval 1 cm^{-1}.

2.3.3.4 The thermal response profile of MCPCNPs

The thermal responses of the MCPCNPs and components were assessed on a differential scanning calorimeter DSC-Q2000 (TA Instruments, USA).

Weighed samples (≈ 8 mg) were crimped into aluminium plates and the thermogram was conducted over a range of 0 to 300 °C, at a scanning rate of 10 °C/min and flushed with nitrogen gas at a rate of 20 ml/min.

2.3.4 Time-of-Flight Secondary Ion Mass Spectrometry (TOF-SIMS)

The formulated samples were analysed for the presence of relevant chemical moieties with a mass spectrometer (TOF-SIMS IV, ION-TOF GmbH, Germany) using a bismuth liquid metal primary ion gun (Bi^{3+}) with a single-stage reflector analyser. Each sample was placed onto the surface of clean silicon wafer. The samples were air-dried on a clean bench before the measurements were taken. Surface analyses was performed over a 500 × 500 μm area at 256 × 256-pixel resolution for 15 scans. As the samples were not conductive, charge compensation was applied in the form of a low energy (<20 eV) electron flood gun and analyses were maintained in the static regime with a primary ion dose density of < 1. Data acquisition and analysis was performed using the software recommended for the mass spectrometer (Surface Lab 6, ION-TOF GmbH, Germany). For mass calibration CH^-, C_2H^- and C_3H^- peaks were used in the negative mode.

2.3.5 High Performance Liquid Chromatography (HPLC) for quantifying curcumin

Analysis of drug payload is crucial to any formulation development as it gives a reliable indication of the amount encapsulated and can be used to study drug release profiles. An HPLC system (Series 200 pump, Perkin Elmer, USA) equipped with UV/Vis detector (Series 200 UV/Vis detector, Perkin Elmer, USA) was operated at a detection wavelength of 425 nm. A reverse phase column (ZORBAX Eclipse Plus C8, 250mm x 4.6 mm, 5 μm, Agilent, USA)

was utilised as the stationary phase and the mobile phase consisted of methanol: 0.01% acetic acid: acetonitrile (5: 43: 52) filtered through 0.45 μm regenerated cellulose membrane filter (WHATMAN, UK) prior to analysis which was run at a flow rate 1.5 ml/min.

Curcumin standard solutions prepared in methanol (0.625-10 μg /ml) were quantified and the peak areas obtained were used to construct standard calibration curves. These standard curves were then used to calculate curcumin concentrations in formulations.

2.3.5.1 HPLC method validation

The HPLC method was adapted and modified from Kim et al. (Kim et al., 2009), thus validation in terms of method repeatability and accuracy was done. Curcumin solutions were prepared in methanol at three different concentrations namely 0.625, 50 and 100 μg/mL, representing the low, medium and high concentrations, respectively. The three concentrations of curcumin solution were analysed in triplicate on the same day to determine intra-day precision and accuracy; whereas triplicate analysis on three separate days were carried out for inter-day precision and accuracy determination.

2.3.6 Encapsulation efficiency and curcumin loading within MCPCNPs

The formed MCPCNPs were centrifuged at 10,000 rpm for 10 min and the centrifuged pellet was rinsed twice with methanol. The curcumin content in the supernatant and the methanol rinse was analysed by injecting 10 μl onto an HPLC system and analysed using the HPLC method described in section 2.3.5. Responses obtained were compared to those from the standard curve of

curcumin in methanol. The percentage encapsulation of curcumin and loading capacity of the MCPCNPs with respect to curcumin was calculated as follows:

$$Encapsulation\ efficiency\ (\%) = \frac{\text{Amount of curcumin added} - \text{unbound curcumin}}{\text{Amount of curcumin added}} \times 100 \qquad (2.1)$$

$$Loading\ capacity\ (\%) = \frac{\text{Entrapped curcumin}}{\text{Curcumin loaded NP weight}} \times 100 \qquad (2.2)$$

2.3.7 Stability studies

The consequences of storage on the physical integrity of MCPCNPs was conducted at 4 ^{0}C for 21 days. Physical characterization of MCPCNPs including particle size, morphology, encapsulation efficiency and drug loading were carried out as described in sections 2.3.3.1, 2.3.3.2 and 2.3.6, respectively. Studies were conducted on day 1, 7, 14 and 21.

2.4 Results and discussion

2.4.1 Modification of citrus pectin

Pectin polysaccharides consist of several side chain polymers including HG, RG-I and RG-II. The backbone of the HG is covalently cross-linked to the rhamnogalacturans, which have branched arabinogalactan side chains (Leclere et al., 2015). Alkaline treatment of pectin results in the disruption of the rhamnogalacturan side chains with a consequent depolymerisation of the backbone and de-esterification of the HG regions. Sustained exposure of the pectin in the alkaline pH also allows the cleavage of the rhamnogalacturans to arabino galactans and galactans, which are crucial in the anticancer trigger cascade. Figure 2.3 presents the FTIR spectra of the CP, (a) in comparison to the MCP, (b).

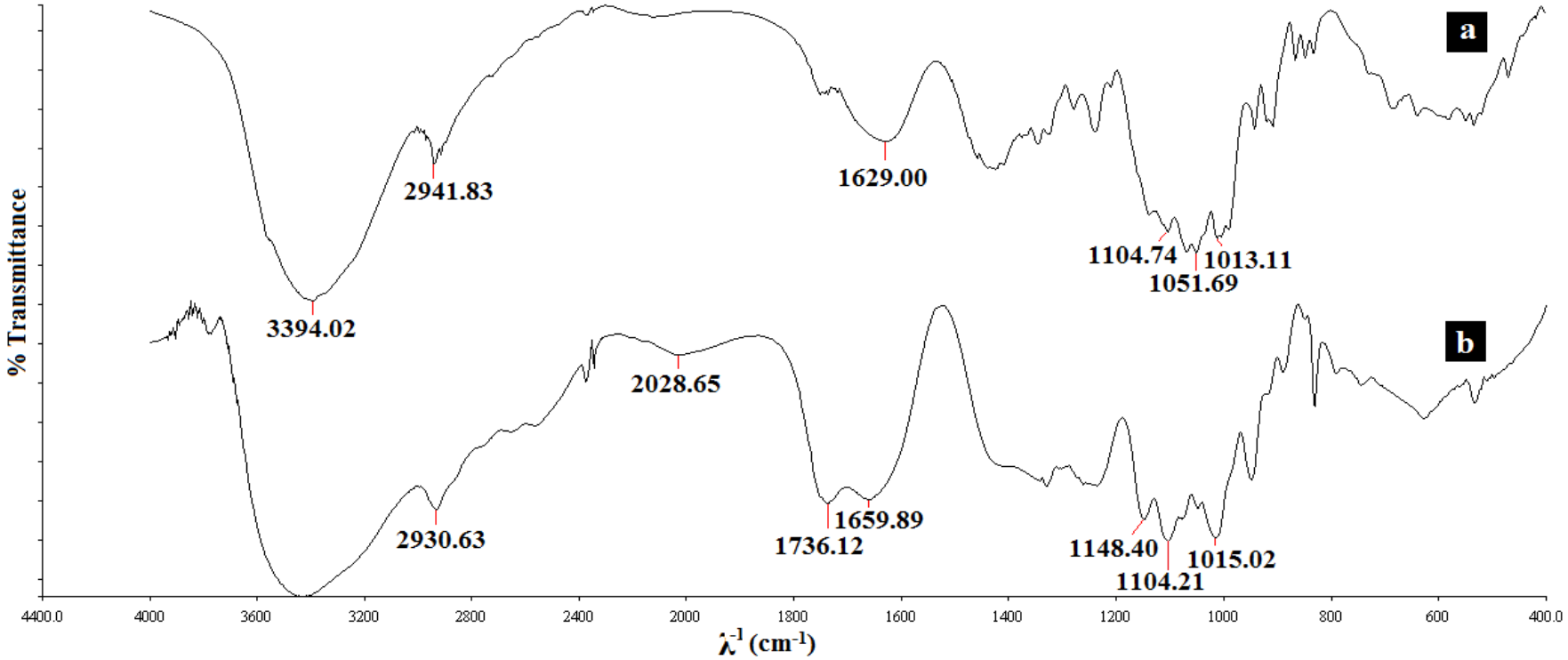


Figure 2.3 FT-IR spectra of CP **(a)** and MCP **(b).**

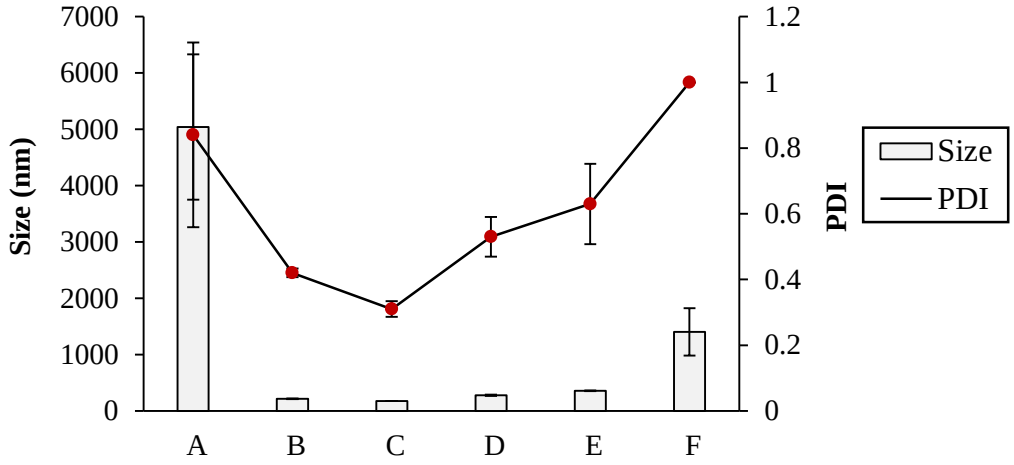
The wide peaks at approximately 3440 cm^{-1} and 2900 cm^{-1} in both spectra are indicative of secondary hydroxyl carboxylic groups, respectively. There is comparatively lower intensity at about 1700 cm^{-1} in CP compared to identical peak in the MCP, which is indicative of a lower degree of methoxy substitution of pectin in CP (Urias-orona et al., 2010). A distinctive absorption band was observed at 1015 cm^{-1} in the MCP spectra and not apparent in the CP spectra, which is consistent with an increase in the D-galacturonic acid sugar units, therefore, we can conclude that the modification procedure yielded the desired galactan moiety.

2.4.2 MCP-chitosan nanoparticle formulations

The use of MCP and chitosan as polymers increases the mechanical strength and hydrophobicity of the nano-formulation, which is likely to lower the rate and extent of drug release from the NP to the surrounding dissolution medium (Chuah et al., 2011). It is believed that the amino group of chitosan is optimally protonated at pH 5 (Andriani et al., 2015). An increase in chitosan concentration from 1 mg/ml to 2.5 mg/ml produced smaller sized nanoparticles (Figure 2.4) and the zeta potential increased concurrently (Figure 2.5). As the chitosan concentration was increased, more of the protonated amino groups of chitosan molecules become available to coacervate with MCP and cross-link with STPP, which is manifested in the consequent increase in the surface charge from +17.1 mV to +35.7 mV. The various orders of addition used altered the size, PDI and zeta potential of the formed particles.

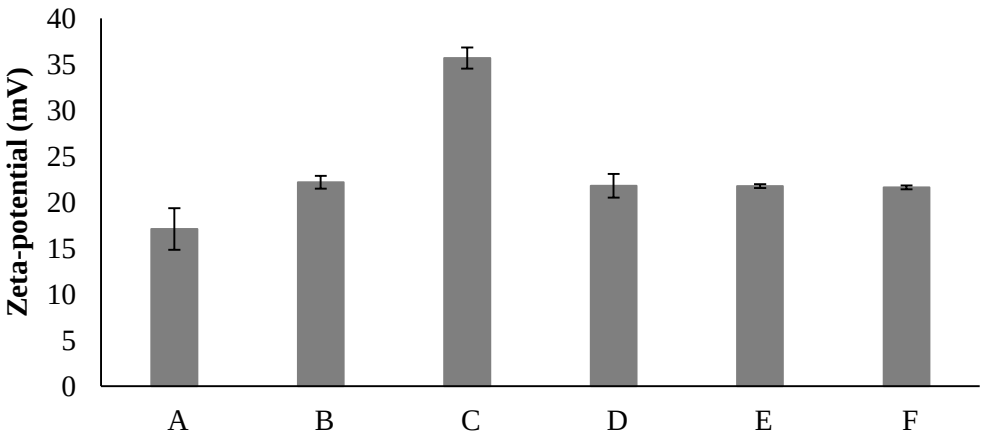
An increase in size and decrease in zeta-potential was observed in sample C (MCP + chitosan + STPP) to sample F (MCP + STPP + chitosan), accordingly. Basically, in Sample F, when STPP was firstly added to the MCP solution

followed by the addition of chitosan solution, the resultant mixture produced microparticles as opposed to nanoparticles. This can be attributed to the negatively charged carboxylic group of MCP and the phosphate group of STPP that repel each other and hence forming excessive inter- and intra-droplet crosslinking. This scenario favours the formation of larger particles and irregular particulate aggregates upon addition of the positively charged chitosan. There is only a few free MCP or STPP to either coacervate or crosslink with the chitosan so that excess of the chitosan particles remained suspended within the medium. This also contributed to high PDI values. As particle size and zeta-potential play important roles in nanoparticulate formulation from a stability and drug delivery point, sample C was selected for the preparation of the coated- curcumin nanoparticles due to the comparatively smaller size and higher zeta potential. Therefore, the MCPCNPs were prepared by ionic gelation, in which 10 ml aliquot of the MCP solution was added to an amber-coloured beaker containing 120 µl of the curcumin solution with vigorous stirring, followed by drop-wise addition of 10 ml of chitosan solution and then drop-wise addition of 15 ml of STPP. Lastly, the mixture was stirred for a further 20 min at 500 rpm at room temperature and the MCPCNPs were collected by centrifugation at 8000 rpm for 20 min, washed twice with distilled water and stored till further use.



(A) and **(B)** 1.0 mg/ml and 1.5 mg/ml of chitosan was used respectively. **(C)** is the control, while **(D)**, **(E)** and **(F)** different orders of addition

Figure 2.5 Size and PDI obtained from the different techniques followed



A) and **(B)** 1.0 mg/ml and 1.5 mg/ml of chitosan was used respectively. **(C)** is the control, while **(D)**, **(E)** and **(F)** different orders of addition

Figure 2.4 Zeta-potential from the different formulation techniques

2.4.3 Physical characterisation of MCPCNPs

2.4.3.1 The hydrodynamic size and surface charge of MCPNPs

In the present study, the NPs were formed from coacervation between the negatively charged carboxylic groups of the MCP and the positively charged amino group of chitosan, followed by the crosslinking between the negative phosphate groups of STPP and the amino groups of chitosan (refer to Figure 2.6), while encapsulating curcumin within the polymeric matrices formed in the process.

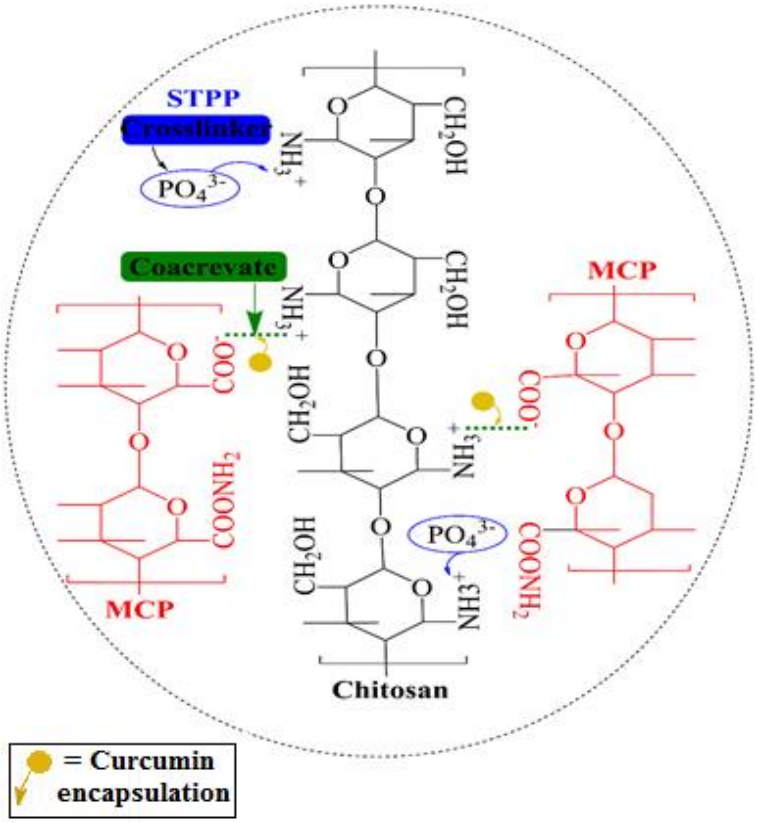


Figure 2.6 Schematic representation of the MCPCNP formation

Such composite nanoformulation comprising of pectin and chitosan has been reported to increase the mechanical strength and hydrophobicity of the formulation, which favours sustained drug release (Wong et al., 2011). There was a slight increase in the size of the nanoparticles, from 174 nm (± 0.889) to

178 nm (± 0.896), with the incorporation of curcumin. This is attributable to the steric effects by curcumin within the polymer chain domains during coacervation between MCP and chitosan, which impedes the process. Moreover, the zeta potential values of the nanoparticles increased slightly from +31.4 mV (± 0.793) to +35.7 mV (± 1.418) after the addition of curcumin. This increase in the surface charge is directly related to the increase in size, whereby, bulkier particles hinder the knitting effects of STPP with the free $–NH_3^+$ groups of chitosan. This leaves relatively more of the free $–NH_3^+$ in the nanoparticle matrix, with a consequent increase in zeta potential.

2.4.3.2 The morphology of MCPCNPs

The morphology of the MCPCNPs was observed using SEM and results are shown in Figure 2.7. The image revealed well-distributed and spherically shaped nanoparticles, consistent with the size observation by the DLS studies.

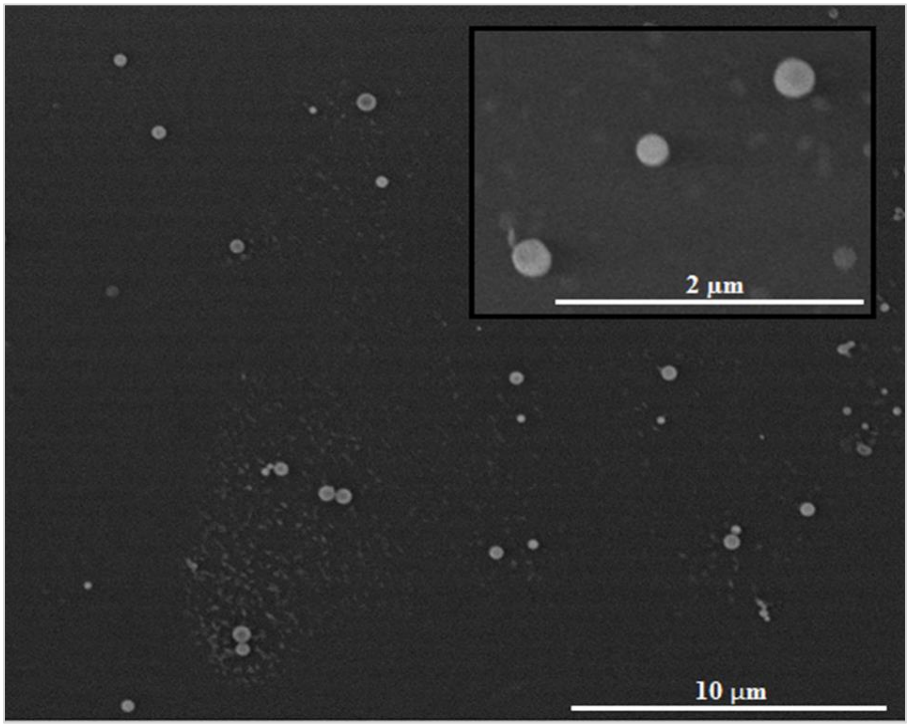


Figure 2.7 SEM image of the MCPCNPs

2.4.3.3 FTIR spectra

The FTIR spectra of the MCPCNPs and the raw materials are presented in Figure 2.8. The disappearance of the amine group of chitosan at 1650.68 cm^{-1}, the phosphate group of STTP at 1211.47 cm^{-1} and the D-galacturonic acid peak of MCP at 1015.02 cm^{-1} in the MCPCNPs spectrum can be attributed to the crosslinking effects of chitosan with MCP and STPP, respectively. The relatively sharper peaks at 3448.22 cm^{-1} in the spectra of the MCPCNPs and MCP-chitosan nanoparticles (NPs without curcumin) indicate a higher density of hydroxyl (-OH) moieties. The intense peaks at 1560.31 cm^{-1} and 1412.57 cm^{-1} in both spectra (MCPCNPs and MCP-chitosan NPs) corresponds to the N-H deformation, known as "amide II band," due to the interaction between the carboxylic groups of MCP and amino groups of chitosan. The only observed difference between the MCPCNPs spectrum and that of the MCP-chitosan NPs is the presence of the peak at 1638.92 cm^{-1} in the former, which is consistent with the presence of enol group moieties of curcumin, thus ascertains the incorporation of curcumin in the formulation.

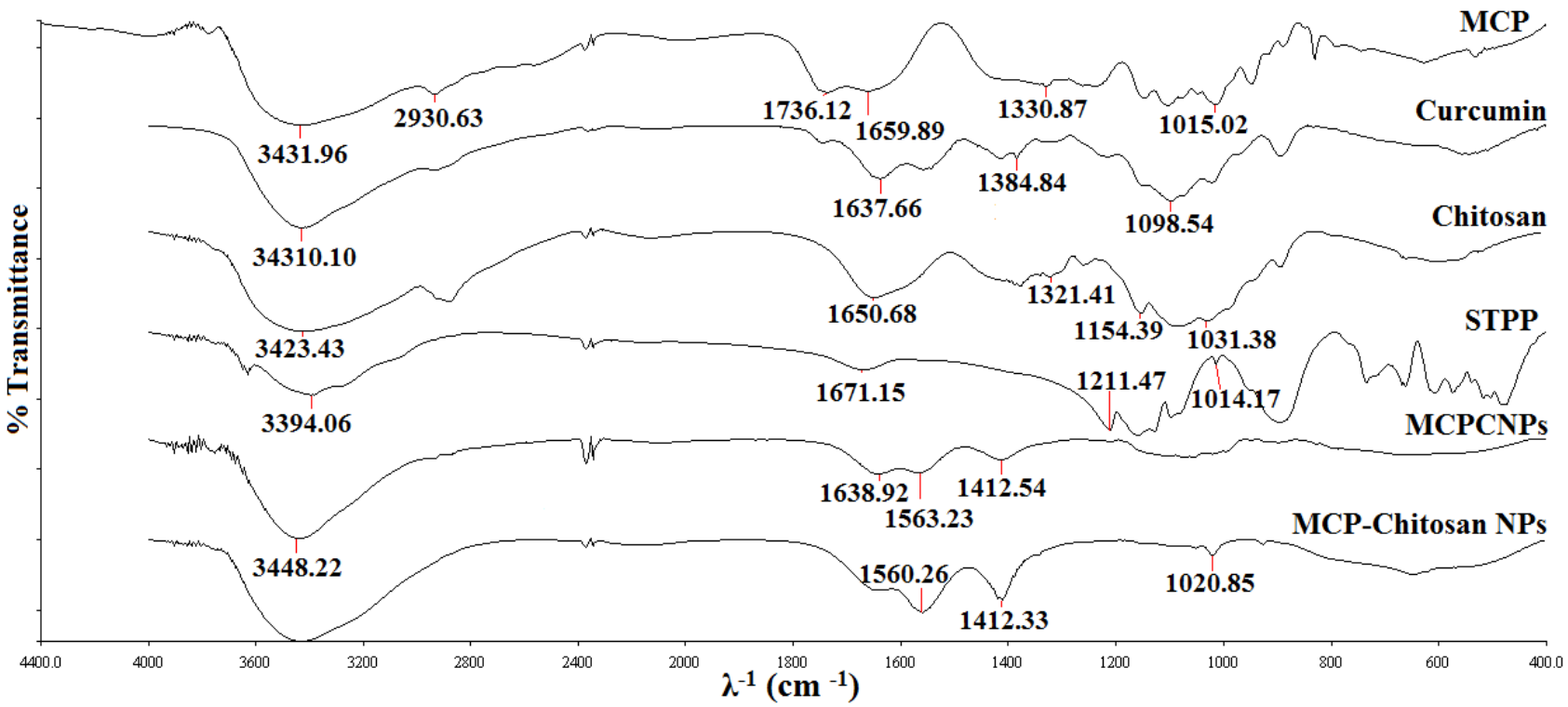


Figure 2.8 FTIR spectra of chitosan, STPP, MCP, curcumin, MCP-chitosan nanoparticles and MCPCNPs.

2.4.3.4 Thermal analyses

Figure 2.9 presents the thermal responses from the MCPCNPs and the raw materials. The melting points of STPP, chitosan and MCP were found to be at 117.2 °C, 112.6 °C and 101.6 °C, respectively. Curcumin exhibited a melting peak at 178.8 °C, however this peak was not observed in the thermogram of the MCPCNPs. There were two melting episodes displayed by the MCPCNPs at 56.9 °C and 128.8 °C. The peak appearing at 128.8 °C is mainly attributed to chitosan. The shift in the melting point of chitosan is due to its interactions with STPP and MCP as part of the crosslinking, whilst the endothermic at 56.9 °C is manifestation of complexes within the MCPCNPs. These complexes are formed from possible weak van der Waal type interactions between the MCP and curcumin thereby destroying the specific structural arrangement of the particular functional head group regions (Chen et al., 2012).

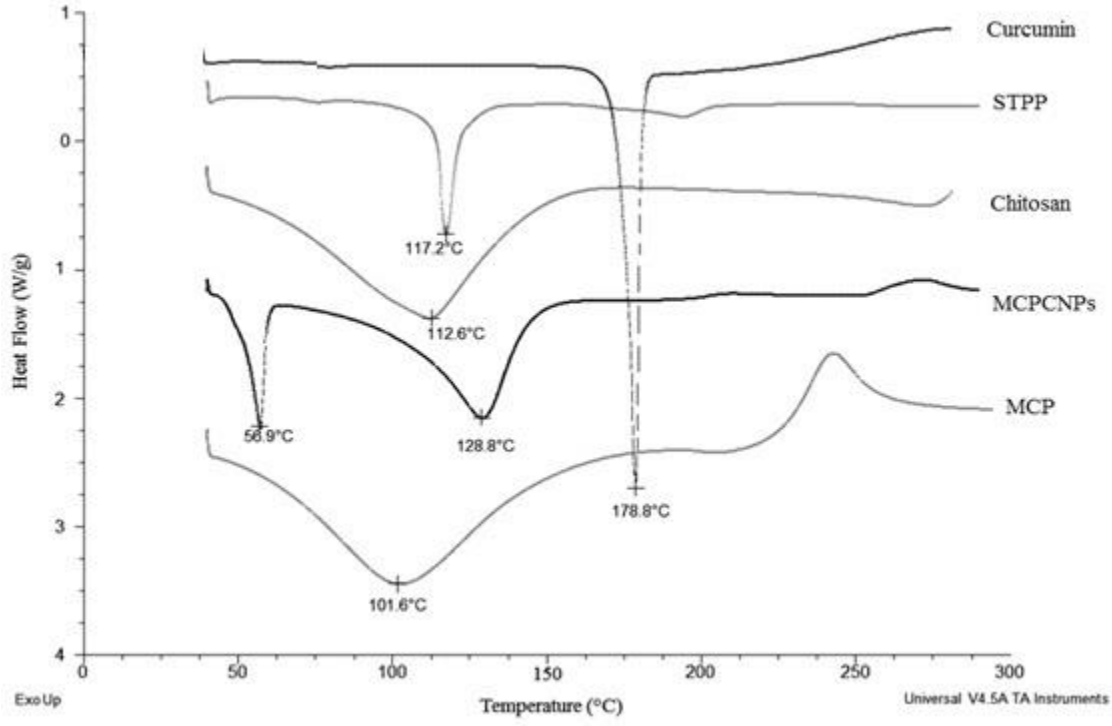


Figure 2.9 DSC profiles of chitosan, STPP, MCP, curcumin and MCPCNPs

Interestingly, the sharp curcumin peak at 178 °C is completely lost in the thermogram of the nanoparticles, affirming the presence of curcumin within the particles in amorphous conformation. These suggestions are in line with karri et al. (Karri et al., 2016) in which curcumin exhibited a characteristic endothermic peak at 182 ◦C, while the curcumin-chitosan nanoparticles presented no peak in this region and only a peak at 125 ◦C was observed. They attributed this to the fact that the crystalline form of curcumin is converted into amorphous form, while the latter melting point corresponds to the chitosan matrix into which curcumin is incorporated (Karri et al., 2016). The MCP peaks disappear in the MCPCNPs thermogram due to the disruption of their joint intermolecular hydrogen bonds by curcumin molecules.

2.4.4 ToF-SIMS analysis of MCPCNPs

ToF-SIMS is a highly sensitive surface analytical technique which provides useful information on the molecular structure and composition of the surface chemistry in pharmaceutical systems (Barnes et al., 2011). Spectra comparison was carried out after a normalization of the intensity, proportionally to the total intensity of each spectrum. Raw materials were used as reference samples in order to select characteristic fragments that could be compared with the fabricated nanoparticles. Characteristic peaks were chosen as peaks that showed a high relative intensity of the raw materials with no significant peaks detected for other materials within the same unit mass. Table 2.1 displays the negative secondary ion peaks determined to be the characteristic peaks from the raw materials used in the fabrication of the MCPCNP.

Table 2.1 Characteristic negative fragments of raw materials used for MCPCNPs fabrication

Component	Peak mass for negative ion (m/z)	
Chitosan		CHO_2 (45)
	C_2H_2O (43)	C_2H_4NO (58)
MCP	$C_{11}H_{21}O_7$ (265)	$C_2H_3O_2$ (59)
	$C_{18}H_{31}O_4$ (311)	$C_3H_3O_2$ (71)
Curcumin	$C_{20}H_{17}O_5$ (337)	
	$C_{21}H_{19}O_6$ (367)	
	PO_2 (63)	
STPP	NaP_2O_5 (165)	
	NaP_2O_6 (63)	

As can be seen from the table, both MCP and chitosan shared the same peak fragments with some extra peaks detected from MCP. The peak fragments obtained from chitosan were in accordance with those observed by D'almeida et al. (D'almeida et al., 2017) and Rodrigues et al. (Rodrigues et al., 2012) . A search in the literature indicates that MCP has not been studied on ToF–SIMS, therefore characteristic peak fragments were determined by acquiring the high mass resolution spectra from a pure MCP deposited onto a silicon wafer. The TPP spectrum consisted of three peaks, however only PO_2 m/z was reported (Al-Qadi et al., 2011). The peak fragment for curcumin (367 m/z) and a specific peak fragment (337 m/z) was detected (J. Lee et al., 2013). Typical peak fragments of chitosan, MCP and STPP were detected in the MCPCNPs spectra, which are $C_2H_3O_2$, C_2H_2O and PO_2 (Figure 2.10), respectively.

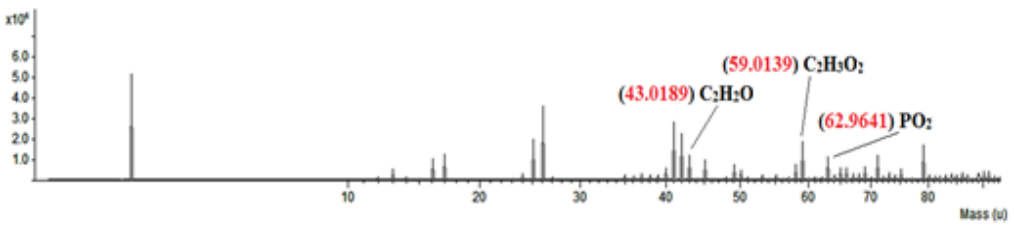


Figure 2.10 Negative ion mass spectra obtained by ToF-SIMS analysis of MCPCNPs between 0 and 80 mass (u).

As shown in Figure 2.11 the mass spectrum of MCPCNPs revealed a peak at 337.2 m/z which is also found in the spectrum for curcumin, albeit at a lower intensity and slightly shifted in the former. The low peak intensity attributable to curcumin is likely due to the fact that TOF-SIMs analysis is based on the molecular fragments obtained from surface scans after bombarded with primary ions. Therefore, curcumin residing in the deeper pockets of the nanoparticles are not accounted for. The shift in peak intensity of curcumin in the nanoparticles suggests that some form of chemical association between curcumin and other components might have occurred. Since the carrier system forms a matrix comprising of the chitosan-modified pectinate composite held in place by the cross-linker (STPP), and fragments ascribable to curcumin located on the surface of the nanoparticles, we can deduce that curcumin is distributed homogeneously within the chitosan-pectinate composite matrix.

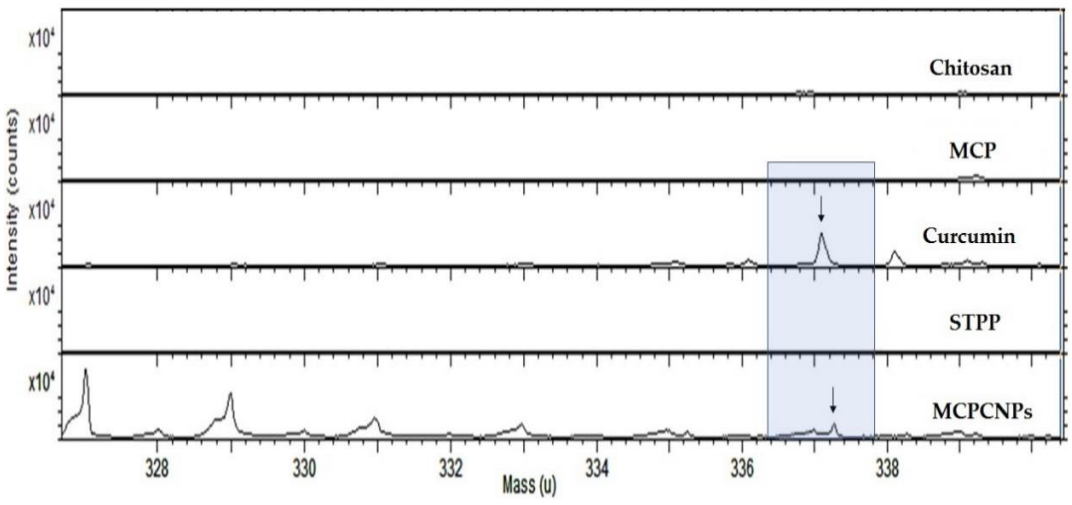


Figure 2.11 Negative ion mass spectra obtained by ToF-SIMS analysis of raw materials and MCPCNPs between 327 and 339 mass (u)

2.4.5 Validation of HPLC method

Calibration curve from standard curcumin solution with a correlation coefficient (R^2) of 1.0, which confirms response linearity within the concentration range of 0.625-10 µg/mL, is shown in Figure 2.12. The peak for the curcumin standard samples appeared at the retention time of about 5.62 minutes and representative chromatograms of curcumin at concentrations 0.625 µg/ml and 10 µg/ml are displayed in Figure 2.13.

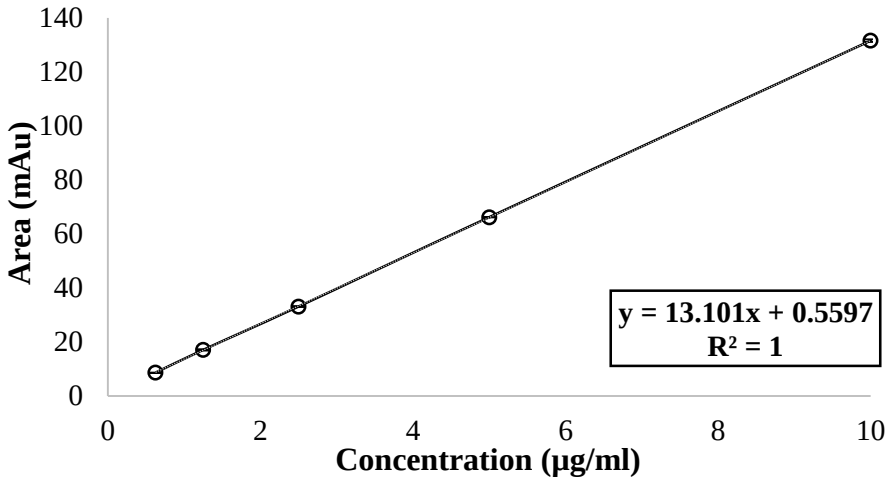


Figure 2.12 Standard calibration curve of curcumin

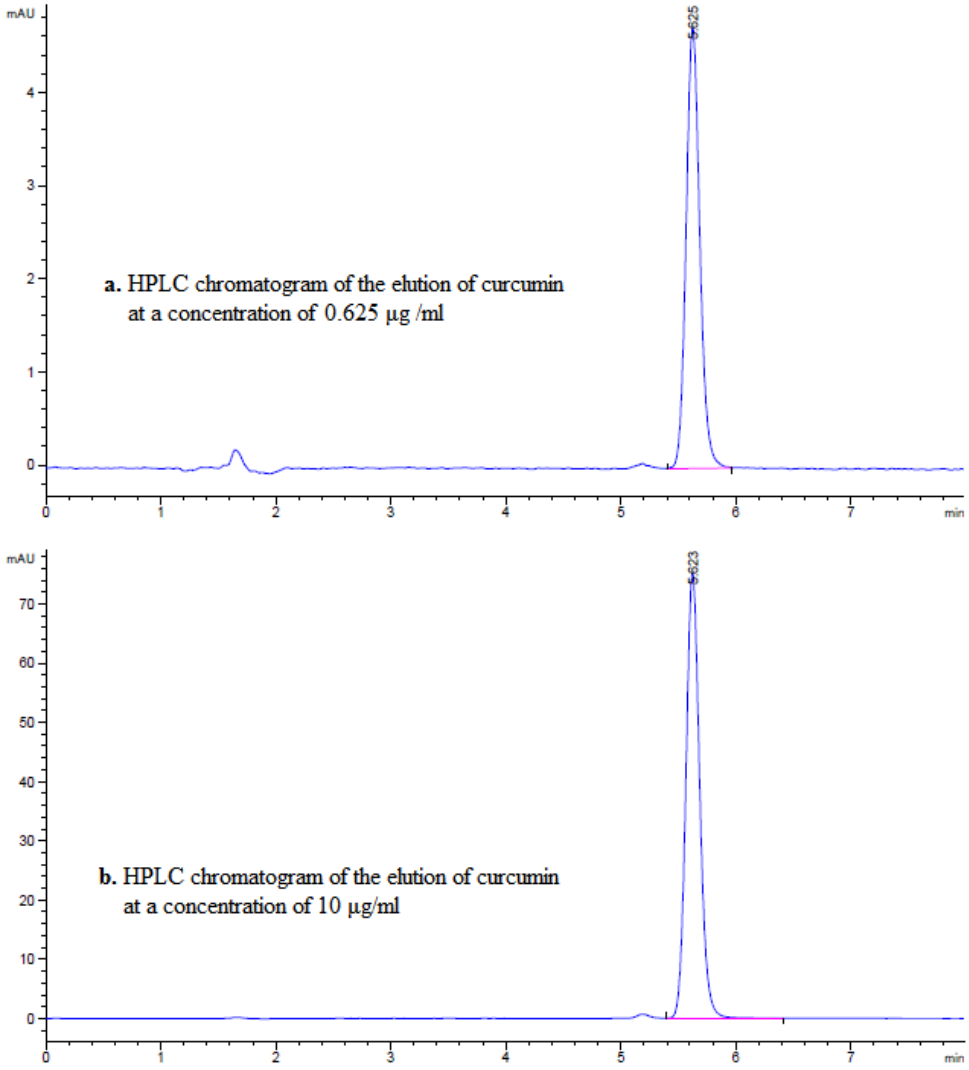


Figure 2.13 Representative chromatograms of curcumin at concentrations 0.625 µg/ml and 10 µg/ml

The intra- and inter-day precision and accuracy were evaluated by analysing three replicates at three different concentration levels of curcumin in methanol, i.e., 0.625, 50 and 100 µg/mL. The intra-day precision of the assay was determined by calculating the relative standard deviation for the analysis of curcumin standards in three replicates. While, the inter-day precision was obtained by the analysis of three replicates curcumin standards on three consecutive days. The accuracy was calculated as

$$Accuracy = \frac{\text{mean concentration found}}{\text{concentration taken}}\ x\ 100 \qquad (2.3)$$

Accuracy and precision data for intra- and inter-day assay for curcumin samples are presented in Table 2.2. The assay values on both the occasions (intra- and inter-day) were found to be within the accepted variable limits defined by FDA guidelines for bioanalytical method validation.

The percentage relative standard deviation (% RSD) were all below 1 %. The accuracy of the method was also assessed, and they were all around 100 %. The limit of detection (LOD) and limit of quantification (LOQ) were calculated from equations (2.4) and (2.5) and found to be 0.048 μg /ml and 0.144 μg /ml, respectively.

$$LOD = 3.3\ \times \frac{\text{Standard deviation of low concentration}}{\text{Slope of curve}} \qquad (2.4)$$

$$LOQ = 10\ \times \frac{\text{Standard deviation of low concentration}}{\text{Slope of curve}} \qquad (2.5)$$

Table 2.2 Precision and accuracy of the HPLC method

	Accuracy (% error)		**Precision** (% RSD)	
Concentration (μg/ml)	***Intra-day*** (n=3)	***Inter-day*** (n=3)	***Intra-day*** (n=3)	***Inter-day*** (n=3)
100	101.36	104.94	0.26	0.45
50	107.04	107.64	0.67	0.28
0.625	100.70	101.09	0.76	0.91

2.4.6 Encapsulation efficiency and drug loading

Encapsulation involves application of technologies in which an active agent is entrapped within a material system that can release its payload at controlled rates under specific conditions (Nedovic et al., 2011). This process ensures controlled release and shields labile compounds from harsh conditions. Encapsulation efficiency and drug loading are two significant parameters of nanomedicines. They are both basically dependent on the mass of the drug in feed, the fabrication method in use, the physicochemical characteristics of the component polymers (such as their hydrophilicity/hydrophobicity and solubility) and other experimental conditions (Shen et al., 2017; Shin et al., 2013). Figure 2.14 shows the encapsulation efficiency and drug loading of the MCPCNPs vs. curcumin-containing NPs prepared with CP (CPCNPs).

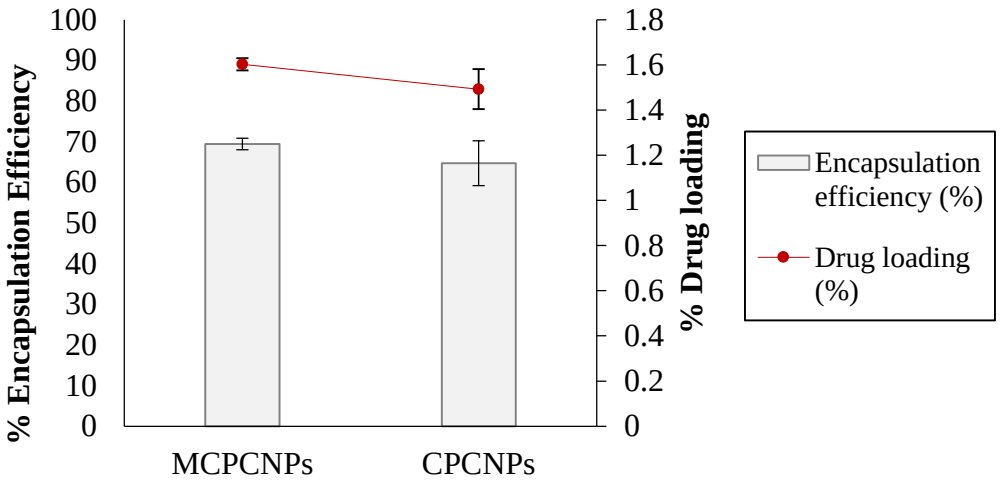


Figure 2.14 The encapsulation efficiency and drug loading of curcumin in MCPCNPs and CPCNPs

The encapsulation efficiency and drug loading of MCPCNPs were 69.43 ± 1.11% and 1.60 ± 0.03%, respectively, which are about 5% and 0.11% higher than that of CPCNPs, correspondingly. This slight increase is probably due to the lower molecular weight of the modified citrus pectin caused by the removal

of neutral sugars during the modification process (Venzon et al., 2015). Usually, z-potential increases along with the decrease of the molecular weight, therefore shorter chains mean more carboxylic acid end groups available (Palacio et al., 2011) to react with chitosan, allowing more curcumin to diffuse and encapsulate into the chitosan-MCP matrix. Moreover, the encapsulation efficiency obtained in the present study is higher than those in a number of reports where pectin-chitosan matrix was utilised for drug encapsulation. For example, Hwang S.W. and Shin J. W. reported an encapsulation efficiency of 62.9 % in curcumin-loaded chitosan-pectin microparticles (Hwang and Shin, 2018). In another study by Maciel et al. in which a polyelectrolyte complex system of chitosan-pectin nano- and microparticles was developed to encapsulate the hormone insulin, an encapsulation efficiency of ≈ 62 % was reported (Maciel et al., 2017). However, the drug loading obtained in the present study is lower than those from several studies, most probably due to the low space capacity of the carrier material (Shen et al., 2017).

2.4.7 Stability studies

The stability of a drug in a dosage form with regard to storage is relevant because it discerns the possible shelf life of that specific formulation (Wilson et al., 2010). The present experiment was conducted to evaluate the impact of storage, in a refrigerator (4 ^{0}C), on the physical properties of the MCPCNPs. Figures 2.15 and 2.16 display the changes in properties over day-21 period. Figure 2.15 shows gradual increase in size of the MCPCNPs over 21 days (from 178 ± 0.896 to 254.7 ± 3.826 nm). This can be attributed to Ostwald's ripening, whereby smaller particles, which tend to have high surface area to volume ratio, provide high surface energy, agglomerate and deposit on larger particles in order to minimize their surface energy (Thanh et al., 2014). This phenomenon is also supported by the SEM images presented in Figure 2.16.

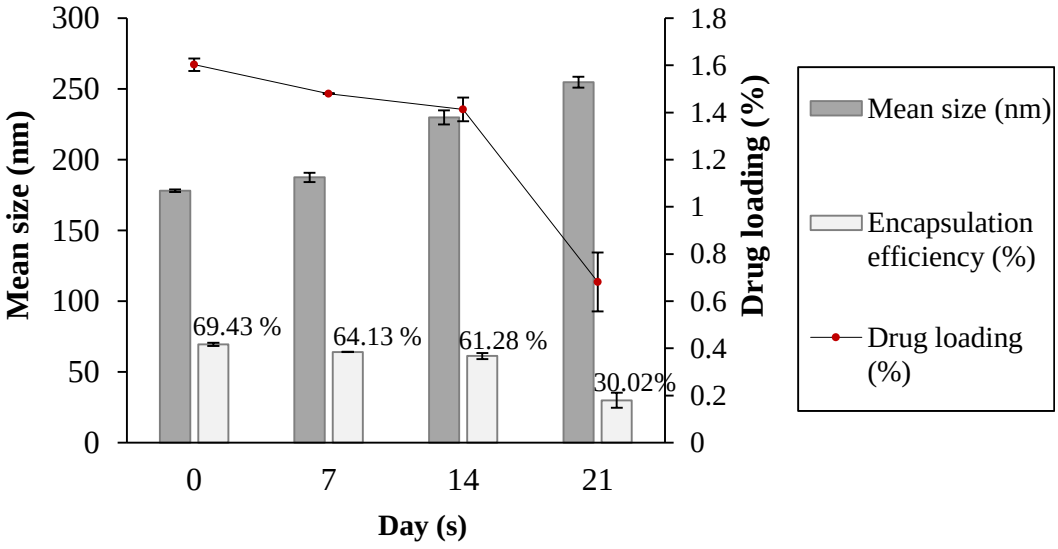


Figure 2.15 Mean particle size, encapsulation efficiency and drug loading values of MCPCNPs at days 0, 7, 14 and 21 during storage at 4 ^{0}C

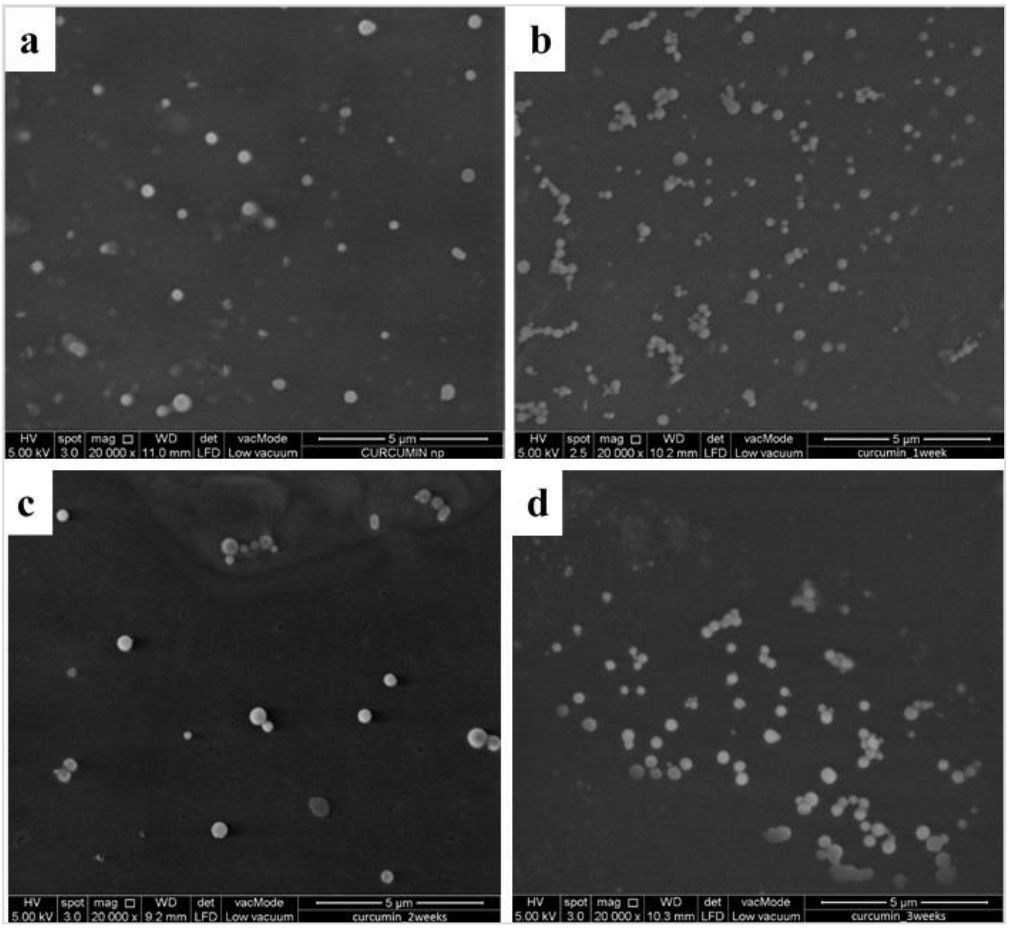


Figure 2.16 Morphology of MCPCNPs at day 0 **(a)**, 7 **(b)**, 14 **(c)** and 21 **(d)** during storage at 4 ^{0}C

The images of the freshly prepared NPs on day 1 (Figure 2.16 (a)) were spherically shaped and well-dispersed with approximate mean particle size of 180 nm. However, after storage for 21 days, the SEM images showed noticeable particle aggregation and significant increase in the approximate particle size to 260 nm as shown in Figure 2.16 (d). The results are consistent with the findings by Hussain A. and Sahudin S. on storage of nanoparticles of a similar size range, albeit pectin was not part of the polymer matrix (Hussain and Sahudin, 2016). The results of storage on the encapsulation efficiency and loading capacity of curcumin in the nanoparticles after 21 days are shown in Figure 2.15. The data demonstrate a slight decrease in the encapsulation efficiency and drug loading

of the MCPCNPs from 69.43 ± 1.17 %, 1.60 ± 0.03 % (day-0) to 61.28 ± 2.17 %, 1.41 ± 0.05 % (day-14), respectively. However, there was a significant decrease on Day-21, where the encapsulation efficiency and dug loading fell to 30.02 ± 5.42 %, 0.68 ± 0.13 %. Usually the degradation of polymeric nanoparticles is affected by the particle size, and larger particles are hypothesized to contribute to faster polymer degradation (Panyam et al., 2003). This is due to the fact that the polymer matrix of larger particles increases the time of release due to the greater distance and may also cause autocatalytic degradation of the polymer material (Singh et al., 2009). Therefore, it can be concluded that as the particle size increases, the particle is more prone to polymer degradation, which causes leakage of the drug from the polymer matrix, consequently decreasing the drug encapsulation efficiency and capacity.

Due to the significant decrease of drug encapsulation efficiency and loading of more than 50% during storage, the shelf-life stability studies were discontinued at day 21. These findings reflect the low storage stability of MCPCNPs. Therefore, the NPs may have to be used within 2 weeks of fabrication or stored in dry form and reconstituted prior to use.

2.5 Conclusion

MCPCNPs have been successfully formulated and optimized in terms of desirable physical properties. The NPs were characterised in terms of size, PDI, zeta potential, morphology, chemical composition and the physical state of curcumin. The encapsulation efficiency was determined, and the stability was investigated. The MCPCNPs appeared to be unstable for storage up to 21 days when in solution. Moreover, curcumin was confirmed to be distributed homogeneously in the chitosan-pectin composite matrix via TOF-SIMS. These

data present us with the incentive for further investigation in terms of swelling behaviour, curcumin release profile and mucoadhesion at relevant physiological conditions. These would be discussed in detail in Chapter 3.

Chapter 3 Evaluating the mucoadhesion propensity and release profile of curcumin from MCPCNPs

3.1 Introduction

There is growing research interest in exploring mucoadhesion of orally administered dosage forms as a means to improving systemic bioavailability of drugs through delayed gastrointestinal transit (Smart, 2005). This is particularly true with nanoparticulate dosage forms and is borne on the fact that prolonged contact with the gastrointestinal epithelia would most likely improve the chances of particulate uptake across the mucosa (Mazzarino et al., 2012). Furthermore, sustained drug delivery can be attained by utilisation of appropriate polymers as carrier systems. Polymers such as chitosan and pectin exhibit mucoadhesive properties and have been widely explored in the design of mucoadhesive dosage forms. They can be used complimentarily in colon-targeted delivery due to their opposing responses to extremes in gastrointestinal pH. Nanoparticles formulated using chitosan and pectin possess strong mucoadhesive properties with the colon due to their ability to form hydrogen bonds with suitable substrates within the mucosa, where their cationic/anionic moieties flexibly penetrate the mucus network (Shaikh et al., 2010). It is worth noting that various synthetic polymers such as polylactic acid, polyadipic acid and cellulose derivatives have also been explored as potential mucoadhesive drug delivery systems (Ways et al., 2018), however, the use of natural polymers in drug delivery has attracted interests due to toxicity concerns associated with synthetic polymers. Furthermore natural polymers are associated with lower production costs (Kavitha et al., 2011).

Therefore, the aim of this chapter is to probe the interaction and behaviour of mucin from porcine stomach with the fabricated MCPCNPs in Chapter 2, under gastrointestinal simulated conditions, using NTA, SEM, electrophoretic light

scattering (ELS) and other relevant techniques. The swelling behaviour and release profile of curcumin from the MCPCNPS will also be examined.

3.2 Materials

Curcumin was purchased from Fluka, (U.S.A). Chitosan (low molecular weight, de-acetylated chitin), sodium tripolyphosphate and phosphate buffered saline tablets (PBS) were purchased from Sigma–Aldrich, USA. Low methoxyl citrus pectin (DE lower than 50) was bought from Genu, CPKelco® (Limeira- SP, Brazil). Trehalose (Nacalai Tesque, Japan) was employed as the cryoprotectant. Mucin type III from porcine stomach (Sigma Aldrich, USA) was utilised for mucoadhesive studies. Micro-BCA protein assay kit (Thermo Scientific, USA) was operated for the colorimetric assay. Acetic acid (R&M chemicals, UK), hydrochloric acid (R&M chemicals, UK), sodium hydroxide (Merck, Germany), sodium acetate (Sigma Aldrich, USA) and potassium dihydrogen phosphate (Merck Millipore, Germany) were used for buffer preparations.

3.3 Methods

3.3.1 MCPCNPs matrix swelling studies

The swelling propensity of the MCPCNPs matrix at physiologically relevant pH of the gastrointestinal tract was studied at pH 1.2 (0.1 M HCl), 5.5 (0.1 M sodium acetate buffer) and 7.0 (0.1 M phosphate buffer). Briefly, 20 ml of the MCPCNPs suspension was added to respective pH solution and then mixed using a rotary shaker (WiseCube®, Witeg Inc., Germany) at 180 rpm. At predetermined time intervals (0 h, 30 min, 1 h, 2 h, 4 h and 6 h) the z-average of the particles in the respective solutions were measured by means of DLS. The swelling capacity of the MCPCNPs was calculated as:

$$Swelling\ capacity\ (\%) = \frac{Z-average \text{ of MCPCNPs at time (t)} - \text{Initial z-average of MCPCNPs}}{\text{Initial z-average of MCPCNPs}} \times 100$$

(3.1)

3.3.2 Mucin adsorption studies

The propensity of the MCPCNPs to adhere to mucus was determined as the amount of mucin adsorbed by the MCPCNPs dispersed in standardised mucin solutions. The amount of mucin adsorbed was also studied as a function of pH representing relevant anatomical sections of the gastrointestinal tract: pH 1.2, pH 5.5, pH 6.25 (0.1 M phosphate buffer) and 7.0. Specifically, 2 ml of the MCPCNPs suspension was mixed in the mucin solutions, vortexed for few seconds and then rotated at 100 rpm maintained at 37 °C for 1 h. The suspension was centrifuged at 4000 rpm for 1 h to separate the free mucin followed by the addition of micro-BCA reagent and then incubation at 37 °C for 2 h and then finally measuring the absorbance at 562 nm. The quantity of mucin in the supernatant was determined from a standard calibration curve treated in a similar way and mucin adsorption (%) was calculated using the equation below:

$$Mucin\ adsorption\ (\%) = \frac{\text{Amount of mucin added} - \text{Amount in supernatant}}{\text{Amount of mucin added}} \times 100 \qquad (3.2)$$

3.3.3 Zeta Potential Measurements

A time-dependent zeta-potential measurement of the MCPCNPs matrix in pH 1.2 and 7.0 were studied after a 30-fold dilution in the respective medium. At predetermined time intervals (0 h, 2 h, 4 h and 6 h) the zeta-potential of the particles was measured using Laser Doppler anemometry (Zetasizer Nano Series, Malvern Instruments Ltd., UK).

The magnitude of mucoadhesion of the nanoparticles with mucin was determined by measuring the changes in the zeta-potential after interaction at

10, 50, 100 and 150 µg/mL of mucin in pH 1.2 and 7.0. Prior to the measurement, the nanoparticle-mucin suspension was vortex-mixed for 1 min followed by incubation at room temperature for 30 minutes.

3.3.4 Morphological analyses

An SEM image of 25 µl of MCPCNPs incubated in 25 µl of 50 µg/mL mucin solution at pH 1.2 and pH 7.0 was obtained on a JEOL 7100F SEM after placing the mixed samples over a carbon tape and air-drying it overnight. The samples were then coated with iridium using a sputter coater in a vacuum. The samples were air-dried for another 24 h before viewing.

3.3.5 AFM

The topography of nanoparticles exposed to 50 µg/mL of mucin solution in pH 7.0 was observed on a Bruker AFM D3100. A drop of the mixture was placed on clean mica substrate and air-dried overnight before viewing. Topographic images were obtained using tapping mode with silicon tip cantilever with a spring constant of 0.7 N/m and a frequency of 150 kHz. All measurements were performed at room temperature.

3.3.6 NTA

The size of the nanoparticles before and after interaction with mucin was measured using the NTA system (NanoSight LM10 Ltd, UK) equipped with LM 14 base unit with a 405-nm blue laser. The size of nanoparticles dispersed in 150 µg/mL mucin in pH 7.0 was also measured. The samples were injected into the sample chamber with sterile syringes (BD Plastipak, Spain). The data was analysed using the NTA 2.2 software. The samples were measured for 30s each and the videos recorded with manual shutter and gain adjustments. All

measurements were performed in triplicate and data are expressed as mean (SD).

3.3.7 Mucoadhesion based on everted caecal sac

A further mucoadhesion study was conducted on rat caecal tissue in order to validate the mucin adsorption studies described above. In this method, adapted from Chuah et al. (Chuah et al., 2014), Sprague-Dawley male rats* were sacrificed in carbon dioxide (CO_2) chamber. The caecum was excised and flushed with ice cold phosphate buffer and everted using a glass rod and tweezers. One ligature was placed at the end of the segment and the sac was filled with 1 ml McCoy's media through the open end and then tightly tied. The sac was then placed in a centrifuge tube containing 60 mg MCPCNPs dispersed in 5 ml McCoy's media and then subjected to gentle shaking at 37 °C for 30 min. Finally, the sac was removed and the tube was centrifuged to retrieve the unattached MCPCNPs. A brief outline is portrayed in Figure 3.1.

$$Attachment\ of\ MCPCNPs\ to\ caecam\ (\%) = \\ = \frac{\text{Weight of MCPCNPs added} - \text{Weight of unattached MCPCNPs}}{\text{Weight of MCPCNPs added}} \times 100$$

* *the sacrificed rats were provided from a separate investigation by Professor Ting Kang Nee from which caecal content was used so that no rat was sacrificed solely for the purpose of this investigation.*

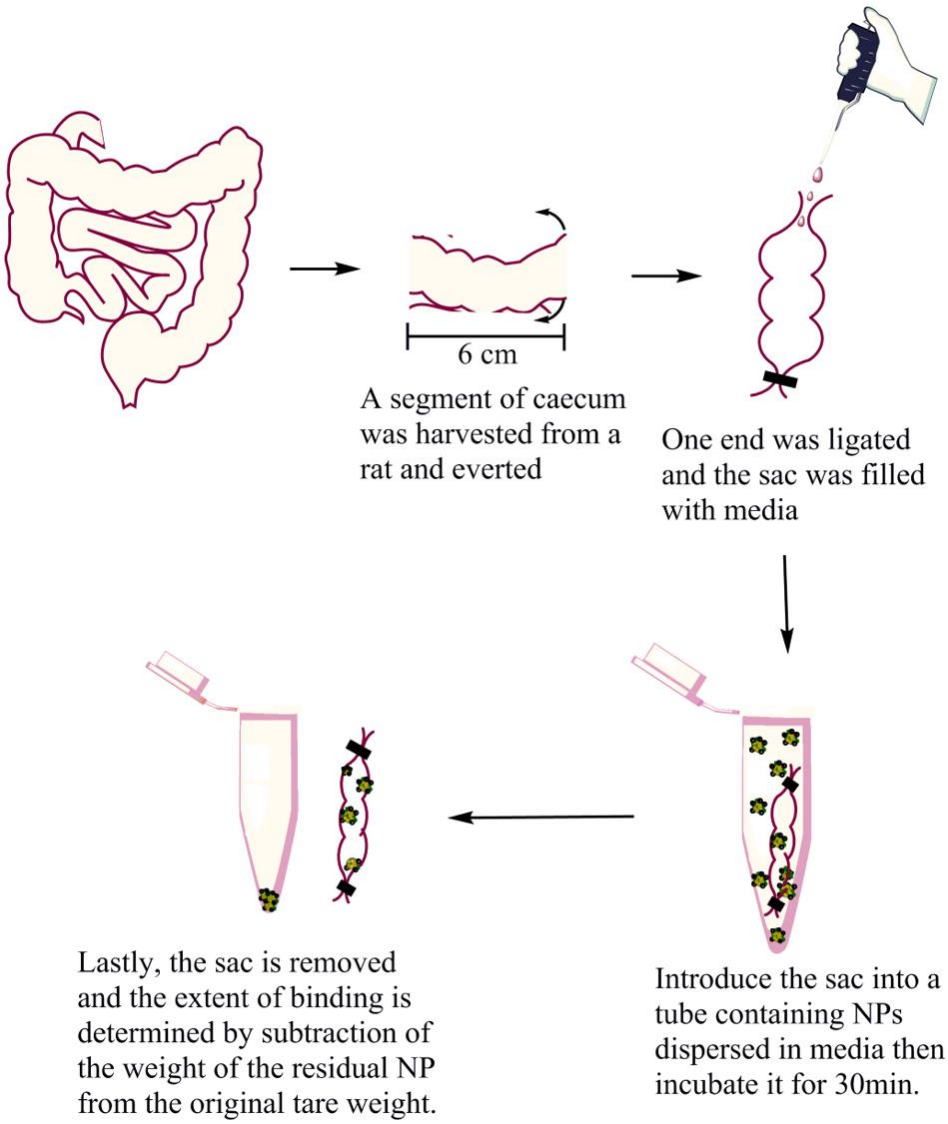


Figure 3.1 Illustration of the everted intestinal sac procedure

3.3.8 Freeze-drying of MCPCNPs

The nanoparticle suspension was centrifuged at 10,000 rpm for 10 min and trehalose, as a cryoprotectant, was added at a concentration of 10% (w/v). The nanoparticle suspension was then stored at -20 ^{0}C for 14 h and lyophilized in the freeze-dryer (ALPHA 1-2 LD plus, Christ, UK) at a vacuum pressure of 0.39 mbar for 48 h. The freeze-dried samples were then stored at 4 ^{o}C for further analyses.

3.3.9 Preparation of 33% w/v rat caecal content

The caecum of one of the Sprague–Dawley male rats used above was ligated, then carefully incised. The caecal contents were removed, weighed and suspended in cold (0–4 °C) phosphate buffer (pH 7.0) to a concentration of 33% (w/v). The suspension was centrifuged at 1200 rpm for 15 min at 4 °C and the supernatant obtained was further centrifuged at 9000 rpm for 30 min. This final supernatant was stored at 4 °C and was used as the colonic release medium.

3.3.10 Curcumin release from the MCPCNPs

1.3 mg of freeze-dried MCPCNPs was suspended in 2 ml of hydrochloric acid (pH 1.2) or 33% w/v caecal medium in a centrifuge tube. The tube was subjected to rotary shaking at 120 rpm maintained at 37 °C for 2 h for the pH 1.2 medium and 24 h for the caecal content medium. At each time point (0, 1, 2, 3, 5, 7, 14 and 24 h), the tube was centrifuged at 10,000 rpm for 10 min to pellet the MCPCNPs and the amount of curcumin released was determined in the supernatant using the HPLC method described previously in Chapter 2. The MCPCNPs pellet was re-suspended in 2 ml of fresh buffer media and the process repeated. The percentage of curcumin released from the MCPCNPs was calculated as follows:

$$Percentage\ released\ (\%) = \frac{\text{Amount of curcumin released}}{\text{Amount of curcumin in the NPs}} \times 100 \quad (3.4)$$

3.4 Results and discussion

3.4.1 Swelling of MCPCNPs matrices

The crucial prerequisite for mucoadhesion between dosage form and epithelia is the ability of the former to swell effectively. Therefore, the swelling ratios of the MCPCNPs were assessed as a function of the three pH buffers (pH 1.2, 5.5 and 7.0) for 0, 0.5, 1, 2, 4 and 6 h using the particle size analyser (Zeta Sizer Nano Series). In all three pH media, the MCPCNPs swelled rapidly (within 30 min), with the highest swelling ratio in pH 5.5 and lowest in pH 1.2 (Figure 3.2).

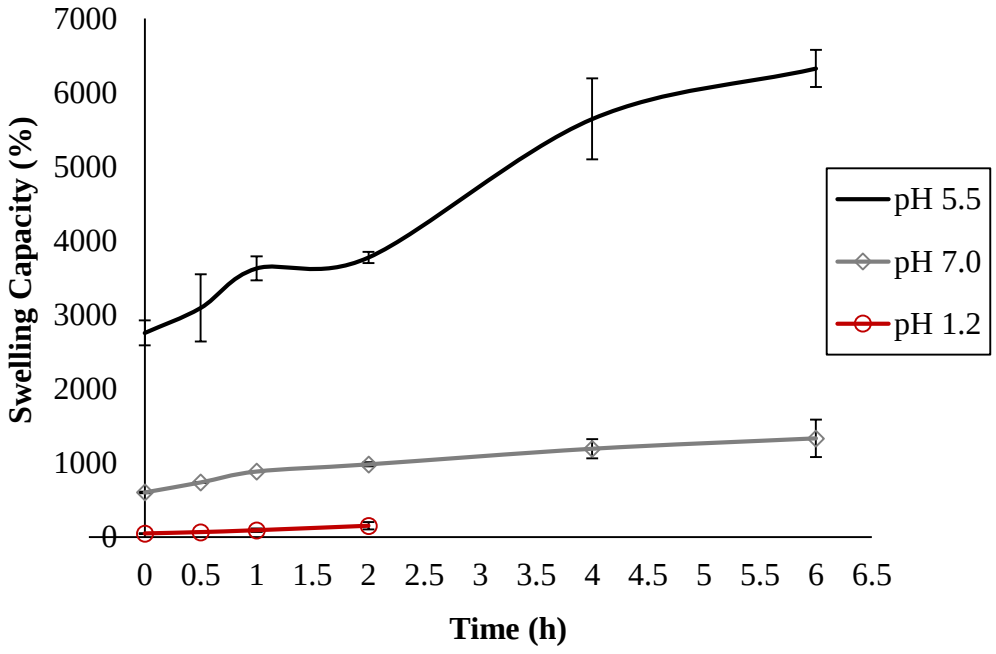


Figure 3.2 Swelling profile of MCPCNPs in pH 1.2, 5.5 and 7.0.

Free chitosan swells in acidic media; however, the swelling of the MCPCNPs in pH 1.2 was restricted due to the formation of polyelectrolyte complex between the amino groups of chitosan and the carboxylate group of MCP. At pH 5.5, the swelling capacity increased significantly due to the complete protonation of the amine groups in chitosan and the ionisation of the carboxyl groups in MCP, thus yielding a significant increase in charge density. This

increase in charge density results in repulsion between polymer segments, creating voids that facilitate the penetration of water within the polymer matrix and causing an increase in the size of the particles. The higher swelling capacities obtained at pH 7.0, relative to that at pH 1.2, can be related to the relatively weaker interactions between chitosan and MCP due to the stronger cationic nature and lower anionic nature of chitosan and MCP at this pH, respectively. This makes the interactions between MCP and chitosan susceptible to dissociations with a consequent compromise in matrix rigidity.

3.4.2 Mucin adsorption assay

In the micro-BCA staining colorimetric assay, the amount of mucin adsorbed on to the MCPCNPs was used as a measure of the extent of mucoadhesion of the MCPCNPs. The advantage of this method over other methods is that it presents lesser batch-to-batch variability thus providing more reproducible data. According to Khutoryanskiy (Khutoryanskiy, 2015) the pH values in the three distinct sections (ascending, transverse and descending regions) of the colon range from 5.20 to 7.02, therefore three broadly isosmotic buffers representing these different sections of the colon were used. Furthermore, mucoadhesion within the pH limits expected in the stomach was also investigated. The spectrophotometric analysis utilised in this investigation provided measurements at very dilute concentrations of mucin (25–200 μg/mL) and displayed a linear relationship ($r > 0.99$) with respect to the concentration of mucin and the absorbance at 562 nm for the adsorption assay in pH 1.2, 5.5, 6.25 and 7.0 (Figure 3.3).

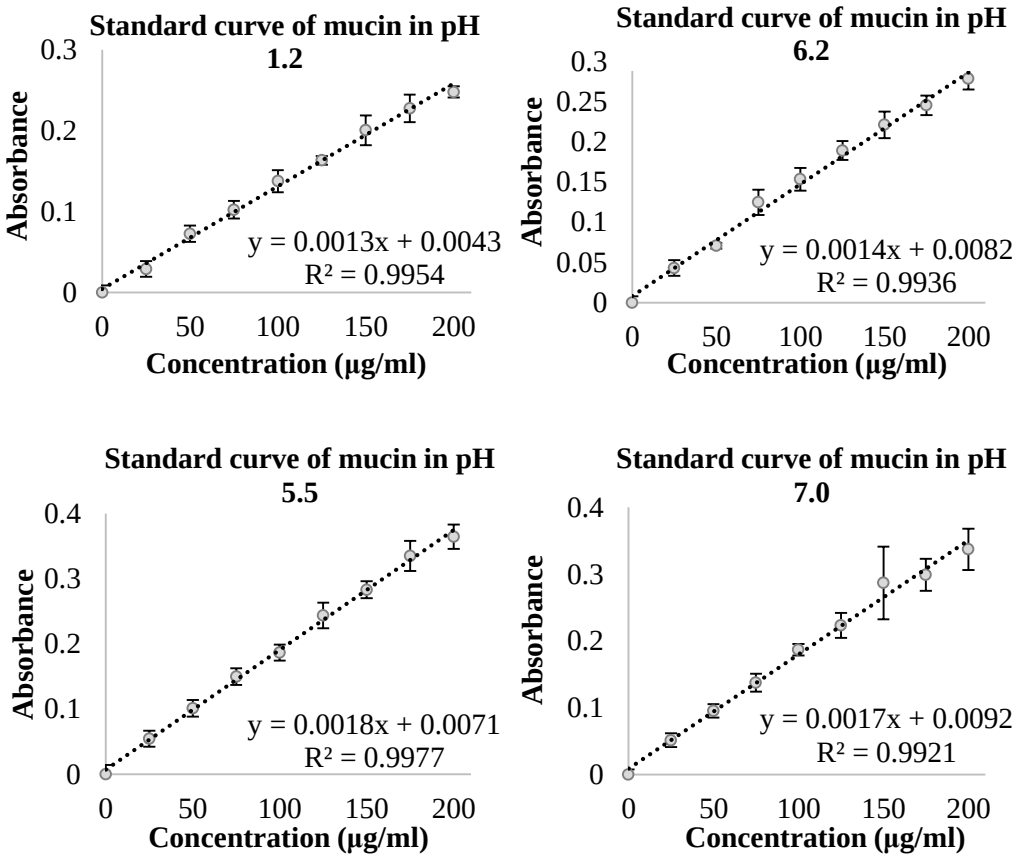


Figure 3.3 The calibration curves of mucin in pH 1.2, 5.5, 6.2 and 7.0

Clearly, the extent of adsorption of mucin on the MCPCNPs is pH-dependent (Figure 3.4) due to the influence of the latter on the degree of ionisation of MCPCNPs and mucin. In this context, the lower percentage of adsorption of mucin on MCPCNPs at pH 1.2 was due to the lower magnitude of ionisation of the principal component in mucin (sialic acid) at this pH. This effectively reduced the extent of interactions between chitosan moieties within MCPCNPs and mucin. On the other hand, higher mucin adsorption capacities were observed at higher pH values (pH 7.0, 5.5 and 6.25). This pH range approximate physiological values within the colon and because sialic acid within mucin has a pKa of 2.6, a negative charge condensation manifests within mucin at such pH values.

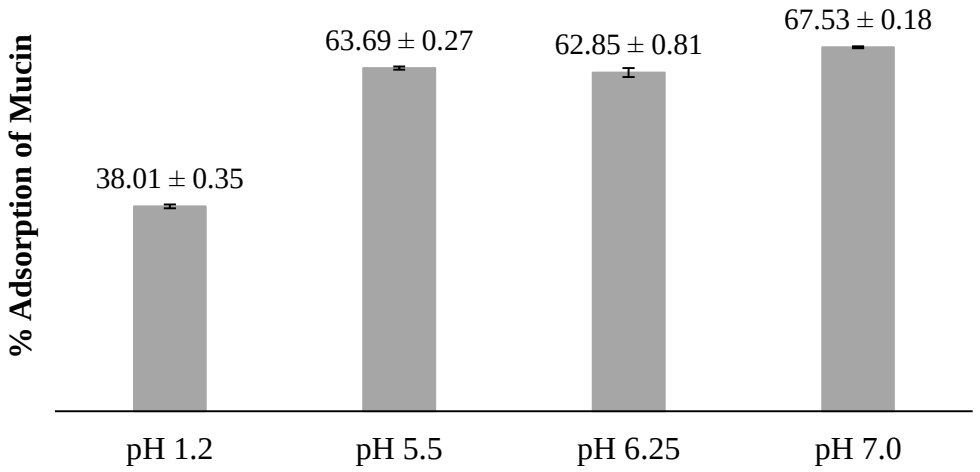


Figure 3.4 Mucin adsorption of MCPCNPs at different pH

Consequently, electrostatic interactions are most favourable at this pH range from the cationic nature of MCPCNPs and the negative charge of sialic acid in mucin. Furthermore, a good correlation can be observed between the swelling capacities of MCPCNPs (Figure 3.2) and mucoadhesion, suggesting that swelling of the MCPCNPs is a precursor to the electrostatic interaction with mucin explained above. Mucoadhesion was further enhanced through physical entanglement between mucin and MCPCNPs. Physical entanglement is chiefly promoted by MCP within the MCPCNPs due to ionisable carboxyl groups of pectin (pKa of 4.0) at pH 5.5-7, which enhances its swelling and physical entanglement with mucin chains. The above data is in agreement with those by Bigucci et al. where polyelectrolyte complexes composed of chitosan and pectin used for delivering vancomycin displayed the best *in vitro* mucoadhesion in colonic pH, with efficiencies between 58–60% (Bigucci et al., 2008). In another report, Gadalla et al. showed that zinc-pectinate chitosan microparticles for colonic delivery of progesterone exhibited high mucoadhesion in colonic pH (≈80%) (Gadalla et al., 2016). They both attributed this observation to the open expanded conformations in pectin and the cationic nature of chitosan which

promoted physical entanglement and electrostatic interaction of the formulation with the negatively charged sialic acid residues in the mucus, respectively.

3.4.3 Zeta- potential as a function of pH

The zeta-potential assessment of the MCPCNPs incubated in simulated pH media for the stomach and colon (pH 1.2 for 2 h and pH 7.0 for 6 h, respectively) is presented in Figure 3.5.

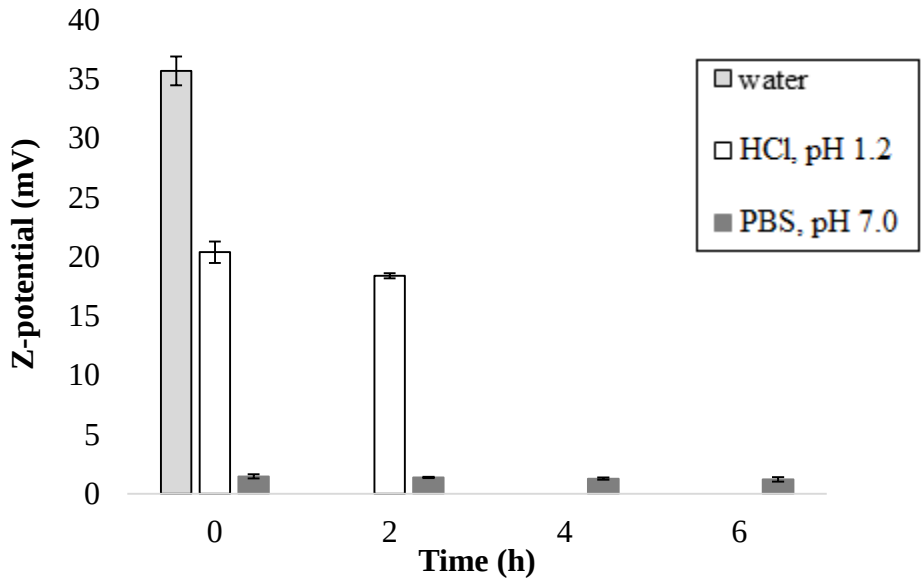


Figure 3.5 Z-potential of NPs incubated in different pH without mucin for specific time intervals

The zeta potential of the MCPCNPs reduced from +35.7 mV (freshly prepared) to +18.2 mV in pH 1.2 after 2 h and to +1.22 mV in pH 7.0 after 6 h. The magnitude of the zeta-potential can be used to predict the colloidal stability of a dispersed system. On the basis of the change in zeta potential obtained for MCPCNPs at pH 1.2, we may infer that the particles are fairly stable at that pH. On the other hand, there was a drastic drop in the zeta-potential at pH 7.0 and this is attributable to the MCPCNPs aggregating due to van der Waal inter-particle attractions. Therefore, a change in pH during gastrointestinal transit of

the MCPCNPs is likely to impose instability to the MCPCNPs. Furthermore, at pH 7.0, there is effective repulsion between the chitosan and MCP chain segments due to cationic charge rendition. This creates voids which facilitate the diffusion of water into the polymer matrix and causes an increase in the size of the particles. These results correlate with swelling study (section 3.4.1) in which the highest swelling ratio was registered in pH presenting the colon and lowest in pH mimicking the stomach. Notwithstanding, this reduction in stability within the gastrointestinal tract is inconsequential due to the short transit duration.

The mucoadhesive propensity of the MCPCNPs was determined using mucin type III at four different concentrations (10, 50, 100, and 150 µg/ml) maintained at the two pH (pH 1.2 and 7.0) used in assessing the z-potential of the MCPCNPs. A drop-in zeta-potential of the MCPCNPs can be used as a measure of the extent of mucoadhesion between the former and mucin (Alkhader et al., 2016). Figure 3.6 shows a drop-in zeta-potential as the mucin concentration was increased, in both pH 1.2 and 7.0.

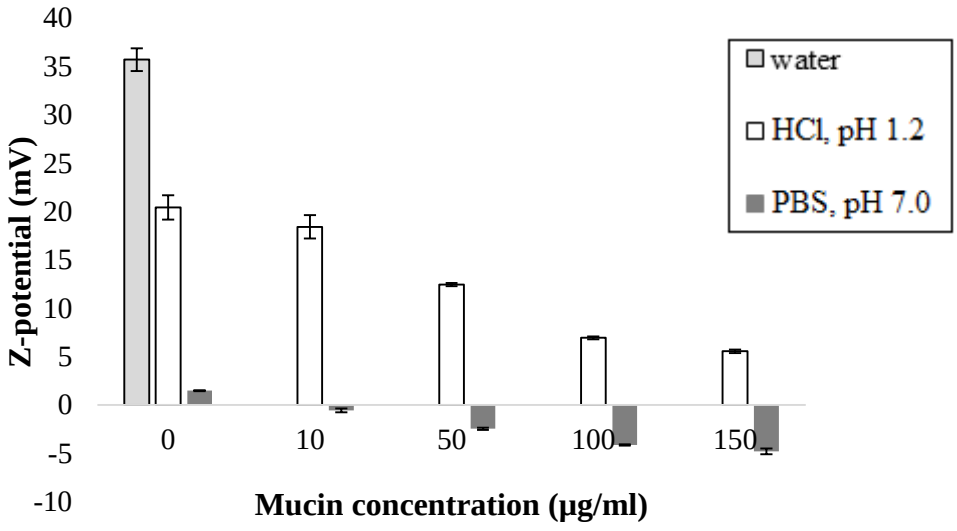


Figure 3.6 Z-potential of NPs incubated in different pH with mucin for specific time intervals.

Compared to the initial value, we observed a marked reduction in the zeta-potential of the MCPCNPs at pH 7.0 compared to in pH 1.2, suggesting that the NPs are more mucoadhesive at pH 7.0. The drop-in zeta-potential at pH 7.0 elaborates the electrostatic interactions between the cationic moieties of MCPCNPs and the negative charge of sialic acid in mucin. These findings are in good agreement with those from Mazzarino et al. (Mazzarino et al., 2012) who reported that the interaction between chitosan-coated nanoparticles and mucin was due to the electrostatic forces between the protonated amino groups of the mucoadhesive polymer and the negatively charged groups of the protein carbohydrate chains. Therefore, in the ultimate performance of the MCPCNPs, we would expect mucoadhesion within the colonic mucosa.

3.4.4 Morphological analyses

In order to study the effect of mucoadhesion of the physical integrity of the MCPCNPs after interaction with mucin in representative physiological media, MCPCNPs were digested in pH 1.2 and pH 7.0 for 10 minutes, removed, air-dried and studied under SEM (Figures 3.7). Figure 3.7 (a) represent nanoparticles without mucin with the size range of 50 to 200 nm. In Figure 3.7 (b) however, MCPCNPs edges appear deformed and distorted after suspension in mucin at pH 7.0, with an increase in the size range (180-350 nm). This increase in size as explained earlier is related to the repulsive forces between like-charged groups within the two polymers. Subsequently, expansion of the matrix and invitation of media causes an increase in particle size which compromise matrix rigidity. A closer look at the morphology of MCPCNPs exposed to pH 7.0 shows that they are somewhat porous compared to the unexposed and acid exposed MCPCNPs.

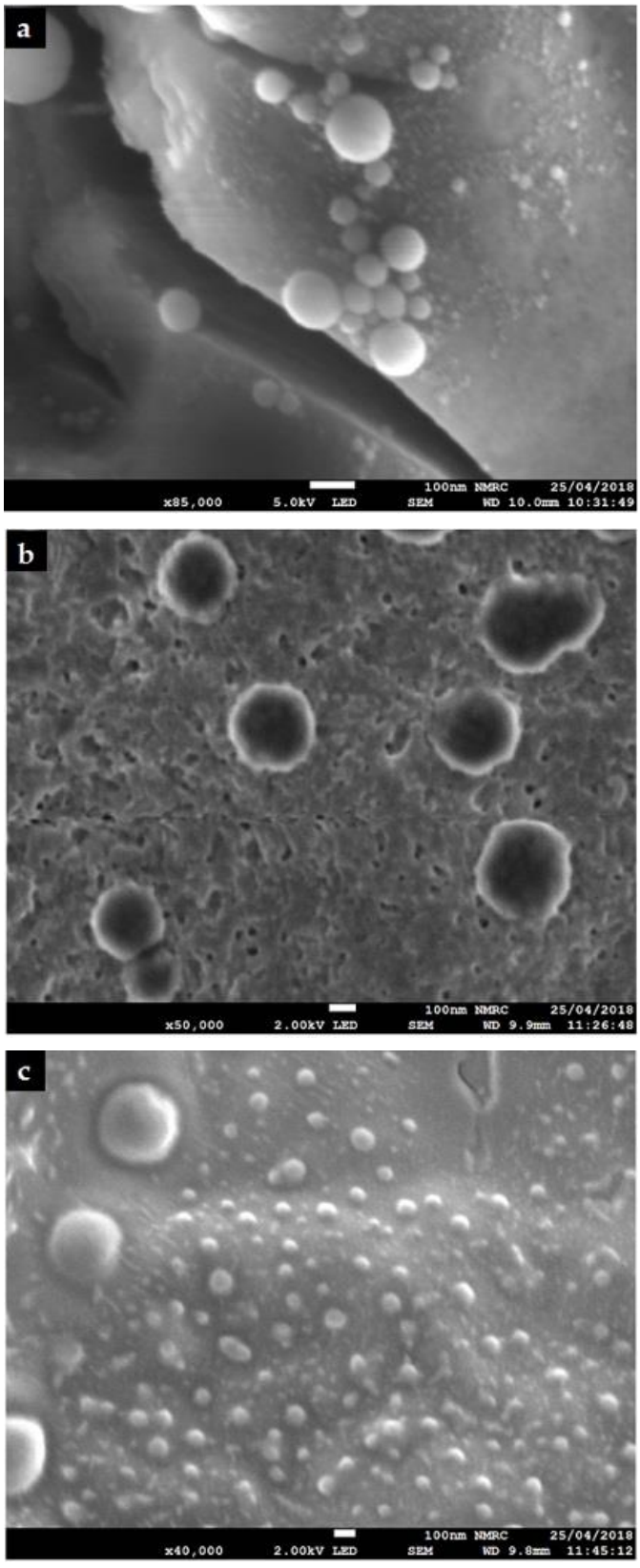


Figure 3.7 SEM images of MCPCNPs **(a)** MCPCNPs exposed to mucin in pH 7.0 **(b)** MCPCNPs exposed to mucin in pH 1.2 **(c)**

Moreover, a thin coating of mucin appears to be decorated around each nanoparticle, which suggests adsorption to the surface of the MCPCNPs. In Figure 3.7 (c), a minimal change in size was observed (50-250 nm) with MCPCNPs exposed to mucin at pH 1.2. This restricted increase in size range at pH 1.2 is attributed to the formation of polyelectrolyte complex between the amino groups of chitosan and the carboxylate group of MCP. This interaction between chitosan and MCP means that there are fewer functional moieties to interact with mucin and therefore, very few MCPCNPs were surrounded by mucin.

3.4.5 AFM

AFM was used to further ascertain the observations made in the SEM analyses above. Visual representation of the MCPCNPS before and after exposure to mucin in pH 7.0 is shown in Figure 3.8.

Firstly, the size range of MCPCNPs after respective exposure to media mirrors the results from the SEM, with larger aggregates of MCPCNP and distorted morphologies. The surface topology of pure MCPCNPs (Figure 4.8 a) appears more homogeneous than those in Figure 4.8 b which also displays coatings of mucin decorated around each nanoparticle (indicated by arrows). Therefore, it may be interpreted that MCPCNPs display intermolecular interaction with mucin. These results are in agreement with those of two other reports that separately studied mucin-chitosan (Dedinaite et al., 2005) and mucin-pectin (Joergensen et al., 2011) interactions. In (Dedinaite et al., 2005), they showed that chitosan, being a positively charged polyelectrolyte, associates with the negatively charged adsorption layer of mucin to form mucin-chitosan complexes in addition to possible contributions from hydrogen bonding. While,

Joergensen et al. reported that the interaction between mucin and pectin was due to the fact that both mucin and pectin are negatively charged which leads to repulsion and cause uncoiling of polymer chains, thus facilitating chain entanglement and physical bond formation (Joergensen et al., 2011).

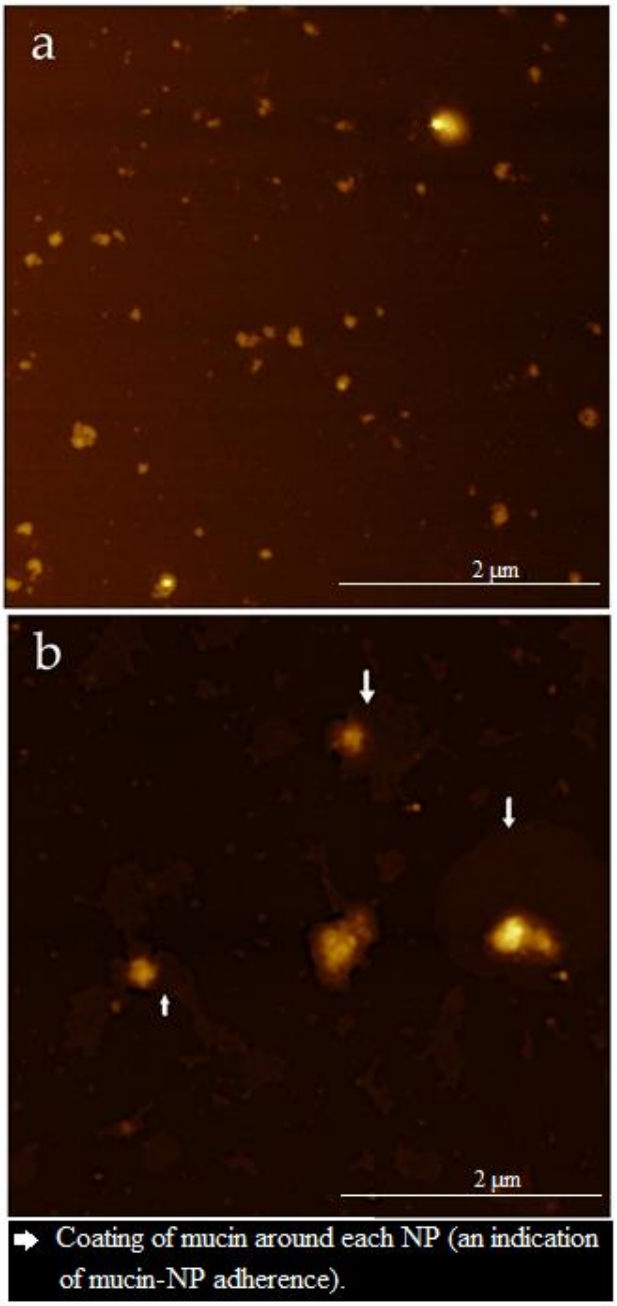


Figure 3.8 AFM images with 5 µm x 5 µm scan sizes of pure MCPCNPs **(a)** and MCPCNPs incubated with mucin in pH 7.0 **(b)**

3.4.6 NTA analysis

To further investigate the observed changes in morphology and increase in the hydrodynamic radius of the particles upon exposure to mucin in pH 7.0, a direct and real-time visualization of the Brownian motion exhibited by MCPCNPs was carried out on NTA. In contrast to the AFM and SEM analyses, this technique gives us some insight on the real-time changes to the MCPCNPs when these are exposed to mucin. The technique is based on visualisation and tracking of particles in solution by an image analysis software that deduces the diffusion coefficient of each particle and allows the determination of its hydrodynamic radius (*NanoSight NTA 2.1 Analytical Software Operating Manual*, 2010). It is superior to electrophoretic light scattering (ELS) in that it directly views the fate of individual nanoparticles as mucin is introduced into the analysis chamber, providing an explicit response of the nanoparticle behaviour. Moreover, NTA does not recapitulate the architecture of a mucosal tissue and the porous structure of the mucus (Moshe et al., 2017). A representative graph showing the size distribution profile of MCPCNPs before and after exposure to mucin for 30 minutes along with snapshots from the NTA video are shown in Figure 4.9. Prior to exposure, the mean size of the MCPCNPs was 218.1 (± 4.9) nm, after the introduction of mucin, the nanoparticles displayed a noticeable increase in size distribution with mean size of 291.7 (± 7.8) nm. These findings are in agreement with the ELS data where the formation of the larger sized MCPCNPs was observed when exposed to mucin in pH 7.0. Moreover, the images showed a drastic increase in the number of nanoparticles detected after exposure to mucin. The MCPCNPs are proposed to have been brought closer together and instantly aggregate upon contact with mucin forming larger clusters, with the

mucin acting like a ‘double-sided’ adhesive. In the present system, electrostatic interactions are possible between the negatively-charged sialic acid units of mucin and the ($-NH_3^+$) groups of chitosan that confers the overall-positive charge to the MCPCNPs. This theory was highlighted by Smart (Smart, 2005) who described that attractive forces will arise (van der Waals’ interactions and electrostatic interactions) when oppositely charged compounds come into contact.

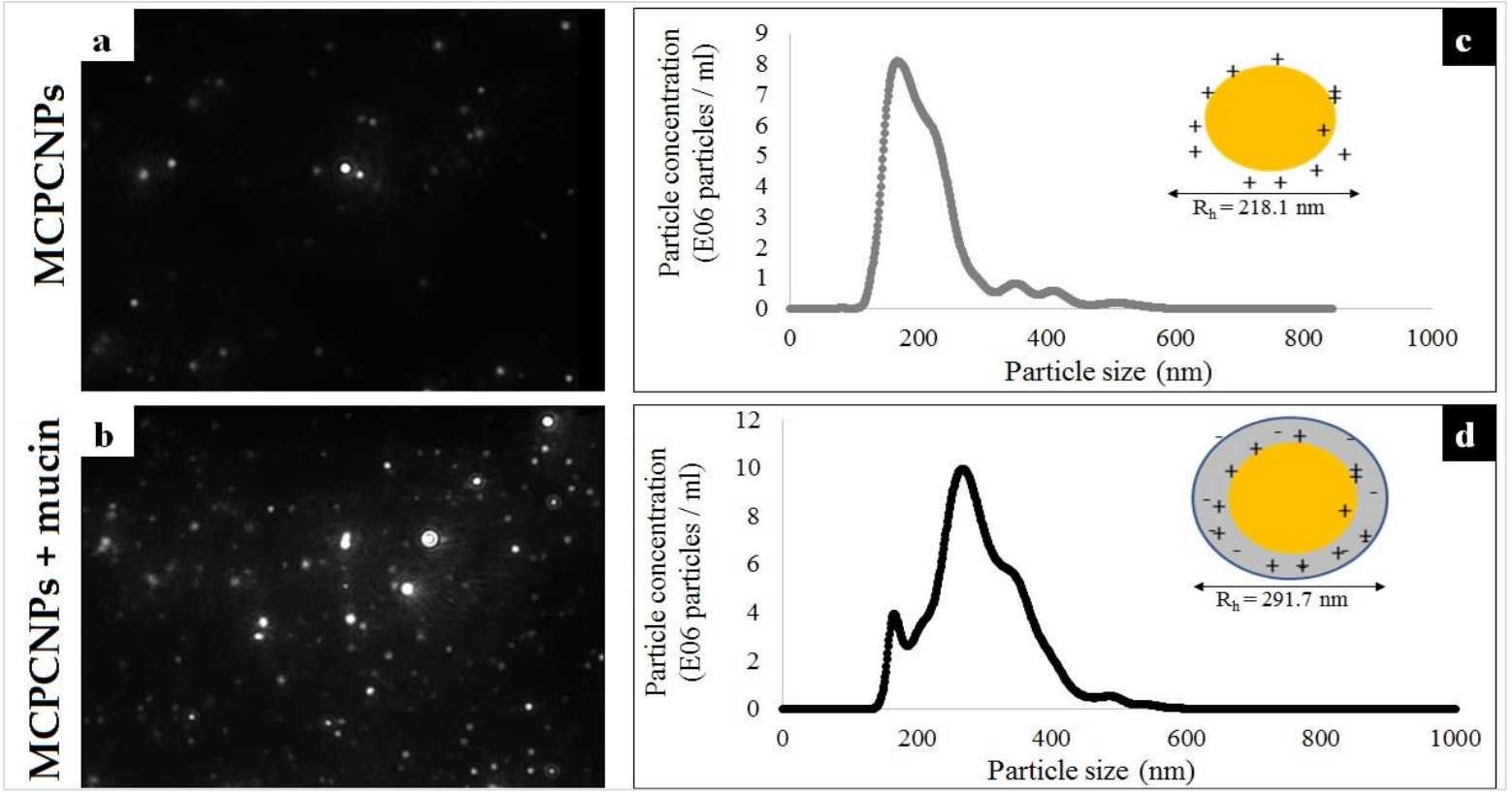


Figure 3.9 NTA results with **(a)** and **(b)** presenting the video snapshots of MCPNPs before and after the addition of mucin, respectively, while **(c)** and **(d)** portray the size distribution profiles of MCPNPs prior to and 30 minutes after addition of mucin, respectively.

3.4.7 Everted caecal sac

For more comprehensive and conclusive understanding of the mechanism involved in mucoadhesion, an *ex-vivo* study was conducted on fresh animal mucosal tissue (caecum). This set-up is a true depiction of the passive nature of the adhesion between the caecal tissue and particles as no external force is applied to the particles. The percentage of MCPCNPs bound to the rat caecum was found to be 66.76 % (±3.86). This substantial percentage in mucoadhesion of the MCPCNPs is in agreement with the previous data obtained by the mucin adsorption assay in section 3.4.2, in which the adherence of the MCPCNPs to the caecal epithelium ascertains the formation of electrostatic attraction between the positive amine groups of chitosan and the negative sialic acids of mucin, as well as the formation of covalent bonds between the carboxylic side chains of the pectin and the cysteine-rich subdomains of the mucus glycoprotein (Pengpong et al., 2014). This final study on mucoadhesion gives credence to all the other studies and confirms the finding that the MCPCNPs are mucoadhesive in colon pH.

3.4.8 Curcumin release studies

Orally administered drug delivery systems intended for the colon should ideally yield minimal release of the payload in gastric media but release maximally in colonic conditions. Firstly, curcumin standard solutions (0.625-10 µg/ml) prepared in pH 1.2 and 33 % caecal content buffer were quantified and the peak areas obtained from HPLC were used to construct standard calibration curves. These standard curves are then used to calculate the released curcumin concentrations in pH 1.2 and the caecal buffer. Figure 3.10 displays the obtained calibration curves.

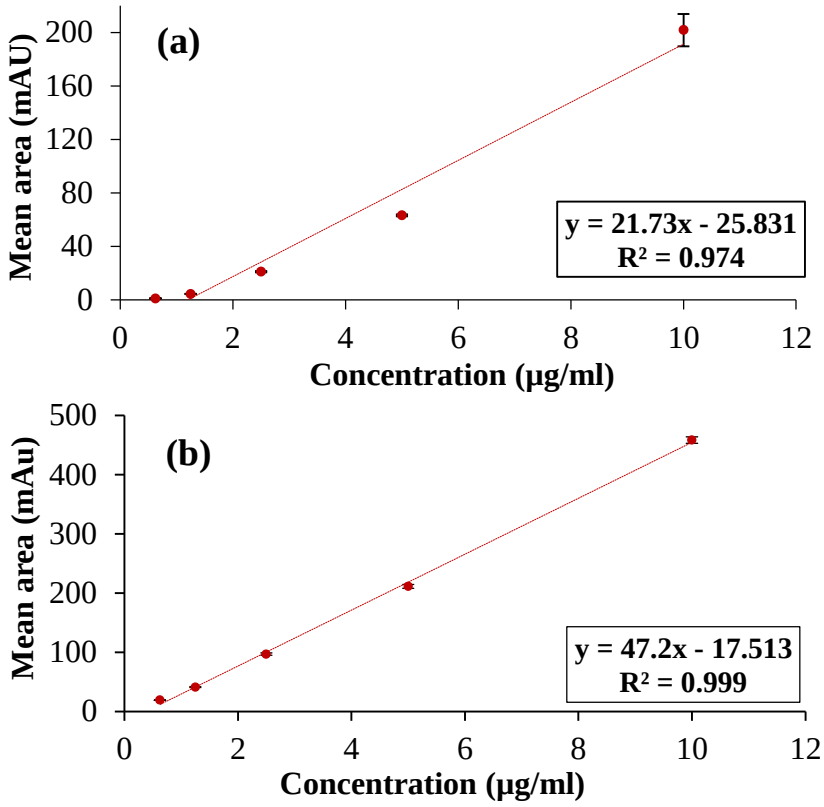


Figure 3.10 Standard calibration curves of curcumin prepared in pH 1.2 **(a)** and 33 % caecal content buffer **(b)**

The *in vitro* release of curcumin from the MCPCNPs at conditions mimicking the pH and times likely to be encountered in the stomach and colon (2 h in pH 1.2 and 24 h in 33% (w/v) caecal media) is presented in Figure 3.11.

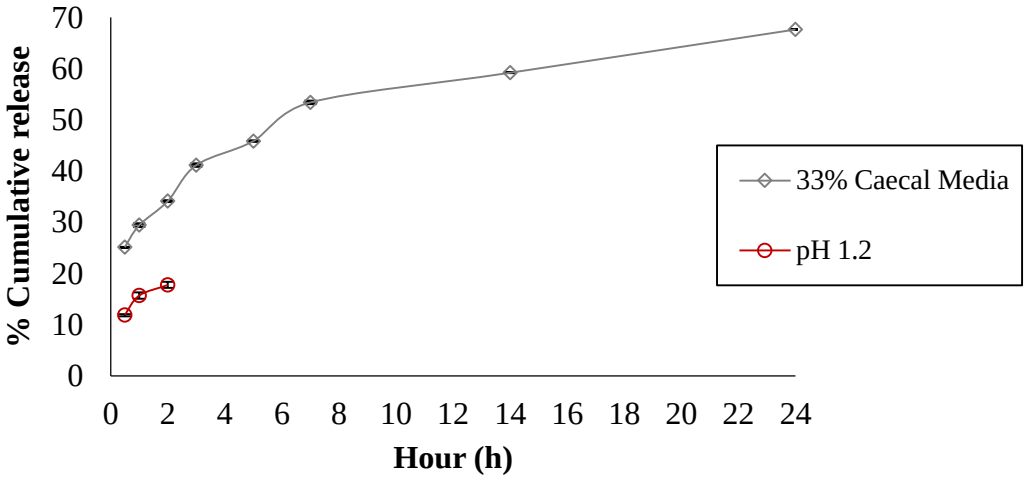


Figure 3.11 In vitro drug release profile of curcumin from MCPCNPs in pH 1.2 for 2 h and 33 % caecal medium for 24 h.

The release of curcumin reached ≈18% over 2 h in acidic conditions due to the poor solubility of curcumin at acidic pH, coupled with the protonation of the charged carboxylic groups (COO−) of pectin which minimises coulombic repulsions between polymer chains and therefore keeps the matrix secluded. Furthermore, at this pH, the amino groups of chitosan also become protonated, which favours a closely-knit gel network with MCP that impedes the diffusion of curcumin within the matrices. On the other hand, a significant release of curcumin was observed in the caecal media over 24 h (≈68%), pointing to the profound effects colonic enzymes exhibit on the integrity of the chitosan-MCP composite matrix, which tends to loosen the polymer matrix network allowing free diffusion of curcumin.

The obtained release results correlate with the swelling capacities profiles presented previously, further approving the released amount of curcumin from the MCP chitosan composite matrix. In order to investigate the mechanism of curcumin release from the MCPCNPs in caecal medium, the data were fitted to the zero-order, first-order, Higuchi and Korsmeyer–Peppas models (AbouAitah et al., 2016) and results are presented in Table 3.1.

Table 3.1 Correlation coefficients of best fits to studied models

Model	r^2 for complete profile
Korsmeyer-Peppas	0.986
Higuchi	0.954
First-order	0.920
Zero-order	0.847

The models were not fitted to the release profile in pH 1.2 medium because less than 18% of curcumin was released within the 2 h study period (stipulated

gastric resident time) and aptly, the release of curcumin in pH 1.2 (stomach) is not very relevant to the present pursuit. Curcumin release was best fitted to the Korsmeyer- Peppas model with a correlation of 0.986 (Table 3.1) and an exponent (n) of 0.27. This indicates that the release mechanism followed a quasi- Fickian diffusion mechanism. We believe that this mechanism is borne by a natural propensity of curcumin to diffuse passively from the porous matrix of the MCPCNPs. Furthermore, diffusion was prompted by degradation of the pectin chains, especially at surface of the particle matrices by enzymes within the caecal medium. A closer study of the profile in the caecal medium reveals a bi-phasic release pattern, with the first inflection (1–7 h) steeper than the second (7–24 h) (Figure 3.10). During the initial phase (first inflection), diffusion is limited to the outer or near outer surfaces of the MCPCNPs matrix, reinforced by enzymatic effects. The second inflection involves release from the deeper domains of the MCPCNPs with lesser enzymatic effects on the matrices and more by passive diffusion of curcumin. We may conclude that curcumin release is largely governed by diffusion, dictated by enzymatic effects on the MCPCNPs matrix that can best be described as a quasi-Fickian diffusion mechanism.

3.5 Conclusion

The MCPCNPs have demonstrable potential for colon delivery of curcumin. The data suggest that the formulation survives acidic pH milieu, with a limited amount of curcumin release, but releases curcumin significantly at media representing the colon. This presents a possible model for colon delivery of curcumin following oral delivery whereby significant curcumin payload is retained within the nanoparticles until colon arrival. Furthermore, the

nanoparticles are mucoadhesive at pH representing the colon region. The MCPCNPs formed spontaneous aggregates upon exposure with mucin at simulated colonic media. The decoration of these nanoparticles with mucin, favoured by the electrostatic forces between both, was confirmed by the changes in particle size and zeta potential values. To further improve the targeting capability of the MCPCNPs toward colon cancer cells, the conjugation of an antibody with the former will be investigated in Chapter 4. The mucoadhesive properties of the formulation are expected to prolong the contact time of curcumin with the cancer cells hence improving treatment outcome. The MCPCNPs are thus well primed for further investigation where the anti-cancer and apoptotic efficacy as well as the cellular uptake will be discussed in Chapter 5.

Chapter 4 Formulation and *in vitro* evaluation of cetuximab conjugated to MCPCNPs

4.1 Introduction

Targeted therapeutic nanoparticles as a delivery system have gained significant attention in recent years because it conquers the limitations associated with conventional therapies such as nonspecific biodistribution, poor water solubility and limited bioavailability (Xin et al., 2017). Generally, NPs are designed to assist therapeutic agents to pass through biologic barriers and they offer several advantages over the free drug in terms of flexibility in the route of administration, minimal toxicity and controlled drug-release capability (Jahan et al., 2017). NPs with specific ligands attached to the surface are capable of recognising relevant moieties within target tissues making them a good potential for site-selective delivery as well as enhanced specificity for drug targeting (Kocbek et al., 2007). For example, mAbs have been established as one of the most successful and widely studied targeting moieties (Adler and Dimitrov, 2012; Geng et al., 2015; Scott et al., 2012).

mAb-conjugated NPs deliver drugs to the inflicted sites by targeting cell-surface biomarkers and thus generating receptor endocytosis of the NP-encapsulated drug. One such cell-surface biomarker is EGFR, a member of the human EGF family of transmembrane receptor tyrosine kinases (Wieduwilt and Moasser, 2008). Overexpression of EGFR has been reported in approximately one third of epithelial malignancies, including colorectal cancer (Chu et al., 2015). The activation of EGFR has become a target for NP mediated cancer treatment as the former stimulates tumour growth, proliferation, angiogenesis, invasion and metastasis (Maya et al., 2014). Recent studies have listed several mAb which efficiently block the downstream signalling pathway of EGFR, however, Cetuximab (Cet) is among the most widely studied anti-EGFR mAb

for colorectal cancer (Goldberg et al., 2018). It is a chimeric mAb (IgG1) that binds to the membrane protein domain of the EGFR and competitively inhibits ligand binding to suppress tumour proliferation (Shigeta et al., 2013).

In previous chapters, I successfully developed MCPCNPs and showed that it has the potential to deliver curcumin safely to the colon where it is expected to manifest its effects locally through prior mucoadhesion to cancer tissue. Recent clinical trials suggest that targeting tumour-specific receptors with mAbs offer the most effective therapeutic approach for the treatment of colorectal cancer (Krzemieniecki et al., 2006). In this Chapter therefore, I will be focusing on the binding strategies required to attach the mAb, Cet, to the surface of the pre-formed MCPCNPs, estimating the amount of mAb attached to the NP surface and studying the physiochemical properties of the formulated system. While in the following Chapter, I will examine whether the anti-tumour activity of MCPCNPs is further enhanced by coupling them with Cet that targets EGFR.

4.2 Materials

Curcumin was purchased from Fluka, (U.S.A). Chitosan (low molecular weight, de-acetylated chitin), sodium tripolyphosphate and phosphate buffered saline tablets (PBS) were purchased from Sigma–Aldrich, USA. Low methoxyl citrus pectin (DE lower than 50) was bought from Genu, CPKelco® (Limeira- SP, Brazil). Trehalose (Nacalai Tesque, Japan) was employed as the cryoprotectant. Cetuximab was purchased from Chembest Research Laboratories, China. Mucin type III from porcine stomach (Sigma Aldrich, USA) was utilised for mucoadhesive studies. Micro-BCA protein assay kit was purchased from Thermo Scientific, USA. (1-ethyl-3-(3-dimethylaminopropyl) carbodiimide hydrochloride) (EDC) (Nacalai Tesque, Japan), N-hydroxysuccinimide (NHS)

(Sigma Aldrich, USA) were used for the antibody conjugation to the NPS. 2-(N-morpholino) ethanesulfonic acid (MES) (Nacalai Tesque, Japan), acetic acid (R&M chemicals, UK), hydrochloric acid (R&M chemicals, UK), sodium hydroxide (Merck, Germany), sodium acetate (Sigma Aldrich, USA) and potassium dihydrogen phosphate (Merck Millipore, Germany) were used for buffer preparations.

4.3 Methods

4.3.1 Preparation of MCPCNPs

MCPCNPs were prepared using the method reported in Chapter 2 section 2.3.2, then freeze-dried as described in Chapter 3 section 3.3.8.

4.3.2 Preparation of Cet-MCPCNPs

Functionalization of the MCPCNPs with Cet was achieved by adapting the EDC–NHS conjugation chemistry as reported by thermofisher manual instruction (Thermo Scientific, 2011). Briefly, 10 mg/ml of lyophilized MCPCNPs in 25 mM MES buffer was treated with 0.4 mg of EDC and 0.6 mg of NHS and stirred for a total of 1 h to activate and stabilize the carboxyl group yielded by the MCP of the NPs. The solution was then centrifuged 10,000rpm for 20 min to separate the activated MCPCNPs and then reconstituted in MES buffer. 1 mg/ml of Cet in MES was added to the activated NPs suspension and stirred for 4 h for Cet conjugation. The NPs were then centrifuged at 10,000rpm for 20 min, washed twice with deionized water to remove any unbound cetuximab and re-suspended in MES buffer for further analysis. The extent of Cet conjugation on MCPCNPs was quantified using a micro -BCA kit (Thermo Scientific, USA) following the manufacturer's instructions. Briefly, 150 µL each of sample and working reagent was pipetted in replicate into a microplate

well then incubated at 37 ^{0}C for 2 h. The absorbance was measured at 562 nm on a plate reader. Absorbance obtained was compared to those from the standard curve of Cet in MES buffer to estimate the percentage of Cet bound to MCPCNPs.

4.3.4 Physiochemical characterisation

The hydrodynamic size distribution (expressed as mean size) and surface charge (expressed as zeta-potential) of the Cet-MCPCNPs were determined after dilution using a Zeta Sizer Nano Series® (Malvern Instruments Ltd., UK) equipped with a 4 mW He-Ne laser at a wavelength of 633 nm. Samples were run in triplicates and presented as mean (± SD). Surface morphology of the Cet-MCPCNPs were analysed by scanning transmission electron microscope (STEM) (Model Quanta 400F, FEI Company USA). A 10 µl aliquot of the sample was drop-casted onto copper stub and left under a drying chamber for 24 h at room temperature before viewing. The FTIR was used to identify the possible interaction between the Cet and MCPCNPs. Spectra were obtained for MCPNP and Cet-MCPCNPs using a Perkin-Elmer FTIR spectrometer (Spectrum RX I) with scans run between 400 and 4000 cm^{-1} at a resolution of 4 cm^{-1} and interval 1 cm^{-1}. An elemental analysis of the MCPCNPs and Cet-MCPCNPs was carried out by a SEM (Model Quanta 400F, FEI Company USA) equipped with an Energy dispersive X-ray (EDX), which can provide a rapid qualitative and quantitative analysis of the elemental composition of NPs.

4.3.5 Entrapment efficiency of curcumin and *in vitro* drug release from Cet-MCPCNPs

To analyse the entrapment efficiency of curcumin in the Cet-MCPCNPs, the amount of curcumin in the supernatant after each step of centrifugation during

the synthesis of NPs was quantified. A standard calibration curve was constructed using standard concentrations of curcumin dissolved in methanol. The curcumin content was analysed by injecting 10 μL onto an HPLC system and analysed using the method described in Chapter 2, section 2.3.5. The encapsulation efficiency was calculated using the formula:

$$Encapsulation\ efficiency\ (\%) = \frac{\text{Amount of curcumin encapsulated}}{\text{Total amount of curcumin added}} \times 100 \qquad (4.1)$$

In vitro curcumin release from Cet-MCPCNPs was conducted as described in Chapter 3 section 3.3.10.

4.3.6 Mucin adsorption studies

The propensity of the MCPCNPs to adhere to mucus was evaluated as stated in Chapter 3 section 3.3.2. However, the amount of mucin adsorbed as a function of pH was conducted at pH 1.2, 5.5 and 7.0.

4.4 Results and discussion

4.4.1 Preparation of Cet-MCPCNPs

The MCPCNPs were prepared by ionic gelation technique as described previously in Chapter 2. Subsequently, the conjugation of the mAb, Cet, to the surface of the MCPCNPs was carried out to aid the targeted delivery of curcumin to tumours at colon. Numerous commercially available crosslinkers provide diverse strategies to link primary amino groups with carboxylates, among which carbodiimide (EDC)/NHS chemistry is the most commonly adopted (Meng et al., 2010). EDC is a water-soluble, zero-length crosslinking agent which reacts with the −COOH group of MCPCNPs without the need for prior organic solvent dissolution, to form an amine-reactive O-acylisourea

intermediate which can directly react with amine group of Cet (Maya et al., 2013). To increase the stability of the formed reactive ester and avoid its rapid hydrolyzation in aqueous solutions, NHS is usually added (Thermo Scientific, 2012). The addition of NHS stabilizes the amine-reactive intermediate by converting it to an amine-reactive NHS ester, in which the resultant NHS-MCPCNPs reacts with the amine group of Cet, forming Cet-MCPCNPs with a stable peptide bond. Figure 4.1 shows the step-wise reaction in the formation of the Cet-MCPCNPs. It is worthwhile to note that the buffer components play a crucial role in stabilizing mAbs and should be devoid of extraneous carboxyl and amine groups (Ramkumar et al., 2017). Sodium phosphate and MES are the most commonly-used buffer components (Goswami et al., 2013), however, MES is suggested to be the primary buffer of choice since it has a pKa of ~6 which allows the preparation of EDC crosslinking with Cet under slightly acidic pH, thus more stabilized environment (Ferreira et al., 2015).

A colorimetric micro BCA protein assay kit was utilized to determine the amount of Cet conjugated on the MCPCNP *via* reduction of the amount in the supernatant from the initial amount. Our data revealed that 61.37 ± 0.70% of the Cet added was incorporated on the surface, which is slightly higher than what was reported by Mato et al. wherein 51.11 % of Cet was conjugated to the surface of PLGA nanoparticles loaded with Sorafenib (Mato et al., 2015).

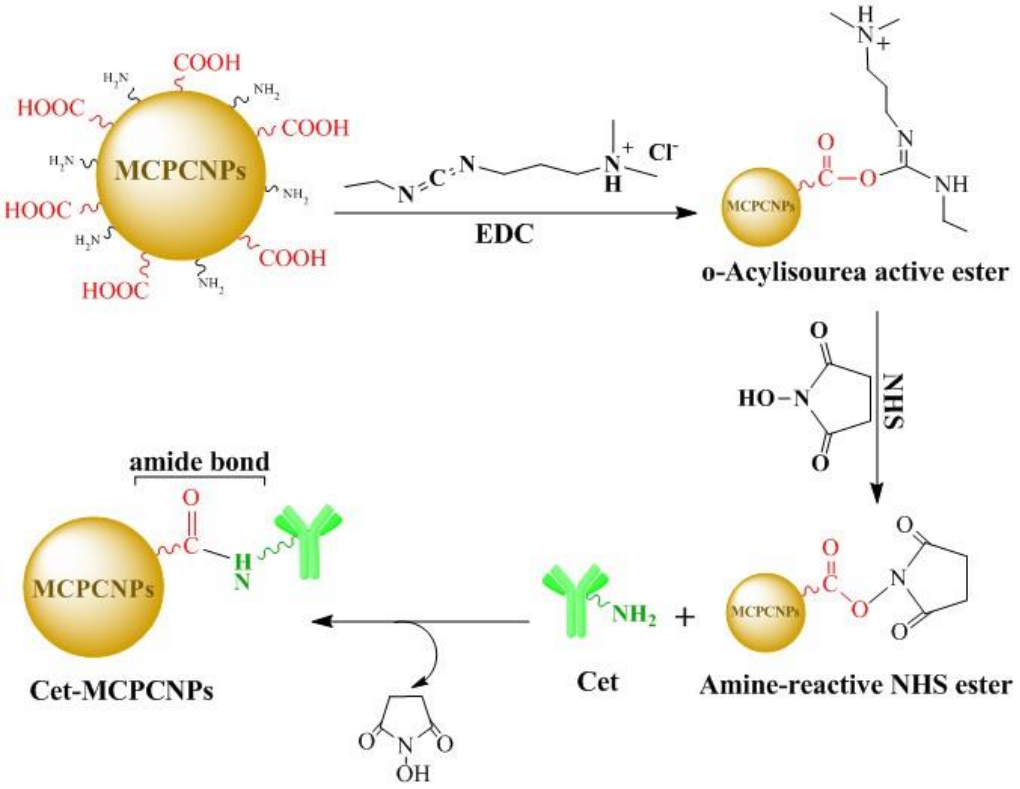


Figure 4.1 Schematic representation of the EDC/NHS conjugation that was employed to crosslink Cet to MCPCNPs

4.4.2 Physiochemical characterisation

An average particle size of 249.33 ± 5.15 nm was obtained for the Cet-MCPCNPs which was in accordance with the sizes observed from the STEM images (Figure 4.2). This indicates an increase of about 72 nm in the size of the MCPCNPs after Cet conjugation. The increase in size can explained by the fact that a typical antibody (150 kDa) is about 15 nm long and about 5 nm in diameter at the base, therefore, the increase in diameter size is consistent with the high molecular weight of the Cet which contributes to an overall increase in NP diameter (Kim et al., 2014). The same tendency of antibody increasing the size of NP was also reported by Maya et al., when they incorporated Cet on the surface of O-carboxymethyl chitosan NPs loaded with paclitaxel. However, the increase in size (≈ 50 nm) observed by these authors was slightly lower,

probably due to the lower conjugation efficiency of the antibody (42±6 %) (Maya et al., 2013). It has been reported that NPs of less than 400 nm in size may accumulate in the tumour through enhanced permeability of actively dividing cells and retention (Deepagan et al., 2012). Therefore, this signifies that the Cet-MCPCNPs will more probably accumulate passively in the tumour vicinity. Figure 4.2 also confirms that the MCPCNPs maintained their spherical morphology after conjugation to Cet and remained well-distributed.

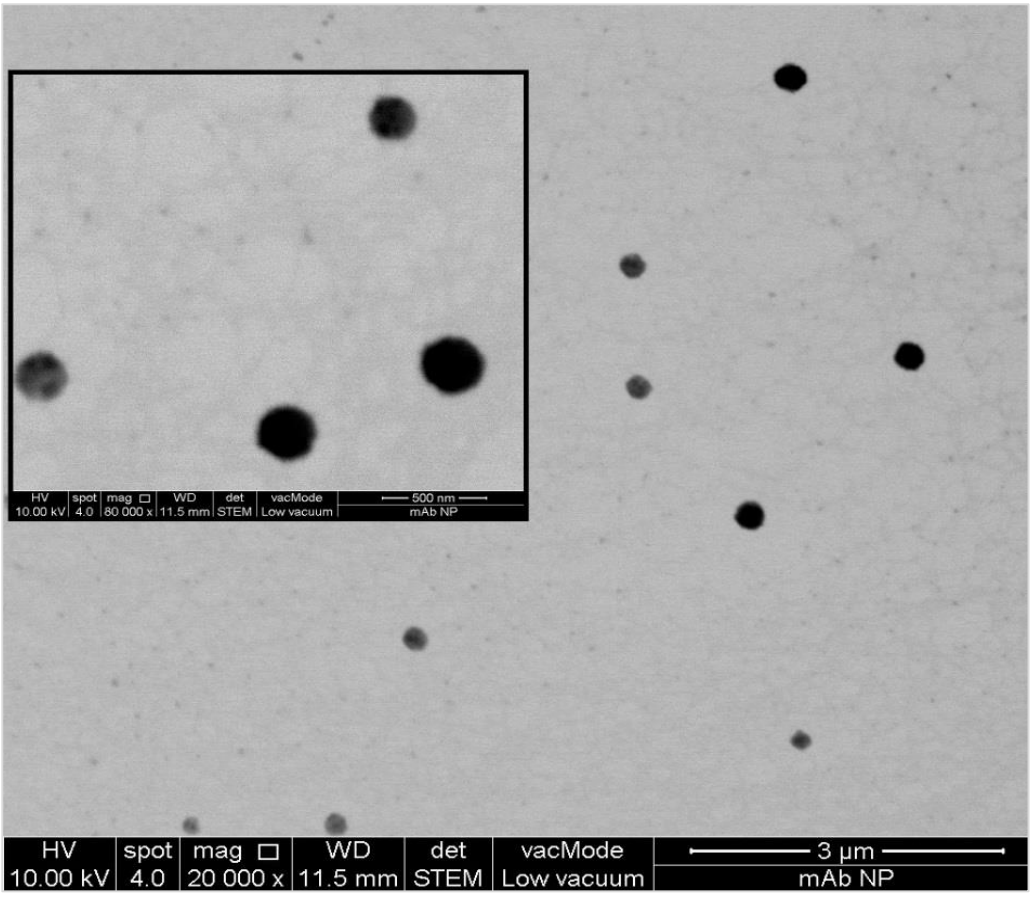


Figure 4.2 STEM image of the Cet-MCPCNPs

Interestingly, a significant increase in the surface charge of MCPCNPs was also observed after the Cet incorporation, from +35.7 ± 1.418 mV to +39.1 ± 0.87 mV, respectively. Most probably due to the amino group neutralisation of the carboxylic groups present on the surface of the MCPCNPs, resulting in a more

positive surface charge in the system. This observation is in good agreement with a number of studies that reported an increase in surface charge after the incorporation of antibodies (Chu et al., 2015; Kutty and Feng, 2013; Mato et al., 2015; Maya et al., 2013).

FTIR spectral analysis was then studied in order to identify the chemical modifications occurring in the nano-matrix due to the conjugation of Cet onto the MCPCNPs surface. Figure 4.3 presents the FTIR spectra of the Cet-MCPCNP, (i) in comparison to the MCPCNPs, (ii). FTIR spectra of both samples displayed strong absorption at 3271 cm^{-1} which may be attributed to the stretching vibration of the O–H groups. In both spectra, an adsorption peak was observed at about 2930 cm^{-1}, which correspond to the asymmetrical C–H stretching vibration. Furthermore, sharp absorption peaks at 1148 cm^{-1} and 1028 cm^{-1} demonstrate stretching vibration due to (C – O) and (C – N) amine bonds, respectively. Typical peak was identified at 3499 cm^{-1} in Figure 4.3 (i) which corresponds to the N-H bending vibration of Cet. Other characteristic absorption peaks were observed at 1399 cm^{-1} and 1211 cm^{-1} which corresponds to the strong (S = O) stretching of Cet. Moreover, the peak at 1239 cm^{-1} which represent the C-N stretching confirms the formation of an amide bond between MCPCNPs and Cet. Usually amide vibrations involve C=O, C-N and N-H groups of a peptide bond which result in characteristic spectral features of proteins (Singh, 2000). The peak at the region 1640-1660 cm^{-1} in the spectra depiction of Figure 4.3 (i) and (ii) (indicated by dashed circle) confirms the presence of curcumin in the NPs

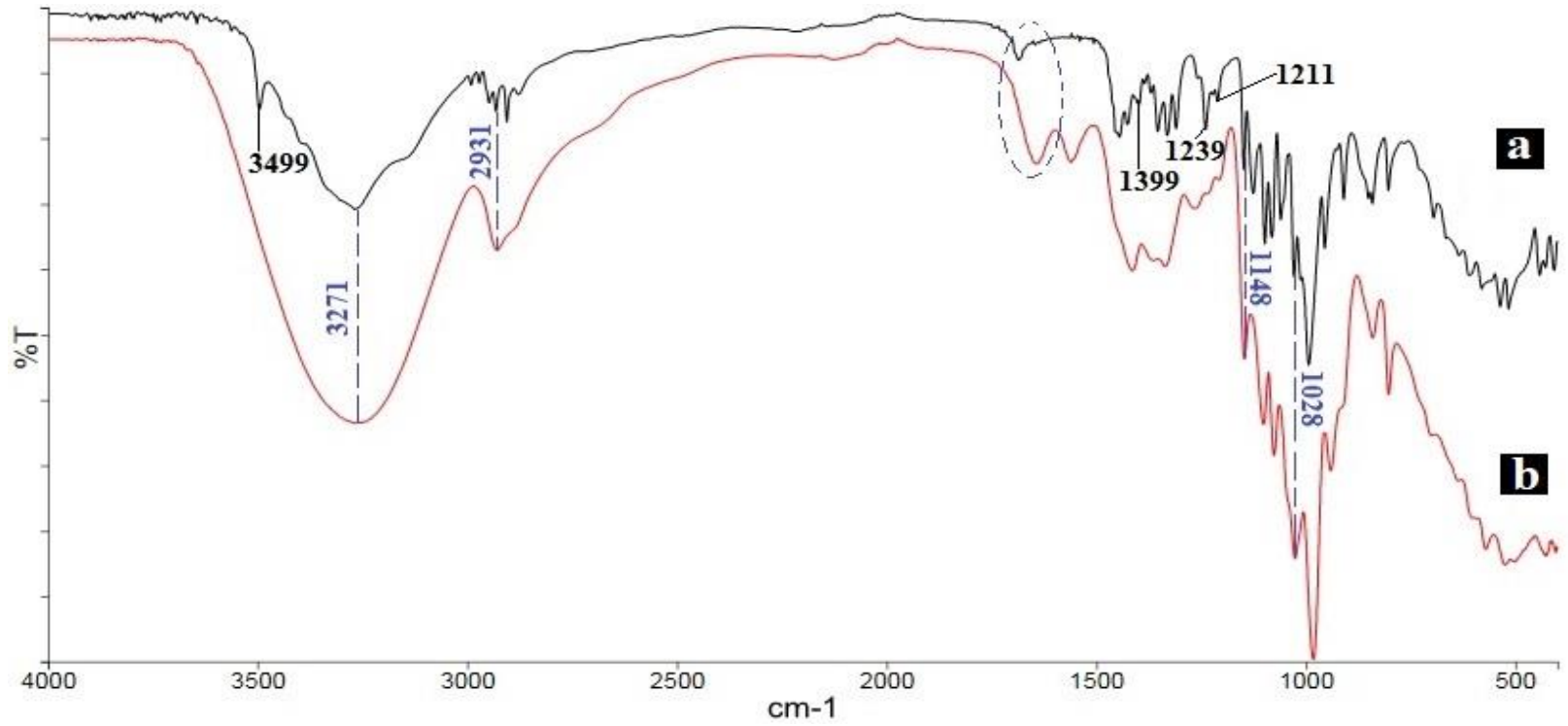


Figure 4.3 FT-IR spectra of Cet-MCPCNP **(a)** and MCPCNP **(b)**

The EDX spectra (Figure 4.4) captured during SEM of both MCPCNP and Cet-MCPCNP were also evaluated to further confirm the conjugation of the Cet with MCPCNP. The EDX analysis of Cet-MCPCNP (Figure 4.4 (b)) revealed strong signal for Sulphur, and thus confirmed the presence of intact Cet which is an elemental component of Cet and absent in the other raw materials used for the fabrication of MCPCNPS. The EDX pattern in both MCPCNPs and Cet-MCPCNPs consisted of Carbon, Oxygen, Phosphorous and Nitrogen. However, the Cet-MCPCNPs consisted of slightly higher weight percentage contribution due to N (3.12 %) which further confirms the presence of Cet and could be attributed to the amide bond formed between the Cet and MCPCNP.

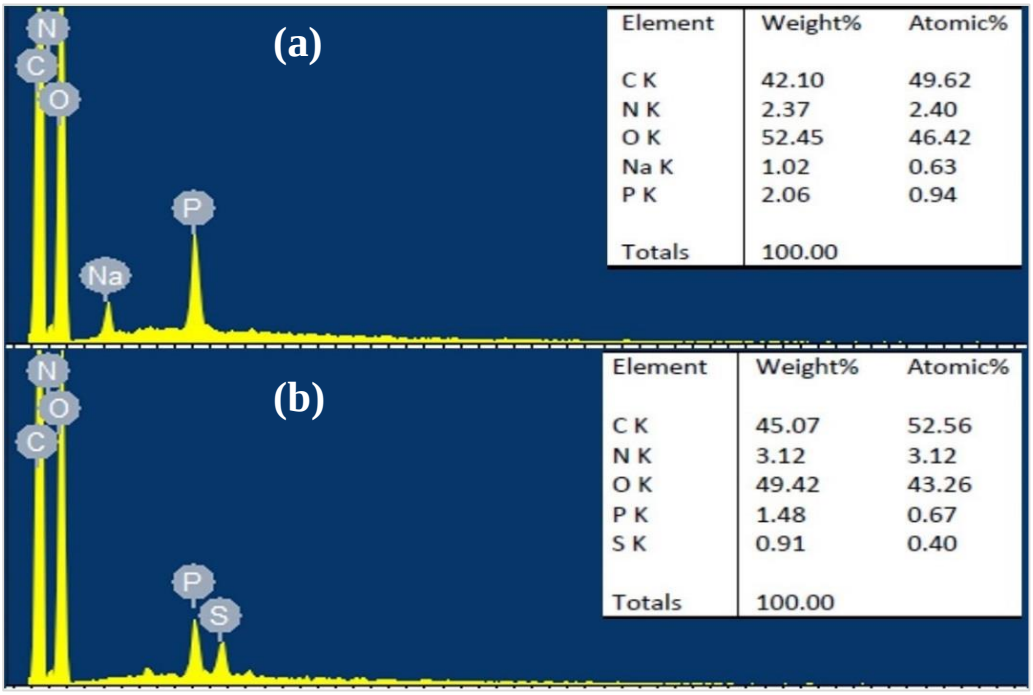


Figure 4.4 EDX chemical mapping of MCPCNPs (**a**) Cet-MCPCNPs (**b**) on a STEM copper grid

4.4.3 Entrapment efficiency and *in vitro* curcumin release

The encapsulation efficiency of the carrier system for curcumin was determined by reading the absorbance of the supernatant of the Cet-MCPCNPs after the formulation process at 425 nm and was found to be 68.43 ± 2.4%. This was a slight decrease in the entrapment efficiency of MCPCNP, which was initially 69.43 ± 1.11% (refer to chapter 2, section 2.4.6). The main factors that affect the entrapment efficiency are the concentrations of polymer and type of drug used. Therefore, since the conjugation of Cet was carried out at pH=5.0 some of the surface bound curcumin would have been lost, which thus explains the slight decrease of entrapped curcumin in Cet-MCPCNPs.

For effective oral delivery of Cet-MCPCNPs *in vivo*, the formulation should be stable enough to deliver the payload to colonic tumours before any dissociation. Therefore, the release profile of curcumin from Cet-MCPCNPs was studied under physiologic conditions mimicking the pH and transit times likely to be encountered in the stomach and colon (2 h in pH 1.2 and 24 h in 33% (w/v) caecal media). The amount of curcumin released into the supernatant over each time point was measured by HPLC. Cet-MCPCNPs showed slow and controlled release of curcumin from the NPs (Figure 4.5), initially, whereby curcumin was bound to diffuse from the highly conjugated chitosan-pectin matrix whose surface is tightly shielded by Cet.

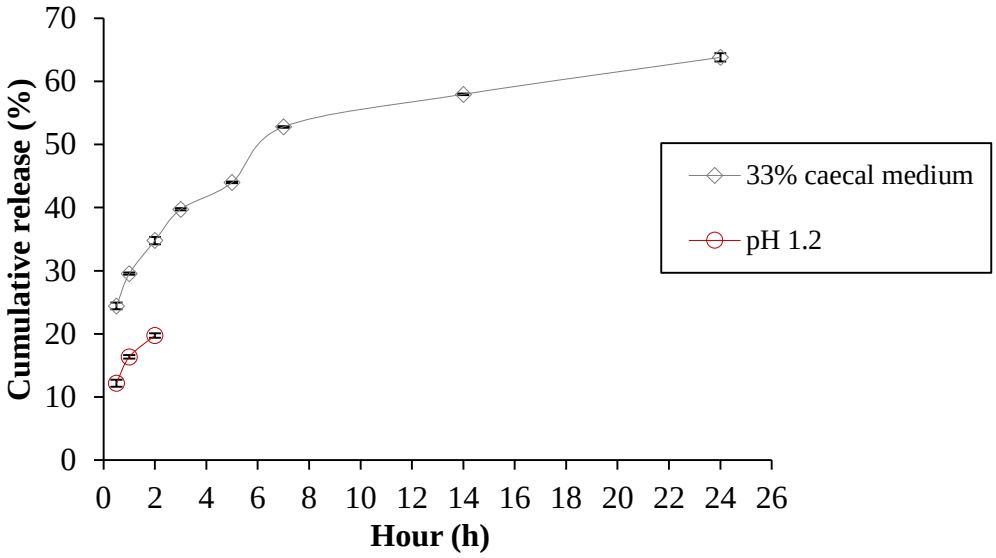


Figure 4.5 *In vitro* drug release profile of curcumin from Cet-MCPCNPs in pH 1.2 for 2 h and 33 % caecal medium for 24 h

In the case of release at pH 1.2, only 19.74 ±0.37 % of curcumin was released from Cet-MCPCNP after a 2 h incubation period, while 63.79 ±0.66 % was released from the NP over 24 h in the caecal medium. The difference in curcumin release observed at two different pH/buffer conditions may be attributed to the pH-dependency in the swelling behaviour of chitosan-pectin matrix, whereby the ionic interaction between amino groups in chitosan and negatively charged MCP is significantly reduced at colonic pH and hence forms a relatively loose network (Pandey et al., 2013). This increases the porosity of the matrix and imbibes water within the Cet-MCPCNPs that allowed the leakage of more curcumin. Furthermore, this higher curcumin release observed in 33% caecal content compared to the acid environment may be attributed to the enhanced colloidal stability of the NP in acidic environment compared to colonic conditions. Interestingly, the release pattern of curcumin from MCPCNPs (presented in Chapter 3, Figure 3.11) and Cet-MCPCNPs (Figure 4.5) is identical to the release in 33 % caecal media in which both appear to

follow a biphasic release pattern, signifying that the conjugation of Cet to the surface of NPs did not alter the properties of the chitosan-modified pectin matrix. However, a negligible decrease in curcumin release from Cet-MCPCNP (≈ -3.38 %) compared to MCPCNP in colonic medium was observed. On the other hand, an increase (≈ +1.98 %) in curcumin release from Cet-MCPCNPs compared to MCPCNPs was observed in pH 1.2. This is because at pH 1.2 the amine groups of Cet become protonated and create repulsive forces between adjacent positive charges and thereby cause Cet to detach from the NP surface thus allowing more curcumin to be diffused out (Maya et al., 2013). In basic media however, there is a limitation in the extent of protonation of the $-NH_2$ of Cet which keeps it attached to the surface of NPs and hence inhibiting the diffusion of curcumin at a faster rate (Prabaharan et al., 2007).

These results are in accord with a study by Kutty et al. in which the release of docetaxel from micelles of vitamin E TPGS was found to be 64.83 % whereas after conjugation with cetuximab, there was a decrease in release to 54.31 % at pH 7.4 (Kutty and Feng, 2013). It is worth noting that the release profile of Cet-MCPCNPs is likely to be enhanced in *in vivo* setup. This is because in targeted drug delivery systems, after receptor mediated endocytosis, proteins become internalized from the cell environment via a set of endosomes to the lysosome in which they will undergo a major degradation (Tokarev et al., 2013) which allows the delivery of curcumin to the internal compartment of the tumour tissue.

4.4.5 Mucin adsorption studies

The mucoadhesive behaviour of Cet-MCPCNPs was studied using the mucus glycoprotein assay, to confirm that the conjugation of an antibody did not alter the mucoadhesion propensity of MCPCNPs. Results are reported as mucoadhesion percentages in Figure 4.6.

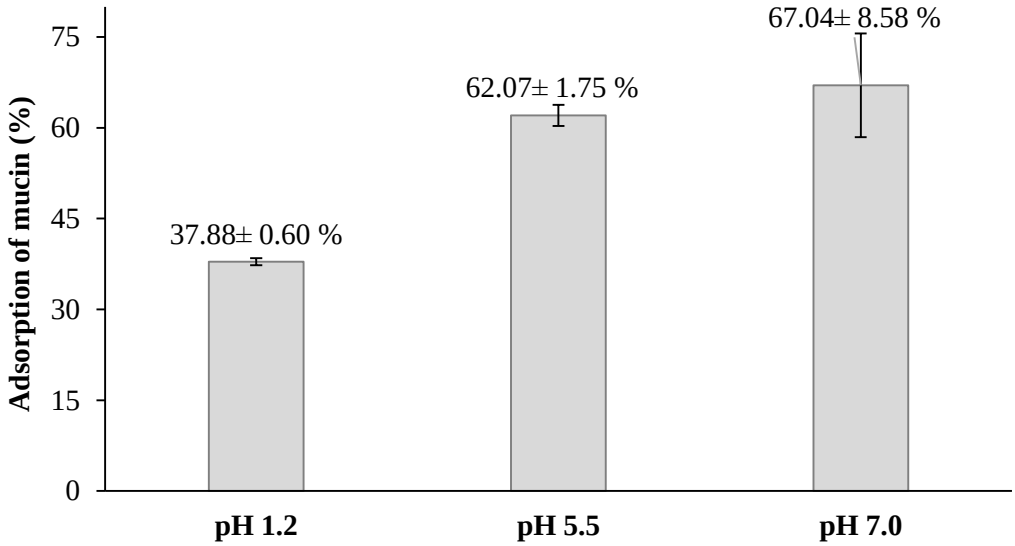


Figure 4.6 Mucin adsorption of Cet-MCPCNPs at different pH

Clearly, a positive correlation can be observed between the amounts of mucin adsorbed onto the NP with increase in pH. Moreover, the results obtained are in good agreement with previous reports on MCPCNPs as described in Chapter 3, Figure 3.4, and hence confirming that the incorporation of Cet did not significantly impact the mucoadhesiveness of the MCPCNP. High percentage mucoadhesion of the NPs is attributed to the hydrogen bond and ionic interactions between the amino groups of chitosan with mucin chains (Hosseinzadeh et al., 2012). Moreover, the cationic nature of Cet-MCPCNPs as a whole, electrostatically interacts with the negatively charged sialic acid residues of mucin whose pKa is 2.6 in colonic medium (Svensson and

Arnebrant, 2010). In general, NPs provide higher mucoadhesion property compared to microparticles due to their larger surface area to volume ratio, which provides more room for mucin adsorption (Moghaddam et al., 2009).

4.5 Conclusion

Cet was successfully attached to surface of MCPCNPs via the carbodiimide (EDC)/ NHS chemistry. The EDX and FTIR analyses confirmed the successful presence of Cet in MCPCNPs. The *in vitro* drug release observed at pH 1.2 and simulated caecal medium support the appropriateness of this formulation for colon delivery. The mucoadhesion propensity of MCPCNPs was not altered after Cet-conjugation. Therefore, the *in vitro* cell evaluation of Cet-MCPCNPs will be investigated in Chapter 5 to confirm whether this combined approach is effective in cancer therapy.

Chapter 5 *In vitro* cell evaluation of formulations

5.1 Introduction

Cell culturing, a process by which cells are detached from their natural environment and then grown in a controlled environment, has generated vast avenues in the study of human and animal tissue in appropriate pathological contexts (Hudu et al., 2016). Drug and chemical testing in recent years have profoundly relied on cell culture technology to overcome some of the drawbacks associated with animal testing and avoiding unethical procedures (Doke and Dhawale, 2015). Cell culture-based practical technologies have evolved in several areas, including the valuation of the efficacy and toxicity of new drugs, and production of vaccines and biopharmaceuticals (Yao and Asayama, 2017). In the field of cancer research, drug-cell interaction, mechanism of action, cell proliferation and drug metabolism have been well developed under the framework of *in vitro* cell culture techniques. Consistency and reproducibility of data can be assured by using a batch of clonal cells. Cell culture procedure is an efficient and cost effective alternative model to animal use (Arango et al., 2013).

In the present objective, the antiproliferative efficacy, cellular uptake, selectivity and therapeutic efficacy of formulated NPs against CRC cell line models will be evaluated in detail. This addresses the issue of non-specificity to cancer treatment whilst at the same time reducing the side effects due to the anticancer agents.

5.2 Materials

Curcumin was purchased from Fluka, (U.S.A). Chitosan (low molecular weight, de-acetylated chitin), sodium tripolyphosphate, RNase A, propidium iodide (PI) and trypan blue were purchased from Sigma–Aldrich, USA. Low methoxyl citrus pectin (DE lower than 50) was bought from Genu, CPKelco® (Limeira-SP, Brazil). Cetuximab (Cet) was purchased from Chembest Research Laboratories, China. Dulbecco's modified eagle's medium (DMEM) 4.5 g/l glucose with L-glutamine and sodium pyruvate free, roswell park memorial institute (RPMI) 1640 medium 1x (with L-glutamine and 25mM HEPES) , foetal bovine serum (FBS), trypsin EDTA, (3-(4,5-dimethylthiazolyl-2)-2,5-diphenyl tetrazolium bromide) (MTT), dimethyl sulfoxide (DMSO), calcium and magnesium free phosphate buffered saline (PBS) pH 7.4, penicillin-streptomycin mixed solution and trehalose were bought from Nacalai Tesque, Japan. Triton X-100 was bought from R&M chemicals, UK.

5.3 Methods

5.3.1 Maintenance of cell culture

Human colorectal adenocarcinoma cell line (HT-29) and (Caco-2) were a kind donation by the National Cancer Council, Malaysia (MAKNA) laboratory, University Putra Malaysia and cultivated in monolayers to 85-90 % confluence in DMEM medium supplemented with 10 % FBS and 1 % penicillin-streptomycin. The human colorectal carcinoma (HCT-116) and normal lung fibroblast (MRC-5) were a donation by the Cell Culture Lab of the University of Nottingham, Malaysia. These cells were harvested in monolayers in supplemented RPMI – 1640 medium. All cell types were maintained at 37 ^{0}C in a humidified atmosphere containing 5 % CO_2. After reaching confluence, the

cells were detached from the flask with trypsin–EDTA. The cell suspension was centrifuged at 1500 rpm for 5 min and then re-suspended in their respective growth medium for further studies.

5.3.2 Subculture of cells

Cells were harvested by aspirating the medium and gently rinsing the cells with Ca^{2+} and Mg^{2+} free PBS. For cell detachment, Trypsin-EDTA was added to the flasks and incubated at 37 ^{0}C for 5 minutes. Flasks were then gently tapped to detach cells from the bottom of the flask. The cells were viewed under inverted microscope (Nikon Eclipse AZ100, Japan) to confirm their detachment, re-suspended in fresh media and then centrifuged at 1500 rpm at 25 ^{0}C (Eppendorf 5424, Germany) for 5 minutes. Lastly, the supernatant was discarded and cells were re-suspended in fresh media. Dilution was carried out to split the cells into different flasks.

5.3.3 Cell counting

Cells were harvested from the flask of confluent cells as ascribed in section 5.3.2. A 15 µL aliquot of cells was mixed with 15 µL of trypan blue and added into the counting chamber of a hemacytometer (Figure 5.1 (a)) and allowed to be drawn into chamber by capillary force. The chamber was then viewed under an inverted microscope (Nikon Eclipse AZ100, Japan) with a 10x objective. The cells in the four outside gridded squares (Figure 5.1 (b)) were counted, excluding the dead cells stained by trypan blue. The number of cells per 1 mm^2 was calculated as the average of the four counted chamber sides. The total number of cells was calculated as follows:

$$\text{Number of cells per 1 mL} = \text{average cells per } 1mm^2 \times 10^4$$

Total number of cells = number of cells per 1 mL x dilution factor of trypan blue x dilution factor of media.

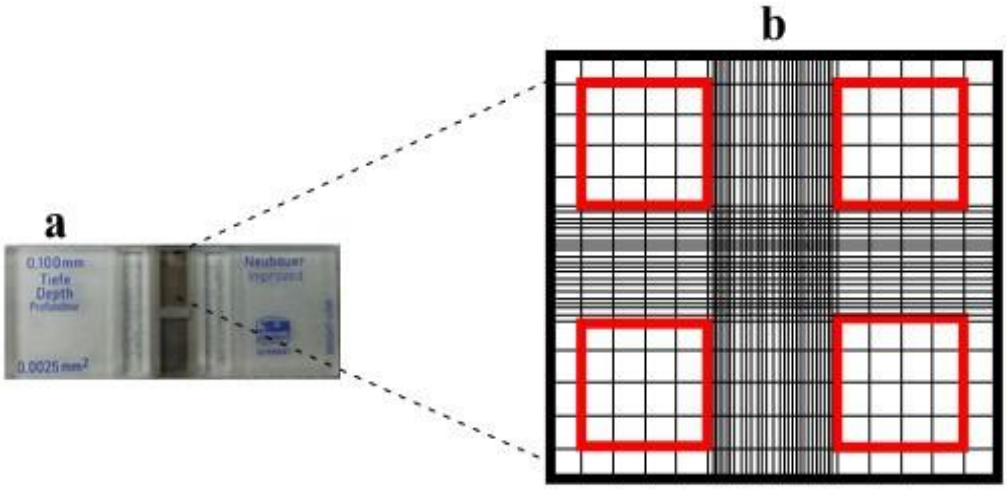


Figure 5.1 Schematic representation of a haemocytometer (a) and its counting grids (b)

5.3.4 Cell cytotoxicity

The cytotoxicity of MCPCNPs was assessed using the MTT assay. The HT-29, Caco-2, HCT-116 and MRC-5 cells were cultured for 24 h in 96 well plates at 2 x 10^3 cells/well and 5 x 10^5 cells/well, respectively and then treated with either curcumin solution (free curcumin), Cet-MCPCNPs, MCPCNPs and/or CPCNPs at four different concentrations of curcumin (2.5, 5, 10 and 20 µg/mL) for a period of 24, 48 and 72 h at 37 ^{0}C in a CO_2 incubator. Cells in media devoid of nanoparticles and cells treated with DMSO acted as negative control while 15 µM of 5-fluorouracil (5-FU) was used as a positive control under the same experimental conditions. A 10 µL aliquot of MTT reagent (5 mg/ml in PBS) was added to each well. After 4 h of dark incubation at 37 ^{0}C, a 100 µL aliquot of DMSO was added and content mixed for 10 min at 50 rpm using a laboratory shaker (S1000 Gyrotwister, Labnet, USA). The absorbance of each well was

then measured at 570 nm using a microplate reader (Epoch, BioTek®, USA). The mean values of the relative growth inhibition compared to untreated cells were presented (n=3).

5.3.5 Cellular uptake

5.3.5.1 Qualitative cellular uptake

Cellular uptake of treatments in HT-29, Caco-2 and HCT-116 were examined on a fluorescent microscope. The cells were seeded in 6 well plates at 1 x 10^5 cells/well at 37˚C for 24h. The culture media were then replaced with treatment media containing either curcumin, MCPCNPs, Cet-MCPCNPs and/or CPCNPs at 2.5 and 20 μg/mL, representing low and high doses of curcumin, respectively. Controls used were untreated cells and cells treated with DMSO. After 4 h, cells were gently washed with PBS and viewed under fluorescent microscope with 535-600 nm (blue filter, FITC channel) to determine the cellular uptake of curcumin.

5.3.5.2 Quantitative cellular uptake

The HT-29, Caco-2 and HCT-116 cells were harvested from a confluent culture flask, seeded and treated as described in section 5.3.5.1. After 4 h, treatment media were aspirated, cells were gently washed with PBS, trypsinized and centrifuged at 1500 rpm for 5 minutes. The cell pellet was then lysed using methanol and vortex-mixed for 1 minute. Lastly, the amount of curcumin taken up by the cells was quantified using the HPLC method described in Chapter 2, section 2.3.5.

5.3.6 Cellular apoptosis

A total of 1×10^5 cells/1.7cm^3 well were seeded on a LAB-TEK chamber slide (Thermo Scientific Nunc, U.K.) and cultured for 24 h to allow adherence of the cells. The cells were then exposed to media containing 20 µg/mL of curcumin, Cet-MCPCNPs and MCPCNPs. Untreated cells and cells treated with DMSO were used as negative controls and positive control, respectively. After 24 h of treatment, cells were fixed with 3.7% formaldehyde for 10 minutes, washed with PBS and left to air-dry for another 10 minutes. Then 1 µg/mL of DAPI in deionized water was added to the wells and incubated in the dark for 10 minutes. Lastly, cells were washed with PBS and viewed under an inverted fluorescence microscope (Colibri 7, Zeiss axio, Germany) equipped with the red filter (430-495 nm), (n=3).

5.3.7 Cell cycle

Caco-2 and HCT-116 cells were seeded at 5 x 10^5 cells/well in 6 well plates. After 24 h, the cells were exposed to 20 µg/mL of curcumin, MCPCNPs and Cet-MCPCNPs. Untreated cells and cells treated with DMSO were used as negative control and as positive control, respectively. After 24 h of treatment, cells were trypsinized, centrifuged at 1800 rpm at 25 ^{0}C for 5 minutes, fixed in 70 % (v/v) cold ethanol for one week and stored in -20 ^{0}C. After a week, cells were washed and centrifuged twice before the addition of 500 µL of PI staining solution. PI staining solution was prepared by mixing 0.1% (v/v) Triton X-100, 10 µg /mL PI and 100 µg/mL RNase A in PBS. Cells were incubated for 30 minutes on ice and finally analyzed by flow cytometry (Flow FACS Calibur, Becton Dickinson, USA) at 488-nm laser line excitation.

5.3.8 Statistical analysis

Statistical analysis was done using the Graph-Pad Prism 7 software. All values are expressed as mean ± standard deviation. The statistical significance between the sets of data was tested by one-way analysis of variance (ANOVA) followed by Turkey's test with $p < 0.05$ considered significant.

5.4 Results and discussion

This section is divided into two sections. Firstly, I wanted to analyse whether the combined effects of curcumin, modified pectin and mucoadhesion of the carrier system, augments the anticancer effects in colon cancer. Therefore, I employed the cell lines HT-29, HCT-116 and MRC-5 with the following treatments: MCPCNPs, curcumin solution and CPCNPs. In the second section however, I aimed to ascertain whether attaching appropriate antibodies to the surface of the MCPCNPs that target EGFR within the CRC cells would augment effectiveness of the treatment. Therefore, I employed the cell lines Caco-2, HCT-116 and MRC-5 with the following treatments: MCPCNPs, curcumin solution and Cet-MCPCNPs.

Section I:

Galectins are carbohydrate binding proteins characterized by their ability to bind to carbohydrate chains that contain β-galactosides resident on glycoconjugates, leading to cell-matrix and cell-cell adhesion (Nielsen et al., 2018). Among all the known galectins, galectin-3 (Gal-3) is specifically involved in a variety of cellular and carcinogenic processes (Newlaczyl and Yu, 2011). Gal-3 is undetectable in normal cell lines, indicating that it is a cancer-specific biomarker (Balan et al., 2010). HT-29 and HCT-116 are among the common model systems used in *in vitro* cancer work with a high expression of Gal-3 (Satelli et al., 2008). However, one of the main differences between HT-29 and HCT-116 is that the former expresses a small proportion of mucus-secreting cells and columnar absorptive cells in culture media and therefore contains relatively higher levels of mucin (Gagnon et al., 2013). MRC-5 have been widely used in literature (Buhrmann et al., 2014; Gandin et al., 2012; Šeklić et al., 2018; Tokunaga et al., 2000) as a control (normal) cell line against colorectal cancer cell lines, therefore, it was utilized as the control in the present study.

5.4.1 Maintenance of cell culture

HT-29, HCT-116 and MRC-5 cells were maintained at standard cell culture conditions. Cells were passaged when confluence was reached every 5-7 and 2-3 days for HT-29, MRC-5 and HCT-116 cells, respectively. Figure 5.2 depicts confluent HT-29, HCT-116 and MRC-5 cells viewed under inverted microscope.

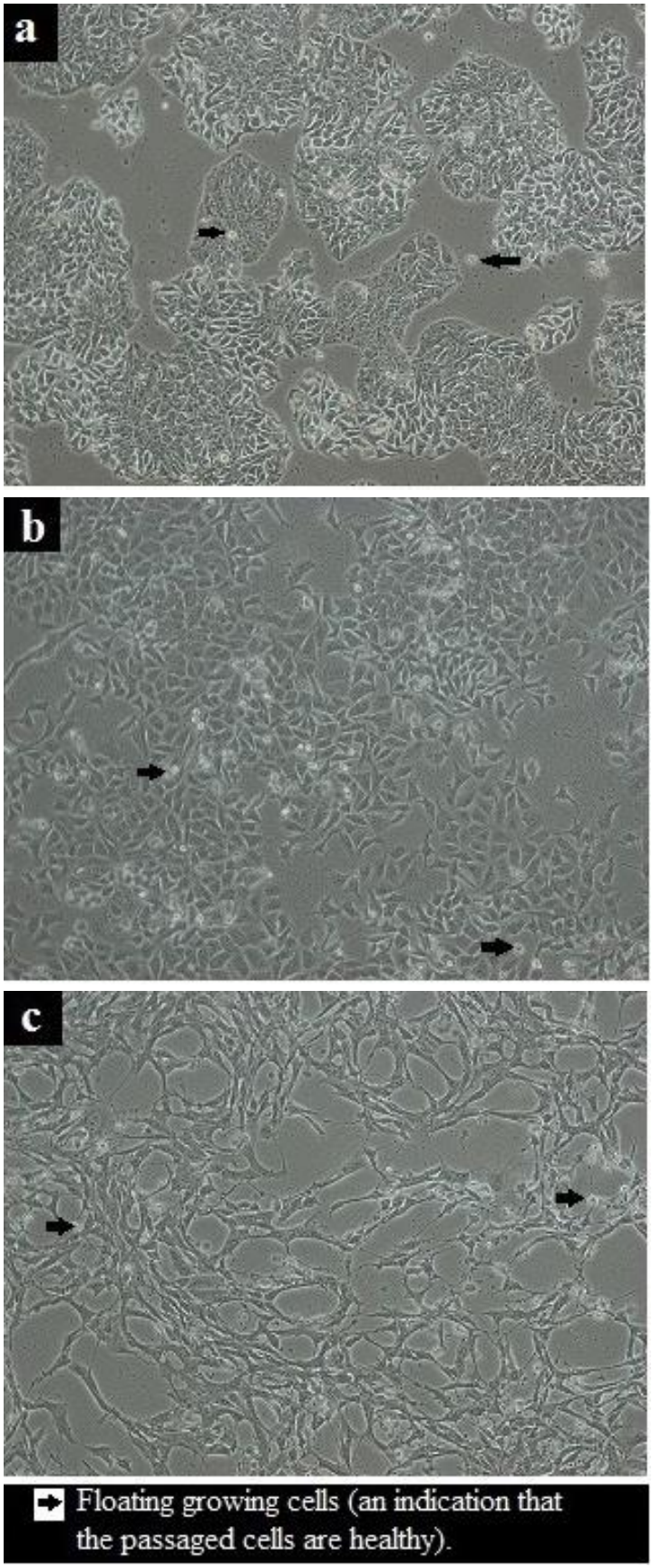


Figure 5.2 HT-29 cells **(a)**, HCT-116 **(b)** and MRC-5 cells **(c)** viewed under an inverted microscope under 10× magnification

5.4.2 Cell cytotoxicity assay

One of the major limitations in the use of curcumin as an effective anticancer agent is its reduced bioavailability and low solubility. However, a targeted nanoformulation of curcumin has the potential to improve its bioavailability and provide enhanced cytotoxic effects toward cancer cells (Gera et al., 2017). Three different formulations (MCPCNPs, CPCNPs and curcumin solution) at four equivalent curcumin concentrations (2.5, 5, 10 and 20 μg/mL) were initially studied by MTT for toxicity on HT-29 and HCT-116 cell lines (Figure 5.3). The cell viability plots reveal that the overall cell viability of both cell lines decreased significantly when treated with increasing concentration of curcumin over the course of 72 hours, (i.e. dose- and time- dependent manner). In general, higher toxicity was induced by MCPCNPs on both HT-29 and HCT-116 cell lines at the four concentrations compared to curcumin solutions and aptly, CPCNPs. However, CPCNPs showed better cytotoxic effect in lower doses in both cell lines when compared to curcumin solution. The IC50 data presented in Table 5.1 reveal that after 72 h of treatment both MCPCNP and CPCNPs exhibited much lower IC50 compared to curcumin solutions in both cell lines.

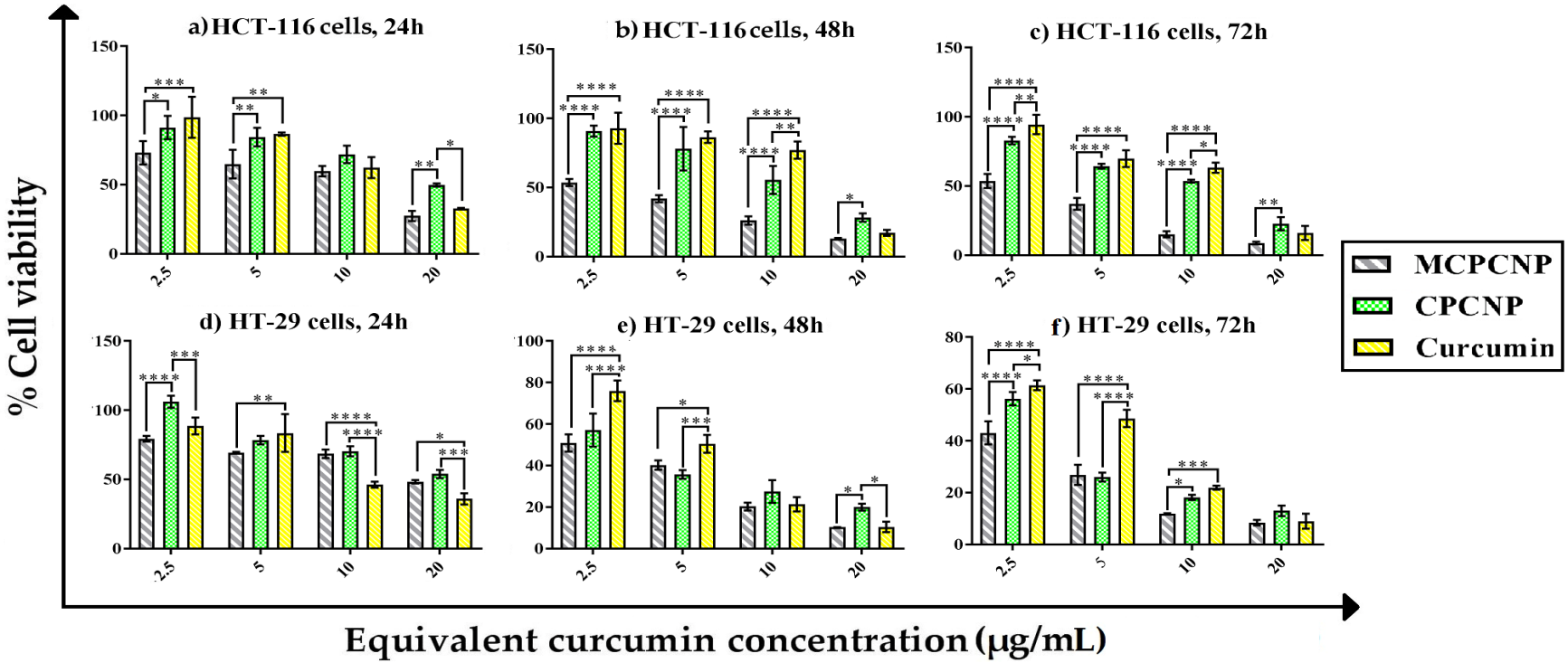


Figure 5.3 Cytotoxicity of MCPCPs, CPCNPs and curcumin solution on HCT-116 (a-c) and HT-29 (e-f) after 24, 48 and 72 h incubation (mean± S.D, n=3). Significance denoted as *($p < 0.05$), ** ($p < 0.01$), *** ($p < 0.001$), **** ($p < 0.0001$).

Table 5.1 IC50 values in µg/mL of MCPCNPs, CPCNPs and curcumin on HCT-116 and HT-29 cell lines. Each value represents means of triplicate determinations (mean ± S.D).

	24h		**48h**		**72h**	
	HT-29	HCT-116	HT-29	HCT-116	HT-29	HCT-116
MCPCNP	19.41± 0.77	11.83± 2.06	0.65± 1.13	2.00± 0.06	0.31± 0.06	0.40± 0.97
CPCNP	20.08± 3.53	19.68± 1.33	0.971± 3.40	13.12± 0.91	0.42± 0.02	11.21± 0.35
Curcumin	13.69± 0.19	14.76± 1.23	6.34± 0.64	13.58± 3.15	4.33± 0.51	11.99± 0.97

These observations highlight a few important points. Firstly, the polymeric encapsulation by the carrier system did not compromise on the therapeutic activity of curcumin. Secondly, the encapsulation of curcumin in the carrier system appear to have prolonged the contact between the nanoparticle and the cells, particularly HT-29, which explains the better treatment outcome. Recall that HT-29 expresses a higher level of mucous cells. Thirdly, mucoadhesion conferred by the chitosan-pectin matrix did augment the efficacy of curcumin, which was further validated by the much lower IC50 values required for toxicity on HT-29. This is in accord with a report by Hosseinzadeh et al. in which an enhanced cytotoxicity effect of chitosan-pluronic nanoparticles loaded with gemcitabine was observed in comparison with drug alone in HT-29 cell lines (Hosseinzadeh et al., 2012). They contend that the mucoadhesive properties of the nanoparticles imparted by chitosan was due to the mucin produced by HT-29 cell line, thus increasing the accumulation of the drug inside the cells.

The superiority in cytotoxicity of MCPCNPs (Figure 5.3) compared to the other treatments may be attributed to the fact that the modification process of citrus pectin results in the production of neutral sugar sequences with a low degree of

branching but rich in galactose. Galactose is capable of inhibiting the growth and migration of colon cancer cells since it is a remarkable antagonist to Gal-3 (Leclere et al., 2013). This agrees with a study that evaluated the preventive effect of modified pectin alginate probiotic microbeads on a Balb/c mouse model of colonic carcinogenesis, proving that the modified citrus pectin increased the bioactivity and chemo-preventative effect against pre-cancerous colonic lesions and adenocarcinoma through inhibition of Gal-3 (Odun-Ayo et al., 2015). It is worth noting that MCPCNPs, CPCNPs and curcumin had negligible toxicity on MRC-5 (Figure 5.4) which confirms the selectivity of the tested formulations/carrier system against colon cancer cells. Therefore, the MTT assay results support the safety of the formulation against normal cells.

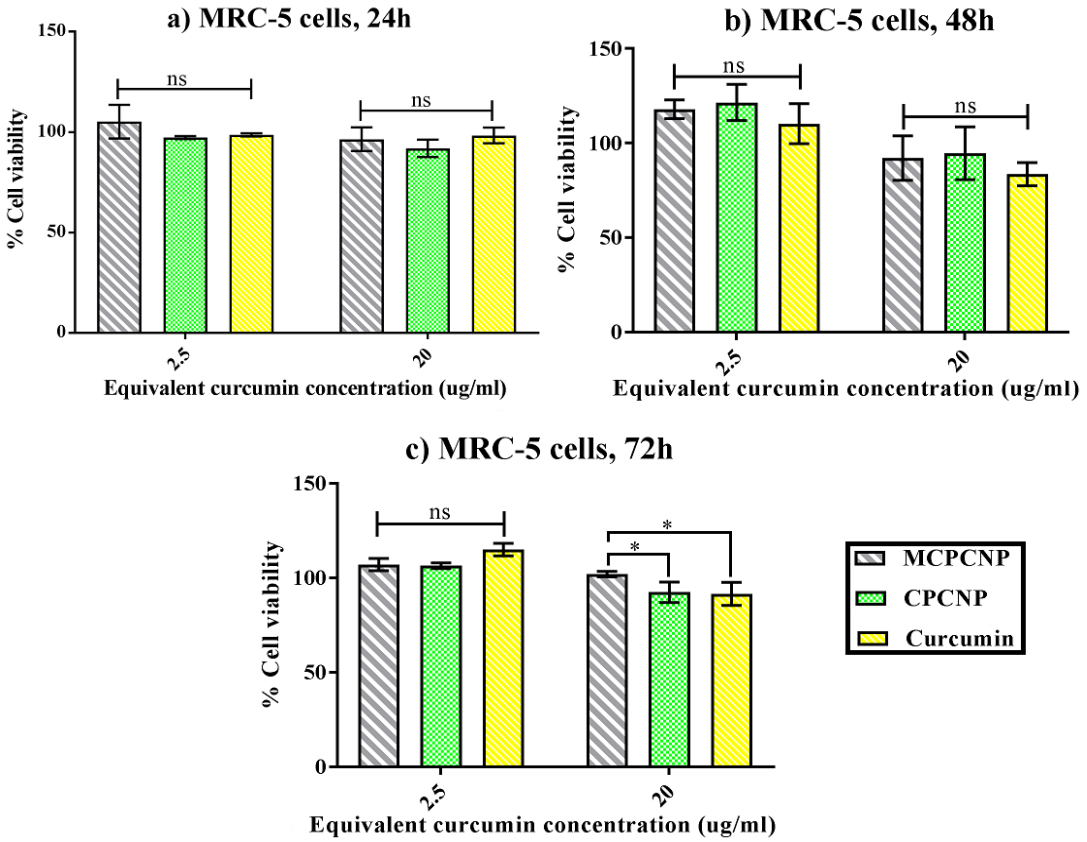


Figure 5.4 Cytotoxicity of MCPCPs, CPCNPs and curcumin solution on MRC-5 (a-c) after 24, 48 and 72 h incubation (mean± S.D, n=3). Significance denoted as *($p < 0.05$), ns (not significant).

5.4.3 Cellular uptake studies through fluorescent microscopy and HPLC

To evaluate the efficiency in cellular uptake of MCPCNPs, CPCNPs and curcumin solution, a 4 h incubation period was considered in reference to a number of reports in which a 4 h incubation period presented the sharpest slope for the cellular uptake kinetics of nanoparticles while a 24 h incubation saturated the cells and hindered the differential cellular uptake efficiency due to surface modifications (Cho et al., 2018; dos Santos et al., 2011; Shoshi et al., 2012). Due to the intrinsic green fluorescence of curcumin, it was possible to qualitatively and quantitatively assess the cellular uptake of MCPCNPs, CPCNPs and curcumin solution without the need for tagging by other fluorescent dyes.

Figures 5.5 and 5.6 display the intracellular fluorescence conferred by HCT-116 and HT-29 cell lines after uptake following treatments. The fluorescence images of untreated cells were captured as controls (not displayed). In general, both cell lines emitted green fluorescence and the morphology of the cells remained unchanged during the treatment period. Moreover, the emitted green fluorescence signifies the uptake of curcumin by the cytoplasm of the cell. At high curcumin concentration (20 µg/mL) both MCPCNPs and CPCNPs displayed a comparatively bright fluorescence intensity, while a slightly weaker green fluorescence signal was observed in cells treated with curcumin solution. At low curcumin concentration (2.5 µg/mL) a brighter fluorescent intensity was observed in cells treated with MCPCNPs compared to those treated with CPCNPs and curcumin solution. These findings indicate that the modification of pectin significantly augmented the internalization of the nanoparticles into the colon cancer cell lines, especially at low drug concentrations.

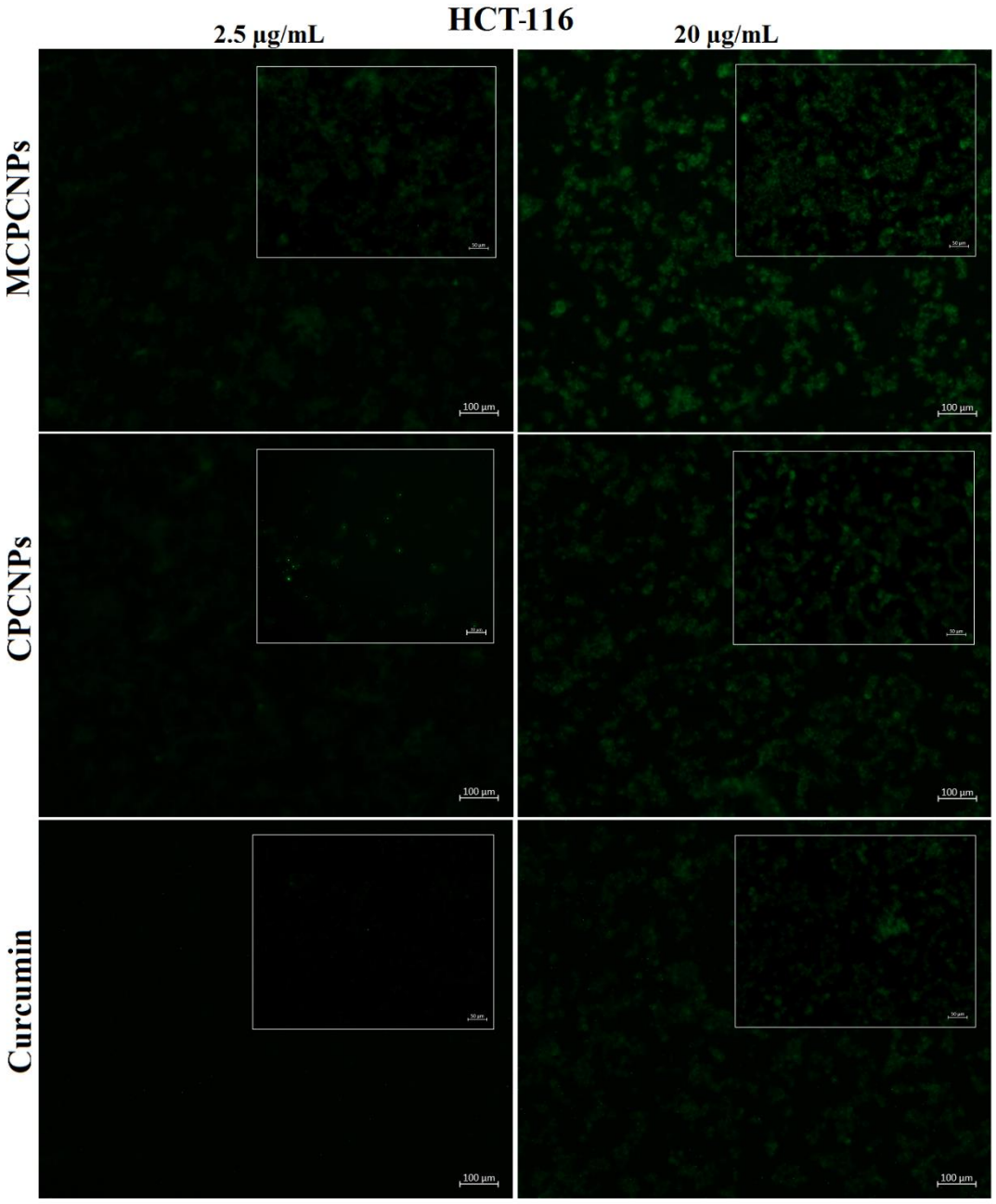


Figure 5.5 Cellular uptake of MCPCNPs, CPCNPs and curcumin solution at 20 µg/mL and 2.5 µg/mL after 4 h incubation [10-20x magnification]

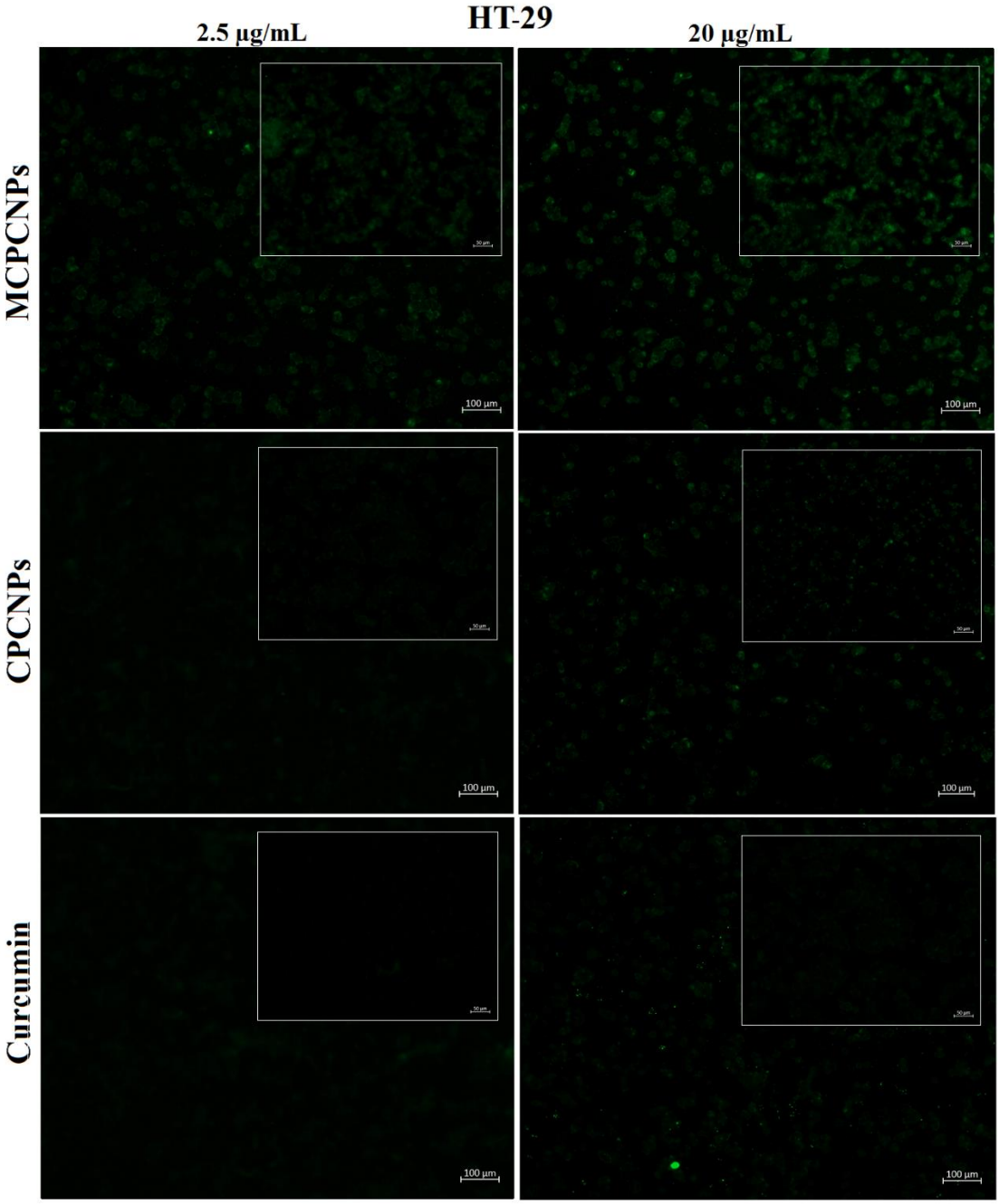


Figure 5.6 Cellular uptake of MCPCNPs, CPCNPs and curcumin solution at 20 µg/mL and 2.5 µg/mL after 4 h incubation [10-20 x magnification]

The quantitative cellular uptake analyses by HPLC (Figure 5.7) shows that in both cell lines the curcumin uptake was highest when treated with MCPCNPs followed by CPCNPs at both treatment concentrations (20 and 2.5 µg/mL). HCT-116 showed better curcumin uptake compared to HT-29 cells at high concentration of MCPCNPs and CPCNPs and a comparable uptake at low concentration. Such cellular uptake behaviour by HCT-116 and HT-29 was recently reported by Vijayakumar et al (Vijayakumar et al., 2019). They attributed it to the fact that the different genotypic profile of the two colonic cell lines dictates a different pathway for the cellular uptake of curcumin (Vijayakumar et al., 2019). On the other hand, curcumin uptake from curcumin solution possessed better uptake by HT-29 cell line than HCT-116. According to Howells et al. this can be attributed to the fact that the regulation of the primary target differs between the two colonic cell lines, which may be a function of p53 status. In HCT-116 (p53 wild-type), p53 plays an important role in governing the response of this cell line to therapeutic agents, making it less sensitive to curcumin compared to HT-29 cell line (p53 mutant) (Howells et al., 2007).

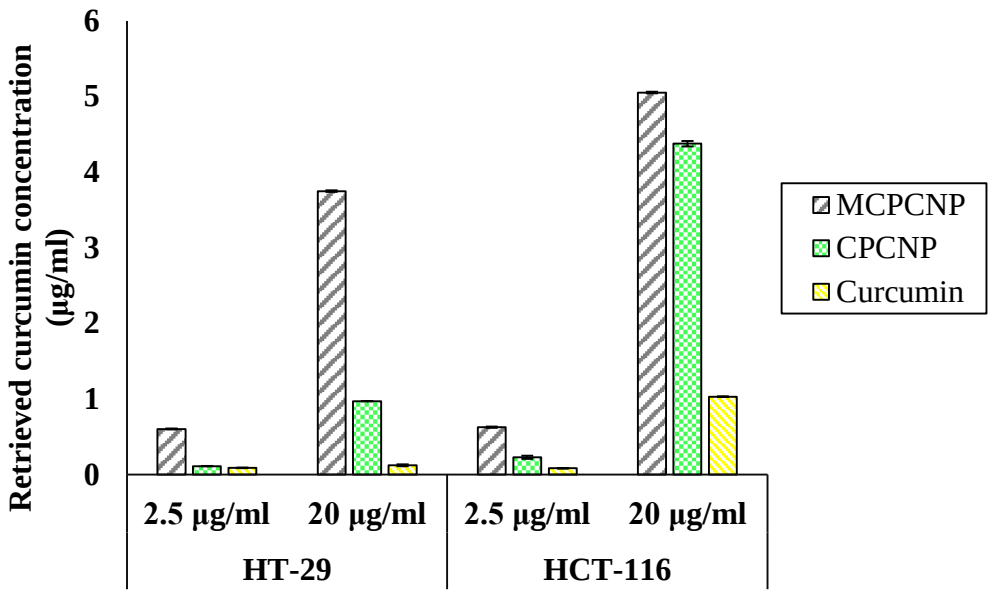


Figure 5.7 Amount of curcumin retrieved from HCT-116 and HT-29 cells after treatment with 20 µg/mL and 2.5 µg/mL of MCPCNPs, CPCNPs and curcumin solution after 4 h incubation. Averaged mean values and standard deviations of triplicates are presented

These findings propose that traversing of particles in HT-29 cell is impeded by the mucus layer, taking longer to reach the underlying epithelial cells. Thus, a reduced cellular uptake of the particles was observed compared to uptake in HCT-116. This explains the improved cytotoxicity effect on HT-29 occurring only after 48 h of treatment in contrast to HCT-116 occurring earlier. Akbari et al. showed that the presence of mucus in Caco-2/HT-29 co-culture caused 40–50% decrease of cellular uptake for coumarin encapsulated in digested cruciferin-chitosan nanoparticles, relating it to the potential mucoadhesive property of the chitosan parts of the particles (Akbari et al., 2017).

Section II:

To examine whether the anti-tumour activity of MCPCNPs is further enhanced in response to cetuximab coupling, we used two colorectal cancer cell lines, CaCo-2, which expresses high EGFR level, and HCT-116 with low EGFR

expression. These cell lines have been used in many other previous studies to assess the efficacy of cetuximab treatment (Li et al., 2014; Shigeta et al., 2013; Xu et al., 2005). Caco-2 and HCT-116 are *KRAS* wild- and mutant-type cell lines, respectively.

5.4.4 Maintenance of cell culture

Caco-2, HCT-116 and MRC-5 cells were maintained at standard cell culture conditions as described in section 5.4.1. Figure 5.8 depicts confluent Caco-2 cells viewed under inverted microscope.

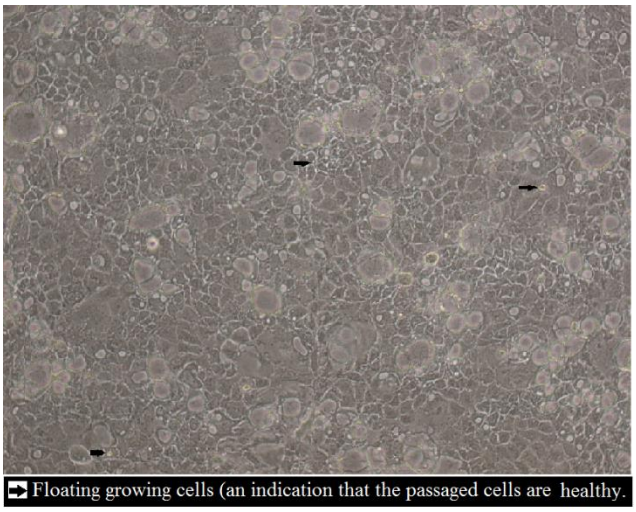


Figure 5.8 Caco-2 cells viewed under an inverted microscope under 10× magnification

5.4.5 Cell cytotoxicity assay

In order to explore and verify the anticancer efficiency of the well-designed Cet-MCPCNPs, MTT assay was employed to evaluate the cell viability of MCPCNPs, Cet-MCPCNPs and Curcumin. Figure 5.9 displays the cytotoxicity data by MTT assay. Cytotoxicity test of the Cet-MCPCNPs was also conducted on normal cell lines (MRC-5) to compare the selective cytotoxic activity of Cet-MCPCNPs in colon cancer cells. Results showed that more than 90% of the cells survived at the highest and lowest doses over the course of 72 h, granting the safety of the formulation against normal cells (Figure 5.10

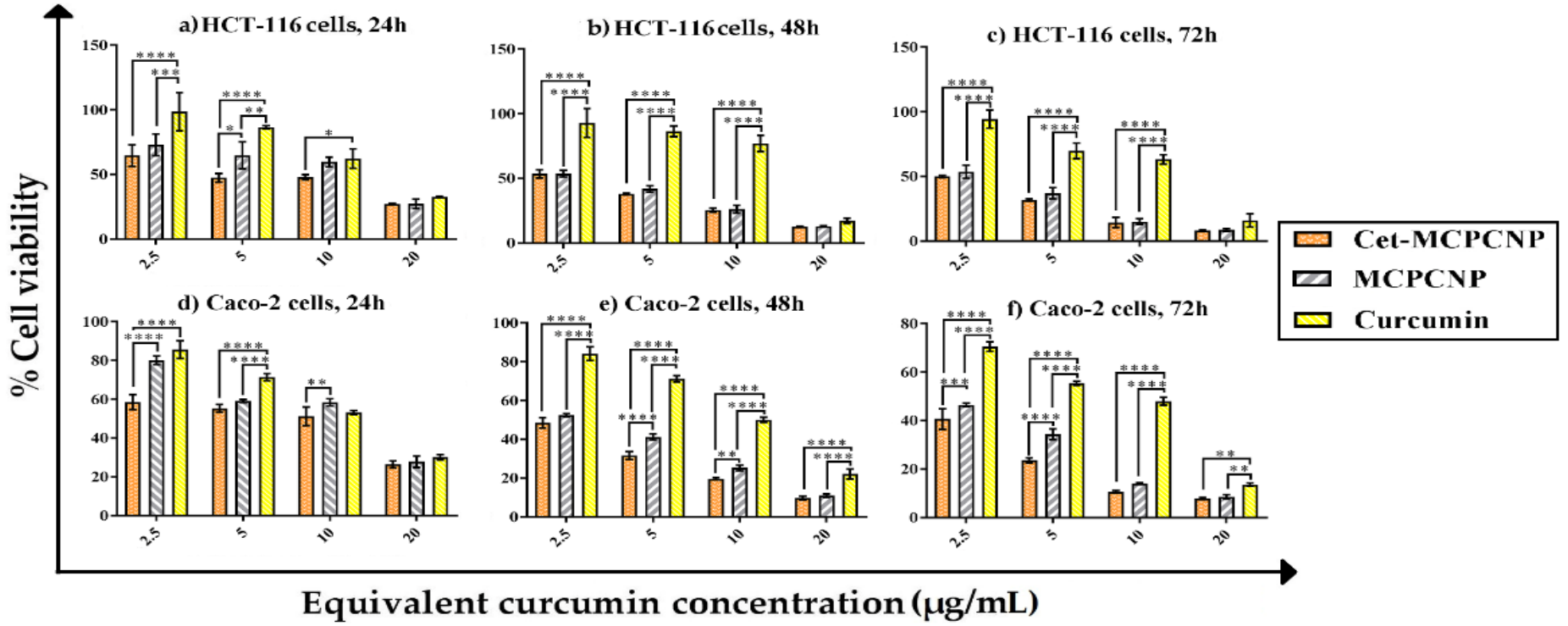


Figure 5.9 Cytotoxicity of Cet-MCPCPs, MCPCNPs and curcumin solution on HCT-116 (a-c) and Caco-2 (e-f) after 24, 48 and 72 h incubation (mean± S.D, n=3). Significance denoted as *($p < 0.05$), ** ($p < 0.01$), *** ($p < 0.001$), **** ($p < 0.0001$).

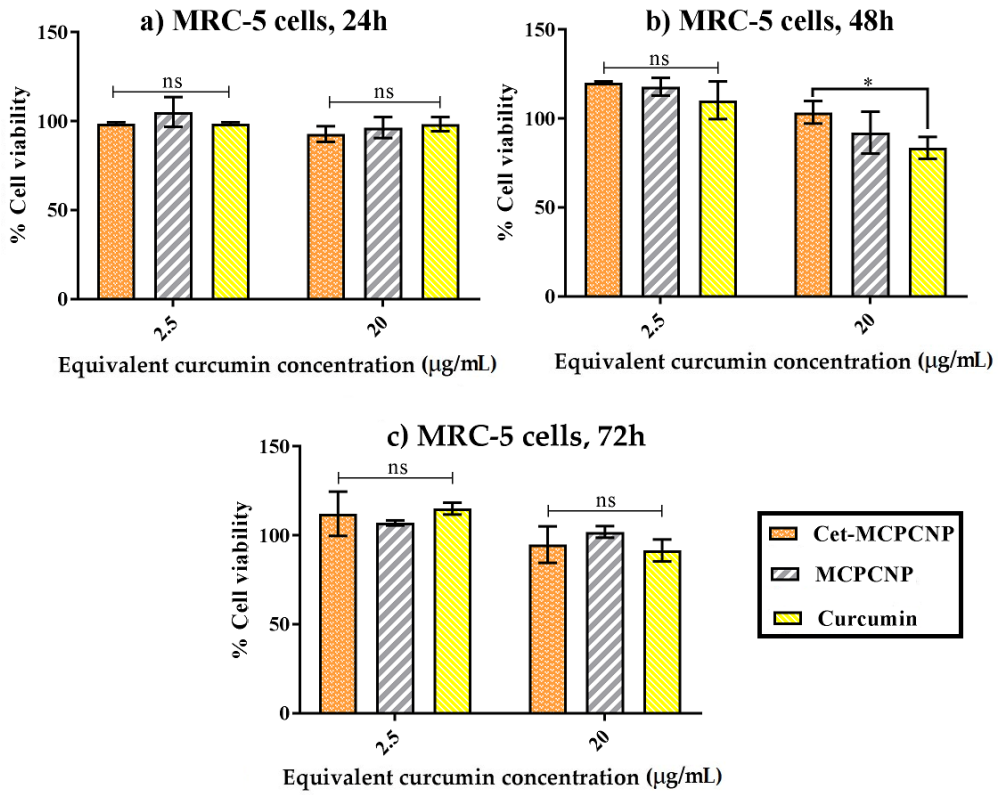


Figure 5.10 Cytotoxicity of Cet-MCPCPs, MCPCNPs and curcumin solution on MRC-5 after 24, 48 and 72 h incubation (mean± S.D, n=3). Significance denoted as *($p < 0.05$), ns (not significant).

As displayed in Figure (5.9), Cet-MCPCNPs showed a more potent anti-cancer effect than MCPCNPs or curcumin solution at equivalent curcumin concentrations in Caco-2 cell lines, whilst comparable cytotoxicity was induced by Cet-MCPCNPs and MCPCNPs against HCT-116 cell lines. This difference can be related to the high expression of functional EGFR in Caco-2 and improved nanoparticle internalization in cells mediated by Cet, implying that combined chemotherapy of Cet and curcumin hold stronger anticancer efficiency than either curcumin or MCPCNPs alone.

Moreover, the better cytotoxicity imposed by Caco-2 compared to HCT-116 is most probably due to the KRAS mutation present in the latter cell lines, in which many studies suggest that patients with KRAS mutated tumours have poorer

response outcomes (Göthel and Schulte, 2012; Knickelbein and Zhang, 2015; Misale et al., 2014; Park et al., 2011) since the potential to respond to growth factor signalling inhibitors is impeded (Skvortsov et al., 2004). In practice, these results also confirm that curcumin-encapsulated in nanoparticles can still exert a strong influence of the lethality on colonic tumours, regardless of protooncogene mutations. However, the slightly lower IC50 values of Cet-MCPCNP compared to MCPCNPs in HCT-116 (Table 5.2) is due to the increased overall charge of the former, which is in according with a number of studies, where the electrostatic interactions between the cationic nanoparticles and the anionic cellular membrane could be the rationale behind higher cell uptake and lower viability (Fröhlich, 2012; He et al., 2010; Mahmoud et al., 2010). In general, the results in Figure 5.8 imply that with increased concentrations of curcumin, corresponding lethality is also increased, suggesting that the *in vitro* anticancer effect of the three different treatments was dose-time- dependent in both cell lines.

Table 5.2 IC50 values in µg/mL of Cet-MCPCNPs, MCPCNPs and curcumin on Caco-2 and HCT-116 cell lines. Each value represents means of triplicate determinations (mean ± S.D).

	24h		**48h**		**72h**	
	Caco-2	HCT-116	Caco-2	HCT-116	Caco-2	HCT-116
Cet-MCPCNP	8.23± 1.46	11.72± 2.04	0.39± 0.99	1.92± 1.25	0.28± 1.83	0.40± 1.58
MCPCNP	11.83± 2.06	11.83± 2.06	1.65± 0.91	2.00± 0.06	0.38± 0.76	0.40± 0.97
Curcumin	12.68± 0.64	14.76± 1.23	11.35± 1.05	13.58± 3.15	8.35± 5.07	11.99± 0.97

5.4.6 Cellular uptake

Curcumin, as both a model drug and fluorescent molecule, was utilized as an indicator to qualitatively and quantitatively estimate the uptake behaviour of Cet-MCPCNPs, MCPCNPs and Curcumin by Caco-2 and HCT-116 after 4h of incubation. The internalization profile of MCPCNPs, Cet-MCPCNPs and curcumin in both cell lines was assessed by monitoring the innate fluorescence signal of curcumin.

As shown in Figures 5.11 and 5.12, higher fluorescence signals were observed in the Caco-2 cells treated with Cet-MCPCNPs, rather than that of MCPCNP, while comparable fluorescent signals were registered for both treatments in HCT-116 cell line. It was also calculated from the HPLC (Figure 5.13) that the fluorescence intensity of Cet-MCPCNP was approximately 2- fold higher than that of MCPCNP after incubation for 4 h in Caco-2, suggesting that Cet-MCPCNP can be readily internalized by Caco-2 cells than its counterpart HCT-116, possibly *via* the EGFR mediated endocytosis pathway. Additionally, the fluorescence signal demonstrated a gradually increased profile with higher treatment doses, indicating that the intracellular uptake of the three treatments were dose-dependent. These results clearly show that the enhanced cellular internalization of Cet-MCPCNPs rather than the increased tumour accumulation is responsible for its anti-tumour efficacy in Caco-2 compared to MCPCNPs. Therefore, it is deduced that the cellular uptake of Cet-MCPCNPs is attained via the concept of active targeting which originated to overcome the limitations of passive targeting.

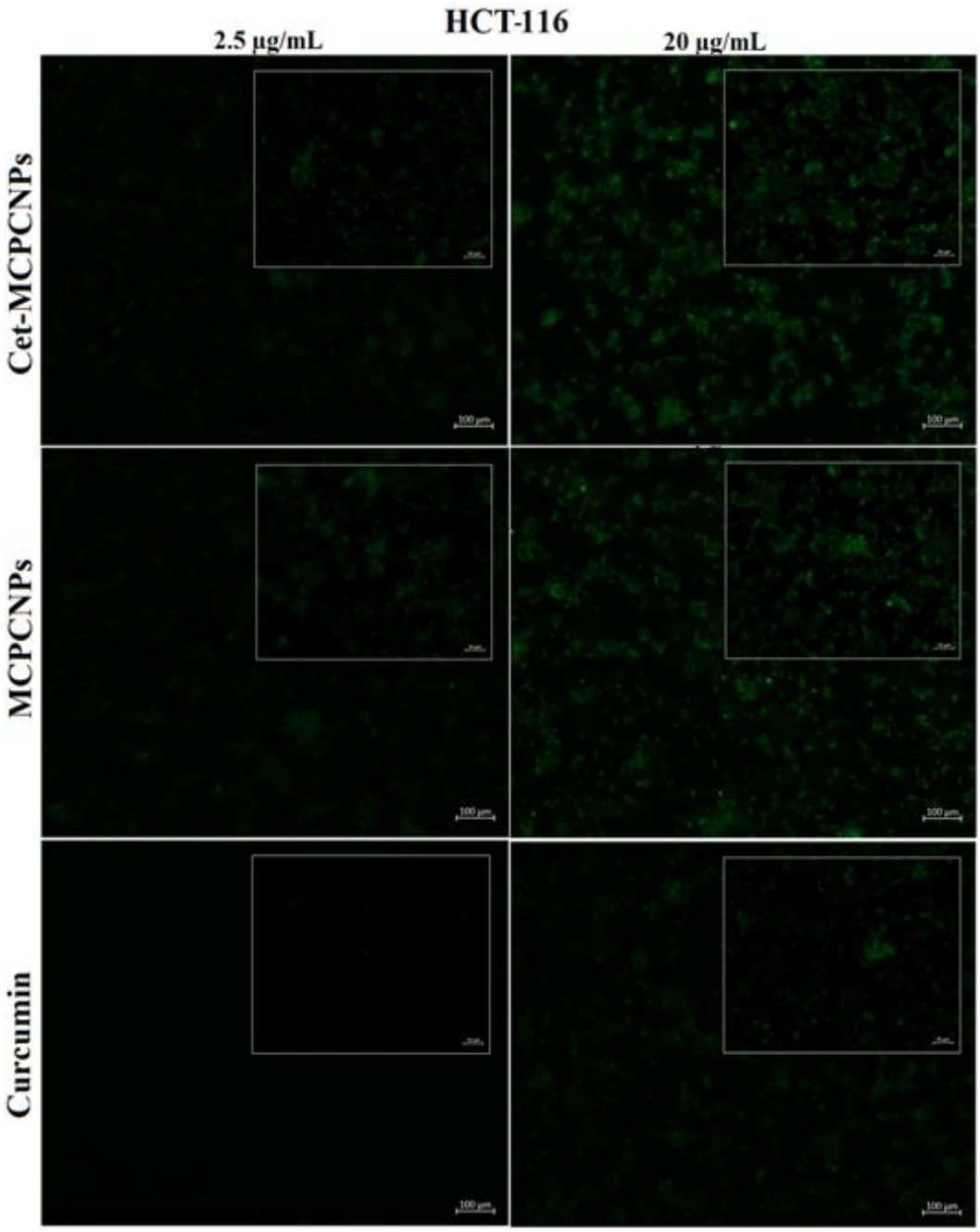


Figure 5.11 Cellular uptake of Cet-MCPCNPs, MCPCNPs and curcumin solution at 20 µg/mL and 2.5 µg/mL after 4 h incubation [10-20x magnification]

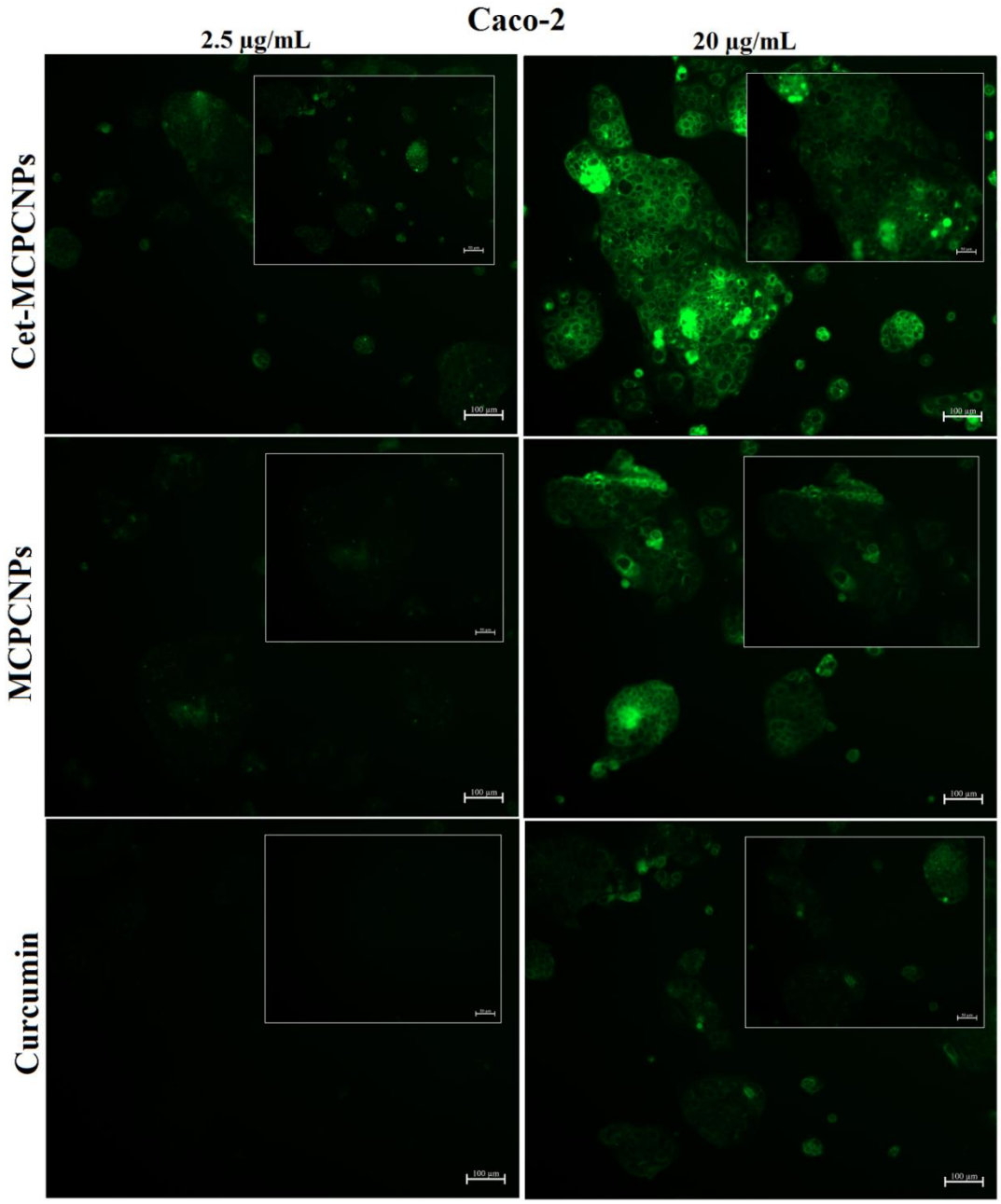


Figure 5.12 Cellular uptake of Cet-MCPCNPs, MCPCNPs and curcumin solution at 20 µg/mL and 2.5 µg/mL after 4 h incubation [10-20x magnification]

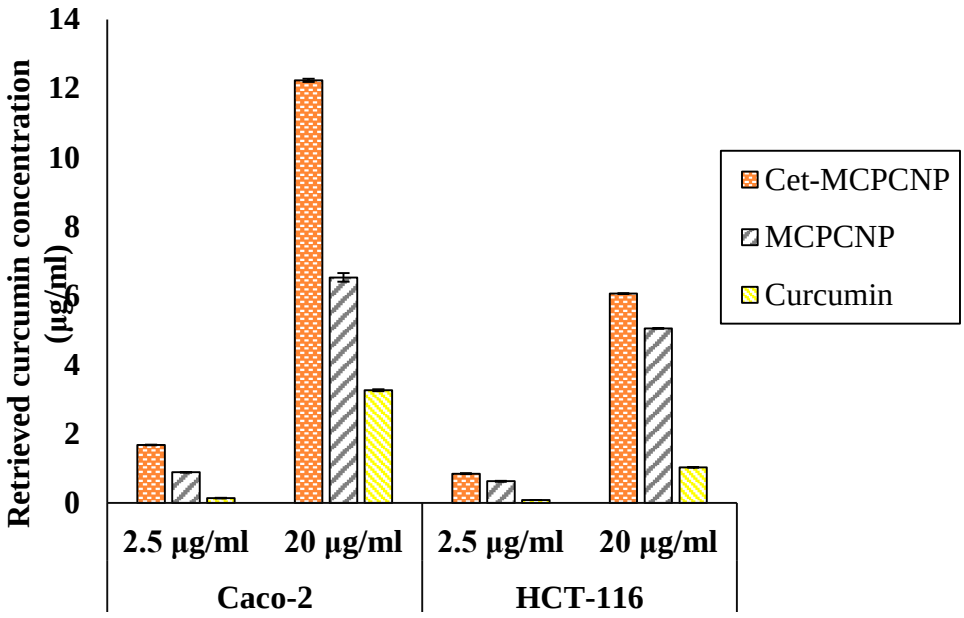


Figure 5.13 Amount of curcumin retrieved from HCT-116 and Caco-2 cells after treatment with 20 µg/mL and 2.5 µg/mL of Cet-MCPCNPs, MCPCNPs and curcumin solution after 4 h incubation. Averaged mean values and standard deviations of triplicates are presented.

In general free curcumin showed lower fluorescence in Figures 5.11, 5.12 and 5.13 compared to encapsulated curcumin, this is because the encapsulation of drug in chitosan-based nanoparticles decrease drug efflux, since chitosan-based nanoparticles act as transmembrane delivery vehicle that help bypass the need for efflux, thus increasing the cell internalization and intracellular accumulation of the drug (Guan et al., 2012).

5.4.7 Cell apoptosis

To assess the effect of formulations on apoptosis, HCT-116 and Caco-2 cells were treated with highest and lowest concentrations of free curcumin, MCPCNPs and Cet-MCPCNPs for 24 h (Figures 5.14 and 5.15). Nuclear staining was carried out using DAPI and nucleolus changes were observed under fluorescent microscope. Fluorescent micrographs of treated HCT-1116 and Caco-2 cells displayed nuclei that were smaller and brighter suggesting

chromatin condensation. Crescent-shaped profiles around the periphery of the nucleus and separate globular structures, as apoptotic features, were also observed. The number of apoptotic cells in cell lines treated with higher concentrations of Cet-MCPCNPS, MCPCNPs and curcumin dramatically increased, when compared with those treated with lower concentration. However, untreated and DMSO receiving HCT-116 and Caco-2 cells showed uniform blue stain. In the present study, DAPI staining also demonstrated that Cet-MCPCNPs induced more apoptosis on Caco-2 cell lines than on HCT-116 cell lines, which was consistent with the results of cytotoxicity assay and confirming that reduction in cell viability was associated with damage to cellular DNA attributed to the NPs.

In general, the results obtained are in good accordance with those by Chen et al. reporting that co-treatment of oral cancer CAR cell with cetuximab and curcumin resulted in cell shrinkage, cytoplasmic membrane blabbing and cell death (Chen et al., 2018). In another study by Yin et al., apoptotic morphology, including chromatin condensation and internucleosomal degradation of DNA were observed in lung cancer cell line (A549) treated with curcumin-loaded polyethylene glycol- polycaprolactone block copolymers (Yin et al., 2013).

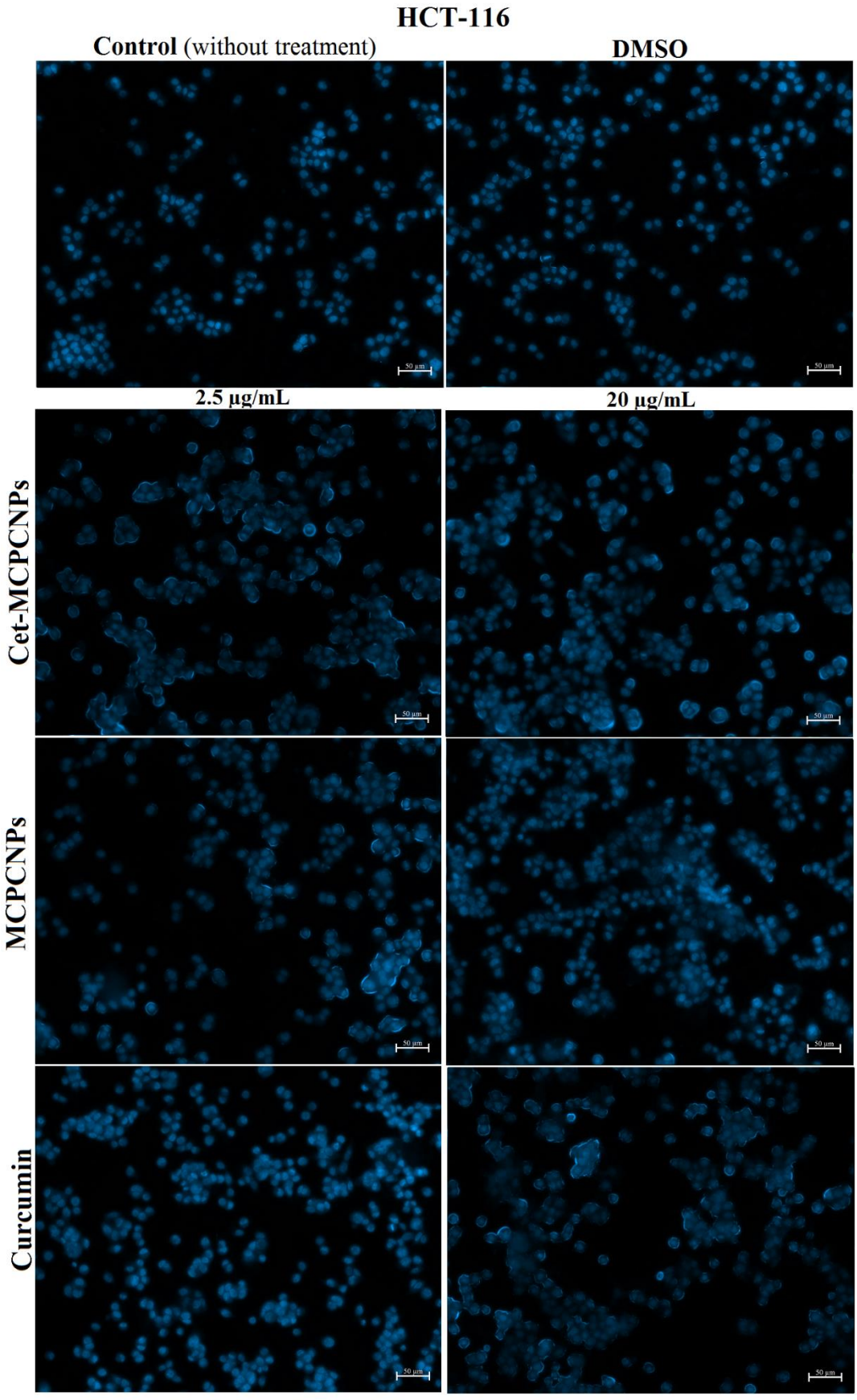


Figure 5.14 Fluorescence micrographs of treated and untreated HCT-116 cells after DAPI staining (20x magnification)

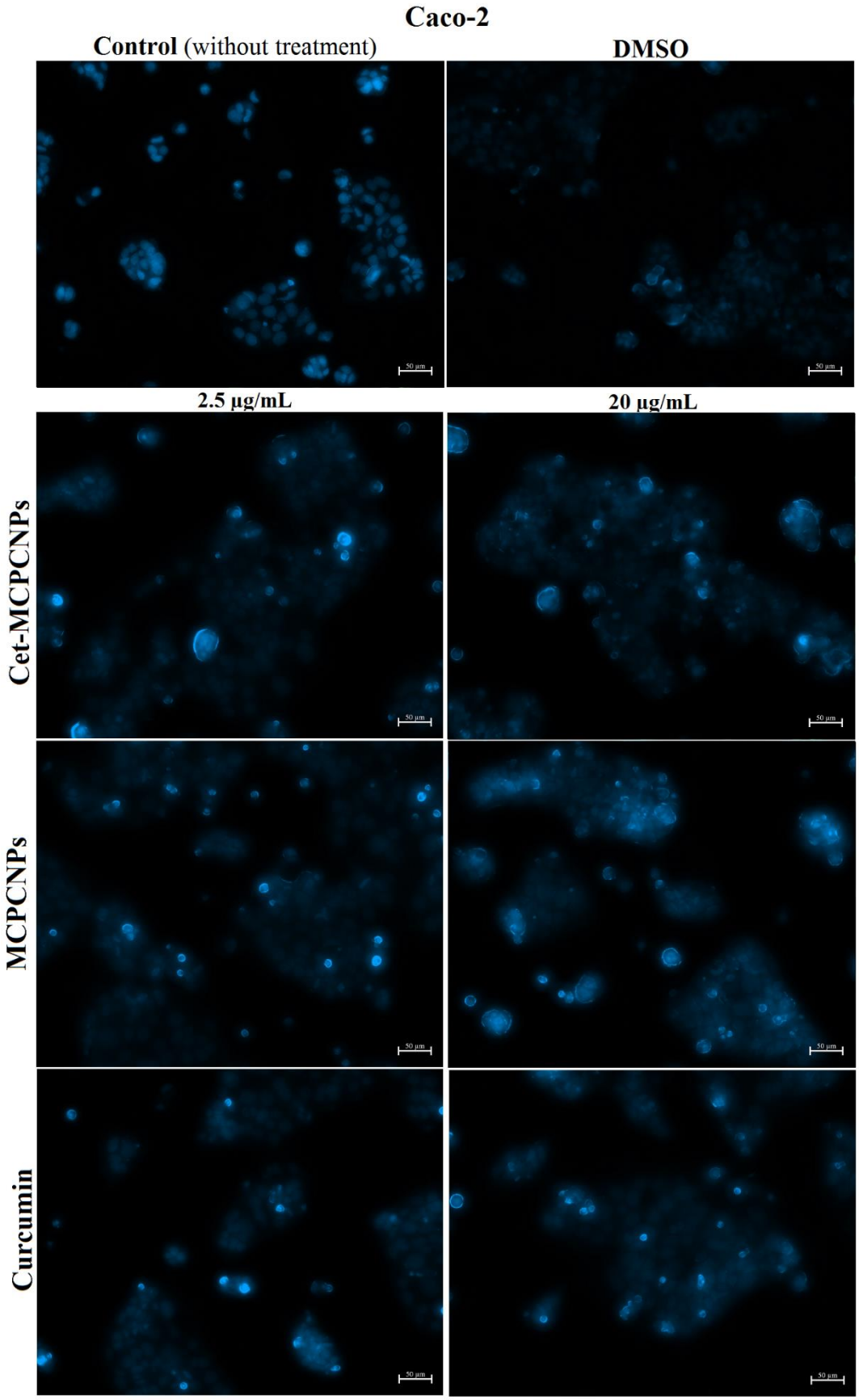


Figure 5.15 Fluorescence micrographs of treated and untreated Caco-2 cells after DAPI staining (20x magnification).

5.4.8 Cell cycle

Flow cytometry was performed to examine the effects of curcumin, MCPCNPs and Cet-MCPCNPs on HCT-116 and Caco-2 cell proliferation. Propidium iodide (PI) staining of nuclei was utilised to assess the time course of the cell cycle profile of these cell lines. RNAase was added to eliminate RNA as PI can stain the latter, causing interference in results. Usually, the amount of nucleic acid dye (PI) incorporated is proportional to the amount of DNA, thus the fluorescence data can be regarded as a measurement of the cellular DNA content (Nunez, 2001; Wang et al., 2017).

The results of the study are presented in Figures 5.16 and 5.17 as cellular DNA content frequency histograms with three distinctive phases namely G_0/G_1, S and G_2/M phase. Usually in the growth phase (G_1), the cell increases in size, yielding RNA and produce protein, to be used for syntheses (Arango et al., 2013). In S phase, the DNA begins to duplicate then enters the G_2 phase, where the biosynthesis and production of microtubules occur (Rhind and Russell, 2012). At the end of the G_2 is a checkpoint that confirms whether the cell can proceed to mitosis. In the mitotic phase (M phase), the cell divides itself into two identical daughter cells and then either continue through to G_1 phase or enter the quiescent phase (G_0). In the G_0 phase, the cell will leave the cycle and quit dividing (Cecchini et al., 2012).

Table 5.1 displays the percentages of cells in their respective phases. Compared to untreated cells, free curcumin, MCPCNPs and Cet-MCPCNPs induced G_2/M cell arrest and decreased population of cells at G_0/G1 in both HCT-116 and Caco-2 cell lines. Initially, Cet-MCPCNPs and MCPCNPS treatment led to a similar proportion of cells in G_2, which is one-fold higher than that from free

curcumin on HCT-116 cells. However, Cet-MCPCNPs showed a higher proportion of cells in G_2 compared to MCPCNPs in Caco-2 cells.

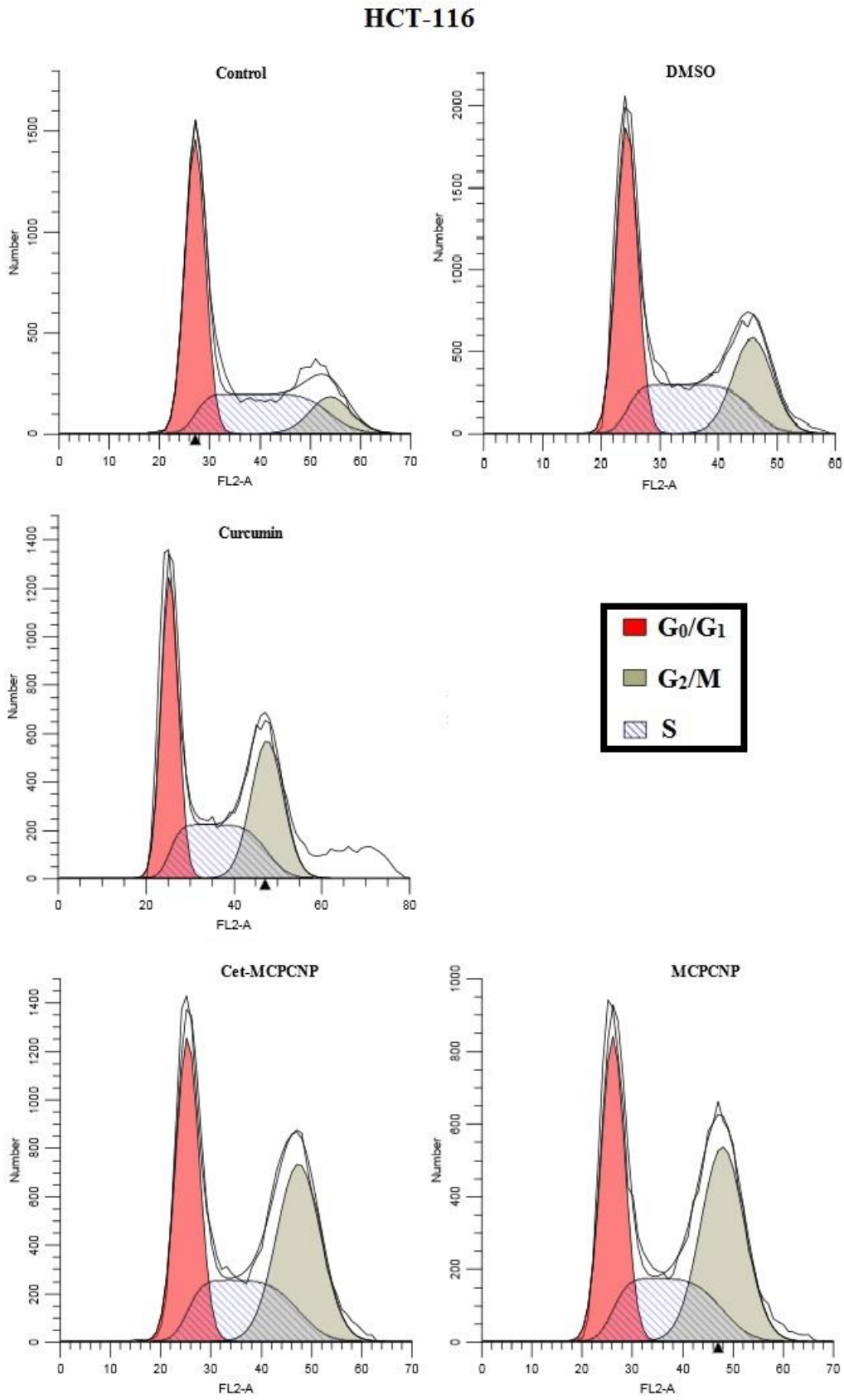


Figure 5.16 DNA histogram of HCT-116 cells treated with control, DMSO, 20 µg/ml free curcumin, 20 µg/ml MCPCNP and 20 µg/ml Cet-MCPCNP analysed by flow cytometry.

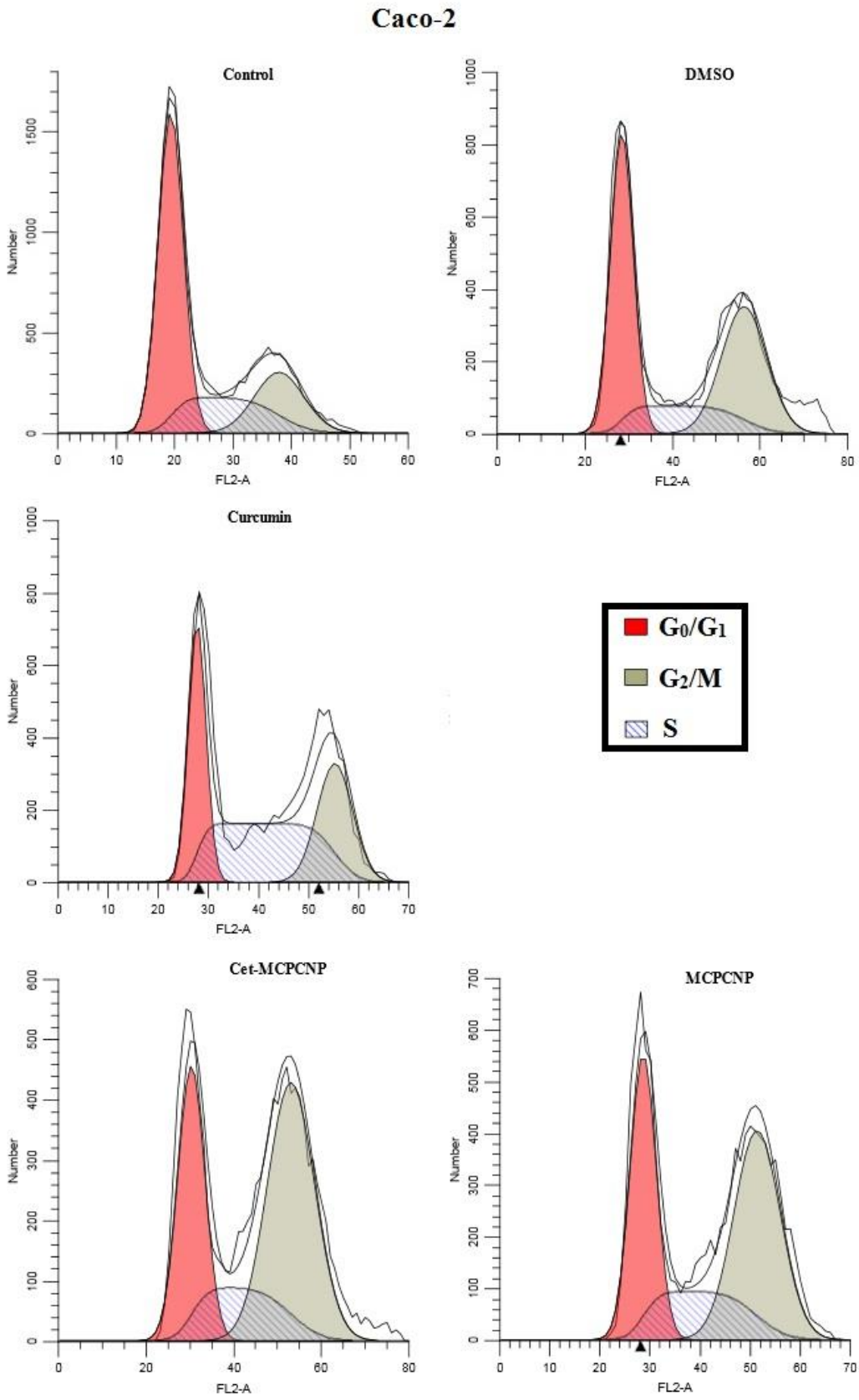


Figure 5.17 DNA histogram of Caco-2 cells treated with control, DMSO, 20 µg/ml free curcumin, 20 µg/ml MCPCNP and 20 µg/ml Cet-MCPCNP analysed by flow cytometry.

Table 5.3 Percentage (%) of cells in the respective phases analysed by flow cytometry. Each value represents means of triplicate determinations (mean ± S.D)

	Caco-2		
	G_0/G_1	S	G_2/M
Control	57.86 ± 0.76	17.71 ± 3.89	24.42 ± 3.59
DMSO	44.38 ± 0.43	19.18 ± 1.38	36.43 ± 0.98
Curcumin	31.61 ± 1.126	38.13 ± 4.41	30.25 ± 3.30
MCPCNP	33.085 ± 1.89	21.14 ± 0.98	45.78 ± 0.90
Cet-MCPCNP	32.29 ± 1.21	13.55 ± 3.67	54.17 ± 2.64
	HCT-116		
	G_0/G_1	S	G_2/M
Control	51.67 ± 0.57	33.35 ± 4.47	14.97 ± 3.90
DMSO	43.94 ± 0.81	29.28 ± 2.60	26.77 ± 1.80
Curcumin	36.91 ± 1.98	32.42 ± 7.75	30.67 ± 5.81
MCPCNP	33.55 ± 1.76	27.35 ± 1.95	39.09 ± 0.77
Cet-MCPCNP	33.69 ± 1.83	26.71 ±1.02	39.60 ± 2.67

Curcumin, in both free and encapsulated in Cet-MCPCNPs or MCPCNPS, induced accumulation of cells in S and G2/M phase of cell cycle. This indicates that curcumin could inhibit cellular proliferation in Caco-2 and HCT-116 cells *in vitro*, and this effect can be augmented when encapsulated in NPs and further enhanced when the latter is conjugated to Cet. Therefore, the obtained findings are consistent with the results of the *in vitro* cell cytotoxicity. It is worth noting that an increase in G_2/M arrest has been associated with enhanced apoptosis, an indicator of better cytotoxicity effect against cancer cells (DiPaola, 2002). Therefore, the obtained findings are an affirmation to *in vitro* cytotoxicity.

Van Erk et al. reported that the downregulation of the expression of polo-like kinase (PLK), by curcumin is accountable for the G_2/M arrest in colon cancer

cells (Van Erk et al., 2004). Weir et al., on the other hand, explained that curcumin downregulates anti-apoptotic Akt signalling, which activates the pro-apoptotic p38 MAPK and generates superoxide radicals that induce G_2/M cell cycle arrest that eventually leads to apoptosis (Weir et al., 2007).

We can conclude that curcumin, MCPCNPs and Cet-MCPCNPs drove cells out of the G_0/G_1 phase, leading to more cells entering S and G_2/M phase and these proportions were further arrested at the G_2/M phase. This means that the curcumin effect on the cell cycle mainly emerges in the G_2/M phase, as contended by (Jaiswal et al., 2002; Sakuma et al., 2014).

5.5 Conclusion

The mucoadhesive properties of the MCPCNPs prolonged the contact time with cancer cells and through the combined effects from the galactan moiety of the modified pectin and the curcumin, improved treatment outcome was realised. The enhanced cellular uptake and anticancer effect of Cet-MCPCNPs concur with our hypothesis. Morphological examination of the nuclei confirmed the apoptotic properties of Cet-MCPCNPs. Cellular uptake studies by fluorescent microscopy and flow cytometry confirmed that there was a superior uptake of curcumin when encapsulated in Cet-MCPCNPs. This was attributable to a combination of appropriate size, positive charge, active targeting as well as the mucoadhesive properties of the Cet-MCPCNPs all in one.

Chapter 6 General conclusions and Future directions

6.1 General conclusion

From the notion that CRC is the second leading cause of cancer-related deaths in the world, there is a realisation of the ever-increasing health burden on society and healthcare systems arising from this disease (Bray et al., 2018; Wolf et al., 2018). The adverse side-effects from chemotherapeutic and radiotherapeutic treatments and the inability of current modalities to effectively deliver optimal therapeutic doses to the tumour site, has prompted the development of interventions that sought to address these constraints with an overarching consequence of reducing toxicity (Senapati et al., 2018; Zhang et al., 2018). The work described in this thesis identifies the aforementioned constrains and aimed to develop a colon-specific drug carrier system that delivers the natural chemotherapeutic agent, curcumin, to the colon through a concerted approach.

Curcumin was selected as the model drug because of its chemopreventive/therapeutic potency in cellular/animal models with CRC and shows comparatively negligible side effects (Femia et al., 2015; Ireson et al., 2002; Patel et al., 2010; Perkins et al., 2002). Due to the poor systemic bioavailability when administered orally, polymer-based nanoparticles have been used as adjuvants in the delivery of curcumin. In the present investigation, modified pectin and chitosan were used as the encapsulant-nanoparticles based on several considerations outlined henceforth. Both polymers are biodegradable, non-toxic and resistant to the digestive enzymes in the GIT (Rampino et al., 2013). MCP serves the dual function of contributing to retaining the integrity of the nanoparticles within the acidic pH of the upper gut and also yielding the galactose moiety within the polymer backbone, which is

known to manifest anticancer properties against galectin 3 (Gal-3) in the colon. The amine moiety of chitosan is destined to promote binding to negatively charged species such as mucin, thus providing the framework for mucoadhesion within the colon mucosa. This would ensure longer residence time within the colon epithelia and promote drug flux. Therefore, chitosan and MCP complement each other in colon-targeting of curcumin due to their opposing responses to extremes in gastrointestinal pH. In this fashion curcumin is also protected from degradation and premature release in the upper gastrointestinal tract (GIT) while ensuring controlled release in the colon (Pandey et al., 2013). Obviously, for the successful deployment of the prototype, the method of fabrication is crucial. This is true because the method adopted regulates the ultimate structure of the prototype and hence, the rate of the payload. In this report therefore, curcumin was encapsulated into modified pectin-chitosan nanoparticles using the ionic gelation method because of its simplicity, convenience, and non-toxicity attributes (de Pinho Neves et al., 2014).

In order to enhance the NP uptake by colonic cancer cells, the clinically approved EGFR antagonistic antibody, Cet, was incorporated onto the surface corona of the NP. Cet is capable of blocking receptor activation and triggering receptor internalization, thus sensitizing EGFR-dependent cells to apoptosis induction (Sotelo Lezama et al., 2014). Therefore, Cet-MCPCNPs can be considered promising with demonstrable mucoadhesive and targeting capabilities. The thesis presented a sequential investigation in the mucoadhesion and the targeting propensity of the formulated nanoparticles. Up to date, there are no reports that elaborate the combined approach of nanoparticulate

mucoadhesion and tumour targeting as a means of enhancing colon cancer treatment from therapeutic agents.

The presence of the galactan moiety from the MCP was confirmed using FTIR and the fabricated NP registered a size of 178 nm and surface charge of +35.7 mV. The size obtained guaranteed the effective diffusion of the NP in epithelia and particularly, tumours because they are leakier. The positive surface charge of the NP facilitated the interaction with anionic sialic acid within mucin and hence effected mucoadhesion. Mucoadhesion was also brought about through physical entanglement of polymer chains in MCPCNP and mucin and van der Waals interactions. The MCP-chitosan composite matrix restricted the cumulative curcumin release to approximately 18% in acidic conditions, implying that around 82% of the curcumin cargo was potentially available for release in the colon. The carboxylic functional moiety of the modified pectin was utilised to conjugate the amine-terminated aspect of Cet through a two-step carbodiimide (EDC) approach and crucially, the incorporation of Cet did not compromise the mucoadhesive and release aspects of the MCPCNPs.

The combined effect of the curcumin payload and galactan moiety from the pectin carrier and the mucoadhesion presented at colonic condition provided an enhanced delivery and an efficient anticancer effect in CRC models. The cytotoxicity study affirmed that the transition of the crystalline phase of curcumin to the amorphous state upon encapsulation did not hinder its anticancer potential and further, the encapsulation into polymeric nanoparticulate did not compromise curcumin's therapeutic activity. The active targeting and/or additional therapeutic effects provided by Cet, enhanced the internalization of MCPCNPs and yielded improved cellular apoptosis effects as

well as cytotoxicity against CRC cell-lines. Importantly, the Cet-MCPCNPs produced synergistic cytotoxic effects in Kras-mutated cell line overcoming drug resistance of an *in vitro* CRC model.

In conclusion, through the combined effects of mucoadhesion and tumour-targeting capability of the NP, we can state that the Cet-MCPCNPs has demonstrable effectiveness against CRC models. Thus, the anticancer effects of curcumin are expected to be exponentially augmented in the ultimate application. This clearly warrants further investigations and possibly, pre-clinical development.

6.2 Future work

Nanocarrier-based platforms can be designed to exploit the pathophysiology of tumour microenvironment to effectively deliver anticancer drugs into the tumours. This strategy remarkably enhances the therapeutic outcomes in oncological management. Additionally, the overexpressed receptors on tumour cells surface have been used as a target to nanocarriers platforms attached with targeting ligands. Subsequently in this study, I developed a mucoadhesive-tumour targeting curcumin containing NP formulation, which established promising data for future clinical translation, however, substantial studies need to be continued in order to shed invaluable light on the applicability of the system to humans. Hence, recommendations for further research are discussed as follows.

The galactan moiety of the modified pectin was only confirmed via FTIR due to limitations of time and resources. A prospective identification via Nuclear Magnetic Resonance (NMR) spectroscopy should be considered for

more definitive results. Moreover, further physical properties of MCP are essential to understand how chemical modification of such a complex polysaccharide can influence their anti-cancer properties.

Drug loading is one of the key features in NP formulation. High drug loaded-NPs are believed to be a prospective approach for bypassing various problems that afflict nanotherapeutics. Usually low drug loaded nanocarriers prompt the use of large amount of excipients which drive up the cost of a nanotherapeutic (Della Rocca et al., 2012). Since the variability of drug loading is often dependent upon the fabrication process, the low drug loading (%) of the current formulation can thus be improved by using the emulsion/solvent evaporation method instead which have reported drug loadings as high as 14% (Chu et al., 2013).

Nanoparticles are often produced in an aqueous suspension form making them physically unstable in which particle aggregates and the hydrolytic action of water on the polymer matrix cause premature drug leakage leading to the formation of undesirable degradation products during long periods of storage (Fonte et al., 2014). This exactly explains the poor storage stability of MCPCNPs that can be improved either by adding surfactants (such as poly (vinylalcohol)) that impede their aggregation or transforming the NP suspension into a solid dosage form by lyophilization. Nevertheless, due to the toxicity issues accompanied with the former, lyophilisation with the use of cryoprotectant like trehalose and sucrose is considered a safer option.

The preliminary *in vitro* studies indicated that the formulation has the propensity to mucoadhere in the colonic mucosa within colonic milieu whilst

retaining its integrity in acidic to alkaline conditions but releases the payload in colonic conditions. Moreover, the cellular studies offered an inclusive depiction of the *in vitro* behaviours of curcumin, MCPCNPs and Cet-MCPCNPs, however, *in vitro-in vivo* correlation might not always present direct relationship. Therefore, animal studies are essential for assessing the effects of formulations on the host and the ability of the drug to exert anti-tumour activity after oral administration. Tumour xenografts implanted in immunocompromised mice such as Balb/c nudes are the accepted standard system for studying human cancers *in vivo*. These models are regarded as the least severe, produce the most satisfactory results and have been used extensively. Moreover, Balb/c nude mice are unable to produce T-cells, therefore, the deficiency in T-cell function allows mice to accept and grow xenografts of normal and malignant tissues. After injecting colonic cell suspension into the right and left flank of the mice, in which the tumour volume reached around 60 mm^3, MCPCNPs, Cet-MCPCNPs or pure curcumin suspension will be administered via oral gavage. Tumour response to the treatment can be measured by the change in tumour volume of the animal, whereby the animal will be weighed on a daily basis and any changes in weight will be noted.

In general, monoclonal antibodies do not have an appreciable oral bioavailability due to their large size, limited membrane permeability, and limited stability toward gastrointestinal protease activity (da Cunha and Weiner, 2012). Therefore, encapsulating Cet-MCPCNPs in a microcapsule or pellet matrix can be a promising strategy to enhance the oral delivery of the formulation to the colon. Consequently, the stress and discomfort associated

with *i.v* treatments are relinquished, and the greater flexibility of orally administered cancer drugs allow patients to forgo hospital visits, which, in turn, positively affect patients' quality of life.

References

AbouAitah, K.E., Swiderska-Sroda, A., Lojkowski, W., Razin, A.-F.M., 2016. pH-controlled Release System for Curcumin based on Functionalized Dendritic Mesoporous Silica Nanoparticles. J Nanomed Nanotechnol 7, 351. https://doi.org/10.4172/2157-7439.1000351

Adler, M.J., Dimitrov, D.S., 2012. Therapeutic antibodies against cancer. Hematol. Oncol. Clin. North Am. 26, 447–81, vii. https://doi.org/10.1016/j.hoc.2012.02.013

Aggarwal, B.B., Kumar, A., Bharti, A.C., 2003. Anticancer potential of curcumin: preclinical and clinical studies. Anticancer Res. 23, 363–98.

Ahirrao, S.P., Gide, P.S., Shrivastav, B., Sharma, P., 2013. Ionotropic Gelation: A Promising Cross Linking Technique for Hydrogels. J. Pharm. Nanotechnol. 2, 1–6.

Ahmadi, F., Oveisi, Z., Samani, S.M., Amoozgar, Z., 2015. Chitosan based hydrogels: characteristics and pharmaceutical applications. Res. Pharm. Sci. 10, 1–16.

Ahmed, T.A., Aljaeid, B.M., 2016. Preparation, characterization, and potential application of chitosan, chitosan derivatives, and chitosan metal nanoparticles in pharmaceutical drug delivery. Drug Des. Devel. Ther. 10, 483–507. https://doi.org/10.2147/DDDT.S99651

Akbari, A., Lavasanifar, A., Wu, J., 2017. Interaction of cruciferin-based nanoparticles with Caco-2 cells and Caco-2/HT29-MTX co-cultures. Acta Biomater. 64, 249–258. https://doi.org/10.1016/J.ACTBIO.2017.10.017

Al-Qadi, S., Grenha, A., Remuñán, C., Remuñán-López, R., 2011. Microspheres loaded with polysaccharide nanoparticles for pulmonary delivery: Preparation, structure and surface analysis. Carbohydr. Polym. 86, 25–34. https://doi.org/10.1016/j.carbpol.2011.03.022

Alexis, F., Pridgen, E.M., Langer, R., Farokhzad, O.C., 2010. Nanoparticle technologies for cancer therapy. Handb. Exp. Pharmacol. 55–86. https://doi.org/10.1007/978-3-642-00477-3_2

Alkhader, E., Billa, N., Roberts, C.J., 2016. Mucoadhesive Chitosan-Pectinate Nanoparticles for the Delivery of Curcumin to the Colon. AAPS PharmSciTech 18, 1009–1018. https://doi.org/10.1208/s12249-016-0623-y

Allouche, J., 2013. Synthesis of Organic and Bioorganic Nanoparticles: An Overview of the Preparation Methods, in: Brayner R., Fiévet F., C.T. (Ed.), Nanomaterials: A Danger or a Promise? Springer London, London, pp. 27–74. https://doi.org/10.1007/978-1-4471-4213-3_2

American Cancer Society, 2018. Colorectal Cancer Stages [WWW Document]. Am. Cancer Soc. URL https://www.cancer.org/cancer/colon-rectal-cancer/detection-diagnosis-staging/staged.html (accessed 12.20.18).

Anand, P., Kunnumakkara, A.B., Newman, R.A., Aggarwal, B.B., 2007. Bioavailability of curcumin: Problems and promises. Mol. Pharm. 4, 807–818. https://doi.org/10.1021/mp700113r

Andriani, Y., Grastianto, Siswanta, Mudasir, 2015. Glutaraldehyde-Crosslinked Chitosan-Pectin Nanoparticles as a Potential Carrier for Curcumin Delivery and Its In Vitro Release Study. Int. J. Drug Deliv. 7, 167–173.

Anitha, A., Deepa, N., Chennazhi, K.P., Lakshmanan, V.-K., Jayakumar, R., 2014. Combinatorial anticancer effects of curcumin and 5-fluorouracil loaded thiolated chitosan nanoparticles towards colon cancer treatment. Biochim. Biophys. Acta - Gen. Subj. 1840, 2730–2743. https://doi.org/10.1016/J.BBAGEN.2014.06.004

Arango, M.-T., Quintero-Ronderos, P., Castiblanco, J., Montoya-Ortíz, G., 2013. Cell culture and cell analysis, in: Anaya JM, Shoenfeld Y, Rojas-Villarraga A (Eds.), Autoimmunity: From Bench to Bedside. El Rosario University Press, Bogota, Colombia, pp. 741–755.

Archer, M.C., 2011. Role of sp transcription factors in the regulation of cancer cell metabolism. Genes Cancer 2, 712–9. https://doi.org/10.1177/1947601911423029

Ascoli, C.A., Aggeler, B., 2018. Overlooked benefi ts of using polyclonal antibodies. Biotechniques 65. https://doi.org/10.2144/btn-2018-0065

Astin, M., Griffin, T., Neal, R.D., Rose, P., Hamilton, W., 2011. The diagnostic value of symptoms for colorectal cancer in primary care: a systematic review. Br. J. Gen. Pract. 61, e231-43. https://doi.org/10.3399/bjgp11X572427

Attili-Qadri, S., Karra, N., Nemirovski, A., Schwob, O., Talmon, Y., Nassar, T., Benita, S., 2013. Oral delivery system prolongs blood circulation of docetaxel nanocapsules via lymphatic absorption. Proc. Natl. Acad. Sci. U. S. A. 110, 17498–503. https://doi.org/10.1073/pnas.1313839110

Awwad, S., Angkawinitwong, U., 2018. Overview of Antibody Drug Delivery. Pharmaceutics 10, 83. https://doi.org/10.3390/pharmaceutics10030083

Balan, V., Nangia-Makker, P., Raz, A., 2010. Galectins as cancer biomarkers. Cancers (Basel). 2, 592–610. https://doi.org/10.3390/cancers2020592

Barnes, T.J., Kempson, I.M., Prestidge, C.A., 2011. Surface analysis for compositional, chemical and structural imaging in pharmaceutics with mass spectrometry: A ToF-SIMS perspective. Int. J. Pharm. 417, 61–69. https://doi.org/10.1016/j.ijpharm.2011.01.043

Barrow, H., Rhodes, J.M., Yu, L.G., 2011. The role of galectins in colorectal cancer progression. Int. J. Cancer 129, 1–8. https://doi.org/10.1002/ijc.25945

Batchelor, D., Russell, P., 2013. SEM and AFM: Complementary Techniques for Surface Investigations. Microsc. Anal. 1–12.

Bennet, D., Kim, S., 2014. Polymer Nanoparticles for Smart Drug Delivery, in: Application of Nanotechnology in Drug Delivery. InTech. https://doi.org/10.5772/58422

Bertrand, N., Wu, J., Xu, X., Kamaly, N., Farokhzad, O.C., 2014. Cancer nanotechnology: the impact of passive and active targeting in the era of modern cancer biology. Adv. Drug Deliv. Rev. 66, 2–25. https://doi.org/10.1016/j.addr.2013.11.009

Betancur, P., Bronner-Fraser, M., Sauka-Spengler, T., 2010. Assembling neural crest regulatory circuits into a gene regulatory network. Annu. Rev. Cell Dev. Biol. 26, 581–603. https://doi.org/10.1146/annurev.cellbio.042308.113245

Bhattacharjee, S., 2016. DLS and zeta potential – What they are and what they are not? J. Control. Release 235, 337–351. https://doi.org/10.1016/j.jconrel.2016.06.017

Bhattacharyya, S., Kudgus, R.A., Bhattacharya, R., Mukherjee, P., 2011. Inorganic nanoparticles in cancer therapy. Pharm. Res. 28, 237–59.

https://doi.org/10.1007/s11095-010-0318-0

Bhumkar, D.R., Pokharkar, V.B., 2006. Studies on Effect of pH on Cross-linking of Chitosan With Sodium Tripolyphosphate: A Technical Note. AAPS PharmSciTech 7, E1–E6.

Bigucci, F., Luppi, B., Cerchiara, T., Sorrenti, M., Bettinetti, G., Rodriguez, L., Zecchi, V., 2008. Chitosan/pectin polyelectrolyte complexes: Selection of suitable preparative conditions for colon-specific delivery of vancomycin. Eur. J. Pharm. Sci. 35, 435–441. https://doi.org/10.1016/J.EJPS.2008.09.004

Boddupalli, B.M., Mohammed, Z.N.K., Nath, R.A., Banji, D., 2010. Mucoadhesive drug delivery system: An overview. J. Adv. Pharm. Technol. Res. 1, 381–7. https://doi.org/10.4103/0110-5558.76436

Bogner, A., Jouneau, P.-H., Thollet, G., Basset, D., Gauthier, C., 2007. A history of scanning electron microscopy developments: Towards "'wet-STEM'" imaging. micron 38, 390–401. https://doi.org/10.1016/j.micron.2006.06.008

Bozzuto, G., Molinari, A., 2015. Liposomes as nanomedical devices. Int. J. Nanomedicine 10, 975–99. https://doi.org/10.2147/IJN.S68861

Bray, F., Ferlay, J., Soerjomataram, I., Siegel, R.L., Torre, L.A., Jemal, A., 2018. Global cancer statistics 2018: GLOBOCAN estimates of incidence and mortality worldwide for 36 cancers in 185 countries. CA. Cancer J. Clin. 68, 394–424. https://doi.org/10.3322/caac.21492

Brigger, I., Dubernet, C., Couvreur, P., 2002. Nanoparticles in cancer therapy and diagnosis. Adv. Drug Deliv. Rev. 54, 631–51.

Bucurescu, A., Blaga, A.C., Estevinho, B.N., Rocha, F., 2018. Microencapsulation of Curcumin by a Spray-Drying Technique Using Gum Arabic as Encapsulating Agent and Release Studies. Food Bioprocess Technol. 11, 1795–1806. https://doi.org/10.1007/s11947-018-2140-3

Buhrmann, C., Kraehe, P., Lueders, C., Shayan, P., Goel, A., Shakibaei, M., 2014. Curcumin Suppresses Crosstalk between Colon Cancer Stem Cells and Stromal Fibroblasts in the Tumor Microenvironment: Potential Role of EMT. PLoS One 9, e107514. https://doi.org/10.1371/journal.pone.0107514

Bunaciu, A.A., Aboul-Enein, H.Y., Fleschin, S., 2010. Application of fourier transform infrared spectrophotometry in pharmaceutical drugs analysis. Appl. Spectrosc. Rev. 45, 206–219. https://doi.org/10.1080/00387011003601044

Çağdaş, M., Sezer, A.D., Bucak, S., 2014. Liposomes as Potential Drug Carrier Systems for Drug Delivery, in: Sezer D. Ali (Ed.), Application of Nanotechnology in Drug Delivery. Intech. https://doi.org/10.5772/58459

Cecchini, M.J., Amiri, M., Dick, F.A., 2012. Analysis of cell cycle position in mammalian cells. J. Vis. Exp. 3491. https://doi.org/10.3791/3491

Chan, J.M., Valencia, P.M., Zhang, L., Langer, R., Farokhzad, O.C., 2010. Polymeric nanoparticles for drug delivery. Methods Mol. Biol. 624, 163–75. https://doi.org/10.1007/978-1-60761-609-2_11

Chen, C.-C., Sureshbabul, M., Chen, H.-W., Lin, Y.-S., Lee, J.-Y., Hong, Q.-S., Yang, Y.-C., Yu, S.-L., 2013. Curcumin Suppresses Metastasis via Sp-1, FAK Inhibition, and E-Cadherin Upregulation in Colorectal Cancer. Evid. Based. Complement. Alternat. Med. 2013, 541695. https://doi.org/10.1155/2013/541695

Chen, C., Yang, W., Wang, D.-T., Chen, C.-L., Zhuang, Q.-Y., Kong, X.-D., 2014. A modified spontaneous emulsification solvent diffusion method for the preparation of curcumin-loaded PLGA nanoparticles with enhanced in vitro anti-tumor activity. Front. Mater. Sci. 8, 332–342. https://doi.org/10.1007/s11706-014-0268-2

Chen, C.F., Lu, C.C., Chiang, J.H., Chiu, H.Y., Yang, J.S., Lee, C.Y., Way, T.D., Huang, H.J., 2018. Synergistic inhibitory effects of cetuximab and curcumin on human cisplatin- resistant oral cancer CAR cells through intrinsic apoptotic process. Oncol. Lett. 16, 6323–6330. https://doi.org/10.3892/ol.2018.9418

Chen, Y., Wu, Q., Zhang, Z., Yuan, L., Liu, X., Zhou, L., 2012. Preparation of curcumin-loaded liposomes and evaluation of their skin permeation and pharmacodynamics. Molecules 17, 5972–5987. https://doi.org/10.3390/molecules17055972

Chiu, M.H., Prenner, E.J., 2011. Differential scanning calorimetry: An invaluable tool for a detailed thermodynamic characterization of macromolecules and their interactions. J. Pharm. Bioallied Sci. 3, 39–59. https://doi.org/10.4103/0975-7406.76463

Cho, W.-S., Jeon, S., Bradley, M., Lee, D.-K., Clavadetscher, J., Chankeshwara, S., 2018. Surface Charge-Dependent Cellular Uptake of Polystyrene Nanoparticles. Nanomaterials 8, 1028. https://doi.org/10.3390/nano8121028

Chu, I.-M., Tseng, S.-H., Chou, M.-Y., 2015. Cetuximab-conjugated iron oxide nanoparticles for cancer imaging and therapy. Int. J. Nanomedicine 10, 3663–3685. https://doi.org/10.2147/IJN.S80134

Chu, K.S., Schorzman, A.N., Finniss, M.C., Bowerman, C.J., Peng, L., Luft, J.C., Madden, A.J., Wang, A.Z., Zamboni, W.C., DeSimone, J.M., 2013. Nanoparticle drug loading as a design parameter to improve docetaxel pharmacokinetics and efficacy. Biomaterials 34, 8424–9. https://doi.org/10.1016/j.biomaterials.2013.07.038

Chuah, L.H., Billa, N., Roberts, C.J., Burley, J.C., Manickam, S., 2011. Curcumin-containing chitosan nanoparticles as a potential mucoadhesive delivery system to the colon. Pharm. Dev. Technol. 18, 1–9. https://doi.org/10.3109/10837450.2011.640688

Chuah, L.H., Roberts, C.J., Billa, N., Abdullah, S., Rosli, R., 2014. Cellular uptake and anticancer effects of mucoadhesive curcumin-containing chitosan nanoparticles. Colloids Surfaces B Biointerfaces 116, 228–236. https://doi.org/10.1016/j.colsurfb.2014.01.007

Churchill, M., Chadburn, A., Bilinski, R.T., Bertagnolli, M.M., 2000. Inhibition of intestinal tumors by curcumin is associated with changes in the intestinal immune cell profile. J. Surg. Res. 89, 169–75. https://doi.org/10.1006/jsre.2000.5826

D'almeida, M., Attik, N., Amalric, J., Brunon, C., Ois Renaud, F., Abouelleil, H., Toury, B., Grosgogeat, B., 2017. Chitosan coating as an antibacterial surface for biomedical applications. https://doi.org/10.1371/journal.pone.0189537.t001

da Cunha, A.P., Weiner, H.L., 2012. Induction of immunological tolerance by oral anti-CD3. Clin. Dev. Immunol. 2012, 425021. https://doi.org/10.1155/2012/425021

Danaei, M., Dehghankhold, M., Ataei, S., Hasanzadeh Davarani, F., Javanmard, R., Dokhani, A., Khorasani, S., Mozafari, M.R., 2018. Impact of Particle Size and Polydispersity Index on the Clinical Applications of Lipidic Nanocarrier Systems.

Pharmaceutics 10. https://doi.org/10.3390/pharmaceutics10020057

Danhier, F., Feron, O., Préat, V., 2010. To exploit the tumor microenvironment: Passive and active tumor targeting of nanocarriers for anti-cancer drug delivery. J. Control. Release 148, 135–46. https://doi.org/10.1016/j.jconrel.2010.08.027

Danley, R.L., 2002. New heat flux DSC measurement technique. Thermochim. Acta 395, 201–208. https://doi.org/10.1016/S0040-6031(02)00212-5

Das, S., Chaudhury, A., Ng, K.-Y., 2011. Preparation and evaluation of zinc–pectin–chitosan composite particles for drug delivery to the colon: Role of chitosan in modifying in vitro and in vivo drug release. Int. J. Pharm. 406, 11–20. https://doi.org/10.1016/J.IJPHARM.2010.12.015

Date, A.A., Hanes, J., Ensign, L.M., 2016. Nanoparticles for oral delivery: Design, evaluation and state-of-the-art. J. Control. Release 240, 504–526. https://doi.org/10.1016/j.jconrel.2016.06.016

de Pinho Neves, A.L., Milioli, C.C., Müller, L., Riella, H.G., Kuhnen, N.C., Stulzer, H.K., 2014. Factorial design as tool in chitosan nanoparticles development by ionic gelation technique. Colloids Surfaces A Physicochem. Eng. Asp. 445, 34–39. https://doi.org/10.1016/J.COLSURFA.2013.12.058

Dedinaite, A., Lundin, M., Macakova, L., Auletta T., 2005. Mucin-Chitosan Complexes at the Solid-Liquid Interface: Multilayer Formation and Stability in Surfactant Solutions. Langmuir 21, 9502–9509.

Deeb, D., Xu, Y.X., Jiang, H., Gao, X., Janakiraman, N., Chapman, R.A., Gautam, S.C., 2003. Curcumin (diferuloyl-methane) enhances tumor necrosis factor-related apoptosis-inducing ligand-induced apoptosis in LNCaP prostate cancer cells. Mol. Cancer Ther. 2, 95–103.

Deepagan, V.G., Sarmento, B., Menon, D., Nascimento, A., Jayasree, A., Sreeranganathan, M., Koyakutty, M., Nair, S. V, Rangasamy, J., 2012. In vitro targeted imaging and delivery of camptothecin using cetuximab-conjugated multifunctional PLGA-ZnS nanoparticles. Nanomedicine 7, 507–19. https://doi.org/10.2217/nnm.11.139

Della Rocca, J., Liu, D., Lin, W., 2012. Are high drug loading nanoparticles the next step forward for chemotherapy? Nanomedicine (Lond). 7, 303–5. https://doi.org/10.2217/nnm.11.191

Dhivya, S., Rajalakshmi, A.N., 2018. A Review on the preparation methods of Curcumin Nanoparticles. PharmaTutor J. 6, 6–10.

Din, F.U., Aman, W., Ullah, I., Qureshi, O.S., Mustapha, O., Shafique, S., Zeb, A., 2017. Effective use of nanocarriers as drug delivery systems for the treatment of selected tumors. Int. J. Nanomedicine 12, 7291–7309. https://doi.org/10.2147/IJN.S146315

DiPaola, R.S., 2002. To arrest or not to G(2)-M Cell-cycle arrest : commentary re: A. K. Tyagi et al., Silibinin strongly synergizes human prostate carcinoma DU145 cells to doxorubicin-induced growth inhibition, G(2)-M arrest, and apoptosis. Clin. cancer res., 8: 3512-3519, 2. Clin. Cancer Res. 8, 3311–4.

Doke, S.K., Dhawale, S.C., 2015. Alternatives to animal testing: A review. Saudi Pharm. J. SPJ Off. Publ. Saudi Pharm. Soc. 23, 223–9. https://doi.org/10.1016/j.jsps.2013.11.002

dos Santos, T., Varela, J., Lynch, I., Salvati, A., Dawson, K.A., 2011. Quantitative

Assessment of the Comparative Nanoparticle-Uptake Efficiency of a Range of Cell Lines. Small 7, 3341–3349. https://doi.org/10.1002/smll.201101076

Doyle, W.M., 1992. Principles and Applications of Fourier Transform Infrared (FTIR) Process Analysis. California.

Duvoix, A., Blasius, R., Delhalle, S., Schnekenburger, M., Morceau, F., Henry, E., Dicato, M., Diederich, M., 2005. Chemopreventive and therapeutic effects of curcumin. Cancer Lett. 223, 181–90. https://doi.org/10.1016/j.canlet.2004.09.041

Eaton, P., Quaresma, P., Soares, C., Neves, C., de Almeida, M.P., Pereira, E., West, P., 2017. A direct comparison of experimental methods to measure dimensions of synthetic nanoparticles. Ultramicroscopy 182, 179–190. https://doi.org/10.1016/j.ultramic.2017.07.001

Ecker, D.M., Jones, S.D., Levine, H.L., 2015. The therapeutic monoclonal antibody market. BioProcess Technol. Consult. 7, 09–14. https://doi.org/10.4161/19420862.2015.989042

Eek, D., Krohe, M., Mazar, I., Horsfield, A., Pompilus, F., Friebe, R., Shields, A.L., 2016. Patient-reported preferences for oral versus intravenous administration for the treatment of cancer: a review of the literature. Patient Prefer. Adherence 10, 1609–21. https://doi.org/10.2147/PPA.S106629

Ettmayer, P., Amidon, G.L., Clement, B., Testa, B., 2004. Lessons Learned from Marketed and Investigational Prodrugs. J. Med. Chem. 47, 2393–2404. https://doi.org/10.1021/jm0303812

Femia, A. Pietro, Soares, P.V., Luceri, C., Lodovici, M., Giannini, A., Caderni, G., 2015. Sulindac, 3,3'-diindolylmethane and curcumin reduce carcinogenesis in the Pirc rat, an Apc-driven model of colon carcinogenesis. BMC Cancer 15, 611. https://doi.org/10.1186/s12885-015-1627-9

Feng, T., Wei, Y., Lee, R.J., Zhao, L., 2017. Liposomal curcumin and its application in cancer. Int. J. Nanomedicine 12, 6027–6044. https://doi.org/10.2147/IJN.S132434

Ferreira, C.M.H., Pinto, I.S.S., Soares Bc, E. V, Soares, H.M.V.M., 2015. (Un)suitability of the use of pH buffers in biological, biochemical and environmental studies and their interaction with metal ions – a review. RSC Adv. 5, 30989–31003. https://doi.org/10.1039/c4ra15453c

Fonte, P., Soares, S., Sousa, F., Costa, A., Seabra, V., Reis, S., Sarmento, B., 2014. Stability study perspective of the effect of freeze-drying using cryoprotectants on the structure of insulin loaded into PLGA nanoparticles. Biomacromolecules 15, 3753–3765. https://doi.org/10.1021/bm5010383

Fröhlich, E., 2012. The role of surface charge in cellular uptake and cytotoxicity of medical nanoparticles. Int. J. Nanomedicine 7, 5577–91. https://doi.org/10.2147/IJN.S36111

Gadalla, H.H., Soliman, G.M., Mohammed, F.A., El-Sayed, A.M., 2016. Drug Delivery Development and in vitro/in vivo evaluation of Zn-pectinate microparticles reinforced with chitosan for the colonic delivery of progesterone Development and in vitro/in vivo evaluation of Zn-pectinate microparticles reinforced with chitosan . Drug Deliv 23, 2541–2554. https://doi.org/10.3109/10717544.2015.1028602

Gagnon, M., Zihler Berner, A., Chervet, N., Chassard, C., Lacroix, C., 2013.

Comparison of the Caco-2, HT-29 and the mucus-secreting HT29-MTX intestinal cell models to investigate Salmonella adhesion and invasion. J. Microbiol. Methods 94, 274–279. https://doi.org/10.1016/j.mimet.2013.06.027

Gandin, V., Pellei, M., Tisato, F., Porchia, M., Santini, C., Marzano, C., 2012. A novel copper complex induces paraptosis in colon cancer cells via the activation of ER stress signalling. J. Cell. Mol. Med. 16, 142–151. https://doi.org/10.1111/j.1582-4934.2011.01292.x

Gazzaniga, A., Maroni, A., Sangalli, M.E., Zema, L., 2006. Time-controlled oral delivery systems for colon targeting. Expert Opin. Drug Deliv. 3, 583–97. https://doi.org/10.1517/17425247.3.5.583

Geng, X., Kong, X., Hu, H., Chen, J., Yang, F., Liang, H., Chen, X., Hu, Y., 2015. Research and development of therapeutic mAbs: An analysis based on pipeline projects. Hum. Vaccin. Immunother. 11, 2769--2776. https://doi.org/10.1080/21645515.2015.1074362

Gera, M., Sharma, N., Ghosh, M., Huynh, D.L., Lee, S.J., Min, T., Kwon, T., Jeong, D.K., 2017. Nanoformulations of curcumin: an emerging paradigm for improved remedial application. Oncotarget 8, 66680–66698. https://doi.org/10.18632/oncotarget.19164

Ghaffari, A., Navaee, K., Oskoui, M., Bayati, K., Rafiee-Tehrani, M., 2007. Preparation and characterization of free mixed-film of pectin/chitosan/Eudragit® RS intended for sigmoidal drug delivery. Eur. J. Pharm. Biopharm. 67, 175–186. https://doi.org/10.1016/J.EJPB.2007.01.013

Gill, P., Moghadam, T.T., Ranjbar, B., 2010. Differential scanning calorimetry techniques: applications in biology and nanoscience. J. Biomol. Tech. 21, 167–93.

Glinsky, V. V., Raz, A., 2009. Modified citrus pectin anti-metastatic properties: one bullet, multiple targets. Carbohydr. Res. 344, 1788–1791. https://doi.org/10.1016/j.carres.2008.08.038

Goldberg, R.M., Montagut, C., Wainberg, Z.A., Ronga, P., Audhuy, F., Taieb, J., Stintzing, S., Siena, S., Santini, D., 2018. Optimising the use of cetuximab in the continuum of care for patients with metastatic colorectal cancer. Esmo Open 3, 353. https://doi.org/10.1136/esmoopen-2018-000353

Goswami, S., Wang, W., Arakawa, T., Ohtake, S., 2013. Developments and Challenges for mAb-Based Therapeutics. Antibodies 2, 452–500. https://doi.org/10.3390/antib2030452

Göthel, M., Schulte, A., 2012. Functional Dissection of the Epidermal Growth Factor Receptor Epitopes Targeted by. Neoplasia 14, 1023–1031. https://doi.org/10.1593/neo.121242

Greenfield, E.A., 2014. Generating Monoclonal Antibodies, in: Antibodies: A Laboratory Manual. Cold Spring Harbor Laboratory Press, Boston, Massachusetts, pp. 203–255.

Greillier, L., Tomasini, P., Barlesi, F., 2015. Necitumumab for non-small cell lung cancer. Expert Opin. Biol. Ther. 15, 1231–1239. https://doi.org/10.1517/14712598.2015.1055243

Guan, M., Zhu, Q.-L., Liu, Y., Bei, Y.-Y., Gu, Z.-L., Zhang, X.-N., Zhang, Q., 2012. Uptake and transport of a novel anticancer drug-delivery system: lactosyl-

norcantharidin-associated N-trimethyl chitosan nanoparticles across intestinal Caco-2 cell monolayers. Int. J. Nanomedicine 7, 1921–1930. https://doi.org/10.2147/IJN.S30034

Guorgui, J., Wang, R., Mattheolabakis, G., Mackenzie, G.G., 2018. Curcumin formulated in solid lipid nanoparticles has enhanced efficacy in Hodgkin's lymphoma in mice. Arch. Biochem. Biophys. 648, 12–19. https://doi.org/10.1016/j.abb.2018.04.012

Gurunathan, S., Kang, M.-H., Qasim, M., Kim, J.-H., 2018. Nanoparticle-Mediated Combination Therapy: Two-in-One Approach for Cancer. Int. J. Mol. Sci. 19. https://doi.org/10.3390/ijms19103264

Guterres, S.S., Alves, M.P., Pohlmann, A.R., 2007. Polymeric nanoparticles, nanospheres and nanocapsules, for cutaneous applications. Drug Target Insights 2, 147–57.

Hamman, J.H., 2010. Chitosan based polyelectrolyte complexes as potential carrier materials in drug delivery systems. Mar. Drugs 8, 1305–22. https://doi.org/10.3390/md8041305

He, C., Hu, Y., Yin, L., Tang, C., Yin, C., 2010. Effects of particle size and surface charge on cellular uptake and biodistribution of polymeric nanoparticles. Biomaterials 31, 3657–3666. https://doi.org/10.1016/J.BIOMATERIALS.2010.01.065

Herbst, R.S., 2004. Review of epidermal growth factor receptor biology. Int. J. Radiat. Oncol. 59, S21–S26. https://doi.org/10.1016/j.ijrobp.2003.11.041

Hewlings, S.J., Kalman, D.S., 2017. Curcumin: A Review of Its' Effects on Human Health. Foods 6, 1–11. https://doi.org/10.3390/foods6100092

Horiba Scientific, 2016. Particle characterisation [WWW Document]. © 1996-2018 HORIBA, Ltd. URL http://www.horiba.com/scientific/products/particle-characterization/particle-size-analysis/details/sz-100-7245/

Hosseinzadeh, H., Atyabi, F., Dinarvand, R., Ostad, S.N., 2012. Chitosan-Pluronic nanoparticles as oral delivery of anticancer gemcitabine: Preparation and in vitro study. Int. J. Nanomedicine 7, 1851–1863. https://doi.org/10.2147/IJN.S26365

Howells, L.M., Mitra, A., Manson, M.M., 2007. Comparison of oxaliplatin- and curcumin-mediated antiproliferative effects in colorectal cell lines. Int. J. Cancer 121, 175–183. https://doi.org/10.1002/ijc.22645

Hua, S., 2014. Orally administered liposomal formulations for colon targeted drug delivery. Front. Pharmacol. 5, 1–4. https://doi.org/10.3389/fphar.2014.00138

Huang, A.-C., Lin, S.-Y., Su, C.-C., Lin, S.-S., Ho, C.-C., Hsia, T.-C., Chiu, T.-H., Yu, C.-S., Ip, S.-W., Lin, T.-P., Chung, J.-G., 2008. Effects of curcumin on N-bis(2-hydroxypropyl) nitrosamine (DHPN)-induced lung and liver tumorigenesis in BALB/c mice in vivo. In Vivo 22, 781–5.

Huang, H.-C., Barua, S., Sharma, G., Dey, S.K., Rege, K., 2011. Inorganic nanoparticles for cancer imaging and therapy. J. Control. Release 155, 344–357. https://doi.org/10.1016/j.jconrel.2011.06.004

Hudu, S.A., Alshrari, A.S., Syahida, A., Sekawi, Z., 2016. Cell Culture, Technology: Enhancing the Culture of Diagnosing Human Diseases. J. Clin. Diagn. Res. 10, DE01-5. https://doi.org/10.7860/JCDR/2016/15837.7460

Hussain, Z., Sahudin, S., 2016. Preparation, characterisation and colloidal stability of chitosan-tripolyphosphate nanoparticles: Optimisation of formulation and process parameters. Int. J. Pharm. Pharm. Sci. 8, 297–308.

Hwang, S.W., Shin, J.S., 2018. Pectin-Coated Curcumin-Chitosan Microparticles Crosslinked with Mg^{2+} for Delayed Drug Release in the Digestive System. Int. J. Polym. Sci. 2018, 1–7. https://doi.org/10.1155/2018/2071071

Ibekwe, V.C., Fadda, H.M., McConnell, E.L., Khela, M.K., Evans, D.F., Basit, A.W., 2008. Interplay between intestinal pH, transit time and feed status on the in vivo performance of pH responsive ileo-colonic release systems. Pharm. Res. 25, 1828–35. https://doi.org/10.1007/s11095-008-9580-9

Ireson, C.R., Jones, D.J.L., Orr, S., Coughtrie, M.W.H., Boocock, D.J., Williams, M.L., Farmer, P.B., Steward, W.P., Gescher, A.J., 2002. Metabolism of the cancer chemopreventive agent curcumin in human and rat intestine. Cancer Epidemiol. Biomarkers Prev. 11, 105–11.

Irving, M.H., Catchpole B, 1992. ABC of Colorectal Diseases ANATOMY AND PHYSIOLOGY OF THE COLON, RECTUM, AND ANUS. BMJ 304, 1106–1108.

Jagetia, G.C., Aggarwal, B.B., 2007. "Spicing up" of the immune system by curcumin. J. Clin. Immunol. 27, 19–35. https://doi.org/10.1007/s10875-006-9066-7

Jahan, S.T., Sadat, S.M.A., Walliser, M., Haddadi, A., 2017. Targeted Therapeutic Nanoparticles: An Immense Promise to Fight against Cancer. J. Drug Deliv. 2017, 1–24. https://doi.org/10.1155/2017/9090325

Jain, S.K., Jain, A., 2008. Target-specific drug release to the colon. Expert Opin. Drug Deliv. 5, 483–98. https://doi.org/10.1517/17425247.5.5.483

Jaiswal, A.S., Marlow, B.P., Gupta, N., Narayan, S., 2002. β-Catenin-mediated transactivation and cell–cell adhesion pathways are important in curcumin (diferuylmethane)-induced growth arrest and apoptosis in colon cancer cells. Oncogene 21, 8414–8427. https://doi.org/10.1038/sj.onc.1205947

Jana, S., Banerjee, A., Gandhi, A., 2014. Preparation and Characterization of Chitosan Based Polyelectrolyte Complex as a Carrier of Aceclofenac. J. PharmaSciTech 3, 68–71.

Janeway, C.J., Travers, P., Walport, M., Shlomchik, M.J., 2001. The structure of a typical antibody molecule, in: Austin, P., Laurence, E. (Eds.), Immunobiology: The Immune System in Health and Disease. Garland Science, New York, p. 93.

Janz, T., Lu, K., Povlow, M.R., Urso, B., 2016. A Review of Colorectal Cancer Detection Modalities, Stool DNA, and Fecal Immunochemistry Testing in Adults Over the Age of 50. Cures 8, e931. https://doi.org/10.7759/cureus.931

Jeught, V.D.K., Xu, H.-C., Li, Y.-J., Lu, X.-B., Ji, G., 2018. Drug resistance and new therapies in colorectal cancer. World J. Gastroenterol. 24, 3834–3848. https://doi.org/10.3748/wjg.v24.i34.3834

Joergensen, L., Klösgen, B., Simonsen, A.C., Borch, J., Hagesaether, E., 2011. New insights into the mucoadhesion of pectins by AFM roughness parameters in combination with SPR. Int. J. Pharm. 411, 162–168. https://doi.org/10.1016/j.ijpharm.2011.04.001

Johnson, K.D., Glinskii, O. V, Mossine, V. V, Turk, J.R., Mawhinney, T.P., Anthony, D.C., Henry, C.J., Huxley, V.H., Glinsky, G. V, Pienta, K.J., Raz, A., Glinsky, V.

V, 2007. Galectin-3 as a potential therapeutic target in tumors arising from malignant endothelia. Neoplasia 9, 662–670. https://doi.org/10.1593/neo.07433

Jonassen, H., Kjoniksen, A.L., Hiorth, M., 2012. Stability of chitosan nanoparticles cross-linked with tripolyphosphate. Biomacromolecules 13, 3747–3756. https://doi.org/10.1021/bm301207a

Jordan, V.C., 2016. A Retrospective: On Clinical Studies with 5-Fluorouracil. Cancer Res. 76, 767–8. https://doi.org/10.1158/0008-5472.CAN-16-0150

Karri, V.V.S.R., Kuppusamy, G., Talluri, S.V., Mannemala, S.S., Kollipara, R., Wadhwani, A.D., Mulukutla, S., Raju, K.R.S., Malayandi, R., 2016. Curcumin loaded chitosan nanoparticles impregnated into collagen-alginate scaffolds for diabetic wound healing. Int. J. Biol. Macromol. 93, 1519–1529. https://doi.org/10.1016/j.ijbiomac.2016.05.038

Katragadda, S., Budda, B., Anand, B.S., Mitra, A.K., 2005. Role of efflux pumps and metabolising enzymes in drug delivery. Expert Opin. Drug Deliv. 2, 683–705. https://doi.org/10.1517/17425247.2.4.683

Kavitha, K., Rupesh Kumar, M., Jagadeesh Singh, S., Correspondence Mythri, F.G., 2011. Novel Mucoadhesive Polymers –A Review. J. Appl. Pharm. Sci. 01, 37–42.

Kaya, M., Sousa, A.G., Crépeau, M.-J., Sørensen, S.O., Ralet, M.-C., 2014. Characterization of citrus pectin samples extracted under different conditions: influence of acid type and pH of extraction. Ann. Bot. 114, 1319–26. https://doi.org/10.1093/aob/mcu150

Khutoryanskiy, V. V., 2015. Supramolecular materials: Longer and safer gastric residence. Nat. Mater. 14, 963–964. https://doi.org/10.1038/nmat4432

Kim, C., Galloway, J.F., Lee, K.H., Searson, P.C., 2014. Universal Antibody Conjugation to Nanoparticles Using the Fcγ Receptor I (FcγRI): Quantitative Profiling Of Membrane Biomarkers. Bioconjug. Chem. 25, 1893–1901. https://doi.org/10.1021/bc5003778

Kim H. John, 2017. Controversial issues in radiotherapy for rectal cancer: a systematic review. Radiat. Oncol. J. 35, 295–305. https://doi.org/10.3857/roj.2017.00395

Kim, H.J., Jang, Y.P., Hee, K., 2009. Direct Analysis of Curcumin in Turmeric by DART-MS. Phytochem. Anal. 20, 372–377. https://doi.org/10.1002/pca.1136

Kim, Y.S., Ahn, Y., Hong, M.H., Joo, S.Y., Kim, K.H., Sohn, I.S., Park, H.W., Hong, Y.J., Kim, J.H., Kim, W., Jeong, M.H., Cho, J.G., Park, J.C., Kang, J.C., 2007. Curcumin attenuates inflammatory responses of TNF-alpha-stimulated human endothelial cells. J. Cardiovasc. Pharmacol. 50, 41–9. https://doi.org/10.1097/FJC.0b013e31805559b9

Knickelbein, K., Zhang, L., 2015. Mutant KRAS as a critical determinant of the therapeutic response of colorectal cancer. Genes Dis. 2, 4–12. https://doi.org/10.1016/j.gendis.2014.10.002

Kocbek, P., Obermajer, N., Cegnar, M., Kos, J., Kristl, J., 2007. Targeting cancer cells using PLGA nanoparticles surface modified with monoclonal antibody. J. Control. Release 120, 18–26. https://doi.org/10.1016/J.JCONREL.2007.03.012

Krzemieniecki, K., Szypt, E., Rashedi, I., Gawron, K., Los, M., 2006. Targeting of solid tumors and blood malignancies by antibody-based therapies — EGFR-pathway as an example. Cent. Eur. J. Biol. 1, 167–82.

https://doi.org/10.2478/s11535-006-0014-6

Kumar, R., Lal, S., 2014. Synthesis of Organic Nanoparticles and their Applications in Drug Delivery and Food Nanotechnology: A Review. J. Nanomater. Mol. Nanotechnol. 3, 1–11. https://doi.org/10.4172/2324-8777.1000150

Kumar, S.S.D., Mahadevan, S., Vijayaraghavan, R., Mandal, B.A., Macfarlane, D.R., 2014. Curcumin loaded poly(2-hydroxyethyl methacrylate) nanoparticles from gelled ionic liquid â€“ In vitro cytotoxicity and anti-cancer activity in SKOV-3 cells. Eur. J. Pharm. Sci. 51, 34–44. https://doi.org/10.1016/j.ejps.2013.08.036

Kutty, R.V., Feng, S.-S., 2013. Cetuximab conjugated vitamin E TPGS micelles for targeted delivery of docetaxel for treatment of triple negative breast cancers. Biomaterials 34, 10160–10171. https://doi.org/10.1016/J.BIOMATERIALS.2013.09.043

Lacour, S., 2013. Emerging questions for emerging technologies: Is there a law for the nano?, in: Brayner R., Fiévet F., C.T. (Ed.), Nanomaterials: A Danger or a Promise? Springer London, London, pp. 357–378. https://doi.org/10.1007/978-1-4471-4213-3

Lange, A., Neves, D.P., Cardoso, C., Müller, L., Gracher, H., Cabral, N., Karine, H., 2014. Factorial design as tool in chitosan nanoparticles development by ionic gelation technique. Colloids Surfaces A Physicochem. Eng. Asp. 445, 34–39. https://doi.org/10.1016/j.colsurfa.2013.12.058

Leclere, L., Cutsem, P. Van, Michiels, C., 2013. Anti-cancer activities of pH- or heat-modified pectin. Front. Pharmacol. 4 OCT, 1–8. https://doi.org/10.3389/fphar.2013.00128

Leclere, L., Fransolet, M., Cote, F., Cambier, P., Arnould, T., Van Cutsem, P., Michiels, C., 2015. Heat-modified citrus pectin induces apoptosis-like cell death and autophagy in HepG2 and A549 cancer cells. PLoS One 10, 1–24. https://doi.org/10.1371/journal.pone.0115831

Lee, J., Kang, M.H., Lee, K.B., Lee, Y., 2013. Characterization of natural dyes and traditional korean silk fabric by surface analytical techniques. Materials (Basel). 6, 2007–2025. https://doi.org/10.3390/ma6052007

Lee, Y.-C., Lee, Y.-L., Chuang, J.-P., Lee, J.-C., 2013. Differences in Survival between Colon and Rectal Cancer from SEER Data. PLoS One 8, e78709. https://doi.org/10.1371/journal.pone.0078709

Leonard, D.N., Chandler, G.W., Seraphin, S., 2012. Scanning Electron Microscopy, in: Characterization of Materials. John Wiley & Sons, Inc., Hoboken, NJ, USA, pp. 1721–1736. https://doi.org/10.1002/0471266965.com081.pub2

Lev-Ari, S., Starr, A., Vexler, A., Karaush, V., Loew, V., Greif, J., Fenig, E., Aderka, D., Ben-Yosef, R., 2006. Inhibition of pancreatic and lung adenocarcinoma cell survival by curcumin is associated with increased apoptosis, down-regulation of COX-2 and EGFR and inhibition of Erk1/2 activity. Anticancer Res. 26, 4423–30.

Li, C., Zhang, Y., Su, T., Feng, L., Long, Y., Chen, Z., 2012. Silica-coated flexible liposomes as a nanohybrid delivery system for enhanced oral bioavailability of curcumin. Int. J. Nanomedicine 7, 5995–6002. https://doi.org/10.2147/IJN.S38043

Li, S., Buchbinder, E., Wu, L., Bjorge, J.D., Fujita, D.J., Zhu, S., 2014. EGFR and

HER2 levels are frequently elevated in colon cancer cells. Discov. Journals 1, 1–8. https://doi.org/10.15190/drep.2014.1

Lipman, N.S., Jackson, L.R., Trudel, L.J., Weis-Garcia, F., 2005. Monoclonal Versus Polyclonal Antibodies: Distinguishing Characteristics, Applications, and Information Resources. ILAR J. 46, 258–268. https://doi.org/10.1093/ilar.46.3.258

Liu, J.K.H., 2014. The history of monoclonal antibody development e Progress, remaining challenges and future innovations. Ann. Med. Surg. 3, 113–116. https://doi.org/10.1016/j.amsu.2014.09.001

M. Ways, T., Lau, W., Khutoryanskiy, V., 2018. Chitosan and Its Derivatives for Application in Mucoadhesive Drug Delivery Systems. Polymers (Basel). 10, 267. https://doi.org/10.3390/polym10030267

Ma, Y., Coombes, A.G.A., 2014. Designing colon-specific delivery systems for anticancer drug-loaded nanoparticles: an evaluation of alginate carriers. J. Biomed. Mater. Res. A 102, 3167–76. https://doi.org/10.1002/jbm.a.34988

Maciel, V.B. V, Yoshida, C.M.P., Pereira, S.M.S.S., Goycoolea, F.M., Franco, T.T., 2017. molecules Electrostatic Self-Assembled Chitosan-Pectin Nano-and Microparticles for Insulin Delivery. Molecules 22, 1–21. https://doi.org/10.3390/molecules22101707

Mahmoud, K.A., Mena, J.A., Male, K.B., Hrapovic, S., Kamen, A., Luong, J.H.T., 2010. Effect of Surface Charge on the Cellular Uptake and Cytotoxicity of Fluorescent Labeled Cellulose Nanocrystals. ACS Appl. Mater. Interfaces 2, 2924–2932. https://doi.org/10.1021/am1006222

MALVERN, 2017. Zetasizer Nano Series. Malvern Instruments Ltd 20. https://doi.org/10.1016/0141-0229(93)90071-9

Malvern Instruments Ltd., 2016. Zetasizer Nano ZS Performance, simplicity, versatility. [WWW Document]. URL http://www.malvern.com/en/products/product-range/zetasizer-range/zetasizer-nano-range/zetasizer-nano-zs/

Marquardt, J.U., Gomez-Quiroz, L., Arreguin Camacho, L.O., Pinna, F., Lee, Y.-H., Kitade, M., Domínguez, M.P., Castven, D., Breuhahn, K., Conner, E.A., Galle, P.R., Andersen, J.B., Factor, V.M., Thorgeirsson, S.S., 2015. Curcumin effectively inhibits oncogenic NF-κB signaling and restrains stemness features in liver cancer. J. Hepatol. 63, 661–9. https://doi.org/10.1016/j.jhep.2015.04.018

Masoud, V., Pagès, G., 2017. Targeted therapies in breast cancer: New challenges to fight against resistance World Journal of Clinical Oncology. World J. Clin. Oncol. 8, 120–134. https://doi.org/10.5306/wjco.v8.i2.120

Mastalier B, Tihon C, Ghiță B, Botezatu C, Deaconescu V, Mandisodza P, Draghici C, Simion S, 2012. Surgical treatment of colon cancer Colentina surgical clinic experience. J. Med. Life 5, 348–353.

Mathew, S.T., 2011. Colon Specific Drug Delivery Systems: A Review on Various Pharmaceutical Approaches. J. Appl. Pharm. Sci. 02, 163–169.

Mato, E., Puras, G., Bell, O., Agirre, M., Hernández, R., Igartua, M., Moreno, R., Gonzalez, G., de Leiva, A., Pedraz, J., 2015. Selective Antitumoral Effect of Sorafenib Loaded PLGA Nanoparticles Conjugated with Cetuximab on Undifferentiated/Anaplastic Thyroid Carcinoma Cells. J. Nanomed.

Nanotechnol. 6, 1–10. https://doi.org/10.4172/2157-7439.1000281

Maya, S., Kumar, L.G., Sarmento, B., Sanoj Rejinold, N., Menon, D., Nair, S. V., Jayakumar, R., 2013. Cetuximab conjugated O-carboxymethyl chitosan nanoparticles for targeting EGFR overexpressing cancer cells. Carbohydr. Polym. 93, 661–669. https://doi.org/10.1016/j.carbpol.2012.12.032

Maya, S., Sarmento, B., Lakshmanan, V.-K., Menon, D., Jayakumar, R., 2014. Actively Targeted Cetuximab Conjugated γ-Poly(glutamic acid)-Docetaxel Nanomedicines for Epidermal Growth Factor Receptor Over Expressing Colon Cancer Cells. J. Biomed. Nanotechnol. 10, 1416–1428. https://doi.org/10.1166/jbn.2014.1841

Mazzarino, L., Travelet, C., Ortega-Murillo, S., Otsuka, I., Pignot-Paintrand, I., Lemos-Senna, E., Borsali, R., 2012. Elaboration of chitosan-coated nanoparticles loaded with curcumin for mucoadhesive applications. J. Colloid Interface Sci. 370, 58–66. https://doi.org/10.1016/j.jcis.2011.12.063

Mehanna, M., Motawaa, A., Samaha, M., 2012. Pharmaceutical Particulate Lipid-Based Carriers. Natl. J. Physiol. Pharm. Pharmacol. | 2, 10–22.

Meng, L., Dobson, J., Kyung Kim, D., 2010. Surface activation and targeting strategies of superparamagnetic iron oxide nanoparticles in cancer-oriented diagnosis and therapy. Nanomedicine 5, 109–133. https://doi.org/10.2217/nnm.09.96

Menon, V.P., Sudheer, A.R., 2007. Antioxidant and anti-inflammatory properties of curcumin. Adv. Exp. Med. Biol. 595, 105–25. https://doi.org/10.1007/978-0-387-46401-5_3

Miladi, K., Sfar, S., Fessi, H., Elaissari, A., 2016. Polymer Nanoparticles for Nanomedicines. https://doi.org/10.1007/978-3-319-41421-8

Misale, S., Yaeger, R., Hobor, S., Scala, E., Liska, D., Valtorta, E., Schiavo, R., Buscarino, M., Siravegna, G., Bencardino, K., Cercek, A., Chen, C., Veronese, S., Zanon, C., Sartore-bianchi, A., Gambacorta, M., Gallicchio, M., Vakiani, E., Boscaro, V., Medico, E., Weiser, M., Siena, S., 2014. Emergence of KRAS mutations and acquired resistance to anti EGFR therapy in colorectal cancer. Nature 486, 532–536. https://doi.org/10.1038/nature11156.Emergence

Mishra, R.K., Anis, A., Mondal, S., Dutt, M., Banthia, A.K., Science, P., Mishra, R.K., Anis, A., Mondal, S., Dutt, M., Banthia, A.K., Science, P., 2009. Preparation and Characterization of Amidated Pectin Based Polymer Electrolyte Membranes. Chinese J. Polym. Sci. 27, 639–646. https://doi.org/10.1142/S0256767909004333

Mishra, R.K., Banthia, A.K., Majeed, A.B.A., 2012. Pectin based formulations for biomedical applications: A review. Asian J. Pharm. Clin. Res. 5, 1–7.

Mitra, T., Sailakshmi, G., Gnanamani, A., 2014. Could glutaric acid (GA) replace glutaraldehyde in the preparation of biocompatible biopolymers with high mechanical and thermal properties? J. Chem. Sci 126, 127–140.

Miura, K., Shima, H., Takebe, N., Rhie, J., Satoh, K., Kakugawa, Y., Satoh, M., Kinouchi, M., Yamamoto, K., Hasegawa, Y., Kawai, M., Kanazawa, K., Fujiya, T., Unno, M., Katakura, R., 2017. Drug delivery of oral anti-cancer fluoropyrimidine agents. Expert Opin. Drug Deliv. 14, 1355–1366. https://doi.org/10.1080/17425247.2017.1316260

Moghaddam, F.A., Atyabi, F., Dinarvand, R., 2009. Preparation and in vitro evaluation

of mucoadhesion and permeation enhancement of thiolated chitosan-pHEMA core-shell nanoparticles. Nanomedicine Nanotechnology, Biol. Med. 5, 208–215. https://doi.org/10.1016/J.NANO.2008.09.006

Moorthi, C., Kathiresan, K., 2013. Curcumin–Piperine/Curcumin–Quercetin/Curcumin–Silibinin dual drug-loaded nanoparticulate combination therapy: A novel approach to target and treat multidrug-resistant cancers. J. Med. Hypotheses Ideas 7, 15–20. https://doi.org/10.1016/j.jmhi.2012.10.005

Moorthi, C., Krishnan, K., Manavalan, R., Kathiresan, K., 2012. Preparation and characterization of curcumin–piperine dual drug loaded nanoparticles. Asian Pac. J. Trop. Biomed. 2, 841–848. https://doi.org/10.1016/S2221-1691(12)60241-X

Morales-Cruz, Moraima, Flores-Fernández, G.M., Morales-Cruz, Myreisa, Orellano, E.A., Rodriguez-Martinez, J.A., Ruiz, M., Griebenow, K., 2012. Two-step nanoprecipitation for the production of protein-loaded PLGA nanospheres. Results Pharma Sci. 2, 79–85. https://doi.org/10.1016/j.rinphs.2012.11.001

Moshe, H., Davizon, Y., Menaker Raskin, M., Sosnik, A., 2017. Novel poly(vinyl alcohol)-based amphiphilic nanogels by non-covalent boric acid crosslinking of polymeric micelles †. Biomater. Sci. 5, 2295. https://doi.org/10.1039/c7bm00675f

Mourdikoudis, S., Pallares, R.M., Thanh, N.T.K., 2018. Characterization techniques for nanoparticles: comparison and complementarity upon studying nanoparticle properties. Nanoscale 10, 12871–12934. https://doi.org/10.1039/C8NR02278J

Muheem, A., Shakeel, F., Jahangir, M.A., Anwar, M., Mallick, N., Jain, G.K., Warsi, M.H., Ahmad, F.J., 2014. A review on the strategies for oral delivery of proteins and peptides and their clinical perspectives. Saudi Pharm. J. 24, 413–428. https://doi.org/10.1016/j.jsps.2014.06.004

Mulik, R., Mahadik, K., Paradkar, A., 2009. Development of curcuminoids loaded poly(butyl) cyanoacrylate nanoparticles: Physicochemical characterization and stability study. Eur. J. Pharm. Sci. 37, 395–404.

Mulik, R., Mönkkönen, J., Juvonen, R.O., Mahadik, K.R., Paradkar, A.R., 2010. Transferrin mediated solid lipid nanoparticles containing curcumin: Enhanced in vitro anticancer activity by induction of apoptosis. Int. J. Pharm. 398, 190–203. https://doi.org/10.1016/j.ijpharm.2010.07.021

Mutlur, S., 2004. Thermal Analysis of Composites Using DSC. pp. 11–33.

Nagavarma, B.V.N., Yadav, H.K.S., Ayaz, A., Vasudha, L.S., Shivakumar, H.G., 2012. Different techniques for preparation of polymeric nanoparticles- A review. Asian J. Pharm. Clin. Res. 5, 16–23.

Nakayama, G., Tanaka, C., Kodera, Y., 2014. Current Options for the Diagnosis, Staging and Therapeutic Management of Colorectal Cancer. Gastrointest. Tumors 1, 25–32. https://doi.org/10.1159/000354995

NanoSight NTA 2.1 Analytical Software Operating Manual, 2010.

Nedovic, V., Kalusevic, A., Manojlovic, V., Levic, S., Bugarski, B., 2011. An overview of encapsulation technologies for food applications. Procedia Food Sci. 1, 1806–1815. https://doi.org/10.1016/j.profoo.2011.09.266

Newlaczyl, A.U., Yu, L.-G., 2011. Galectin-3 – A jack-of-all-trades in cancer. Cancer Lett. 313, 123–128. https://doi.org/10.1016/J.CANLET.2011.09.003

Nicholas E. Madhu, Panaganti Shanker, Prabakaran L., Jayveera N. K, 2011. NOVEL COLON SPECIFIC DRUG DELIVERY SYSTEM: A REVIEW. Int. J. Pharm. Sci. Res. 2545–2561. https://doi.org/http://dx.doi.org/10.13040/IJPSR.0975-8232.2(10).2545-61

Nicolet, T., All, C., 2001. Introduction to Fourier Transform Infrared Spectrometry. A Thermo Electron Bussines 1–8. https://doi.org/10.1080/09638280110110640

Nielsen, M.I., Stegmayr, J., Grant, O.C., Yang, Z., Nilsson, U.J., Boos, I., Carlsson, M.C., Woods, R.J., Unverzagt, C., Leffler, H., Wandall, H.H., 2018. Galectin binding to cells and glycoproteins with genetically modified glycosylation reveals galectin-glycan specificities in a natural context. J. Biol. Chem. 293, 20249–20262. https://doi.org/10.1074/jbc.RA118.004636

Normanno, N., De Luca, A., Bianco, C., Strizzi, L., Mancino, M., Maiello, M.R., Carotenuto, A., De Feo, G., Caponigro, F., Salomon, D.S., 2006. Epidermal growth factor receptor (EGFR) signaling in cancer. Gene 366, 2–16. https://doi.org/10.1016/j.gene.2005.10.018

Nugent, S.G., Kumar, D., Rampton, D.S., Evans, D.F., 2001. Intestinal luminal pH in inflammatory bowel disease: possible determinants and implications for therapy with aminosalicylates and other drugs. Gut 48, 571–577. https://doi.org/10.1136/gut.48.4.571

Nunez, R., 2001. DNA measurement and cell cycle analysis by flow cytometry. Curr. Issues Mol. Biol. 3, 67–70.

Oda, K., Matsuoka, Y., Funahashi, A., Kitano, H., 2005. A comprehensive pathway map of epidermal growth factor receptor signaling. Mol. Syst. Biol. https://doi.org/10.1038/msb4100014

Odun-Ayo, F., Mellem, J., Naicker, T., Reddy, L., 2015. Chemoprevention of Azoxymethane-induced Colonic Carcinogenesis in Balb/c mice Using a Modified Pectin Alginate Probiotic. Anticancer Res. 35, 4765–75.

Oliveira, G.F., Ferrari, P.C., Carvalho, L.Q., Evangelista, R.C., 2010. Chitosan–pectin multiparticulate systems associated with enteric polymers for colonic drug delivery. Carbohydr. Polym. 82, 1004–1009. https://doi.org/10.1016/J.CARBPOL.2010.06.041

Olson, B.J.S.C., Markwell, J., 2007. Assays for Determination of Protein Concentration.

Pabla B., Bissonnette M., Konda J. V., 2015. Colon cancer and the epidermal growth factor receptor: Current treatment paradigms, the importance of diet, and the role of chemoprevention. World J. Clin. Oncol. 6, 133–141. https://doi.org/10.5306/wjco.v6.i5.133

Padma, V.V., 2015. An overview of targeted cancer therapy. BioMedicine 5, 19. https://doi.org/10.7603/s40681-015-0019-4

Padmanaban, G., Nagaraj, V.A., Rangarajan, P.N., 2012. SPECIAL SECTION: MALARIA RESEARCH Artemisinin-based combination with curcumin adds a new dimension to malaria therapy. Curr. Sci. 102.

Pal, S.L., Jana, U., Manna, P.K., Mohanta, G.P., Manavalan, R., 2011. Nanoparticle: An overview of preparation and characterization. J. Appl. Pharm. Sci. 01, 228–234.

Palacio, J., Orozco, V.H., López, B.L., 2011. Effect of the molecular weight on the

physicochemical properties of poly(lactic acid) nanoparticles and on the amount of ovalbumin adsorption. J. Braz. Chem. Soc. 22, 2304–2311. https://doi.org/10.1590/S0103-50532011001200010

Pandey, S., Mishra, A., Raval, P., Patel, H., Gupta, A., Shah, D., 2013. Chitosan-pectin polyelectrolyte complex as a carrier for colon targeted drug delivery. J. Young Pharm. 5, 160–6. https://doi.org/10.1016/j.jyp.2013.11.002

Panyam, J., Dali, M.M., Sahoo, S.K., Ma, W., Chakravarthi, S.S., Amidon, G.L., Levy, R.J., Labhasetwar, V., 2003. Polymer degradation and in vitro release of a model protein from poly(D,L-lactide-co-glycolide) nano-and microparticles. J. Control. Release 92, 173–187. https://doi.org/10.1016/S0168-3659(03)00328-6

Park, J.H., Han, S.W., Oh, D.Y., Im, S.A., Jeong, S.Y., Park, K.J., Kim, T.Y., Bang, Y.J., Park, J.G., 2011. Analysis of KRAS, BRAF, PTEN, IGF1R, EGFR intron 1 CA status in both primary tumors and paired metastases in determining benefit from cetuximab therapy in colon cancer. Cancer Chemother. Pharmacol. 68, 1045–1055. https://doi.org/10.1007/s00280-011-1586-z

Particle Sciences, 2009. Emulsions and Emulsification. Bethlehem,USA.

Patel, M.M., 2014. Getting into the colon: approaches to target colorectal cancer. Expert Opin. Drug Deliv. 11, 1343–1350. https://doi.org/10.1517/17425247.2014.927440

Patel, V.B., Misra, S., Patel, B.B., Majumdar, A.P.N., 2010. Colorectal cancer: chemopreventive role of curcumin and resveratrol. Nutr. Cancer 62, 958–67. https://doi.org/10.1080/01635581.2010.510259

Pengpong, T., Sangvanich, P., Sirilertmukul, K., Muangsin, N., 2014. Design, synthesis and in vitro evaluation of mucoadhesive p-coumarate-thiolated-chitosan as a hydrophobic drug carriers. Eur. J. Pharm. Biopharm. 86, 487–497. https://doi.org/10.1016/j.ejpb.2013.11.009

Perkins, S., Verschoyle, R.D., Hill, K., Parveen, I., Threadgill, M.D., Sharma, R.A., Williams, M.L., Steward, W.P., Gescher, A.J., 2002. Chemopreventive efficacy and pharmacokinetics of curcumin in the min/+ mouse, a model of familial adenomatous polyposis. Cancer Epidemiol. Biomarkers Prev. 11, 535–40.

Pozzi, F., Furlani, P., Gazzaniga, A., Davis, S., Wilding, I., 1994. The time clock system: a new oral dosage form for fast and complete release of drug after a predetermined lag time☆. J. Control. Release 31, 99–108. https://doi.org/10.1016/0168-3659(94)90255-0

Prabaharan, M., Reis, R.L., Mano, J.F., 2007. Carboxymethyl chitosan-graft-phosphatidylethanolamine: Amphiphilic matrices for controlled drug delivery. React. Funct. Polym. 67, 43–52. https://doi.org/10.1016/J.REACTFUNCTPOLYM.2006.09.001

Pragati, S., Kuldeep, S., Ashok, S., Satheesh, M., 2009. Solid Lipid Nanoparticles : A Promising Drug Delivery Technology ABSTRACT : Nanomedicine 2, 509–516.

Prasad, S., Gupta, S.C., Tyagi, A.K., Aggarwal, B.B., 2014. Curcumin, a component of golden spice: From bedside to bench and back. Biotechnol. Adv. 32, 1053–1064. https://doi.org/10.1016/j.biotechadv.2014.04.004

Quiñones, J.P., Peniche, H., Peniche, C., 2018. Chitosan based self-assembled nanoparticles in drug delivery. Polymers (Basel). 10, 1–32. https://doi.org/10.3390/polym10030235

Rachmawati, H., 2013. Curcumin nanoforms promise better therapeutic values. Int. J. Res. Pharm. Sci. 4, 211–220.

Rachmawati, H., Yanda, Y.L., Rahma, A., Mase, N., 2016. Curcumin-Loaded PLA Nanoparticles: Formulation and Physical Evaluation. Sci. Pharm. 84, 191–202. https://doi.org/10.3797/scipharm.ISP.2015.10

Rajalakshmi, R., Y, I.M., Aruna, U., Vinesha, V., Rupangada, V., Krishna, S.B., 2014. Chitosan Nanoparticles — An Emerging Trend In Nanotechnology Chitosan Nanoparticles - An Emerging Trend In Nanotechnology. Int. J. Drug Deliv. 6, 204–229.

Ramkumar, S.C., Murali, A., Preethi, G., Chandrasekaran, B., Saravanan, P., Jaisankar, S.N., 2017. Polycarbodiimide and polyurethane cross-linkers for leather finishing. Leather Footwear J. 17, 181–192. https://doi.org/10.24264/lfj.17.4.1

Rampino, A., Borgogna, M., Blasi, P., Bellich, B., Cesàro, A., 2013. Chitosan nanoparticles: Preparation, size evolution and stability. Int. J. Pharm. 455, 219–228. https://doi.org/10.1016/j.ijpharm.2013.07.034

Rao, J.N., Wang, J.-Y., 2010. Intestinal Architecture and Development, in: Regulation of Gastrointestinal Mucosal Growth. Morgan & Claypool, San Rafael (CA). https://doi.org/NBK54098

Rao, J.P., Geckeler, K.E., 2011. Polymer nanoparticles: Preparation techniques and size-control parameters. Prog. Polym. Sci. 36, 887–913. https://doi.org/10.1016/j.progpolymsci.2011.01.001

Rao, W., Zhang, W., Poventud-Fuentes, I., Wang, Y., Lei, Y., Agarwal, P., Weekes, B., Li, C., Lu, X., Yu, J., He, X., 2014. Thermally responsive nanoparticle-encapsulated curcumin and its combination with mild hyperthermia for enhanced cancer cell destruction. Acta Biomater. 10, 831–42.

Recillas, M., Silva, L.L., Peniche, C., Goycoolea, F.M., Rinaudo, M., Román, J.S., Argüelles-Monal, W.M., 2011. Thermo- and pH-responsive polyelectrolyte complex membranes from chitosan-g-N-isopropylacrylamide and pectin. Carbohydr. Polym. 86, 1336–1343. https://doi.org/10.1016/j.carbpol.2011.06.047

Rex K. Douglas, Johnson A. David, Anderson C. Joseph, Schoenfeld S. Phillip, Burke A. Carol, Inadomi M. John, 2009. ACG PRACTICE GUIDELINES 739. Am. J. Gastroenterol 104, 740–750. https://doi.org/10.1038/ajg.2009.104

Rhind, N., Russell, P., 2012. Signaling pathways that regulate cell division. Cold Spring Harb. Perspect. Biol. 4. https://doi.org/10.1101/cshperspect.a005942

Riesco, A., Santos-Buitrago, B., De, J., Rivas, L., Knapp, M., Santos-García, G., Talcott, C., 2017. Epidermal Growth Factor Signaling towards Proliferation: Modeling and Logic Inference Using Forward and Backward Search. Biomed Res. Int. 2017, 11. https://doi.org/10.1155/2017/1809513

Rocha-Lima, C.M., Soares, H.P., Raez, L.E., Singal, R., 2007. EGFR targeting of solid tumors. Cancer Control 14, 295–304.

Rodrigues, S., Rosa Da Costa, A.M., Grenha, A., 2012. Chitosan/carrageenan nanoparticles: Effect of cross-linking with tripolyphosphate and charge ratios. Carbohydr. Polym. 89, 282–289. https://doi.org/10.1016/j.carbpol.2012.03.010

Romero, G., Moya, S.E., 2012. Synthesis of organic nanoparticles, in: Frontiers of Nanoscience. Elsevier LTD., pp. 115–141. https://doi.org/10.1016/B978-0-12-

415769-9.00004-2

Sadtler, V., M., J., Marie, E., 2012. Low Energy Emulsification Methods for Nanoparticles Synthesis, in: Hashim A. Abbass (Ed.), The Delivery of Nanoparticles. InTech, Croatia, pp. 509–524. https://doi.org/10.5772/35087

Sakuma, S., Maruyama, C., Kohda, T., Fujimoto, Y., 2014. Curcumin inhibits the proliferation of a human colorectal cancer cell line Caco-2 partially by both apoptosis and G2/M cell cycle arrest Corresponding author*. Int. J. Pharmacol. Res. 4, 84–90. https://doi.org/10.7439/ijpr

Sarmento, B., Ferreira, D., Veiga, F., Nio Ribeiro, A., 2006. Characterization of insulin-loaded alginate nanoparticles produced by ionotropic pre-gelation through DSC and FTIR studies. Carbohydr. Polym. 66, 1–7. https://doi.org/10.1016/j.carbpol.2006.02.008

Satelli, A., Rao, P.S., Gupta, P.K., Lockman, P.R., Srivenugopal, K.S., Rao, U.S., 2008. Varied expression and localization of multiple galectins in different cancer cell lines. Oncol. Rep. 19, 587–594. https://doi.org/10.3892/or.19.3.587

Saveyn, H., De Baets, B., Thas, O., Hole, P., Smith, J., Van Der Meeren, P., 2010. Accurate particle size distribution determination by nanoparticle tracking analysis based on 2-D Brownian dynamics simulation. J. Colloid Interface Sci. 352, 593–600. https://doi.org/10.1016/j.jcis.2010.09.006

Scott, A.M., Allison, J.P., Wolchok, J.D., 2012. Monoclonal antibodies in cancer therapy. Cancer Immun. 12, 14.

Šeklić, D.S., Obradović, A.D., Stanković, M.S., Živanović, M.N., Mitrović, T.L., Stamenković, S.M., Marković, S.D., 2018. Proapoptotic and Antimigratory Effects of Pseudevernia furfuracea and Platismatia glauca on Colon Cancer Cell Lines. Food Technol. Biotechnol. 56, 421–430. https://doi.org/10.17113/ftb.56.03.18.5727

Senapati, S., Mahanta, A.K., Kumar, S., Maiti, P., 2018. Controlled drug delivery vehicles for cancer treatment and their performance. Signal Transduct. Target. Ther. 3, 1–19. https://doi.org/10.1038/s41392-017-0004-3

Sercombe, L., Veerati, T., Moheimani, F., Wu, S.Y., Sood, A.K., Hua, S., 2015. Advances and Challenges of Liposome Assisted Drug Delivery. Front. Pharmacol. 6, 286. https://doi.org/10.3389/fphar.2015.00286

Sh Rashidova, S., Yu Milusheva, R., Semenova, L.N., Yu Mukhamedjanova, M., Voropaeva, N.L., Vasilyeva, S., Faizieva, R., Ruban, I.N., 2004. Characteristics of Interactions in the Pectin-Chitosan System. Chromatographia 5, 779–782. https://doi.org/10.1365/s10337-004-0289-6

Shaffer A. Eldon, Alan Bryan, Thomson B. R. Alan, 2005. First Principles of Gastroenterology: The Basis of Disease and an Approach to Management, 5th ed. Medicine Group, Canada.

Shafras M, Rafeek R.A.M, P.G., 2017. Monoclonal Antibodies and Its Clinical Aspects. J. Pharm. Care 5, 29–36.

Shaikh, R., Raj Singh, T.R., Garland, M.J., Woolfson, A.D., Donnelly, R.F., 2011. Mucoadhesive drug delivery systems. J. Pharm. Bioallied Sci. 3, 89–100. https://doi.org/10.4103/0975-7406.76478

Shaikh, R., Raj Singh, T.R., Garland, M.J., Woolfson, A.D., Donnelly, R.F., 2010. Mucoadhesive drug delivery systems. J. Pharm. Bioallied Sci. 3, 89–100.

https://doi.org/10.4103/0975-7406.76478

Sharma, B., Dhuldhoya, N., Merchant, S., Merchant, U., 2006. An Overview on Pectins. Times Food Process. J. 44–51.

Sharma, S., Saltz, L.B., 2000. Oral chemotherapeutic agents for colorectal cancer. Oncologist 5, 99–107. https://doi.org/10.1634/THEONCOLOGIST.5-2-99

Shen, S., Wu, Y., Liu, Y., Wu, D., 2017. High drug-loading nanomedicines: progress, current status, and prospects. Int. J. Nanomedicine 12, 4085–4109. https://doi.org/10.2147/IJN.S132780

Shigeta, K., Hayashida, T., Hoshino, Y., Okabayashi, K., Endo, T., Ishii, Y., Hasegawa, H., Kitagawa, Y., 2013. Expression of Epidermal Growth Factor Receptor Detected by Cetuximab Indicates Its Efficacy to Inhibit In Vitro and In Vivo Proliferation of Colorectal Cancer Cells. PLoS One 8. https://doi.org/10.1371/journal.pone.0066302

Shin, G.H., Chung, S.K., Kim, J.T., Joung, H.J., Park, H.J., 2013. Preparation of chitosan-coated nanoliposomes for improving the mucoadhesive property of curcumin using the ethanol injection method. J. Agric. Food Chem. 61, 11119–11126. https://doi.org/10.1021/jf4035404

Shoshi, A., Schotter, J., Schroeder, P., Milnera, M., Ertl, P., Charwat, V., Purtscher, M., Heer, R., Eggeling, M., Reiss, G., Brueckl, H., 2012. Magnetoresistive-based real-time cell phagocytosis monitoring. Biosens. Bioelectron. 36, 116–122. https://doi.org/10.1016/J.BIOS.2012.04.002

Simonova, D., Karamancheva, I., 2013. Application of Fourier Transform Infrared Spectroscopy for Tumor Diagnosis. Biotechnol. Biotechnol. Equip. 27, 4200–4207. https://doi.org/10.5504/BBEQ.2013.0106

Singh, B.R., 2000. Basic Aspects of the Technique and Applications of Infrared Spectroscopy of Peptides and Proteins. Am. Chem. Soc. 1, 1–36.

Singh B, Carpenter G, Coffey RJ, 2016. EGF receptor ligands: recent advances. F1000 5Research 5, 1–11. https://doi.org/10.12688/f1000research.9025.1

Singh, N., Khanna, R.C., 2012. Colon targeted drug delivery systems – A Potential Approach INTRODUCTION: The oral route of drug. PHARMA Innov. 1, 40–47.

Singh, R., Lillard, J.W., Jr., 2009. Nanoparticle-based targeted drug delivery. Exp. Mol. Pathol. 86, 215–23. https://doi.org/10.1016/j.yexmp.2008.12.004

Sinha, V.R., Kumria, R., 2003. Microbially triggered drug delivery to the colon. Eur. J. Pharm. Sci. 18, 3–18.

Sionkowska, A., 2011. Current research on the blends of natural and synthetic polymers as new biomaterials: Review. Prog. Polym. Sci. 36, 1254–1276. https://doi.org/10.1016/j.progpolymsci.2011.05.003

Skvortsov, S., Sarg, B., Loeffler-Ragg, J., Skvortsova, I., Lindner, H., Ott, H.W., Lukas, P., Illmensee, K., Zwierzina, H., 2004. Different proteome pattern of epidermal growth factor receptor-positive colorectal cancer cell lines that are responsive and nonresponsive to C225 antibody treatment, Mol Cancer Ther.

Smart, J.D., 2005. The basics and underlying mechanisms of mucoadhesion. Adv. Drug Deliv. Rev. 57, 1556–1568. https://doi.org/10.1016/j.addr.2005.07.001

Soenen, S.J., Rivera-Gil, P., Montenegro, J.-M., Parak, W.J., De Smedt, S.C.,

Braeckmans, K., 2011. Cellular toxicity of inorganic nanoparticles: Common aspects and guidelines for improved nanotoxicity evaluation. Nano Today 6, 446–465. https://doi.org/10.1016/j.nantod.2011.08.001

Sotelo Lezama, M.J., Sastre Valera, J., Díaz-Rubio García, E., 2014. Impact of cetuximab in current treatment of metastatic colorectal cancer. Expert Opin. Biol. Ther. 14, 387–399. https://doi.org/10.1517/14712598.2014.883376

Subramani, P.A., Panati, K., Lebaka, V.R., Reddy, D.D., Narala, V.R., 2017. Nanostructures for Curcumin Delivery: Possibilities and Challenges. Nano-Microscale Drug Deliv. Syst. 393–418. https://doi.org/10.1016/B978-0-323-52727-9.00021-2

Svensson, O., Arnebrant, T., 2010. Mucin layers and multilayers — Physicochemical properties and applications. Curr. Opin. Colloid Interface Sci. 15, 395–405. https://doi.org/10.1016/J.COCIS.2010.05.015

Tao, Y., Andrew, G.P., Jones, D.S., 2014. Mucoadhesion and Characterization of Mucoadhesive Properties, in: Neves, D.J., B., S. (Eds.), Mucosal Delivery of Biopharmaceuticals. Springer, pp. 35–44. https://doi.org/10.1007/978-1-4614-9524-6_2

Thakor, A.S., Gambhir, S.S., 2013. Nanooncology: The future of cancer diagnosis and therapy. CA. Cancer J. Clin. 63, 395–418. https://doi.org/10.3322/caac.21199

Thanh, N.T.K., Maclean, N., Mahiddine, S., 2014. Mechanisms of Nucleation and Growth of Nanoparticles in Solution. Chem. Rev. 114, 7610–7630. https://doi.org/10.1021/cr400544s

Thermo Scientific, 2012. Crosslinking technology: Reactivity chemistries, applications and structure references. USA.

Thermo Scientific, 2011. NHS and Sulfo-NHS [WWW Document]. Thermo Fish. Sci. Inc. URL www.thermoscientific.com/pierce (accessed 8.27.19).

Tian, X., Nejadnik, M.R., Baunsgaard, D., Henriksen, A., Rischel, C., Jiskoot, W., 2016. A Comprehensive Evaluation of Nanoparticle Tracking Analysis (NanoSight) for Characterization of Proteinaceous Submicron Particles. J. Pharm. Sci. 105, 3366–3375. https://doi.org/10.1016/j.xphs.2016.08.009

Tokarev, A.A., Alfonso, A., Segev, N., 2013. Overview of Intracellular Compartments and Trafficking Pathways, in: Segev, N. (Ed.), Trafficking Inside Cells: Pathways, Mechanisms and Regulation. Landes Bioscience and Springer Science, Chicago, Illinois.

Tokunaga, E., Oda, S., Fukushima, M., Maehara, Y., Sugimachi, K., 2000. Differential growth inhibition by 5-fluorouracil in human colorectal carcinoma cell lines. Eur. J. Cancer 36, 1998–2006. https://doi.org/10.1016/S0959-8049(00)00200-8

Tuorkey, M.J., 2014. Curcumin a potent cancer preventive agent: Mechanisms of cancer cell killing. Interv. Med. Appl. Sci. 6, 139–46. https://doi.org/10.1556/IMAS.6.2014.4.1

Urias-orona, V., Rascón-chu, A., Lizardi-mendoza, J., Carvajal-Millán, E., Gardea A., A., Ramírez-Wong, B., 2010. A Novel Pectin Material : Extraction , Characterization and Gelling Properties. Int. J. Mol. Sci. 11, 3686–3695. https://doi.org/10.3390/ijms11103686

Usmiati, S., Richana, N., Mangunwidjaja, D., Noor, E., Prangdimurti, E., 2014. The Using of Ionic Gelation Method Based on Polysaccharides for Encapsulating the

Macromolecules-A Review, in: International Conference on Food Security and Nutrition. IACSIT Press, Singapore, pp. 79–84. https://doi.org/10.7763/IPCBEE

Vallianou, N.G., Evangelopoulos, A., Schizas, N., Kazazis, C., 2015. Potential anticancer properties and mechanisms of action of curcumin. Anticancer Res. 35, 645–51.

Van Erk, M.J., Teuling, E., Staal, Y.C., Huybers, S., Van Bladeren, P.J., Aarts, J.M., Van Ommen, B., 2004. Time- and dose-dependent effects of curcumin on gene expression in human colon cancer cells. J. Carcinog. 3, 8. https://doi.org/10.1186/1477-3163-3-8

van Hoogevest, P., Wendel, A., 2014. The use of natural and synthetic phospholipids as pharmaceutical excipients. Eur. J. Lipid Sci. Technol. 116, 1088–1107. https://doi.org/10.1002/ejlt.201400219

Venzon, S.S., Canteri, M.H.G., Granato, D., Demczuk, B., Maciel, G.M., Stafussa, A.P., Haminiuk, C.W.I., 2015. Physicochemical properties of modified citrus pectins extracted from orange pomace. J. Food Sci. Technol. 52, 4102–4112. https://doi.org/10.1007/s13197-014-1419-2

Viennois, E., Chen, F., Merlin, D., 2013. NF-κB pathway in colitis-associated cancers. Transl. Gastrointest. Cancer 2, 21–29. https://doi.org/10.3978/j.issn.2224-4778.2012.11.01

Vijayakumar, A., Baskaran, R., Baek, J.-H., Sundaramoorthy, P., Yoo, B.K., 2019. In Vitro Cytotoxicity and Bioavailability of Ginsenoside-Modified Nanostructured Lipid Carrier Containing Curcumin. AAPS PharmSciTech 20, 1–8. https://doi.org/10.1208/s12249-019-1295-1

Villiers M. Melgardt, Aramwit Pornanong, Kwon S. Glen, 2008. Nanotechnology in Drug Delivery. Springer Science & Business Media, p. 662 pages.

Vogel, R., Pal, A.K., Jambhrunkar, S., Patel, P., Thakur, S.S., Reátegui, E., Parekh, H.S., Saá, P., Stassinopoulos, A., Broom, M.F., 2017. High-Resolution Single Particle Zeta Potential Characterisation of Biological Nanoparticles using Tunable Resistive Pulse Sensing. Sci. Rep. 7, 17479. https://doi.org/10.1038/s41598-017-14981-x

Voutou, B., Stefanaki, E.-C., 2008. Electron Microscopy: The Basics, Physics of Advanced Materials Winter School. Greece.

Wang, F., Wang, Y.-H., Wang, J.-J., Xu, H.-L., Wang, C.-M., 2017. Eriodictyol-induced anti-cancer and apoptotic effects inhuman hepatocellular carcinoma cells are associated with cell cycle arrest and modulation of apoptosis-related proteins. J. Bangladesh Pharmacol. Soc. 11, 285–291.

Wang, Y., Li, P., Truong-Dinh Tran, T., Zhang, J., Kong, L., 2016. Manufacturing Techniques and Surface Engineering of Polymer Based Nanoparticles for Targeted Drug Delivery to Cancer. Nanomaterials 6, 26. https://doi.org/10.3390/nano6020026

Watanabe, T., Itabashi, M., Shimada, Y., Tanaka, S., Ito, Y., Ajioka, Y., Hamaguchi, T., Hyodo, I., Igarashi, M., Ishida, H., Ishiguro, M., Kanemitsu, Y., Kokudo, N., Muro, K., Ochiai, A., Oguchi, M., Ohkura, Y., Saito, Y., Sakai, Y., Ueno, H., Yoshino, T., Fujimori, T., Koinuma, N., Morita, T., Nishimura, G., Sakata, Y., Takahashi, K., Takiuchi, H., Tsuruta, O., Yamaguchi, T., Yoshida, M., Yamaguchi, N., Kotake, K., Sugihara, K., 2012. Japanese Society for Cancer of the Colon and Rectum (JSCCR) guidelines 2010 for the treatment of colorectal

cancer. Int. J. Clin. Oncol. 17, 1–29. https://doi.org/10.1007/s10147-011-0315-2

Ways, T.M.M., Lau, W.M., Khutoryanskiy, V. V., 2018. Chitosan and its derivatives for application in mucoadhesive drug delivery systems. Polymers (Basel). 10. https://doi.org/10.3390/polym10030267

Weir, N.M., Selvendiran, K., Kutala, V.K., Tong, L., Vishwanath, S., Rajaram, M., Tridandapani, S., Anant, S., Kuppusamy, P., 2007. Curcumin induces G2/M arrest and apoptosis in cisplatin-resistant human ovarian cancer cells by modulating Akt and p38 MAPK. Cancer Biol. Ther. 6, 178–84.

Wieduwilt, M.J., Moasser, M.M., 2008. The epidermal growth factor receptor family: biology driving targeted therapeutics. Cell. Mol. Life Sci. 65, 1566–84. https://doi.org/10.1007/s00018-008-7440-8

Wilken, R., Veena, M.S., Wang, M.B., Srivatsan, E.S., 2011. Curcumin: A review of anti-cancer properties and therapeutic activity in head and neck squamous cell carcinoma. Mol. Cancer 10, 12. https://doi.org/10.1186/1476-4598-10-12

Wilson, B., Samanta, M.K., Santhi, K., Sampath Kumar, K.P., Suresh, B., 2010. Chitosan nanoparticles as a new delivery system for the anti-Alzheimer drug tacrine. Nanomedicine Nanotechnology, Biol. Med. 6, 144–152. https://doi.org/10.1016/j.nano.2009.04.001

Wolf, A.M.D., Fontham, E.T.H., Church, T.R., Flowers, C.R., Guerra, C.E., LaMonte, S.J., Etzioni, R., McKenna, M.T., Oeffinger, K.C., Shih, Y.-C.T., Walter, L.C., Andrews, K.S., Brawley, O.W., Brooks, D., Fedewa, S.A., Manassaram-Baptiste, D., Siegel, R.L., Wender, R.C., Smith, R.A., 2018. Colorectal cancer screening for average-risk adults: 2018 guideline update from the American Cancer Society. CA. Cancer J. Clin. 68, 250–281. https://doi.org/10.3322/caac.21457

Wong, T.W., Colombo, G., Sonvico, F., 2011. Pectin matrix as oral drug delivery vehicle for colon cancer treatment. AAPS PharmSciTech 12, 201–214. https://doi.org/10.1208/s12249-010-9564-z

Wu, X., Zhang, J., He, X., Wang, C., Lian, L., Liu, H., Wang, J., Lan, P., 2012. Postoperative Adjuvant Chemotherapy for Stage II Colorectal Cancer: A Systematic Review of 12 Randomized Controlled Trials. J. Gastrointest. Surg. 16, 646–655. https://doi.org/10.1007/s11605-011-1682-8

Xin, Y., Yin, M., Zhao, L., Meng, F., Luo, L., 2017. Recent progress on nanoparticle-based drug delivery systems for cancer therapy. Cancer Biol. Med. 14, 228–241. https://doi.org/10.20892/j.issn.2095-3941.2017.0052

Xing, Y., Zhao, J., Conti, P.S., Chen, K., 2014. Radiolabeled nanoparticles for multimodality tumor imaging. Theranostics 4, 290–306. https://doi.org/10.7150/thno.7341

Xu, H., Yu, Y., Marciniak, D., Rishi, A.K., Sarkar, F.H., Kucuk, O., Majumdar, A.P.N., 2005. Epidermal growth factor receptor (EGFR)-related protein inhibits multiple members of the EGFR family in colon and breast cancer cells. Mol. Cancer Ther. 4, 435–42.

Xu, Z.P., Zeng, Q.H., Lu, G.Q., Yu, A.B., 2006. Inorganic nanoparticles as carriers for efficient cellular delivery. Chem. Eng. Sci. 61, 1027–1040. https://doi.org/10.1016/j.ces.2005.06.019

Yadav, K.S., Sawant, K.K., 2010. Modified nanoprecipitation method for preparation of cytarabine-loaded PLGA nanoparticles. AAPS PharmSciTech 11, 1456–65.

https://doi.org/10.1208/s12249-010-9519-4

Yallapu, M., Dobberpuhl, R., Maher, M., Jaggi, M., Chauhan, C., 2012. Design of curcumin loaded cellulose nanoparticles for prostate cancer. Curr. Drug Metab. 13, 120–8.

Yallapu, M.M., Jaggi, M., Chauhan, S.C., 2013. Curcumin nanomedicine: a road to cancer therapeutics. Curr. Pharm. Des. 19, 1994–2010.

Yao, T., Asayama, Y., 2017. Animal-cell culture media: History, characteristics, and current issues. Reprod. Med. Biol. 16, 99–117. https://doi.org/10.1002/rmb2.12024

Yin, H., Zhang, H., Liu, B., 2013. Superior anticancer efficacy of curcumin-loaded nanoparticles against lung cancer. Acta Biochim Biophys Sin 45, 634–640.

Yordanov Georgi, 2012. Poly(alkyl cyanoacrylate) nanoparticles as drug carriers: 33 years later. Bulg. J. Chem. 1, 61–73.

You, J., Dai, D.-B., He, W.-J., Li, G., Song, S.-C., Wei, Y.-H., Li, F.-Z., Xu, X.-L., 2014. Preparation of curcumin-loaded long-circulating liposomes and its pharmacokinetics in rats. Zhongguo zhong yao zazhi = China J. Chinese Mater. Med. 39, 1238–42.

Zhang, Q.Y., Wang, F.X., Jia, K.K., Kong, L.D., 2018. Natural product interventions for chemotherapy and radiotherapy-induced side effects. Front. Pharmacol. 9. https://doi.org/10.3389/fphar.2018.01253

Zhao, L.-M., Shi, L.-E., Zhang, Z.-L., Chen, J.-M., Shi, D.-D., Yang, J., Tang, Z.-X., 2011. Preparation and application of chitosan nanoparticles and nanofibers. Brazilian J. Chem. Eng. 28, 353–362.